Methanol Conversion to Olefins and Propene Oligomerization over Modified SAPO-34 and Dealuminated Mordenite

Miles van Niekerk (BSc. Chem. Eng.)

Submitted to University of Cape Town

In fulfillment of the requirements for the degree of

DOCTOR OF PHILOSOPHY

Department of Chemical Engineering
University of Cape Town
Rondebosch
Cape Town
South Africa

September 1992

BUT 660 VANN

92/16447

ACKNOWLEDGEMENTS

Thanks are definitely due to my two supervisors; Dr Jack Fletcher and Professor Cyril O'Connor and also to Dr Masami Kojima who was involved in the supervision of the early stages of this work.

One of the greatest things about my post-graduate "epoch" was working with the guys in the Catalysis Unit, especially the "Ou Manne" Bo, Alex and Stefan who taught me many things, including a little about catalysis. Thanks also to Jannie, Rein and Steve for their input, both social and academic and to James for the constructive discussion and help with the SAPO oligomerization and TPR work.

Salutations to Connie, Leslie and Pam who were so helpful with the catalyst characterization. Rob Senekal and Tony Barker cannot be left out since without them and their hard work I would have had no experimental equipment and Basil would still be just a glint in my eye.

For their financial contribution to my research and quality of life, AECI, SASOL, the FRD are gratefully acknowledged.

Thanks to Pete, my good friend and business partner, for putting up with my cranky temperament (often work related). Also to Peggy, thanks for your patience and understanding and I will try to spare you from ever having to proof-read something like this ever again. Finally, I would like to thank my mother, Esme, for all her help and encouragement for without it I would not have gotten here.

SYNOPSIS

SAPO-34 and mordenite, catalysts with quite different pore structures, are known to be suitable for methanol conversion to light olefins and propene oligomerization to a distillate type product, respectively. In this study, these catalysts were modified in various ways and the effect of these modifications on the activity and selectivity of the above two reactions investigated.

SAPO-34, a small-pore silicoaluminophosphate molecular sieve, is highly selective in the formation of ethene and propene from methanol, but deactivates rapidly due to coke formation. This catalyst was synthesized and modified in various ways in an attempt to increase the catalyst lifetime and selectivity to ethene. Mild hydrothermal conditions encountered during deep-bed calcination of SAPO-34 were found to increase the catalyst lifetime. A number of further modifications were made to this deep-bed calcined material in an attempt to increase further the lifetime of this material. These modifications were :

(i) Silanization - in order to neutralize the acidity on the external surface of the crystallites and hence reduce pore-mouth blockage by coke species on the crystallite external surface;
(ii) Steaming - to investigate the effect of more severe hydrothermal conditions than those encountered under deep-bed-calcination conditions;
(iii) Acid site poisoning by ammonia - in an attempt to reduce the rate of coke formation which takes place readily on strong acid sites;
(iv) Boron impregnation - in order to reduce the intercrystalline void volume and thereby sterically hinder the formation of bulky coke molecules within the SAPO-34 pores;
(v) Acid and caustic treatments - in order to reduce the catalyst acidity and thereby limit the rate of the coke formation reaction.

All of the above modifications resulted in reduced catalyst lifetimes relative to that of the deep-bed calcined catalyst. Various synthesis modifications were also tested, including the incorporation of nickel and cobalt into the synthesis gel in order to substitute these metals into the catalyst framework. None of the modifications described above resulted in any significant changes in methanol conversion product selectivities. With regard to SAPO-34, the results of this investigation indicate that the methanol conversion product selectivities are altered

by changes in catalyst pore structure rather than changes in acidity. It was, however, shown that the lifetime of these SAPO-34 materials were directly dependent on the amount of strong acidity they contained, as measured by the temperature programmed desorption of ammonia.

Dealuminated mordenite has been reported to display lifetimes comparable to that of ZSM-5 for olefin oligomerization to distillate fuel type products. In this study, mordenite was synthesized and dealuminated and the activities and selectivities of these materials as well as commercially obtained dealuminated mordenites investigated for methanol conversion to olefins as well as olefin oligomerization.

In the characterization of these dealuminated mordenites, it was found that the amount of framework aluminium in these materials could be exclusively determined using temperature programmed desorption of ammonia. Infrared spectroscopy, on the other hand, was found to be an unreliable method for determining the framework silicon/aluminium ratio. Infrared spectroscopy, does however, give an indication on the manner in which the mordenite samples were dealuminated, in particular the 955 cm^{-1} band which is assigned to vibrations from new $O_3Si\text{-}O\text{-}SiO_3$ bonds formed on aluminium extraction by dealumination under non-hydrothermal conditions. The formation of these new bonds takes place only under conditions where silicon migration is inhibited (non-hydrothermal dealumination) and may be restricted to materials which have an abundance of 5-rings and no more than one 4-ring attached to each T-atom.

The rate at which mordenite may be dealuminated is enhanced for materials with reduced crystallite sizes, and consistent with the findings of this study, a series of events was proposed for mordenite dealumination using nitric acid :

(i) Framework dealumination occurs simultaneously in the main channels and the side pockets;

(ii) Extra-framework aluminium species in the main channels are hydrated oxy-hydroxy species which readily diffuse out of the crystallite into the bulk leaching medium;

(iii) As the main channel species diffuse out of the crystallites, partially hydrated extra-framework species within the side pockets migrate into the main channels where they become fully hydrated and, in turn, diffuse out of the crystallites.

The activity of dealuminated mordenites for methanol conversion to olefins and propene oligomerization was found to be significantly influenced by crystallite size and the amount of extra-framework aluminum present in the zeolite pores. The use of large crystallites and the presence of extra-framework material within the pores reduced reactant and product residence times within the mordenite crystallites, thus increasing the probability of these species being converted to coke. If dealumination is accomplished using mineral acid treatment only, extreme dealumination is not desirable as this results in crystal collapse which leads to a reduced methanol conversion and propene oligomerization catalytic activity. Dealumination accomplished using hydrothermal treatment, which facilitates the replacement of extracted aluminium by silicon, is desirable as catalysts prepared in this way have increased MTO activities.

Commercial processes have been developed for both methanol conversion and propene oligomerization based on the zeolite catalyst ZSM-5. Neither the SAPO-34 nor the mordenite catalysts have methanol conversion lifetimes which are comparable to that of ZSM-5. Whereas the SAPO-34 catalysts produce a significantly improved light olefin selectivity in comparison to ZSM-5, the strong acid site strength and wide pore diameter of mordenite results in a relatively low light olefin selectivity. With regard to the use of these catalysts for propene oligomerization, the lifetimes of the mordenite catalysts are, as expected from its structural properties, significantly less than those obtained using ZSM-5. SAPO-34, as a result of their weak acidity and small pore diameter, exhibit negligible propene oligomerization activity.

TABLE OF CONTENTS

Page

3 RESULTS

4 DISCUSSION

LIST OF FIGURES

LIST OF TABLES

NOMENCLATURE

MN	Norton mordenite
ZM	Zeocat mordenite
M1	Mordenite, synthesis 1
M2	Mordenite, synthesis 2
Ni1	Nickel SAPO-34, synthesis 1
Ni2	Nickel SAPO-34, synthesis 2
Ni3	Nickel SAPO-34, synthesis 3
Co1	Cobalt SAPO-34
S1	SAPO-34, synthesis 1
S2	SAPO-34, synthesis 2
S3	SAPO-34, synthesis 3
S3*	SAPO-34, synthesis 3, deep bed calcined

Suffixes

-H	Sample was in the hydrogen form
-Na	Sample was in the sodium form
-2AW	Sample was washed in acid twice
-2AR	Sample was refluxed in acid twice
-4AR	Sample was refluxed in acid four times
-2AR(NH3)	Ammonium form of the sample was refluxed in acid twice
-4AR(NH3)	Ammonium form of the sample was refluxed in acid four times
-SIL	Sample was silanized
-STM	Sample was steamed
-NH3	Sample was poisoned using NH_3
-BRN	Sample was impregnated with boron
-ACD	Sample was treated with acid
-CAU	Sample was treated with a caustic solution

Chapter 1

INTRODUCTION

1.1 SYNTHETIC FUELS

Historically, routes used in the production synthetic fuels from coal (via syngas) have revolved primarily around the Fischer-Tropsch process which has been in commercial use in South Africa since 1954 [Dry, 1990]. Over the past two decades, a number of synfuel related processes have been developed around the unique structural and chemical properties of molecular sieves. In combination with the existing technology available for the conversion of coal, natural gas and biomass to methanol, these processes provided the final link in a new route for the production of synthetic fuels (Figure 1.1) [Tabak and Yurchak, 1990].

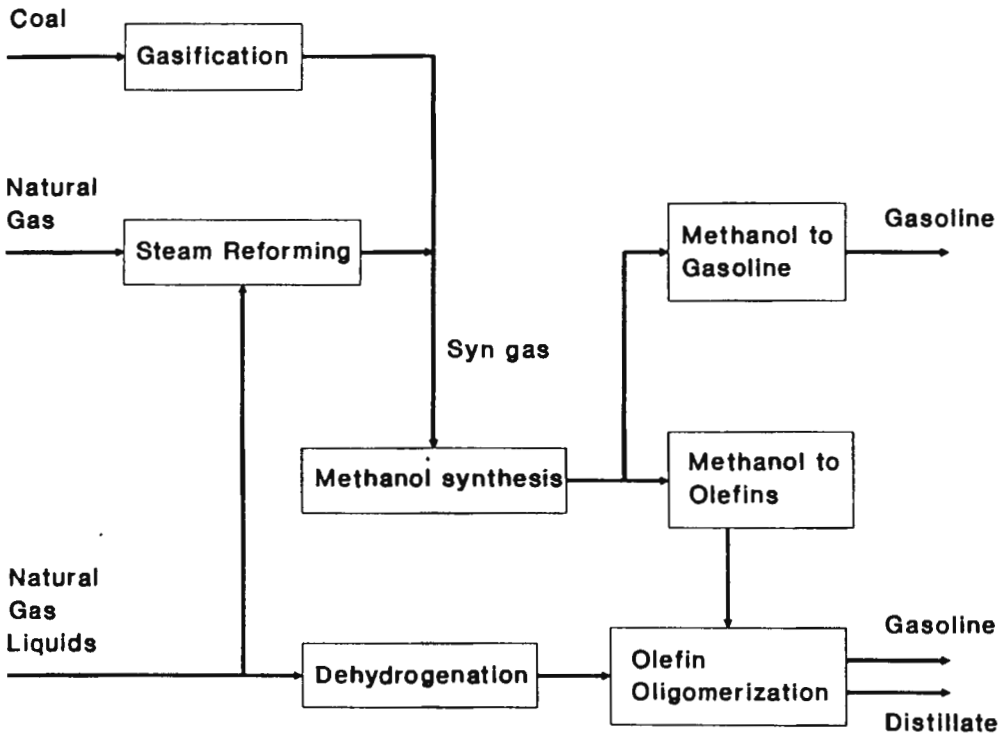

Figure 1.1 : The production of synthetic fuels from methanol. (From Avidan, 1988)

The processes developed for the production of synthetic fuels include the conversion of methanol directly to gasoline (MTG) and the conversion of methanol to light olefins (MTO). The Mobil fixed bed MTG process has been in commercial operation in Motunui, New Zealand, since 1985, producing approximately 14 500 bbl/day of high quality gasoline. The light olefins produced in the MTO process may be converted to gasoline and high quality distillate by oligomerization (MOGD or SPGK) or used as feedstocks in fine chemicals production. Light olefin

oligomerization also produces a high quality jet fuel and the oligomerization of heavier olefins produces good quality lube oils.

The MTO-MOGD route (Figure 1.2) is of particular interest since a very wide range of products may be produced, ranging from high value light olefins to heavy duty lube oils. In regard to the South African situation, the low cetane diesel produced by the oligomerization of C_3 and C_4 Fischer-Tropsch products over non-zeolite catalysts creates a need for a high cetane diesel blending stock. In addition, olefin oligomerization favours the production of aromatic-free fuels, a health and environmental consideration that is receiving increasing worldwide attention.

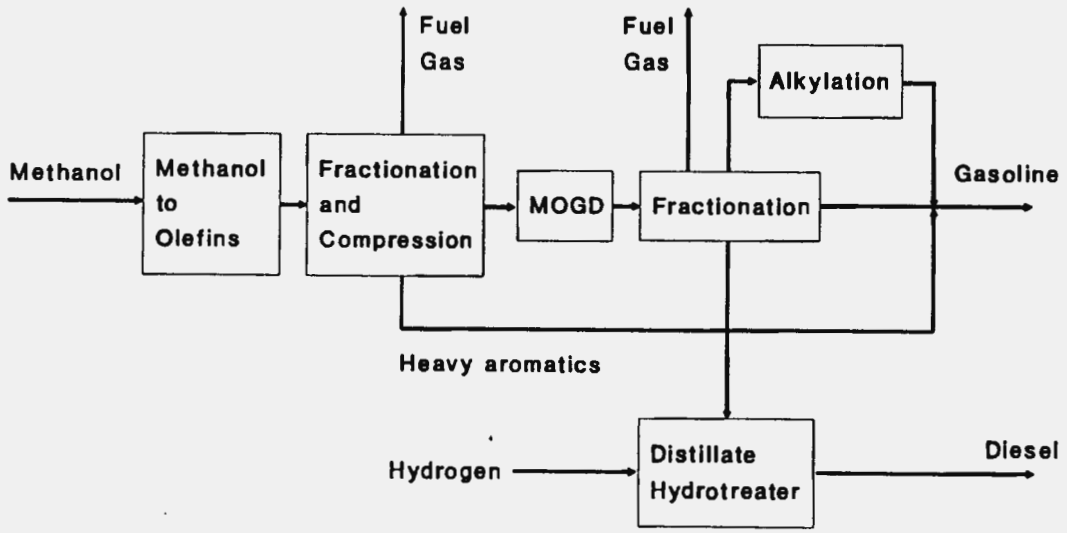

Figure 1.2 : The production of synthetic fuels from methanol via the MTO/MOGD process. (From Avidan, 1988)

Both the MTO and MOGD processes have been operated on a semi-commercial scale. The MTO process was tested on a pilot plant scale (4 bbl/day) which produced similar yields when scaled up to a 100 bbl/day in a fluidized bed demonstration plant in West Germany [Avidan, 1988]. The MOGD process has been demonstrated in a 210 bbl/day test where stable operation was achieved for the production of both gasoline and distillate [Tabak and Yurchak, 1990].

The scope of this investigation will cover the route for production of synthetic fuels via the conversion of methanol to light olefins (MTO) followed by the oligomerization of light olefins for the production of gasoline and distillate. These

reactions are studied separately, using two different microporous materials, SAPO-34 and mordenite, which are known to be suitable for methanol conversion to light olefins and olefin oligomerization, respectively.

In the sections which follow, various aspects relating to the methanol conversion and olefin oligomerization reactions are discussed. The concepts, structures and uses of various microporous materials are reviewed; specific attention being paid to the two microporous materials used in this study.

1.2 METHANOL CONVERSION TO OLEFINS AND GASOLINE

The catalytic conversion of methanol to hydrocarbons over pentasil type zeolites was announced by the Mobil Research and Development Corporation in 1979. As mentioned, this reaction is of industrial interest for the conversion of syngas (via methanol) to higher value chemicals and fuels.

Much work has been done on the selective transformation of methanol to light olefins and there is still much debate as to the mechanism of hydrocarbon formation from methanol. Many reaction conditions and catalyst compositions have been investigated with the aim of increasing the selectivities of ethene and propene while maintaining high methanol conversions with as little catalyst deactivation as possible. Reaction conditions that have been investigated include temperature, pressure, space velocity and feed composition. Variables associated with the ZSM-5 catalyst such as Si/Al ratio, catalyst particle size and morphology have also been investigated.

1.2.1 Reaction mechanism

Chemical reactions with molecular sieve catalysts are in most cases assumed to occur within the internal pore structure of the zeolite. Reacting molecules must diffuse into the micropores to interact with the catalytic sites and the product molecules then have to diffuse out. The pore structure of the molecular sieve may influence both the kinetics and the mechanism of the reaction.

The methanol conversion process may be divided into four different stages:-

(i) The reaction of methanol to give dimethyl ether and water.
(ii) The formation of the first hydrocarbon product.
(iii) The formation of higher olefins.
(iv) Aromatic formation and hydrogen transfer.

Product selectivities may therefore be influenced by controlling the extent of reaction (by varying reactant space velocity, i.e. feed and product residence times, see Figure 1.3).

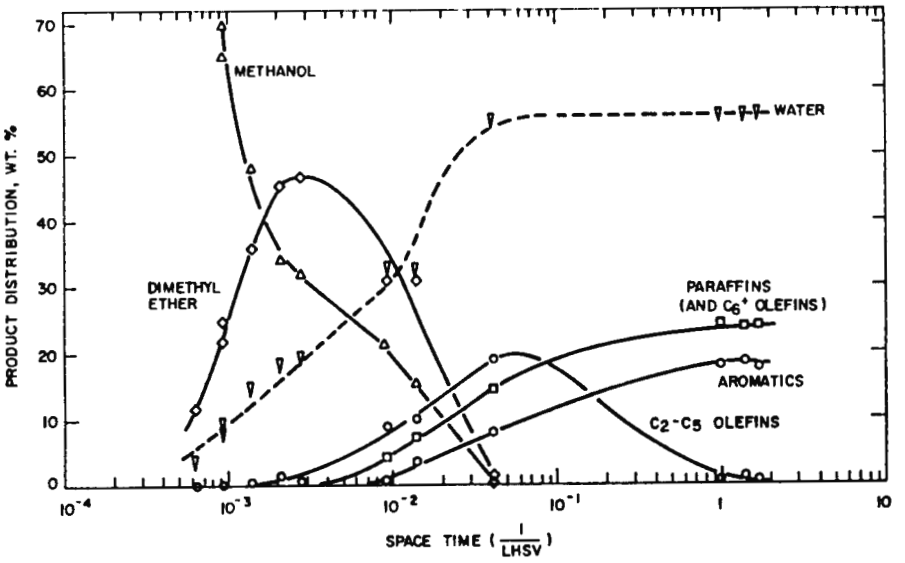

Figure 1.3 : The effect of changing the extent of reaction on hydrocarbon product selectivities. (From Chang and Silvestri, 1977)

The reaction of methanol to give dimethyl ether and water

The formation of dimethyl ether and water is accepted as the first step in the methanol conversion process. With a suitable catalyst and mild reaction conditions (<300°C, atmospheric pressure), the reaction as shown below may be carried out exclusively [Kaeding and Butter, 1980].

$$CH_3OH + H\ zeolite \rightleftharpoons CH_3\text{-}OH_2^+ + zeolite^-$$
$$CH_3OH + CH_3^+\text{---}OH_2 \rightleftharpoons CH_3\text{-}O^+(CH_3)\text{-}H + H_2O$$
$$CH_3\text{-}O^+(CH_3)\text{-}H + zeolite^- \rightleftharpoons CH_3OCH_3 + H\ zeolite$$

The formation of the first hydrocarbon product

Hutchings and Hunter [1990] have recently reviewed various experimental observations concerning the mechanism of the formation of the primary reaction products in the formation of hydrocarbons from methanol and dimethyl ether. These authors concluded that the mechanism of the first C-C bond formation over bifunctional acid-base catalysts involved a radical type reaction whereas that over the zeolite ZSM-5 involved the formation of a methyloxonium surface intermediate

species. This methyloxonium species may lead to the subsequent formation of an oxonium methylide species, an important intermediate in the formation of ethene.

Reacting methanol diluted with nitrogen over ZSM-5 at 300°C, Kaeding and Butter [1980] found the hydrocarbon selectivity to ethene to approach 100% at very low methanol conversions, indicating that ethene was the first hydrocarbon product formed. The following mechanism was proposed :

CH_3OCH_3 + H zeolite $\rightleftharpoons$ $CH_3\text{-}OH^+\text{-}CH_3$ + zeolite$^-$
$CH_3OH^+CH_3$ + $CH_3\text{-}O\text{-}CH_3$ + zeolite$^-$ $\longrightarrow$ CH_3OH + $CH_3CH_2\text{-}O\text{-}CH_3$ + H zeolite
$CH_3CH_2\text{-}O\text{-}CH_3$ + H zeolite $\rightleftharpoons$ $CH_3CH_2\text{-}OH^+\text{-}CH_3$ + zeolite$^-$
H--$CH_2CH_2\text{-}OH^+\text{-}CH_3$ + zeolite$^-$ $\longrightarrow$ $CH_2{=}CH_2$ + CH_3OH + H zeolite

Methyl ethylether, the intermediate in this reaction, was detected in the reaction products.

Radiotracer studies carried out by Mole and Whiteside [1982] provide support for an oxonium-ylide mechanism for the initial formation of ethene. Due to the relatively low reactivity of ethene under methanol conversion conditions it is unlikely that most of the methanol is converted to higher hydrocarbons via ethene. Mole [1983] suggested that most of the ethene is formed directly from methanol (via oxonium-ylide) if large amounts of olefins of three or more carbon atoms are not present. The proposed oxonium-ylide mechanism is as follows:

$2\,CH_3OH \rightleftharpoons CH_3OCH_3 + H_2O$	(dehydration)
$CH_3OCH_3 + R^+ \rightleftharpoons CH_3\text{-}O^+(R)\text{-}CH_3$	(O protonation/alkylation)
$CH_3\text{-}O^+(R)\text{-}CH_3 + B \longrightarrow BH^+ + CH_3\text{-}O^+(R)\text{-}CH_2^-$	(oxonium-ylide formation)
$CH_3\text{-}O^+(R)\text{-}CH_2^- \longrightarrow CH_3CH_2\text{-}OR$	(Stevens rearrangement)

(B: base; R: H or alkyl group)

Dehydration after the Stevens type rearrangement will give ethene. If the rearrangement takes place as follows:

$CH_3\text{-}O^+(R)\text{-}CH_2^- \longrightarrow CH_3\text{-}O\text{-}CH_2R$ (R: alkyl group)

then dehydration will produce a higher olefin of three or more carbon atoms. This mechanism explains why the formation of ethene is often accompanied by the presence of higher olefins [Mole and Whiteside, 1982].

Due to the low reactivity of ethene in comparison to propene and methanol, Dejaifve et al. [1980] suggested that ethene protonated by Brønsted acid sites, forms a carbenium type surface species which may either desorb as ethene or react further with methanol, dimethyl ether or ethene. Earlier work performed by these authors indicated that the reaction of the surface species is faster than the desorption of gaseous ethene. It was also found that the surface species desorbs faster than the gaseous ethene chemisorbs.

Dessau [1986] showed that the ethene/propene ratio increased as the methanol contact time was increased (reaction at a low partial pressure of methanol in nitrogen) suggesting that ethene is formed directly from methanol only in the initiation phase of the reaction, the bulk of the ethene being formed from secondary equilibration of higher olefins.

From electron spin resonance studies, Clarke et al. [1986] detected the presence of free radicals when investigating the reaction of DME over ZSM-5. The free radicals were detected in the temperature range 171-360°C at 101 kPa and only in the presence of the catalyst. Fewer free radicals were detected in the presence of aged catalyst even though the coked material contained a high concentration of free electrons. The mechanism proposed by Clarke et al. is as follows:

$S + CH_3OCH_3 \longrightarrow S\text{-}H + .CH_2\text{-}O\text{-}CH_3$

$2\ .CH_2\text{-}O\text{-}CH_3 \longrightarrow CH_3\text{-}O\text{-}[CH_2]_2\text{-}O\text{-}CH_3$ and $S\text{-}H \longrightarrow .S + .H$

or

$.CH_2\text{-}O\text{-}CH_3 \longrightarrow :CH_2 + .O\text{-}CH_3$

$:CH_2 + CH_3\text{-}O\text{-}CH_3 \longrightarrow CH_3CH_2\text{-}O\text{-}CH_3$

(.S : a surface radical)

These results suggest that the first C-C bond is formed by the direct coupling of the initial free radicals or alternatively, that methene is generated with subsequent insertion into a C-H bond.

Studies done by Hunter et al. [1987] provide some evidence against the involvement of free radicals in the formation of the first C-C bond. NO, a well known radical scavenger at temperatures up to 600°C, was found to have little effect on the conversion of DME to hydrocarbons. Chang et al. [1989] however, found that the addition of 450 ppm of NO to the methanol feed inhibited hydrocarbon formation completely although the formation of DME was unaffected. Using different concentrations of NO it was shown that Brønsted acid site poisons were being generated. These results were duplicated when NH_3 was used in the place of NO. As a result of these findings, Chang et al. claimed that the role of free radicals in the initiation phase of the reaction remained uncertain although the free radical mechanism remained an attractive option.

The formation of higher olefins

A number of mechanisms have been proposed for the formation of higher olefins from methanol or dimethyl ether. Dejaifve et al. [1980] suggested that propene and butene are formed via a C_2 surface species and that a similar mechanism may hold for the formation of higher olefins. Kaeding and Butter [1980] proposed a combination of lower olefin alkylation by methanol or dimethyl ether, oligomerization and cracking. It has also been found that the MTO reaction has an autocatalytic nature, the rate of reaction being enhanced by the presence of olefins [Ono and Mori, 1979, 1981]. Chen and Reagan [1979] found that the rate of olefin formation via an autocatalytic route was 50 times greater than the initial rate of ethene formation from methanol and dimethyl ether.

To simulate the early stages of reaction, Kaeding and Butter [1980] co-fed equimolar amounts of ethene and methanol over ZSM-5 at 350°C and found propene to be the major hydrocarbon product. Kaeding and Butter proposed that the initial propene is formed by the alkylation of ethene with methanol or dimethyl ether. When propene and methanol were co-fed, the major hydrocarbon reaction product was found to be butene. Higher olefins may also be produced by the same mechanism.

$ROCH_3$ + H zeolite $\rightleftharpoons$ R-OH^+-CH_3 + zeolite$^-$ (R : H or CH_3)

R-OH^+-CH_3 + CH_2=CH_2 $\longrightarrow$ ROH + $CH_3CH_2CH_2^+$

$CH_3CH_2CH_2^+$ + H zeolite$^-$ $\longrightarrow$ CH_3CH=CH_2 + H zeolite

Mole and Whiteside [1982] proposed that the conversion of methanol to hydrocarbons and water consists largely of the electrophilic methylation of olefins of three or more carbon atoms. This is described as a homologation process. Repeated homologation followed by carbonium ion cracking will produce two olefin molecules which may also participate in the homologation process.

Whereas the homologation process described above may explain the formation of olefins of three or more carbon atoms, it cannot explain the formation of ethene (ethene is not formed in substantial amounts over ZSM-5 under normal methanol conversion conditions). ^{13}C labeling experiments performed by Mole and Bett [1983] showed that some of the ethene product was comprised of carbon atoms from aromatics and alkyl aromatics. It was suggested that this aromatic process was an indirect route to the formation of ethene, the direct route being the oxonium-ylide mechanism.

Dessau [1987] suggested that it is unlikely that aromatics play a large role in the formation of ethene because ethene may be obtained under conditions where no aromatics are formed. It is also expected that the methylation of olefins is more rapid than the methylation of aromatics. Supporting this view, Dass et al. [1987] found that when passing methanol over ZSM-5 (370°C) the methylation of the methyl group of toluene to form ethylbenzene did not occur. In the light of these results, ethylbenzene cannot be regarded as an intermediate in the formation of ethene.

Studies performed by Chu and Chang [1984] at low methanol conversions showed ethene to be the initial hydrocarbon product formed. After an apparent induction period the yields of propene, butene and pentene increased while the yield of ethene decreased. It was proposed that an autocatalytic process involving mainly alkylation of olefins by C_1 intermediates becomes increasingly important once the initial olefins are formed. It was suggested that subsequent reaction steps include ß scission, oligomerization and aromatization.

Wu and Kaeding [1984] proposed at least two major reaction types for the production of higher olefins, the first reaction type being the alkylation of olefins with methanol and the second being a group of thermodynamic equilibrium reactions, the major reactions being dimerization, cracking and skeletal and double bond isomerization. Except for the production of ethene, Wu and Kaeding found

that the methanol conversion product distribution agreed well with that predicted by the Flory equations. This suggested the dominance of the alkylation reaction for the production of higher oligomers. Infrared results of Sayed [1987] showed that the alkylation reaction was favoured over the oligomerization reaction. In agreement with these results, Dessau [1986, 1987] suggested that as soon as sufficient olefins exist, methylation of these olefins account for the bulk of the methanol conversion. As a result, most of the olefins produced (including ethene) are produced during the dominant autocatalytic phase of the reaction by alkylation, oligomerization and cracking of higher olefins.

Along with the alkylation reaction, oligomerization of the lower olefins also contributes to the formation of higher olefins. Kaeding and Butter [1980] found that feeding ethene diluted with nitrogen produced a hydrocarbon product consisting of mostly C_2 dimer.

Oligomerization:-

$$CH_2{=}CH_2 + H\ zeolite \rightleftharpoons CH_3{}^+CH_2 + zeolite^-$$
$$CH_3{}^+CH_2 + CH_2{=}CH_2 \rightleftharpoons CH_3CH_2CH_2CH_2{}^+ \longrightarrow CH_3CH_2CH^+CH_3$$
$$C_4H_9{}^+ + C_2H_4 \rightleftharpoons C_6H_{13}{}^+ \rightleftharpoons \text{etc.}$$

Cracking:-

$$C_6H_{13}{}^+ + zeolite^- \rightleftharpoons 2\,C_3H_6 + H\ zeolite$$

Aromatic formation and hydrogen transfer

Under more severe reaction conditions, the yields of aromatics and paraffins are increased. Dejaifve et al. [1980] described the initial step in the formation of aromatics as a concerted cycloaddition of an olefin and a carbenium ion which is favoured by the unique structural properties of the zeolite. It was suggested that aromatics are essentially obtained by the reaction of the lower olefins formed with high yield in the early stages of the reaction.

1.2.2 The effect of reaction conditions

There are many parameters that affect the conversion of methanol over zeolite and molecular sieve catalysts. Product distributions and conversion levels are influenced by reaction temperature, reactant space velocity and reactant partial pressure.

Reaction temperature

The rate of reaction and the product distribution are strongly affected by temperature. The temperatures usually used in the conversion of methanol to olefins range between 350°C and 550°C.

Sunavala and Sunavala [1988] studied the thermodynamics of hydrocarbon synthesis from methanol. A relatively simple system was considered, consisting of 8 paraffins, 2 olefins and 5 aromatics. Equilibrium compositions and hydrocarbon distributions of the products at 327°C, 427°C and 627°C and pressures in the range 101 kPa to 5050 kPa were calculated. Results showed that, on raising the reaction temperature, the olefin fraction increased and the aromatic fraction decreased. When the reaction pressure was raised, the olefin fraction decreased while little change was seen in the aromatic fraction.

Using a simple model for a consecutive reaction (the starting material being oxygenates, viz. methanol and DME, the intermediates being olefins and the final products being aromatics and paraffins), Chang et al. [1984] showed that the formation of olefin "intermediates" was more strongly affected by temperature than the formation of aromatic "final products". This selectivity enhancement is said to be due to the decoupling of olefin formation from aromatization brought about by differences in the activation energy and acid dependency of the two reactions.

Kaeding and Butter [1980] varied the methanol conversion temperature from 400°C to 500°C and found only a slight change in the C_2-C_4 olefin/paraffin ratio but the amount of aromatics formed was increased from 15% to 25% (methanol conversion 100%, WHSV 1 hr^{-1}). Wu and Kaeding [1984], on the other hand, found that increasing the reaction temperature from 327°C to 389°C increased the methanol conversion from 0.03% to 31% and reduced the hydrocarbon selectivity

to ethene from 50% to 7% (Si/Al ratio 800, WHSV 1.8 hr^{-1}, feed 57% methanol in water). The C_2-C_4 olefin selectivity was reduced from 74% to 58% but it was noticed that the propene selectivity remained almost constant over the temperature range investigated.

Investigating the effect of reaction temperature over SAPO-34, Marchi and Froment [1991] found that increased reaction temperatures resulted in significant increases in catalyst lifetime. Other temperature-lifetime trends have also been reported. Langner [1982] found that the coking rate for the methanol conversion reaction over ZSM-5 was a minimum at 450°C (reduced diffusion at lower temperatures and increased coking rate at higher temperatures) and Schulz et al. [1987] found that increasing the reaction temperature from 375°C to 475°C resulted in a reduction in catalyst utilization and lifetime.

In European Patent 418 142, detailing the selective formation of ethene over NiAPSO-34, Inui [1990] showed that the ethene selectivity over NiAPSO-34 increased with reaction temperature, but only up to 450°C, after which the formation of CO and CO_2 was found to increase. Marchi and Froment [1991] found that increased reaction temperatures resulted in significant increases in light olefin selectivity over SAPO-34. Similar results were reported by Liang et al. [1990] who also showed that the selectivity towards ethene improved significantly (at the expense of the propene and butene selectivities) as the reaction temperature was increased.

In summary, increasing the reaction temperature generally results in increased methanol conversion levels and light olefin selectivities. The effect of reaction temperature on catalyst lifetime varies and seems to depend on the nature of the catalyst and the effect of temperature on hydrocarbon diffusion and coking rates.

Total pressure, methanol partial pressure and diluent

Investigating the effect of total pressure, Chang et al. [1984] found that, despite equivalent contact times, increasing the pressure decreased the total conversion as well as the C_2-C_5 olefin selectivity. In another series of experiments, Chang et al. changed the methanol partial pressure by co-feeding water while keeping the total pressure constant at 303 kPa. It was found that decreasing the methanol

partial pressure from 101 kPa to 40 kPa increased the hydrocarbon selectivity to C_2-C_5 olefins from 65% to 77% at complete methanol conversion. These results extended those of Chang et al. [1979] who showed that olefin selectivity was greatly enhanced at subatmospheric methanol partial pressures.

Prinz and Riekert [1988] found that the addition of water to the methanol vapor phase increased the induction period (the initial stage of reaction where the conversion increases to its steady state value or plateau) for the reaction and reduced the conversion of methanol to hydrocarbons. The hydrocarbon selectivity to light olefins and the ethene/propene ratio in the reaction products was increased at low conversions when the feed was diluted with water. Using dimethyl ether (no water present) as feed eliminated the induction period for the reaction but did not affect the hydrocarbon product distribution. The induction period was also eliminated when small amounts of propene were added to the methanol feed to the reactor.

For methanol conversion over SAPO-34, Marchi and Froment [1991] found that a reduction in methanol partial pressure increased the catalyst lifetime as well as the C_2-C_4 olefin selectivity. The use of nitrogen for diluting the methanol instead of water was found to have no effect on the catalyst lifetime. Liang et al. [1990] also found a slight increase in light olefin selectivity when the methanol partial pressure was reduced (keeping the methanol space velocity constant), the ethene selectivity increasing at the expense of the other light olefins at the low methanol partial pressures.

From the various findings reported above, it can be seen that the reduction of either total pressure or methanol partial pressure results in increased light olefin selectivities. A reduction in methanol partial pressure results in an increase in the methanol conversion lifetime of SAPO-34 but the choice of methanol diluent has no effect on catalyst lifetime.

Space velocity

Dejaifve et al. [1980] carried out methanol conversion over ZSM-5 of different Si/Al ratios at different space velocities (370-380°C; crystal size 2.5-3.5 microns). Keeping the Si/Al ratio constant (Si/Al 79), it was found that changing the WHSV

from 0.7 hr^{-1} to 11 hr^{-1} changed the conversion to hydrocarbons from 60% to 4%, showing the strong effect of WHSV on conversion levels. The change in WHSV had little effect on the product distribution except for the formation of aromatics which decreased from 4.6% to 0.5% of the total hydrocarbons formed.

Chang et al. [1984] showed that in changing the Si/Al ratio from 35 to 835, the LHSV had to be reduced from 24 hr^{-1} to 0.5 hr^{-1} to obtain the same methanol conversion and hydrocarbon product distribution. Methanol conversion at 500°C over catalysts with Si/Al ratios of 35, 71 and 250 gave similar methanol conversion levels and hydrocarbon product distributions when the $WHSV_{Al}$ (feed rate of methanol per Al atom) was kept constant.

Similar findings were reported by Kanazirev et al. [1986] who investigated the effect of Si/Al ratio on methanol conversion at very low methanol partial pressures and showed that the conversion of methanol to dimethyl ether at a fixed temperature depended only on the $WHSV_{Al}$. Methanol conversion to hydrocarbons at a constant $WHSV_{Al}$ but different Si/Al ratios gave product distributions that were very similar at methanol conversion levels of 100%. These results were found for a range of space velocities showing the strong relationship between selectivity and activity and the aluminium content of the ZSM-5 catalyst.

Dessau [1986] fed methanol diluted in nitrogen (400°C, partial pressure of methanol 1 kPa, total pressure 101 kPa) over ZSM-5 at a range of different flowrates. The conversion of methanol in all the experiments was 100%. Increasing the flow from 5 cm^3/min.g to 4 700 cm^3/min.g decreased the amount of ethene produced from 21% to 1% and the ethene/propene ratio from 1.06 to 0.02. These results showed that low space velocities were needed to increase the hydrocarbon selectivity to ethene at a fixed Si/Al ratio. The selectivity of ethene and propene was a maximum at a feed flowrate of 155 cm^3/min.g.

From plots of product selectivity versus liquid hourly space velocity (LHSV) at 500°C and atmospheric pressure [Chang et al., 1984], it may be seen that the space velocity needed for maximum olefin selectivity for a specified ZSM-5 Si/Al ratio is just lower than that needed to give 100% conversion. It can also be seen that for a constant Si/Al ratio the olefin selectivity passed through a maximum as the LHSV was increased. The highest selectivity to C_2-C_5 olefins was obtained at 500°C, at a LHSV of 0.1 hr^{-1} over ZSM-5 with a Si/Al ratio of 250.

For methanol conversion over SAPO-34, Liang et al. [1990] found very little change in product selectivity for changes in WHSV ranging from 4 g/g/hr to 13 g/g/hr. Similar results were reported by Marchi and Froment [1991] who also found that changes in methanol space velocity had no effect on the amount of methanol converted before the catalyst was deactivated (i.e. the same amount of products would be formed by the time the catalyst has deactivated, irrespective of the rate at which the feed is passed over the catalyst).

From these various studies it can be seen that increased space velocities generally result in reduced methanol conversion levels. For ZSM-5, similar conversion levels and product selectivities may be obtained by keeping the (methanol/acid site) ratio constant. Although little change in light olefin selectivity with space velocity was reported for methanol conversion over SAPO-34, light olefin selectivity was found to be a strong function of space velocity for methanol conversion over ZSM-5.

1.2.3 The effect of catalyst acidity and morphology

Methanol conversion levels and product selectivities are also affected by the nature of the catalyst being used. Other than changes in catalyst pore structure (i.e. different catalyst types), modifications of catalyst acidity and morphology also produce changes in methanol conversion lifetimes and selectivities.

Catalyst acidity

Chang et al. [1984] compared the methanol conversion product distributions obtained over ZSM-5 of different Si/Al ratios (371°C) with those obtained over partially ion exchanged ZSM-5 with a constant Si/Al ratio of 70. The experimental results showed the hydrocarbon selectivity to be dependent on the "effective" Si/Al ratio (i.e. the proton concentration). From plotted data of hydrocarbon selectivity (371°C, 101 kPa, LHSV 1 hr^{-1}) it is seen that an effective maximum Si/Al ratio of about 250 was needed to give 100% methanol conversion. The hydrocarbon selectivity to C_2-C_4 olefins under these conditions was approximately 20%.

Wu and Kaeding [1984] compared the product distributions obtained by keeping the methanol space velocity constant and by varying the Si/Al ratios. Using a

WHSV of 4.0-4.3 hr^{-1} (450°C, 101 kPa) at which methanol conversions were all 100%, it was shown that increasing the Si/Al ratio (decreasing the amount of acidity) from 18 to 800 produced a uniform increase in the C_2-C_4 olefin selectivity from 10% to 59%. The selectivities of C_2-C_4 paraffins and aromatics were reduced from 40% to 3% and 29% to 4%, respectively.

Similarly, Marchi and Froment [1991] studied methanol conversion over SAPO-34 and found that catalysts with smaller amounts of acidity (lower Si/Al ratios) resulted in an increase in the initial olefin yield. There was, however, no difference in catalyst lifetime as a result of these differing Si/Al ratios. Regarding the effect of Si/Al ratio on the MTO induction period, Prinz and Riekert [1988] showed this was increased, and the reaction rate lowered when the Si/Al ratio was increased (crystal size and morphology kept constant).

Dealumination of mordenites (reduction in the amount of acidity) has been found to result in increased catalyst lifetimes for methanol conversion [Meyers et al., 1988]. Niwa et al. [1988] also found that dealuminated mordenites exhibited increased methanol conversion activity but reported that extensive dealumination resulted in only minimal additional activity. The light olefin selectivity was found to be reduced for the dealuminated mordenites exhibiting longer lifetimes.

Suzuki et al. [1987] investigated the effect of the water content of the synthesis mixture on the physiochemical properties and the performance of ZSM-5 type catalysts in the methanol conversion reaction. Reduction of the H_2O/Si ratio (80-8) of the synthesis gel resulted not only in the synthesis of smaller crystals (5 microns reduced to 0.2 microns) but also in an increase in the Si/Al ratio (a reduction in the amount of acidity) of the outer surface of the zeolite crystals.

Methanol conversion at 540°C (LHSV 2 hr^{-1}) showed that ZSM-5 samples prepared with low H_2O/Si ratios had greatly improved lifetimes (H_2O/Si ratio : 80-8; lifetime at above 97% conversion : 20-70 hours). Although this increase in lifetime was attributed to reduced coking (and hence reduced pore blockage) on the exterior surface of the crystallites, it is likely that the smaller crystallite size of this material may have been a contributing factor.

In a similar series of experiments [Suzuki et al., 1988], ZSM-5 crystallization times were varied, resulting in the synthesis of material with similar bulk Si/Al ratios,

relative crystallinities and crystallite sizes but with a different surface Si/Al ratios. Methanol conversion at 540°C (WHSV 1.98 hr^{-1}) showed catalysts with less surface acidity exhibited reduced coking rates and increased lifetimes (lifetime : 20-50 hours). In confirmation, dealumination of the external surface of a catalyst (using $SiCl_4$) with a relatively high amount of surface acidity resulted in an increase in catalyst lifetime (45-56 hours).

Catalyst morphology and particle size

Zeolites are a thermodynamically metastable phase, so different preparation techniques do not necessarily produce zeolites with the same physical, chemical and catalytic properties [Suzuki et al., 1988].

Sugimoto et al. [1987] investigated the correlation between the crystal size and catalytic properties of ZSM-5 for the conversion of methanol to gasoline. Lifetime studies (370°C, WHSV 2 hr^{-1}) showed that the conversion level of methanol to hydrocarbons remained at 100% for the small crystallite material (< 0.2 microns) for 90 hours but for the larger crystallites (aggregates of large primary particles) it dropped to 10% after only 50 hours. On the basis of the coke content and surface areas of the spent catalysts, it was suggested that ZSM-5 with a large external/internal surface area ratio (small crystals) is much less affected by coking than ZSM-5 with a smaller surface area ratio, a possible reason for this being that coking occurs mainly on the external surface of ZSM-5 [Bibby et al., 1986] (higher coke contents are needed to reduce accessibility to the crystallite interior of small crystals).

Similar results were reported by Herrmann et al. [1987] who investigated the effect of ZSM-5 crystal size on various reactions, including methanol conversion to olefins. The crystal sizes investigated ranged from 5 to 21 microns and the Si/Al ratios from 10 to 165. For methanol conversion to hydrocarbons at 340°C (606 kPa, WHSV 10 hr^{-1}), conversion over the catalysts decreased with increasing crystal size, leading to the conclusion that for the larger crystals, the volume of the zeolite was not properly utilized (probably due to diffusional resistance, i.e. the particle effectiveness factor decreases significantly in this size range).

1.3 OLEFIN OLIGOMERIZATION

As previously mentioned, the oligomerization of light olefins forming a higher olefin oligomer product is an attractive route to the formation of synthetic gasoline and distillate fuels. Manipulation of reaction conditions allows a high degree of flexibility with regard to the relative amounts of gasoline and distillate that is produced, this depending on product demand. Oligomerization of light olefins produces a high quality jet fuel and the oligomerization of heavier olefins produces good quality lube oils.

There are at present two commercially available processes for the production of gasoline and distillate fuels by olefin oligomerization over zeolite based catalysts. The Mobil Olefins to Gasoline and Distillate (MOGD) process uses the catalyst ZSM-5 and has been demonstrated on a semi-commercial scale (210 bbl/day) at the Mobil refinery in Paulsboro [Maxwell and Stork, 1991]. The more recently announced Shell Polygasoline Kero Process (SPGK) produces both gasoline and mid-range distillate and is based on a modified zeolite system [Maxwell and Stork, 1991].

1.3.1 Reaction mechanism

Polyolefin chain formation from *n* reacting molecules is classified as oligomerization when $2 < n < 100$ and as polymerization when $n > 100$. Oligomerization the presence of aluminosilicate gels and zeolites is classified as cationic oligomerization and is initiated on Brønsted acid sites after the adsorption of olefins on these sites [Skupinska, 1991]. When the light olefin is propene, the primary reaction product is 2-methylpentene :

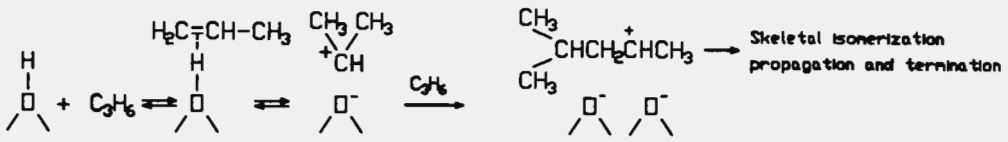

The strong acidity of zeolites results in the formation of numerous non-oligomer products from side reactions such as isomerization, cracking, aromatization and hydrogen transfer. The size of the oligomer products also depends on the stability of the intermediate carbocation and it has been shown that for ZSM-5, the trimer was the dominant reaction product, this being ascribed to the greater stability of the tertiary carbocation of the dimer than that of the secondary carbocation of the monomer. The more stable dimer, therefore, has an improved chance of further reaction.

Propene oligomerization over zeolite Y at between -60°C and 40°C has been found to take place through surface alkoxy derivatives which are formed in the reaction between protonated olefins and zeolite surface oxygen atoms. This reaction does not proceed with a carbocation as an intermediate species, and the primary reaction products are C_9 hydrocarbons :

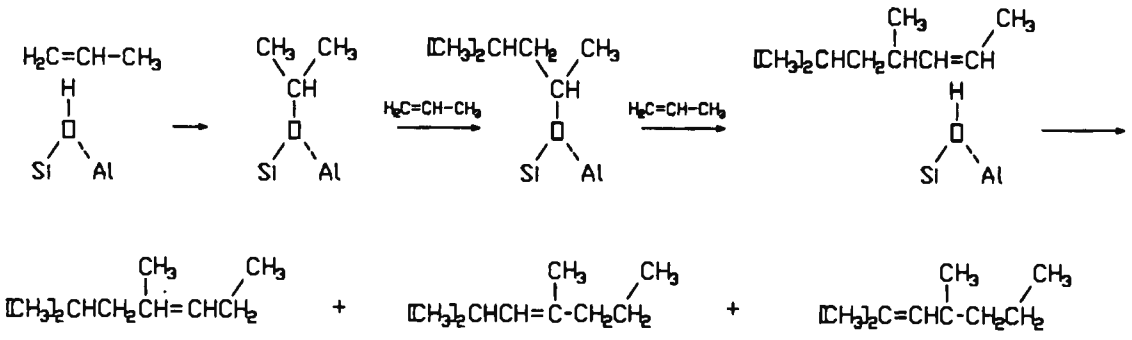

Oligomerization over non-zeolite catalysts

Oligomerization of olefins to higher olefins may be carried out over numerous homogeneous and heterogeneous non-zeolitic catalysts. These include inorganic oxides, cation exchange resins, clays, amorphous silica-alumina and phosphoric acid supported on kieselguhr (which is used in the CATPOLY process). Oligomerization mechanisms over some of the above catalysts and over several transition-metal complexes have been recently reviewed by Skupinska [1991].

1.3.2 The effect of reaction conditions

The reaction sequence, and hence the product distribution, of light olefins over zeolite catalysts is influenced by thermodynamic factors, kinetic considerations and shape-selective constraints [Quann et al, 1988]. The scarcity of thermodynamic and chemical data for higher molecular weight olefins has necessitated the use of group properties which are applied to carbon number isomer or oligomer groupings [Alberty, 1987], allowing the reaction to be modelled by allocating oligomerization and cracking rate constants to these various groups. Several models have been proposed which allow for product formation via non-oligomerization reactions such as isomerization, cracking and co-polymerization [Tabak et al., 1986].

Quann et al. [1988] reported equilibrium olefin distributions with carbon numbers ranging from C_2-C_{50} (Figure 1.4). These values were calculated based on restricted isomer group extrapolation and isomers of butene, pentene and hexene were assumed to be equilibrated. High temperatures and low pressures favour the formation of light olefins whereas low temperatures and high pressures favour higher molecular weight olefins.

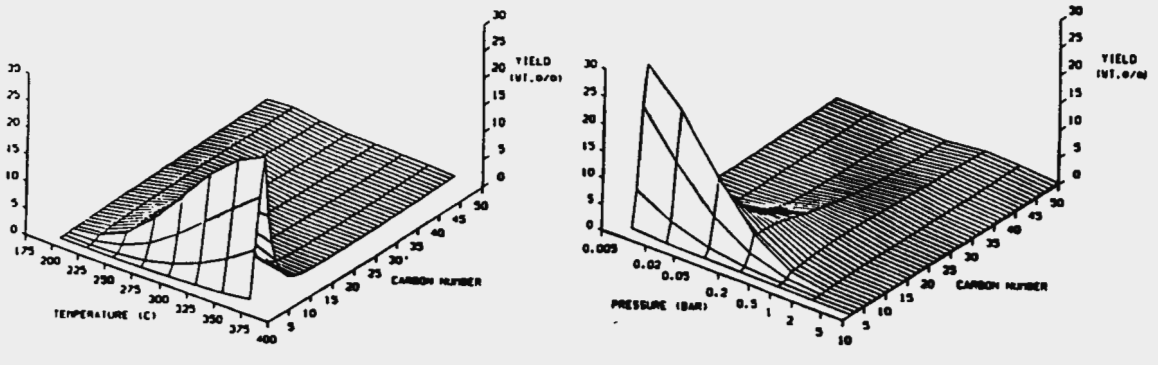

Figure 1.4 : The effect of temperature and pressure on olefin equilibrium distribution. (From Avidan, 1988)

The relative production of gasoline and distillate is controlled by the reaction temperature and pressure. Production of a predominantly gasoline product is undertaken at relatively high reaction temperatures (285-375°C) and low reaction pressures (404-3030 kPa), conditions which favour increased cracking and

reduced chain propagation. The production of a heavy distillate fraction, however, requires relatively low temperatures (190-310°C) and high pressures (4040-10100 kPa) which reduce the amount of cracking and encourage chain propagation. Typical MOGD product quality is shown in Table 1.1.

Specification	MOGD Product	Industry standards
Diesel fuel		
Specific gravity (15°C)	.79	.84-.88
Flash point (°C)	60	52 min
Pour point (°C)	<-50	-7 max
Cetane number	50	45 min
Sulfur (wt%)	<0.002	0.5 max
Viscosity at 40°C (cS)	2.5	1.9-4.1
Jet fuel (kerosene)		
Specific gravity (15°C)	.78	.78-.80
Freeze point (°C)	<-60	-40 max
Smoke point (mm)	28	18 min
Sulfur (wt%)	<0.002	0.3 max
Viscosity at 40°C (cS)	2.5	1.9-4.1
Composition (%)		
Paraffin	95	
Olefin	1	
Aromatic	4	
Gasoline		
Research octane number	92	
Motor octane number	79	
Specific gravity	0.73	
Composition (%)		
Paraffin	3	
Olefin	94	
Naphthene	1	
Aromatic	2	

Table 1.1 : Actual MOGD product quality and industry standards. (From Tabak and Yurchak, 1990)

1.3.3 The effect of acidity and morphology

Molecular sieves with relatively weak acid strength will have a reduced cracking activity producing a product with more clearly defined oligomer groupings and less non-oligomerization reaction products. Due to shape-selective constraints arising from the catalyst pore structure, the location of the acidity is also important. The

selective poisoning of the acid sites on the exterior of the ZSM-23 catalyst, ensuring that all reaction takes place within the zeolite, has been shown to result in the formation of a more linear oligomerization product [Skupinska, 1991].

Similar findings have been reported for oligomerization over ZSM-5 where the amount of exterior surface acidity is reduced by either synthesis modification or silanization. Reduction of exterior surface acidity of ZSM-5 results in reduced coking rates (ZSM-5 cokes mainly on the exterior surface of the crystallite) which, in turn, result in increased catalyst lifetimes [Suzuki et al., 1987]. Of the range of Si/Al ratios investigated for propene oligomerization over ZSM-5, Schwarz [1991] found that an intermediate Si/Al ratio of approximately 40 gave the longest catalyst lifetime (200-250°C, 5050 kPa, WHSV 12 hr^{-1}).

Variation of crystallite size also effects the accessibility of the acid sites. The average diffusion path required to reach acid sites in the interior of large crystals is longer than that in smaller crystals resulting in a reduction in the global reaction rate. The ratio of exterior surface area to acid sites is also less for larger crystals and hence the blocking of a certain area of crystallite surface (by coke formation) will result in the effective isolation of a greater number of acid sites than would be the case for smaller crystallites. The concept of depth of effective reaction surface was proposed by Schwarz [1991] for the significantly improved lifetimes of very small ZSM-5 crystals. It was proposed that oligomerization only takes place up to a certain depth from the exterior of the crystallite surface (diffusion limitations) and hence much of the pore volume of large crystals is unused.

As with the conversion of methanol to hydrocarbons, olefin oligomerization is affected by the molecular sieve pore structure. The extent of oligomer chain branching has been shown to depend on the molecular sieve pore diameter [Skupinska, 1991]. The relative degree of chain branching was shown to decrease in the order of decreasing channel diameter (i.e. omega > HY > mordenite > ZSM-5 > offretite > boralite), zeolite omega having the greatest pore diameter (10 Å) and thus allowing the highest degree of branching. The presence of large cages within the pore structure allows the formation of bulky hydrocarbons which may be trapped within these cages and thereby block pores and restrict access to acid sites. This situation is made worse for molecular sieves which have only 1-dimensional pore systems and the blockage of a pore mouth restricts access to all the acid sites within that pore.

1.4 CATALYST DEACTIVATION DUE TO COKE FORMATION

When hydrocarbon reactions are catalyzed over molecular sieves, carbonaceous materials (coke) gradually deposit on the catalyst surface. These deposits lead to a reduction in the catalyst activity and selectivity due to the poisoning of acid sites and changes in the macro and micro-porous structure of the catalyst [Eisenbach and Gallei, 1979]. Although combustion of this coke may restore the original activity and selectivity of the catalyst, production capacity is decreased and increasingly severe operating conditions are required to account for the coke [Froment, 1982].

Much effort has been made to limit coke formation and to obtain a better insight into the mechanisms of coking which are complex and depend on the chemistry of the process, catalyst properties and operating conditions [Guisnet and Magnoux, 1989]. Much work is still being done in quantifying the relative effects of these variables on catalyst deactivation and a number of techniques which are suitable for the investigation of coke formation on molecular sieves have been recently reviewed [Karge, 1991].

1.4.1 Deactivation mechanisms and resulting coke species

There are two major deactivation mechanisms resulting from coke formation: active site poisoning by irreversible coke adsorption and pore blockage (stops reactants from reaching uncoked active sites). Site poisoning and pore blockage may act separately or in combination, depending largely on the catalyst structure but also on the nature of the reactants used and the reaction conditions employed.

For methanol conversion over chabazite, McLaughlin and Anthony [1985] found the amount of intra-crystalline coke to be four orders of magnitude greater than that removed from the outer surface of the catalyst, leading to the conclusion that deactivation was due mainly to pore blockage. Intra-crystalline coke was composed of aromatics ranging from toluene and xylene through the homologous series of polyaromatics up to and including pyrene (a tetracyclic structure, the molecular size of which is in good agreement with the dimensions of the internal cavities of chabazite). The coke on the outer surface of the catalyst was found to

consist of a diversified mixture of polynuclear aromatics, their polyalkylated derivatives and high molecular weight hydrocarbons.

Bibby et al. [1986] studied methanol conversion over ZSM-5 and found that the volume of coke formed during the reactions exceeded the reduction in pore volume of the catalyst, indicating that coke is deposited on the external surface of the catalyst. These results were in agreement with those of Dejaifve et al. [1981] who, studying the same reaction over HZSM-5, HM and HY, showed that for ZSM-5 (and to a small extent for HM and HY), most of the coke is formed on the external surface of the catalyst. Schulz et al. [1991] also found that HZSM-5 deactivates through surface coverage and hence pore mouth blockage (475°C) but found that deactivation of HY proceeded via acid site poisoning followed by pore filling. Froment [1982] suggested that coke precursors formed in the channels of ZSM-5 have to migrate to the external surface of the catalyst before they can be transformed into coke, the pore size and structure of ZSM-5 not permitting the formation of these bulky coke molecules.

Reporting slightly different results, Magnoux et al. [1987] studying cracking of *n*-heptane over HZSM-5, HM and HY found that initial deactivation was due to acid site poisoning, and only at higher coke contents did the amount of inaccessible acid sites become greater than the number of coke molecules (indicating pore blockage). This mechanism of deactivation had some resemblance to that reported by Naccache et al. [1986] who studied the reaction of methanol with chlorobenzene and toluene over HZSM-5, HM and HY. The pore volumes of deactivated catalysts were found to be only two thirds of the pore volume of the fresh catalyst indicating that deactivation was due to acid site poisoning and not pore blockage.

Results of electron microscopy studies of external coke deposits on USHY, offretite and ZSM-5 after *n*-heptane cracking [Gallezot et al., 1988] were similar to those of Bibby et al. [1986] except that for USHY it was found that part of the coke was in the form of 1 nm thick carbon filaments protruding from the zeolite meso and micropores. These filaments were found to have a similar structure to that of the linear polyaromatic, pentacene, whereas the structure of the coke found on the external surface of HZSM-5 was found to be polyaromatic/graphitic. These results are similar to those of Shiring et al. [1983] who suggested that the coke either migrates from the pores to the catalyst surface or the coke itself provides active

sites for coke formation. The latter is possible since coke formation proceeds via the formation of carbonium ions and carbonium ions are able to interact with other hydrocarbon molecules to produce larger carbonium ions.

In summary, it seems that the mechanism of deactivation and the nature of the coke species is largely dependent on the structure of the catalyst but also, to a lesser extent, the nature of the reactants.

1.4.2 Factors affecting coke formation

Since coke formation on zeolite catalysts is a complex problem, there is still considerable debate in this field. A number of questions arise as to the effect of reactant nature, reaction conditions and catalyst characteristics on coke formation and catalyst deactivation [Karge et al., 1989].

Nature of reactant

Appleby et al. [1962] studied a number of reactions over silica-zirconia-alumina and found that with a catalytic cracking feedstock, aromatic components are a major source of coke. Coke formation also increased with increasing molecular weight and basicity of the aromatics. Olefins were found to lead to heavy coke deposition and coke production increased as the degree of unsaturation increased for a given aliphatic skeleton. Even in the reaction of low molecular weight materials such as C_4 olefins and dienes, polymerization and dehydrocyclyzation occur which lead to the formation of higher boiling aromatics and coke.

Walsh and Rollman [1977] found that reactant contribution to coking varied from one catalyst to another. Using a mixed feed of *n*-hexane and benzene it was found that aromatics were the major contributors to coke formation on zeolite Y but on mordenite, which has less acidity, aromatics and paraffins contributed almost equally to the formation of coke. Infrared studies of hexene and hexane over HY, CaY and Pt/CaY [Eisenbach and Gallei, 1979] showed that a paraffin gas phase resulted in a much lower coking rate than an olefinic gas phase.

Reaction conditions

For a given catalyst and reaction, the formation of coke is strongly affected by temperature. Studying methanol to hydrocarbons over NaHY, HL, HT and HZSM-5, Langner [1982] found increased coke deposition on large pore zeolites (NaHY, HL and HT) at higher reaction temperatures. These results are not in agreement with those of Walsh and Rollman [1977] and Naccache et al. [1986] who found that increased reaction temperatures resulted in reduced coke yields. Eisenbach and Gallei [1979] showed that although no equilibrium concentration of coke could be found for a given reaction temperature, the rate at which the maximum coke concentration is reached is a function of temperature.

Langner found that HZSM-5 showed the lowest tendency for coke formation, coke deposition increased at high and also low reaction temperatures, passing through a minimum at 450°C. The results at low reaction temperatures were explained by the low mobility of strongly adsorbed coke precursors which could lead to pore blockage. At higher temperatures (450°C), the mobility of these species increases, allowing for increased hydrogen transfer and hence the formation of monoaromatics which are easily desorbed from the catalyst surface.

Shiring et al. [1983] studying coking by C_6 and C_7 hydrocarbons on HY and REY found that the initial coking rate as well as the final coke content were greater with increased feed rates and ascribed this to reduced diffusional resistance. It was also found that, for the same feed rate, an increased sample weight resulted in less coke being deposited per gram of sample and that, by increasing the hydrocarbon concentration in the carrier gas, the initial specific coking rate was increased and the ultimate amount of coke deposited on the coke was decreased.

Catalyst acidity

The coking rate of zeolite catalysts is strongly affected by the catalyst acidity and thus the catalyst aluminium content. Infrared coking studies done by Eisenbach and Gallei [1979] over NaY (NaY has very few acid sites) showed no coke formation on the catalyst between 130°C and 330°C, indicating the importance of the OH groups in the formation of coke. The large influence of OH groups is

expected because they are adsorption sites as well as acidic sites which induce the elimination of hydrogen thus lead to coke formation.

Studying methanol conversion over ZSM-5, Bibby et al. [1986] found that the overall rate of coke formation increased with increasing aluminium content of the catalyst (keeping catalyst particle size and morphology constant). The initial rate of coke formation and the total amount of coke formed was not related to the aluminium content or the total amount of methanol converted. Gaseous hydrocarbons and dimethyl ether were still formed after liquid production stopped, indicating that coke first forms on the strongest acid sites and then on the progressively weaker sites.

Dejaifve et al. [1981] found that for the conversion of methanol to hydrocarbons, the coking rates per acid site in HZSM-5, HM and offretite were almost identical. Results of Naccache et al. [1986] for the reaction of methanol with chlorobenzene and toluene over HZSM-5, HM and HY also suggest that the coke formation is controlled by acid site density. It was proposed that bimolecular reactions such as oligomerization, cyclization and hydrogen transfer which lead to the formation of coke need high concentrations of acid sites which are lacking in silicon rich zeolites. These findings were in agreement with those of Walsh and Rollman [1977] who found that for the reaction of hexane and trimethylbenzene over HM, coke yields generally decreased with decreasing acidity.

Namba et al. [1986] found that selective dealumination of aluminium from the external surface of ZSM-5 crystallites reduces the aging rate of the catalyst for the cracking of cumene. In contradiction of these results and those of many other researchers, Ducarme and Vedrine [1985] found that for toluene alkylation with methanol, resistance to aging by coking is observed to increase linearly with the surface aluminium content and crystal size.

Catalyst pore structure

A major step in the formation of carbonaceous residues is the reaction and conversion of alkylaromatics eventually leading to the formation of polyaromatics and polyalkylaromatics which are coke precursors in many molecular sieves. These reactions may be prevented to a certain extent by the structural constraints

imposed by catalysts with smaller pores [Dejaifve et al., 1981]. For the conversion of methanol to hydrocarbons over ZSM-5, offretite and HY it was demonstrated that the coking and aging behavior of these zeolites were essentially determined by their structural properties. Initial coking activities were directly related to the availability of acid sites but consequent coking and aging rates depended on the pore size and the nature of the channel network.

Similar results were reported by Rollman and Walsh [1979] who showed a correlation between the coking tendency and the shape selectivity of zeolite catalysts of different structure, composition and crystal size. The amount of coke deposited on the catalyst (during *n*-hexane and 3-methylpentane cracking) per gram of paraffin converted was found to decrease with increasing catalyst shape selectivity, showing that the aging rate of the catalyst was an intrinsic property of its pore structure.

Xylene isomerisation studies over ZSM-5 and ZSM-11 by Ducarme and Vedrine [1985] showed that for very large crystals, coke plugging of the channel entrances was found to be a determining factor, resulting in high deactivation rates. Small crystals and dense aggregates of tiny particles formed by high pressure compression deactivated slowly (small pore volume limits the growth of coke precursors), leading to the conclusion that the intercrystalline pore volume plays a definite role in the deactivation of ZSM-5 and ZSM-11.

1.5 $AlPO_4$ BASED MOLECULAR SIEVES AND ZEOLITES

Aluminophosphate ($AlPO_4$) based molecular sieves and zeolites are both porous solids which have pore diameters which are similar to molecular dimensions. These two materials are similar in that they are both composed of crystalline frameworks which consist of tetrahedrally coordinated "T" atoms (Si, Al, P, Ga, Be etc.) which are linked to one another via oxygen atoms. Other microporous materials which exhibit molecular sieving abilities include coal, oxides, glasses, carbon and alkali graphite intercalation compounds [Rabo, 1979].

The history of $AlPO_4$ based molecular sieves dates back to the early 1980's. $AlPO_4$ based molecular sieves, unlike zeolites, do not occur naturally and the first successful syntheses of this new family of molecular sieves were only reported in 1982 [Wilson et al., 1982]. Since then, a variety of different of $AlPO_4$ based molecular sieve structures have been synthesized, representing the formation of structures with more than 200 different chemical compositions. These molecular sieves have received much interest with regard to their use as adsorbents and shape selective catalysts which are thermally stable to very high temperatures. This field is still relatively new and the discovery of many other $AlPO_4$ based structures with a wide spectrum of compositions may be expected, leading to a variety of different applications.

Unlike that of $AlPO_4$ based molecular sieves, the history of zeolites began in 1756 when the Swedish mineralogist Cronstedt discovered the first zeolite mineral, stilbite. The first successful investigations into zeolite synthesis were started in the mid to late 1930's. Until the 1950's, zeolites were thought to occur only as minor constituents in cavities in basaltic or volcanic rock. In the late 1950's and early 1960's, major geologic discoveries revealed a widespread occurrence of a number of natural zeolites, in quantities large enough to allow their commercial use. Zeolites were initially used in separation and purification processes and were first used in 1962 as cracking catalysts. Today, zeolites are also used as catalysts in the production of many fine chemicals and as fillers in paper, pozzolanic cements and concrete, in fertilizer and soil conditioners and as dietary supplements in animal husbandry [Flanigen, 1991].

1.5.1 The structure of $AlPO_4$ based molecular sieves and zeolites

The concepts of primary and secondary building units may be used to describe different framework topologies. Primary building units consist of small cations (eg. P^{5+}, Si^{4+}, Al^{3+}, Ga^{2+} etc.) in tetrahedral coordination with four oxygen atoms (Figure 1.5).

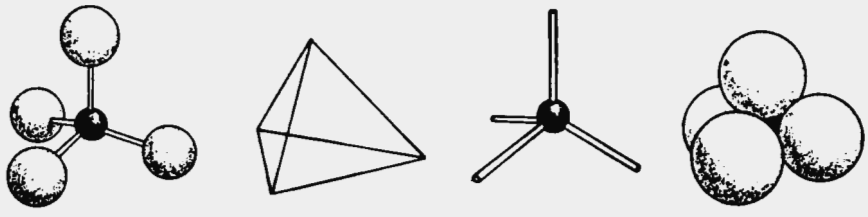

Figure 1.5 : Methods of representing primary building units; TO_4 tetrahedra. (From Breck, 1984)

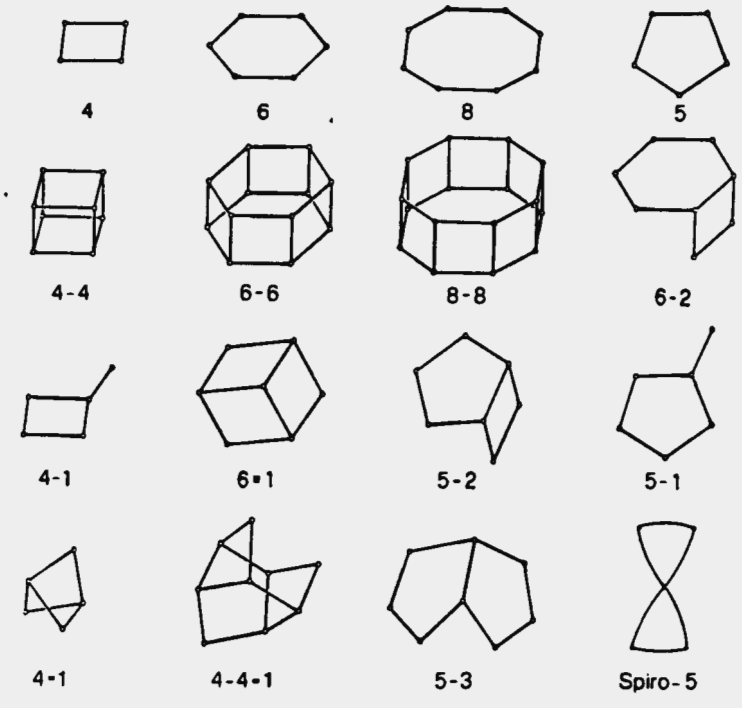

Figure 1.6 : Secondary building units. The small circles represent the tetrahedrally coordinated cations and the linking oxygens are shown as straight lines. (From van Koningsveld, 1991)

Secondary building units (SBUs), composed of small groupings of linked TO_4 tetrahedra (primary building units), were invented [Meier, 1968]; to aid the visualization of framework construction on the assumption that a particular framework may be built from one SBU only, although some frameworks do need two SBUs to describe their structure [van Koningsveld, 1991]. The two simplest SBUs are the 4-ring and the 6-ring (Figure 1.6). Methods involving structural subunits (SSUs), which are of greater complexity than the SBUs, have also been developed to describe various framework topologies. SAPO-34 is composed of 6-6 SBUs arranged in layers in the sequence ABCABC which are connected by tilted 4-rings. The framework of mordenite may be made up of 5-1 SBUs only (Table 1.2).

Zeolite	SBU	Zeolite	SBU
A	4-4	Analcime	4
Bikitaite	5-1	Brewsterite	4
Chabazite	4, 6-6	Dachiardite	5-1
Edingtonite	4-1	Epistilbite	5-1
Erionite	6, 6-6	Faujustite	6-6
Ferrierite	5-1	Gismondine	4
Gmelinite	6-6	Heulandite	4-4=1
Sodalite	6	L	4, 6-6
Levynite	6, 6-6	Mordenite	5-1
Offretite	6, 6-6	Stilbite	4-4=1
X	6-6	Y	6-6

Table 1.2 : Selected zeolites and their secondary building units (SBUs). (From Breck, 1984)

1.5.2 Shape selectivity effects in molecular sieves and zeolites

Molecular sieving by dehydrated zeolite crystals is caused by the size and/or shape differences between the pore apertures and the molecules concerned [Breck, 1984]. Shape selectivity may be divided into various categories; reactant selectivity, product selectivity, restricted transition state selectivity and even parameters such as diffusion and coulombic field effects may give rise to differences in selectivity.

Reactant selectivity occurs when only selected reactants (usually specified by molecular size or linearity) are allowed access to the active sites within the zeolite

pores. Selective hydrocracking of *n*-paraffins (selectoforming) in jet fuel, kerosene or heating oil improves their characteristics with respect to pour point, freezing point and viscosity. A constraint index (CI) calculated from the ratio in the logarithms of the cracking rate constants of *n*-hexane and 3-methyl pentane over a particular zeolite gives a relative indication of reactant selectivity.

Product selectivity arises in situations where molecules have access to the zeolite pore volume and acid sites, but certain reaction products are stericly restricted from leaving the pore volume. This type of selectivity is seen for methanol conversion over small pore zeolites where the reaction products are linear or short chain hydrocarbons. Restricted transition state selectivity may often be useful (reduction in coking) where the steric restrictions of certain pore systems are such that bulky transition states, necessary in particular reactions, are prevented, thus inhibiting those reactions.

Differences in the diffusivity of reactants or products also gives rise to differences in selectivity. Molecules which have a higher diffusivity will have shorter residence times within the pore structure than molecules with lower diffusivities which may be equilibrated to different molecules or may even react further producing larger species which could become trapped within the pore volume.

Selectivity arising from coulombic field effects are encountered in situations where coulombic field interactions between zeolites and sorbed molecules are functions of aluminium content. For example, the aluminium content of a zeolite may be reduced thereby making the material hydrophobic but leaving the hydrocarbon sorption capacity unaffected.

Recently Santilli and Zones [1990] reported what they refer to as secondary shape selectivity, where the catalytic selectivity of a molecular sieve may be effected by one of the reactants. An example of this phenomena was reported for the cracking of *n*-hexane and *n*-hexadecane over the zeolite SSZ-16. These two hydrocarbons were found to be converted to a similar extent when reacted separately but when reacted simultaneously, the conversion of *n*-hexadecane was almost completely retarded whereas that of *n*-hexane was relatively unchanged.

1.5.3 Post-synthesis modifications of molecular sieves and zeolites

There are numerous ways in which $AlPO_4$ based molecular sieves and zeolites may be modified, most of these modifications falling into two basic groups; modifications to the catalyst acidity and modifications to the catalyst morphology. A review of the effect of various modifications of zeolites and molecular sieves on the catalytic properties of these materials has recently been published [Szostak, 1991]. Modifications which were used in this work include; acid treatment, caustic treatment, hydrothermal treatment, silanization, boron impregnation and acid site poisoning.

Acid treatment

Mineral acids are used for dealumination of various zeolites which have a good resistance to acid attack. The framework structure of these materials remain intact when aluminium is extracted. Zeolites with high aluminium contents (eg. zeolite Y) and $AlPO_4$ based molecular sieves have very little resistance to attack by mineral acids which destroy their framework structures. Acid treatment is often used in the dealumination of mordenite, and these treatments and their effects on the mordenite acidity, activity and morphology are covered in more detail in 1.7.3.2 and 1.7.3.3.

Caustic treatment

It has been suggested [Kokatailo, 1989] that caustic treatment of zeolites may remove intercrystalline and intracrystalline amorphous species while leaving the zeolite crystal structure intact. This being the case, material which has received a caustic treatment should have a higher active zeolite content.

Hydrothermal treatment

Hydrothermal treatment or "steaming" of zeolites results in the extraction of aluminium from the framework but, unlike acid treatment, these newly formed extra-framework aluminium species are not removed from the zeolite pores. The

hydrothermal treatment conditions facilitate aluminium and silicon migration which may result in the framework vacancies being filled by silicon atoms and the migration of aluminium atoms towards the crystallite exterior surface.

Whereas severe hydrothermal treatment (above 300 mm Hg water partial pressure, 540°C) of ZSM-5 has been found to result in decreased ZSM-5 hexane cracking activity, mild steaming (below 300 mm Hg water partial pressure, 540°C) has resulted in as much as a four-fold increase in hexane cracking activity [Lago et al., 1986]. Hydrothermal treatment of ZSM-5 has also been shown to result in significant increases in hexene oligomerization activity [Andersen, 1991]. These increases in activity have been ascribed to the formation of "super acid sites" involving the aluminium extracted during hydrothermal treatment. Although several proposals have been put forward, there is still debate as to the exact nature of these super acid sites [Brunner et al., 1989; Zholobenko et al, 1990; Dessau et al., 1986];.

Deep bed calcination conditions allow a very mild form of hydrothermal treatment of the catalyst as the temperature is ramped to the final calcination temperature. The hydrothermal treatment is brought about by the dehydration of the zeolite, water being desorbed at between 130°C and 250°C. The hydrothermal treatment experienced by the catalyst is more severe for the catalyst at the exit to the bed than at the inlet, this effect being enhanced when the depth of the catalyst bed is increased.

Silanization

Treatment of zeolites with $SiCl_4$ vapor may result in the replacement of aluminium framework atoms by silicon [Beyer and Belenykaja, 1980], thereby resulting in a reduction in the number of acid sites. Silicon alkoxide vapor deposition, using a bulky silane species such as tetramethoxysilane and tetraethoxysilane, which cannot access the zeolite pores [Hidalgo et al., 1984], results in a coating of the external surface of the crystallite with layers of silica [Niwa et al., 1986] resulting in a partial or complete elimination of exterior surface acidity.

Silanization may also result in a reduction in accessibility to the pore volume of zeolites by vapor deposition at the pore mouth openings on the exterior surface of

the crystallite [Holderich and van Bekkum, 1991]. The narrowed pore mouth openings may result in considerable changes in the adsorption properties of zeolites as has been reported for mordenite which was treated with diborane and silane [Thijs et al., 1986]. These narrowed pore mouth openings may also result in increases in product shape selectivity [Hibino et al., 1991; Niwa et al., 1984; Sato et al., 1987].

Silanization of $AlPO_4$ based molecular sieves might result in an increase in catalyst acidity (at the interface between the crystallite and the silica coating) as acidity in these materials is due to the presence of silicon, not aluminium, as is the case with zeolites. There has, however, been little data presented in the literature concerning the silanization of $AlPO_4$ based molecular sieves and it is not even certain that silicon can be added onto the exterior surface of these materials by silanization.

Boron impregnation

It was suggested by Barrer [1982] that replacement of aluminum by boron should be possible and this was later proven using ^{11}B NMR and XRD [Coudurier and Vedrine, 1986;; Wendlandt et al., 1988;; Meyers et al., 1985; and Tarramasso et al., 1980]. Boron incorporation into the ZSM-5 framework results in a shrinkage in unit cell dimensions which increases the zeolite shape selectivity [Sayed et al., 1989]. Although incorporation of boron into the framework structure results in a loss of acidity and hence a loss in catalyst activity, deposition of boron within the catalyst pore structure may result in changes in shape selectivity. In this study, SAPO-34 was impregnated with boron to restrict the volume available for coke formation in the chabazite cages.

Acid site poisoning

The adsorption of basic molecules onto acid sites, renders these sites inactive. If the temperature of the catalyst is increased, the basic molecules will start desorbing from the weak acid sites and in this way, the strong acid sites, which facilitate hydrogen transfer and thus coke formation, may be selectively poisoned. The exterior of the crystallites may be selectively poisoned by using bulky basic molecules which will not have access to the pore structure.

1.6 $AlPO_4$ BASED MOLECULAR SIEVES

Towards the end of the 1970's, the Union Carbide Laboratories set about the development of a new generation of aluminophosphate ($AlPO_4$) based molecular sieves [Flanigen et al., 1986]. These $AlPO_4$ molecular sieves, first reported by Wilson et al. [1982], consisted of tetrahedrally coordinated aluminium and phosphorus (T atoms) linked via oxygen atoms into a crystalline framework structure. The addition of silicon to the aluminium and phosphorus framework resulted in the synthesis of the first silicoaluminophosphate (SAPO) molecular sieves [Lok et al., 1984]. Incorporation of metal cations into the $AlPO_4$ or SAPO framework results in the formation of MeAPO and MeAPSO structures, respectively [Messina et al., 1985; Wilson and Flanigen, 1986].

1.6.1 The structure and acidity of $AlPO_4$ based molecular sieves

$AlPO_4$ materials exhibit invariant chemical composition of alternating Al and P tetrahedra (P/Al ratio = 1). Theoretically, this results in an electrically neutral framework structure which would have no ion exchange capacity. The addition of silicon into the $AlPO_4$ framework results mainly in the substitution of silicon for phosphorus (SAPO). This leads to the formation of a framework with a net negative charge on the AlO_4 unit adjacent to the P deficient TO_4 site [Rabo, 1988]. As a result, the net negative charge may be balanced by an exchangeable cation, giving the SAPO materials an ion exchange capacity. When the exchangeable cation is H^+, the SAPO materials display a hydrophylic character and a wide spectrum of carboniogenic catalytic activity [Rabo, 1988] (due to the Brønsted acidity of the hydroxyl structure).

MeAPO and MeAPSO molecular sieves contain metals which include the divalent forms of Co, Fe, Mg, Mn and Zn and trivalent Fe. Metal substitution appears to take place exclusively for Al, again resulting in the formation of a framework with a net negative charge. The incorporation of the additional elements Li, Be, B, Ga, Ge, As and Ti, leads to the formation of the so-called ElAPO and ElAPSO framework compositions. As with the SAPO materials, MeAPO and MeAPSO molecular sieves exhibit an ion exchange capacity and the potential for the formation of Brønsted acid sites (exchangeable cation being H^+) [Flanigen et al., 1986].

The major structures of the $AlPO_4$ and SAPO based molecular sieves are identified by an integer (eg. $AlPO_4$-5, SAPO-5) which is arbitrarily chosen to denote a particular structure type [Rabo, 1988]. There are more than 24 known 3-dimensional structure types of which at least 14 are microporous and 6 are 2-dimensional layer type materials. The pore sizes of the various microporous

Species	Structure Type	Pore Diameter (Å)	H_2O Pore Volume (cc/g)
Very large pore			
VPI-5	Novel, detm.	12.5	0.35
Large pore			
5	Novel, detm.	8.0	0.31
36	Novel	8.0	0.31
37	Faujustite	8.0	0.35
40	Novel	7.0	0.33
46	Novel, detm.	7.0	0.28
Intermediate pore			
11	Novel, detm.	6.0	0.16
31	Novel	6.5	0.17
41	Novel	6.0	0.22
Small pore			
14	Novel, detm.	4.0	0.19
17	Erionite	4.3	0.28
18	Novel	4.3	0.35
26	Novel	4.3	0.23
33	Novel	4.0	0.23
34	Chabazite	4.3	0.30
35	Levynite	4.3	0.30
39	Novel	4.0	0.23
42	Linde type A	4.3	0.30
43	Gismondine	4.3	0.30
44	Chabazite-like	4.3	0.34
47	Chabazite-like	4.3	0.30
Very small pore			
16	Novel	3.0	0.30
20	Sodalite	3.0	0.24
25	Novel	3.0	0.17
28	Novel	3.0	0.21

Table 1.3 : Selected structures of $AlPO_4$ based molecular sieves. (From Flanigen, 1991)

materials range from very small (6-rings : diameter 3 Å) to the recently discovered very large pore VPI-5 (18-rings : diameter 12.5 Å) [Davis et al., 1988] and selected structure types and their pore sizes and volumes are listed in Table 1.3. Although several structure types have topologies similar to those of various zeolite crystals (Table 1.3), at least 15 novel crystal structures have been reported [Rabo, 1988].

$AlPO_4$ based molecular sieves are synthesized by hydrothermal crystallization from aluminophosphate gels containing all the framework elements and a structure directing organic template which fills the pore structure [Flanigen et al., 1986]. These molecular sieves are generally synthesized in the range 100-250°C under autogenous pressure for synthesis times ranging from 2 hours to several days. Structural control is influenced by the type and concentration of the template, reactant gel composition and gel pH [Flanigen et al., 1988].

1.6.2 The catalytic activity of $AlPO_4$ based molecular sieves

Using *n*-butane cracking as a test for Brønsted acidity, Rastelli et al. [1982] reported pseudo first order rate constants for a number of $AlPO_4$ based molecular sieves (Table 1.4). These results indicated that the catalytic performance of various MeAPO and MeAPSO materials was affected by both the metal and the structure type.

Very high yields of light olefins have been reported for the conversion of methanol to olefins over SAPO-34 [Kaiser, 1985; Marchi and Froment, 1991; Liang et al., 1989]. The high yields of C_2-C_4 olefins were attributed to the small pore structure (pore diameter : 4.3 Å) and weak acidity (in comparison to that of zeolites) of the SAPO-34 catalyst. Inui [1991] reported ethene selectivities of above 90% at total methanol conversion over NiAPSO-34 and suggested that this exceptional selectivity was due to the control of the amount and/or strength of the catalyst acidity.

Pellet et al. [1986] investigated the catalytic activity of several SAPO materials for propene oligomerization (Table 1.5) and found only the medium pore materials to be active. The small pore diameter of SAPO-34 prevented the formation of

Species	k_A (cc/g)	Species	k_A (cc/g)
$AlPO_4$-5	0.05	BeAPO-5	3.4
CoAPO-5	0.4	MAPO-5	0.5
MnAPO-5	1.2	SAPO-5	0.2-16.0
MAPSO-5	2.6	ZAPSO-5	1.5
$AlPO_4$-11	<0.05	SAPO-11	0.5-3.5
MAPO-36	11.0-24.0	CoAPO-36	11.0
MnAPO-36	6.8	MAPSO-36	18.0
BeAPO-34	3.7	CoAPO-34	5.0-15.0
FAPO-34	0.1-0.6	MAPO-34	7.0-29.0
MnAPO-34	2.5-5.2	ZAPO-34	13.0
SAPO-34	0.1-7.6	BeAPSO-34	7.6
GAPSO-34	10.0		
MAPO-39	0.05		
Chabazite	7.0	NH_4Y	2.0

Table 1.4 : Pseudo first order rate constants for *n*-butane cracking over $AlPO_4$ based molecular sieves. (From Flanigen, 1986)

Molecular sieve	SAPO-5	SAPO-11	SAPO-31	SAPO-34	LZ-105
Temperature (°C)	700	700	700	700	703
Pressure (psig)	25	25	50	25	25
Time (hours)	4.3	4.2	5.5	2.33	3.5
WHSV (wrt. C_3=)	0.98	0.94	1.04	0.53	0.90
C_3= Conv. (%)	0	86	76	42	82
C_5+ Selec. (%)	-	77	83	20	37
Liquid prod. refractive index	-	1.43	1.43	-	1.52
215°C+ Fraction	-	0.08	0.10	-	0.2

Table 1.5 : Vapor phase propene oligomerization over various $AlPO_4$ based molecular sieves. (From Pellet et al., 1986)

Mol. Sieve	SAPO-11	FAPO-11	MnAPO-11	SAPO-31	FAPO-31	MnAPSO-31	LZ-105
Tot. conversion (%)	85	90	90	86	89	85	94
Double bond Isom.(%)	46	2	28	82	42	43	2
Skeletal Isom.(%)	42	71	64	14	53	45	12
Oligomerization (%)	4	2	1	2	1	4	55
Cracking (%)	3	2	2	1	1	3	26

Table 1.6 : Reaction of 1-hexene over $AlPO_4$ based molecular sieves, 650°F, 40 psig, WHSV 5.5 g/g/hr. (From Pellet et al., 1988)

significant amounts of gasoline range product and the large pore diameter of the SAPO-5 material allowed the formation of high molecular weight hydrocarbons which plugged the catalyst pores thus deactivating the catalyst. Pellet et al. [1988] also investigated the reaction of hexene over various SAPO/MeAPSO materials and found the oligomerization activity of these materials to be significantly less than that of the zeolite LZ-105 (Table 1.6).

1.6.3 SAPO-34

SAPO-34 is a crystalline silicoaluminophosphate which has a 3-dimensional pore structure and is an isomorph of the naturally occurring zeolite chabazite which was first reported in 1933. The pore structure of SAPO-34 is constrained by 8-rings, which gives this silicoaluminophosphate small pore characteristics and hence enhanced shape selectivity towards short chain linear hydrocarbons.

1.6.3.1 Structure of SAPO-34

The crystal structure of chabazite consists of 6-6 SBUs arranged in layers in the sequence ABCABC and are connected by tilted 4-rings. The crystal structure is rhombohedral with unit cell dimensions of 9.46 Å and a rhombohedral angle ranging between 92.0° and 94.1°, depending on the degree of dehydration. The pore structure of chabazite and SAPO-34 is made up of a 3-dimensional network of ellipsoidal sorption cages (Figure 1.7) which are connected via 8-rings. These sorption cages are 11 Å long and 6.5 Å in diameter and the major and minor dimensions of the 8-rings are 4.4 Å and 4.1 Å, respectively.

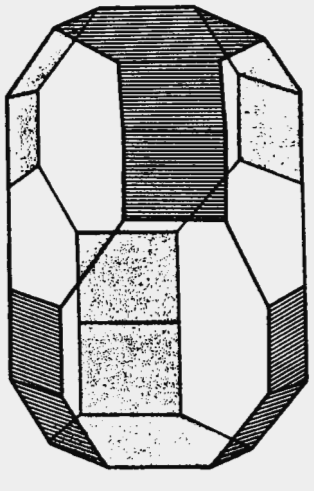

Figure 1.7: Chabazite cage.
(From Rabo, 1979)

On the basis of the sorption properties of molecules of various sizes, Barrer and Ibbitson [1944] estimated the effective size of the 8-ring openings in chabazite to be between 4.89 Å and 5.58 Å. The void volume of chabazite, as determined using water at 25°C, is 0.27 cm^3/g, resulting in a void fraction of 0.45 [Barrer and Sutherland, 1956].

An interesting effect arising from the presence of the ellipsoidal sorption cages, is the reduced diffusivity of *n*-pentane with respect to that of other linear paraffins in H-chabazite [Chen et al., 1988]. A similar effect has been observed with zeolite T (an intergrowth of errionite and offretite) where the diffusivity of C_4-C_8 linear paraffins decreases with increasing carbon number whereas that of the larger C_8-C_{12} linear molecules increased with increasing carbon number (Figure 1.8). This effect (dubbed the "window" or "cage" effect) was ascribed to the similarity between the molecular dimensions of the *n*-octane molecule and that of the errionite sorption cage (15.1 Å; slightly longer than the chabazite sorption cage).

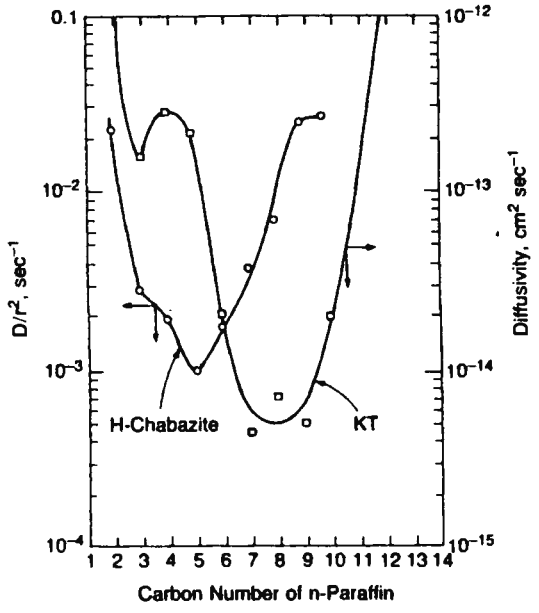

Figure 1.8 : Diffusion of *n*-paraffins in H-chabazite and KT. (From Chen, 1988)

The product distribution of cracked products of $C_{22}H_{46}$ and $C_{23}H_{48}$ over errionite followed the trend in the paraffin diffusivities, being significantly reduced for *n*-octane [Chen et al., 1969]. In addition, the relative cracking rate constants of *n*-octane over errionite and offretite were found to be reduced with respect to that of C_6-C_7 and C_9-C_{12} linear paraffins [Gianneti and Perrotta, 1975], showing that molecules which fit "snugly" into the sorption cages have a reduced reactivity as well as a reduced diffusivity.

1.6.3.2 Synthesis and modification of SAPO-34

The first patent detailing the synthesis of SAPO-34, US 4 440 871, was issued to Lok et al. [1984] of Union Carbide Corporation. Synthesis times employed in the various examples of US 4 440 871 ranged between 50 and 336 hours but later work [Inui et al., 1990a] showed that crystallization times as short as 2 hours were sufficient for the synthesis of SAPO-34. The only modifications of SAPO-34 reported until now, have been synthesis modifications where the silicon content has been varied or metals have been added to the synthesis, resulting in changes in acidity and the formation of MeAPSO-34 materials, respectively.

The synthesis of SAPO-34 requires the combination of phosphorus, aluminium and silicon sources in the presence of a structure directing template. Phosphoric acid, which is used almost exclusively as a phosphorus source, is combined with the aluminium source and stirred until homogeneous with the addition of as little water as possible. The aluminium source is usually either a hydrated aluminium oxide (a pseudo boehmite) or aluminium isopropoxide. Thereafter, the organic template tetraethylammonium hydroxide (TEAOH) is added. In Example 36 of US Patent 4 440 871, isopropylamine was also used successfully as a template for SAPO-34. The silicon source, usually in the form of fumed silica or an aqueous silica solution, is added to the gel either before or after the addition of the organic template.

The first patent detailing the synthesis of CoAPSO-34, EP 0 161 489, was issued in 1984, also to Lok et al. [1984] of Union Carbide Corporation. Nickel and cobalt are usually added to the synthesis gel in either the sulfate, nitrate or acetate form. The synthesis of NiAPSO-34, notably for the selective production of ethene, was first reported and patented in 1990 [Inui et al., 1990a; Inui, 1990b]. Bennet and Marcus [1988] suggested that the occupancy of a tetrahedral site by cobalt might be expected to distort the crystal framework. No reference has been made as to the effect of the incorporation of other metals into a tetrahedral framework position.

Detailed studies were undertaken by Weyda and Lechert [1990] on the effect of different variables on the crystallization of SAPO-5. It was found that the rate of crystallization was increased at higher synthesis temperatures and that crystallization took place at an initial gel pH ranging from 4 to 7. The Al/P ratio was also found to have a significant effect on the crystallization rate and the final relative crystallinity of the synthesis product. The addition of excess water to the synthesis

gel resulted in the formation of a product with a lower relative crystallinity. Similar results were found when the initial SiO_2 or Al_2O_3 contents of the gel were increased (standard starting composition : $Al_2O_3/P_2O_5/0.4SiO_2$). These results show that the rate of crystallization and final crystallinity of the synthesis product are controlled by all the synthesis variables and it is most likely that the trends found for SAPO-5 would also be found for SAPO-34.

1.6.3.3 Catalytic activity of SAPO-34

As previously mentioned, SAPO-34 has shown a very high selectivity toward linear C_2-C_4 olefins during the conversion of methanol. This enhanced selectivity has been attributed to the shape selective effect of the 8-ring sorption cage windows and also the relatively low strength of the acid sites in comparison to those of most zeolites [Marchi and Froment, 1991; Inui, 1991].

Marchi and Froment [1991] varied the SAPO-34 acidity by changing the Si/Al ratio of the catalyst and found that although the initial C_2-C_4 olefin formation was increased for samples with a reduced number of acid sites, the catalyst lifetime was unchanged. The amount of acidity was measured using diffuse reflectance FTIR however and may therefore not be. a true indication of the number of catalytically accessible acid sites.

Flanigen et al. [1988] reported typical maximum *n*-butane cracking activities over various MeAPSO-34 structures (Figure 1.9) which showed that other than BeSAPO-34 and FeSAPO-34, all the other MeAPSO-34 materials tested were catalytically more active than unmodified SAPO-34 (typical maximum *n*-butane cracking activity k_A = 6-7 $cm^3/g.min$).

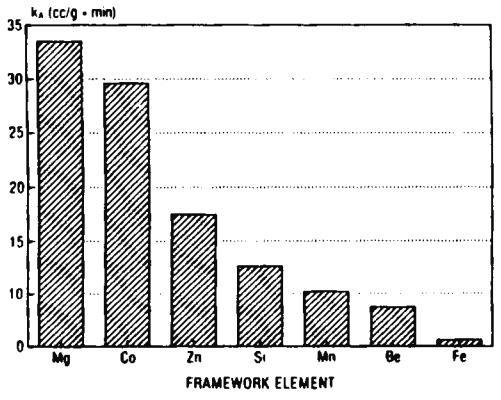

Figure 1.9 : Typical maximum *n*-butane cracking activities for MeAPO-34 structures. (From Flanigen et al. 1988)

Hocevar et al. [1990] studied the temperature programmed desorption of methanol and DME over various SAPO-34 and MeAPSO-34 catalysts. The reported reaction rates for methanol dehydration over ZSM-5, SAPO-34 and Co/Mg/CrSAPO-34 (Table 1.7) were found to be inversely proportional to the DME TPD peak temperatures of the various catalysts. Exceptionally high selectivities toward ethene were reported by Inui [1990a, 1990b] for the conversion of methanol to olefins over NiAPSO-34. It was proposed that these selectivities were a result of strict control of the amount and strength of the acid sites.

Sample	Conc.of Me (mol/g cat.)	T_{des} (K)	DME/MeOH (mol/mol)	React.Rate (mol/g.hr)
SAPO-34	2.14E-3 (Si)	402	0.021	0.19
CoAPSO-34	1.26E-3 (Co)	490	0.014	0.10
MnSAPO-34	0.65E-3 (Mn)	508	0.007	0.08
CrSAPO-34	*1.31E-3 (Si)	417	0.019	0.11
H-ZSM-5	0.83E-3 (Si)	525	0.128	0.54

Table 1.7 : DME TPD data and initial reaction rates for methanol dehydration over various MeAPSO-34 structures. (From Hocevar et al., 1990)

* Cr not incorporated into framework but functions as an extraframework species that blocks the active sites.

Thomson et al. [1990] studied hydrocarbon synthesis from CO hydrogenation over Pd supported on SAPO molecular sieves, and found that Pd/SAPO-34 and Pd/ZSM-5 were both less active than Pd/SAPO-5, Pd/SAPO-11 or Pd/Al_2O_3. This reduction in activity was ascribed to an increased activation energy for both Pd/ZSM-5 and Pd/SAPO-34 with respect to the other catalysts. The total selectivity to C_1-C_4 hydrocarbons was higher than that of the other catalysts and the iC_4/nC_4 ratio of the Pd/SAPO-34 hydrocarbon product was much lower than that of the other catalysts. It was concluded that the hydrocarbon product distribution was determined, not only by the catalyst's acidity, but also by the catalyst pore size and structure.

1.7 ZEOLITES

Zeolites were first recognized by Cronstedt in 1752, who derived the name from the Greek words "zeo" and "lithos" meaning "to boil" and "stone" due to the observed intumescence of the mineral when it was heated in a blowpipe flame [Flanigen, 1991]. It was almost 180 years later before the first analysis of a zeolite, analcime, was reported [Taylor, 1930]. In 1984, the list of zeolite minerals (i.e. non-synthetic zeolites) included 34 species although the basic framework structures of only 30 of these minerals were known at the time. It was estimated that natural zeolite reserves in the Basin and Range Province of the western United States alone, amounted to 100 million tons of clinoptilolite and over 15 million tons of erionite, mordenite, phillipsite and chabazite [Deffeyes, 1968].

The first synthesis of zeolites was started in the mid to late 1930's and between 1949 and 1954 Milton and Breck discovered several commercially significant zeolites, including A, X and Y [Flanigen, 1991]. These early synthetic zeolites were used for the drying of refrigerant and natural gas and in 1959, Union Carbide marketed one of the first bulk industrial separation processes, the "ISOSIV" process, for normal/isoparafin separation, utilizing the shape selective properties of zeolites. In 1962, Mobil Oil first introduced zeolite Y as a catalytic cracking catalyst and later developed several commercial processes around the catalyst ZSM-5, which was first synthesized by Argauer and Landolt in 1972.

At present, the application of zeolites may be divided into four main areas [Moscou, 1991] :

- Adsorbents, desiccants and separations
  mainly used as drying agents and in separation processes where the zeolite shape selectivity is utilized
- Catalysts
  petroleum refining (mostly catalytic cracking and hydrocracking), synfuels production and petrochemicals production
- Detergents
  very large market, mostly for zeolite A
- Miscellaneous
  natural and synthetic zeolites for waste water treatment, nuclear effluent treatment, animal feed supplements and soil improvement

Zeolite usage is greatest in Western Europe, the United States and Japan (Figure 1.10) and in 1988 the estimated zeolite usage in these three areas amounted to approximately 550 thousand metric tons [Moscou, 1991].

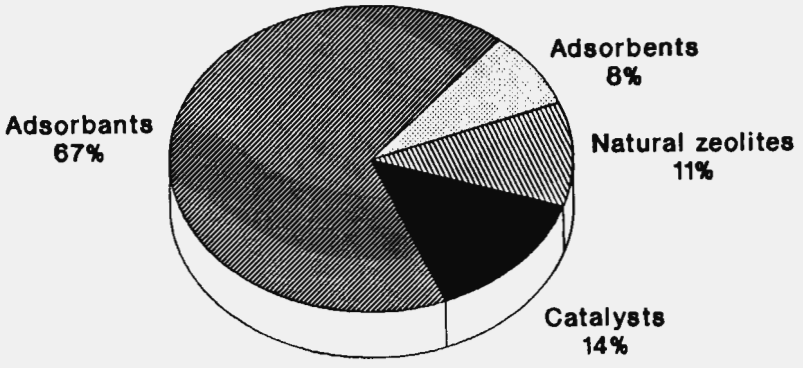

Figure 1.10 : Estimated zeolite consumption in the United States, Western Europe and Japan in 1988 and the relative consumption in various applications. (From Moscou, 1991)

1.7.1 The structure and acidity of zeolites

Zeolites are framework aluminosilicates enclosing regular pores or cavities which may be occupied by large ions and water molecules, both of which have considerable freedom of movement, permitting ion-exchange and reversible dehydration. Zeolites consist of tetrahedrally coordinated aluminium and silicon atoms (T atoms, sometimes Ga, Be, P are also present) that are linked together via oxygen atoms into a crystalline framework structure.

Various framework topologies may be encountered, pore structures ranging from 1-dimensional (non-interconnecting parallel pores, eg. mordenite) to 2-dimensional (heulandite) and 3-dimensional pore systems (faujustite, chabazite). Zeolites are frequently characterized according to the size of the T-O rings (Table 1.8) that characterize the pore structure (or the restrictions within the pore structure) and may range from large (12-rings : diameter 7-8 Å) to very small (6-rings : diameter 2-3 Å).

Zeolite Name	Channel System	Pore size * T atoms/ring	Free aperture (Å)	Largest molecule Adsorbed at RT
Large pore				
Faujustite (X, Y)	3D	12	7.4	$(C_2F_5)_3N$
Gmelinite	3D	12	7.0	C_3H_8
L	1D	12	7.1	$(C_4H_9)_3$
Mordenite	1D	12	6.7x7.0	C_6H_6
Medium/intermediate pore				
Dachiardite	2D	10	3.7x6.7	-
Epislitbite	2D	10	3.2x5.3	H_2O
Ferrierite	2D	10	4.3x5.5	C_2H_4
Heulandite	2D	10	4.4x7.2	NH_3
Stilbite	2D	10	4.1x6.2	H_2O
ZSM-5	3D	10	5.2x5.8	-
Small pore				
A	3D	8	4.2	C_2H_4
Bikitaite	1D	8	3.2x4.9	-
Brewsterite	2D	8	2.3x5.0	H_2O
Chabazite	3D	8	3.7x4.2	n-parafins
Edingtonite	2D	8	3.5x3.9	H_2O
Gismondine	3D	8	3.1x4.4	H_2O
Levynite	2D	8	3.2x5.1	N_2, O_2
Very small pore				
Analcime	1D	6	2.6	NH_3
Sodalite	3D	6	2,6	H_2O

Table 1.8 : Channel systems and pore sizes for selected zeolites. (From Breck, 1984)
* Pore sizes of largest channel only

As both aluminium and silicon are tetrahedrally coordinated, the incorporation of aluminium into the zeolite framework results in the formation of a net framework negative charge associated with the AlO_4 unit. This net negative charge gives zeolites a cation exchange capacity, and when the exchangeable cation is H^+, the hydroxyl group that is formed is a strong proton donor, acting as a Brønsted acid site. Lewis acid sites are thought to be formed by the dehydroxylation of a Brønsted acid site which is in the vicinity of a second Brønsted acid site. The second Brønsted acid site loses its acidity and exhibits a net negative charge which is balanced by the positive charge on the now tri-coordinated aluminium from the first Brønsted acid site.

Zeolites are generally synthesized from the hydrothermal crystallization of reactive alkali metal aluminosilicate gels at between 100°C and 200°C. In the early 1960's experimentation with the use of structure directing organic templates, such as

quaternary ammonium cations, led to the synthesis of the first high silica zeolites. Synthesis times vary from 2-3 hours to several days and the gel pH (pH 10-12) is generally higher than that used for the synthesis of $AlPO_4$ based molecular sieves due to the reduced stability of the amine templates (used for $AlPO_4$) at higher pH values.

1.7.2 Zeolites for catalysis

Zeolites are used as catalysts mainly in the areas of petroleum refining, synfuels production and petrochemicals production although much work is being done on the use of zeolites in the synthesis of specialized fine chemicals [Holderich and van Bekkum, 1991].

Petroleum refining

Fluidized catalytic cracking (FCC) is one of the largest fields of zeolite catalytic application (over 300 metric tons of zeolite Y per annum). The initial use of zeolite Y in FCC led to the evolution of rare earth exchanged Y and steam stabilized Y (USHY). ZSM-5 is used as an additive in FCC for enhancing the octane number of the product.

Hydrocracking catalysts are almost exclusively zeolite Y, the pore size and acidity of this material being ideal for cracking the large molecules found in vacuum gas oil, producing high naphtha (gasoline range) or distillate (diesel fuel range) fraction products. USHY containing base transition metals or palladium are the main catalyst types used for the production of naphtha [Pujado et al., 1992].

The production of *n*-paraffins is desirable because of their high cetane index (fuels) and viscosity index (lube oils). In catalytic dewaxing, the longer chain *n*-paraffins are removed in order to reduce the pour point of the product. The strong acidity of ZSM-5 and mordenite (sometimes in combination with other transition metals) and the suitability of their pore structures for processing small *n*-paraffins, makes these two catalysts ideal for the cracking of the long chain *n*-paraffins to form a lighter hydrocarbon product.

Paraffin isomerization is an application for which mordenite based zeolite catalysts are receiving more and more attention due to their simplicity of operation and increased tolerance of feed impurities. Paraffin isomerization is an important reaction in the production of high octane gasoline as it promotes the formation of highly branched paraffin isomers [Pujado et al. 1992].

Synthetic fuels

The production of synthetic fuels includes processes such as the production of high quality gasoline and distillate fuels from natural gas via methanol and the oligomerization of olefins to form higher oligomers (also gasoline and distillate range products). Catalytic conversion of methane to higher hydrocarbons, steam reforming, methanol synthesis and Fischer-Tropsch synthesis also play an important role in the synthetic fuels industry but these technologies are less reliant on the use of zeolites.

Mobil's fixed bed methanol-to-gasoline (MTG) process, using the catalyst ZSM-5, gives good yields of high quality gasoline and is already in commercial operation in Motuni, New Zealand [Chang and Silvestri, 1987]. Process efficiency was improved by the development of a second generation MTG process based on a fluidized bed reactor which may be operated to produce LPG as well as better yields of high quality gasoline compared to that obtained in the fixed bed process. The fluidized bed MTG process has been demonstrated on a pilot scale in Wesseling, FRG, and is ready for commercialization [Tabak and Yurchak, 1990].

The reaction path in the conversion of methanol to gasoline over ZSM-5 proceeds through the production of olefin intermediates and thus, operation at partial conversion yields products that are rich in light olefins. Alternatively, methanol conversion at higher temperatures (at complete methanol conversion) results in the formation of a predominantly olefin product (MTO). Chabazite has also been found to be highly selective in the formation of light olefins from methanol although this catalyst has a very high deactivation rate in comparison to that of ZSM-5. A fluidized bed reactor configuration is considered favorable for MTO since it allows steady state operation with good heat and mass transfer at maximum olefin selectivity and total methanol conversion [Tabak and Yurchak, 1990].

What may be seen as the next step following the MTO process, is the oligomerization of olefins for the formation of a higher oligomer gasoline or distillate type product. Both Mobil and Shell have commercial processes for this reaction: the Mobil Olefins to Gasoline and Distillate (MOGD) process, using the catalyst ZSM-5, and the Shell Higher Olefin Process (SHOP - selective production of higher alpha-olefins). The MOGD process is flexible enough to regulate the relative yields of gasoline and distillate product depending on the product demand. The MOGD distillate product is of low density and is typically used as a blending stock because of its low pour point and low sulfur content. In addition, the MOGD product makes excellent jet fuel, arising from its high isoparaffin content [Tabak and Yurchak, 1990].

Petrochemicals

Petrochemical production includes important processes such as aromatic alkylation, xylene isomerization and aromatic disproportionation and transalkylation. The alkylation of aromatics requires strong acid sites with low multiple alkylation or disproportionation activity and zeolite Y and ZSM-5 are commonly used in these applications. Xylene isomerization reactions often utilize the shape selectivity of zeolites and boron substituted ZSM-5 and mordenite is often used in this application.

Disproportion and transalkylation reactions require strong acid sites and ZSM-5 and mordenite are also used in this application. The aim of most aromatic disproportionation and transalkylation reactions is generally to maximize the formation of xylenes, and the selective production of p-xylene from the disproportionation of toluene over ZSM-5 has recently been commercialized by Mobil Oil Co [Pujado et al., 1992].

1.7.3 MORDENITE

Mordenite is a crystalline aluminosilicate belonging to the zeolite group of minerals. The name was suggested by How in 1864 for a fibrous mineral found in radial aggregates, in Morden County, Nova Scotia, Canada [Passaglia, 1975]. Mordenite was synthesized for the first time by Barrer in 1948 and its structure

determined by Meier [Meier, 1961]. Davis [1958] showed that mordenite, ptilolite. flokite and arduinite were the same mineral. Since its discovery, mordenite has received increasing attention as an acid catalyst in various industrially important reactions and also as a molecular sieve in various gas-liquid and liquid-liquid separations [Bajpai, 1982].

1.7.3.1 The structure of mordenite

Natural mordenite occurs in compact masses in a radial fibrous structure, these fibers usually being surrounded and connected by microcrystalline quartz and sometimes calcite and hematite [Passaglia, 1975]. The crystal structure of mordenite is orthorhombic, and has unit cell dimensions; a=18.13 Å, b=20.49 Å and c=7.52 Å [Smith, 1979], with a general chemical composition; $Na_8Al_8Si_{40}.24H_2O$ [Eberly, 1963]. A table of interatomic distances and bond angles along with a computer generated x-ray diffraction spectrum is presented in Appendix III.

Mordenite has a complex structure composed of horizontal 4-rings interspersed by tilted 5-rings which share a single edge [Smith, 1979]. These combine to form twisted 12-rings which make up parallel adsorption channels [Eberly, 1963]. These channels have approximately elliptical openings with major and minor openings of 6.95 Å and 5.81 Å, respectively. The walls of the channels are made up of 5-, 6- and 8-rings, the 8-rings forming windows/cavities at periodic intervals along the channels (dimensions between 3.87 Å and 4.72 Å). These cavities do not connect the parallel channels directly because they are staggered, thus preventing diffusion from taking place from one channel to another [Smith, 1979]; this may be seen in Figure 1.11.

There are four related "mordenite structures with similar x-ray diffraction patterns, the most commonly occurring mordenite having a Cmcm structure. Sherman and Bennet [1973] noticed that three other structures could be obtained; Cmmm, Imcm and Immm, which would all have similar unit cell dimensions although the 4-rings lie at different heights along the c axis with respect to one another. The Cmcm and Imcm structures have one-dimensional large pore systems and Cmmm and Immm have two-dimensional pore systems, with the second pore system being composed of small pores [Rabo, 1979].

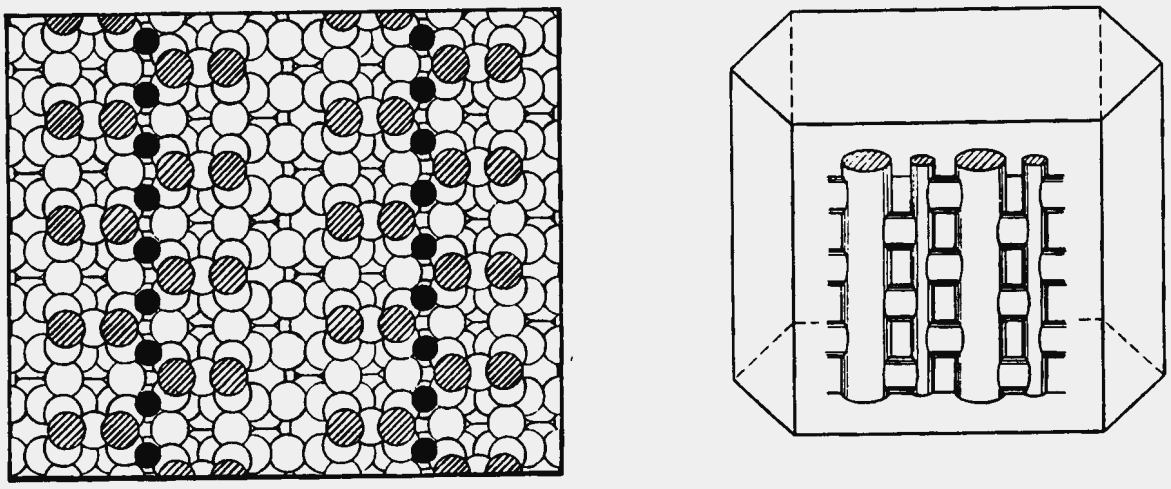

Figure 1.11 : Structure of interconnecting channels. (From Barrer and Peterson, 1964 and Rigutto, 1991)

Figure 1.12 shows a cross-section of mordenite along the c axis with the main pores and side pockets shown as Va and Vb, respectively. The volume of the main pore is 480 $Å^3$/unit cell and that of the side pockets 428 $Å^3$/unit cell. The total pore volumes of NaM and HM were determined by Satterfield and Frabetti [1967] to be 0.189 cm^3/g and 0.199 cm^3/g and the volumes of the main channels are 0.107 cm^3/g and 0.113 cm^3/g. Barrer and Peterson [1964] sorbed O_2, N_2, Ar, *n*-C_4, *i*-C_4, C_6H_6 and neo-C_5H_{12} onto mordenite and found the sorption volume of N_2 to agree well with the estimated volume of the main channels and side pockets. The saturation volumes of the hydrocarbons never exceeded that of the main channels and it was suggested that molecules with a critical dimension of greater than that of *n*-C_4H_{10} had no access to the side pockets.

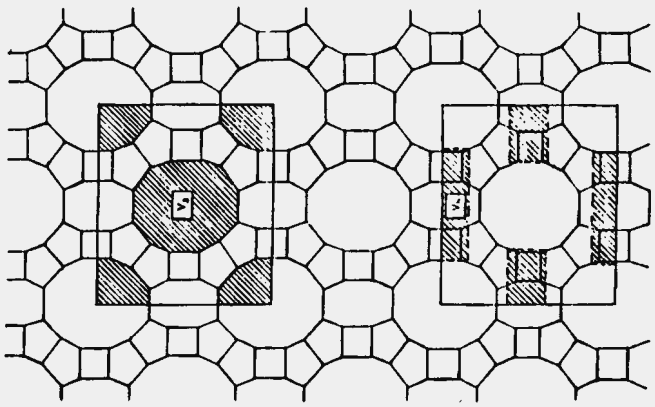

Figure 1.12 : Pore volumes of mordenite main channels and side pockets. (From Eberly, 1963)

Mordenite may be classified as either large port (LPM) or small port (SPM), the distinction arising from the sorption properties of the zeolite. Although the effective diameter of the mordenite channels is about 6.6 Å, SPM can only sorb molecules which are smaller than 4.2 Å [Raatz et al., 1983]. LPM channels have effective diameters of 8 Å and sorption properties which agree much better with the structure proposed by Meier [1961]. LPM was first synthesized by Keogh and Sand [1961] and although most natural mordenites are of the SPM variety, Wu and Ma [1988] reported the discovery of a natural mordenite, Jinyunite, which appears to have LPM sorption properties.

Meier [1968] suggested that stacking faults normal to the c axis may restrict channels to 8-ring windows, although Sanders [1985] could find no evidence for this using electron diffraction techniques and transmission electron microscopy. Another explanation for the reduced sorption properties of SPM are the presence of cations or amorphous material in the channels, although there is as yet no proof that either of these explanations are correct. It has been found though, that the transformation of SPM to LPM is accomplished by the extraction of approximately 20% of the aluminium from the mordenite framework [Raatz et al., 1983].

1.7.3.2 Synthesis and dealumination of mordenite

Mordenite was first synthesized by Barrer in 1958 who later found that when using gels as a starting material, temperatures of at least 250°C and Si/Al ratios of 6 were required [Barrer, 1959]. Water/Al_2O_3 ratios of several hundred were used and the resulting mordenites had channel diameters of approximately 4 Å (small port mordenite), similar to that found in natural mordenites. Large port mordenite was first synthesized by Sand in 1961, having channel diameters of approximately 8 Å, thus confirming the structure proposed by Meier [1961]. The reduction in channel diameter of small port mordenite was ascribed to either crystal stacking faults or pores blocked with amorphous material [Whittemore, 1972].

Sand [1968] demonstrated that gel water content was very important in the synthesis of large port mordenite. Depending on the starting materials employed, the crystallization kinetics could be altered and the crystal size varied from less than one micron to over 100 microns, with a range of crystal morphologies being produced. Sand also reported that the use of low synthesis temperatures

necessitated long crystallization times (75°C, 168 hours) whereas the use of higher temperatures allowed rapid crystallization (260°C, 4 hours).

Mordenite is synthesized in an alkali medium (pH approximately 12) although high pH gels result in the dissolution and recrystallization of the mordenite into different phases [Bodart et al., 1986]. Bodart et al. [1986] found that although both crystallinity and crystallite size increased with synthesis time, the pH of the synthesis gel remained unchanged and suggested that the synthesis comprised of only one nucleation step. Reduction of the pH to between 7 and 8, results in a retardation in crystallization and the formation of smaller crystallites.

The mordenite composition may be modified by varying the synthesis gel composition (Figure 1.13). Early synthetic mordenites had Si/Al ratios ranging between 4.5 and 5.5. The synthesis of siliceous mordenites was first reported by Whittemore in 1972, with Si/Al ratios ranging between 6 and 10. Siliceous mordenite may also be synthesized by ageing of the synthesis gel or the addition of benzyltrimethylammonium ions to the synthesis gel [Ueda et al, 1980]. Gaffney et al. [1989] reported that isomorphous substitution of boron for aluminium was possible, but only in aluminium deficient gels where aluminium does not compete with boron for tetrahedral sites in the growing crystallites.

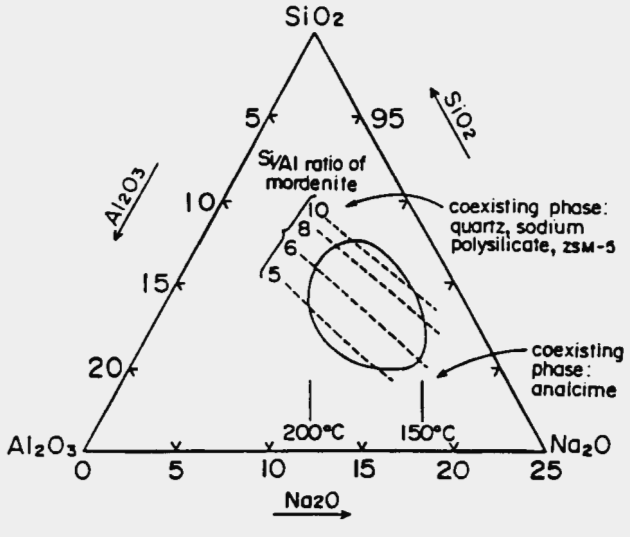

Figure 1.13 : Composition diagram of synthesis gel composition and temperature required for the synthesis of siliceous mordenite. (From Inaoka et al. 1990)

Post-synthesis dealumination of mordenite

Siliceous mordenite may also be produced by the post-synthesis extraction of aluminium or the substitution of aluminium by silicon. Extraction of aluminium may be accomplished by thermal treatment, hydrothermal treatment, treatment with mineral or organic acids or treatment with a variety of metal halides, oxyhalides or metal alcoholates [Fejes et al., 1988].

Dealumination under anhydrous conditions results in the appearance of a new infrared band at approximately 950-970 cm^{-1}. This new band was assigned to the stretching vibration of new Si-O bonds (characterized by different bond lengths and angles from those encountered in the undisturbed lattice) left behind after dehydration of the vacancies produced in the dealumination process [Dunken et al, 1983] :

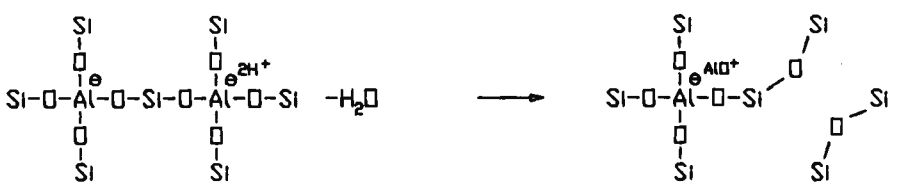

The disappearance of this band after hydrothermal treatment at 500°C was ascribed to hydration and structural reorganization [Fejes et al, 1988] :

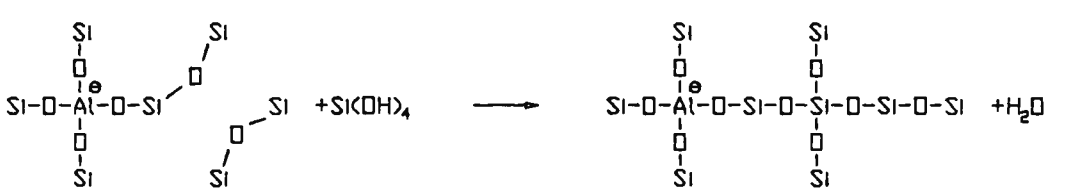

Musa et al. [1987] and Fejes et al. [1988] also reported the appearance of a new infrared band at 955 cm^{-1} and agreed with the assignment of Dunken et al. [1983]. Beyer et al. [1984], however, assigned this new band to the presence of OH nests created after aluminium extraction as was proposed by Kiovsky et al. [1978] and

has been found with zeolite Y [Kerr, 1969]. Although it has been suggested that the formation of OH nests may be an intermediate step in the formation of the new Si-O bonds, Mishin et al. [1973 a, b] concluded that the formation of these new bonds takes place, at least in part, without the intermediate formation of the OH groups.

There has been some uncertainty regarding the assignment of the 620-630 cm^{-1} band which has been associated with alternating SiO_4 and AlO_4 tetrahedra [Ha et al., 1979], vibrations in single 4-rings [Flanigen, 1976] and more recently to isolated AlO_4 tetrahedra in single 4-rings [Van Geem et al., 1988]. There is also some uncertainty regarding the estimation the Si/(Si+Al) ratio of dealuminated mordenites from the position of the asymmetric stretching T-O band since dissimilar correlations have been reported [Bremer et al., 1983; Musa et al., 1987].

Dealumination of mordenite under hydrothermal conditions has been found to favour silicon migration, resulting in the formation of a highly siliceous ultrastable mordenite with an extremely regular crystal structure [Musa et al., 1987]. This sequence of events follows the mechanism proposed by Beyer et al. [1984] where aluminium is removed from 5-rings and the vacancies which are created are filled by migrating silicon atoms.

1.7.3.3 The catalytic activity of dealuminated mordenite

Dealuminated mordenites have been found to exhibit increased hexane cracking activities [Weller and Brauer, 1969] although Goovaerts et al. [1989] showed that although this trend held for large port mordenites, severely dealuminated small port mordenites (bulk aluminium < 1wt%) had reduced cracking activities. Kranich et al. [1970] found that initial dealumination (up to Si/Al = 15) resulted in increased 1-butene isomerization activity but further dealumination resulted in a drop in activity. Similar results were reported by Koradia et al. [1980] for the isomerization of *n*-pentane.

Eberly and Kimberlin [1970] found that the cracking and hydrocracking activity of mordenites increased with dealumination and ascribed this to reduced diffusional resistance as a result of the removal of amorphous material from the zeolite pores. For highly dealuminated mordenites, Kranich et al. [1971] reported that cumene

Post-synthesis dealumination of mordenite

Siliceous mordenite may also be produced by the post-synthesis extraction of aluminium or the substitution of aluminium by silicon. Extraction of aluminium may be accomplished by thermal treatment, hydrothermal treatment, treatment with mineral or organic acids or treatment with a variety of metal halides, oxyhalides or metal alcoholates [Fejes et al., 1988].

Dealumination under anhydrous conditions results in the appearance of a new infrared band at approximately 950-970 cm^{-1}. This new band was assigned to the stretching vibration of new Si-O bonds (characterized by different bond lengths and angles from those encountered in the undisturbed lattice) left behind after dehydration of the vacancies produced in the dealumination process [Dunken et al, 1983] :

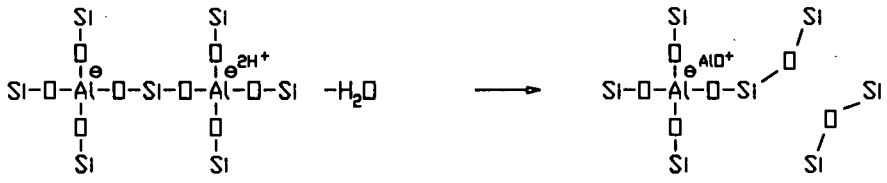

The disappearance of this band after hydrothermal treatment at 500°C was ascribed to hydration and structural reorganization [Fejes et al, 1988] :

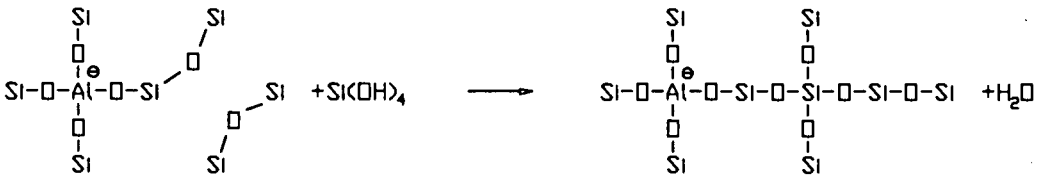

Musa et al. [1987] and Fejes et al. [1988] also reported the appearance of a new infrared band at 955 cm^{-1} and agreed with the assignment of Dunken et al. [1983]. Beyer et al. [1984], however, assigned this new band to the presence of OH nests created after aluminium extraction as was proposed by Kiovsky et al. [1978] and

cracking and hydrocracking was reduced. Bhavikatti and Patwardhan [1981] found that although aluminium deficient mordenites exhibited lower initial toluene disproportionation activity, the rate of these samples was low in comparison to the aluminium rich samples. Similar results were found by Pardillos et al. [1989] for o-dichlorobenzene isomerization.

Bandiera et al. [1984] reported that dealuminated mordenites exhibited a high resistance to deactivation as a result of reduced hydrogen transfer (due to the small number of acid sites) and had longer methanol conversion lifetimes at high methanol space velocities than ZSM-5. Karge and Boldingh [1988] also reported decreased coking and deactivation rates for ethylbenzene dealkylation over dealuminated mordenites. Niwa et al. [1988]; and Sawa et al. [1989] found that reduction in aluminium content up to approximately 0.35 mmols/g resulted in increased methanol conversion lifetimes but small reductions thereafter resulted in a significant reductions in catalyst lifetime.

In summary, it seems that dealumination affects mordenite catalytic activity for various reactions in different ways. Mordenite dealumination frequently results in increased catalytic activity, possibly due to the removal of material which can block the zeolite pores, but excessive or extreme dealumination often results in reduced catalytic activity.

1.8 RESEARCH OBJECTIVES

From the preceding sections, it can be seen that methanol may be converted to light olefins which may be either oligomerized to form high quality synfuels or used as feedstocks in the manufacture of high value fine chemicals. The methanol conversion and olefin oligomerization reactions are catalyzed by various molecular sieves and zeolites, SAPO-34 and dealuminated mordenite being two materials which have received much recent attention in this field. It is evident that there are a number of areas which need elucidation, especially with respect to the effect of various catalyst modifications on the activity and selectivity of SAPO-34 and mordenite for these reactions.

Although SAPO-34 and MeAPSO-34 catalysts have been found to be highly selective for the formation of light olefins from methanol, the effect of catalyst acidity on selectivity and lifetime is still unclear. The 90%+ ethene selectivities reported by Inui [1990] for methanol conversion over NiAPSO-34 are of special interest in this regard. In addition, little work has been reported on the post-synthesis modification of SAPO-34 catalysts for the improvement of either catalyst lifetime (which is relatively short for SAPO-34) or light olefin selectivity.

With regard to the mordenite catalysts, although the catalytic activity of these materials is often found to increase with initial dealumination (as is the case with methanol conversion), the reason for this increase in activity and the subsequent decrease in activity as found for severely dealuminated materials is still not clear. Investigation of this phenomenon required a thorough physiochemical characterization of the four different series of dealuminated mordenites that were used in this study. In the characterization of these dealuminated mordenites there is some uncertainty with regard to the structure of the dealuminated material especially with regard to the way in which the catalyst structure is affected by the type of dealumination procedure employed. This uncertainty is compounded by disparate assignments in the literature to the 930-960 cm^{-1} and 620-630 cm^{-1} structural infrared vibrations.

In the work that follows, the effect of various modifications to the SAPO-34 and mordenite catalysts are investigated with respect to the methanol conversion and propene oligomerization reactions. Optimum catalyst modifications and reaction conditions (especially with respect to catalyst lifetime) for the SAPO-34 and

mordenite catalysts were determined for the methanol conversion reaction and optimum mordenite morphology and extent of dealumination were determined for the propene oligomerization reaction. The activities, selectivities and lifetimes of these catalysts are compared to those reported in the literature for other zeolites.

Chapter 2

EXPERIMENTAL

2.1 CATALYST SYNTHESIS AND MODIFICATION

2.1.1 SAPO-34

2.1.1.1 SAPO-34 synthesis

Three batches of SAPO-34 were synthesized, S1 and S2 according to Example 34 of US patent 4 440 871 and S3 according to Example 33. CoAPSO-34 (Co1) and NiAPSO-34 (Ni1, Ni2, Ni3) were synthesized according to European Patent 0 161 488, substituting nickel acetate for cobalt acetate in the case of NiAPSO-34. Synthesis conditions are given in Table 2.1. The pH of the synthesis gel of the Ni1 catalyst was 7.7 and, as much of the product was amorphous, NaOH was added to the synthesis gel of Ni2 increasing the pH to 11.3 (TEAOH:NaOH molar ratio of 140:1) in an attempt to increase the crystallinity of the resulting product. All the catalysts described, were synthesized at autothermal pressures in a stainless steel autoclave (Figure 2.1), the inside dimensions of which were 90 mm (depth) and 70 mm (diameter). The synthesis gel was stirred using a magnetic stirrer and stirrer bar.

Four attempts were made to synthesize SAPO-34 using tetraethylammonium bromide (TEABr) instead of tetraethylammoniumhydroxide (TEAOH). None of these syntheses produced any material with the SAPO-34 structure, even when

Synthesis conditions	S1	S2	S3	Co1	Ni1	Ni2	Ni3
Temperature (°C)	200	200	150	100	100	100	100
Synthesis Time (hours)	48	48	133	96	96	96	133
pH	11.6	8.8	-	10.9	7.7	11.3	-
Charged masses (g)							
TEAOH (20%)	54.3	54.3	54.4	63.3	63.7	58.0	63.8
Phosphoric acid	17.3	17.3	17.1	17.9	17.8	15.5	18.0
Fumed silica	-	-	.47	-	-	2.82	-
LUDOX (40%)	1.18	3.30	-	7.75	7.79	-	7.79
Aluminium isopropoxide	30.2	30.2	30.2	31.6	31.6	28.9	31.6
Water	37.0	37.0	26.1	19.9	19.6	47.5	17.2
Co acetate	-	-	-	1.07	-	-	-
Ni acetate	-	-	-	-	1.07	3.12	1.50
NaOH	-	-	-	-	-	0.11	-

Table 2.1 : Synthesis conditions and charge masses for SAPO-34 and MeAPSO-34 catalysts.

NaOH was added to the synthesis gel in order to increase the gel pH. The products which were formed were either berlinite ($AlPO_4$) or tridymite (monoclinic silicon oxide). An additional batch of NiAPSO-34 was synthesized using the method described by Inui [1990], where Ni sulfate is used instead of Ni acetate but the synthesis product consisted mostly of SAPO-5.

2.1.1.2 SAPO-34 modification

Catalyst modifications and the investigation into the effects of various reaction conditions were carried out on S3 which had been "**deep-bed**" calcined in flowing air (standard gas hourly space velocity 100 hr^{-1}) at 550°C for 18 hours in a packed bed (15 g catalyst, 16 mm diameter, 180 mm deep). The S3 material calcined in this manner is referred to as S3*.

In contrast to this S3* material, Co1, Ni1, Ni2, Ni3, S1, S2 as well as a sample of S3 were specifically calcined in a "**shallow bed**" of 5 mm depth to avoid any physical or chemical changes brought about by deep bed calcination conditions.

Acid treatment consisted of stirring 1.0 g of S3* in 20 ml of 0.1 N HNO_3 for 4 hours after which the suspension was filtered and the solids washed in 500 ml of flowing distilled water before drying in air overnight at 80°C. The resulting catalyst is referred to as S3*-ACD.

Caustic treatment was similar to the acid treatment except that a 0.1 N NaOH solution was used in place of the 0.1 N HNO_3. The resulting catalyst is referred to as S3*-CAU.

Hydrothermal treatment was carried out by passing a wet nitrogen stream (50 ml/min, 12 kPa water vapor pressure) over a packed bed of S3* material (1.5 g catalyst, 16 mm diameter, 18 mm deep) for 120 minutes at 300°C. The catalyst was cooled to room temperature in dry flowing nitrogen. These steaming conditions had previously been found to enhance the activity of ZSM-5 for hexane cracking and hexene oligomerization [Andersen, 1991]. The resulting catalyst is referred to as S3*-STM.

Strong acid sites of S3* material were selectively **poisoned** by adsorbing **ammonia** onto the catalyst at 100°C for 1 hour. Physisorbed ammonia and ammonia adsorbed on the weaker acid sites was removed by heating the catalyst at 10°C/minute to 400°C in flowing helium and maintaining this temperature for a further 1 hour. The resulting catalyst is referred to as S3*-AMM.

Boron impregnation was achieved by refluxing 1.0 g of S3* in 100 ml of a saturated boric acid solution for 4 hours. The suspension was filtered and the solids washed in 500 ml of flowing distilled water before drying in air at 80°C overnight. The resulting catalyst is referred to as S3*-BRN.

Silanization was accomplished by passing 0.5 g/hr of tetraethoxysilane through a 1.25 g bed of S3* for 1.5 hours at 350°C. Excess tetraethoxysilane was flushed from the catalyst with nitrogen at 350°C for 1 hour. Subsequently, the catalyst was calcined in flowing dry air for 10 hours at 500°C followed by cooling to room temperature in flowing dry nitrogen. The resulting catalyst is referred to as S3*-SIL.

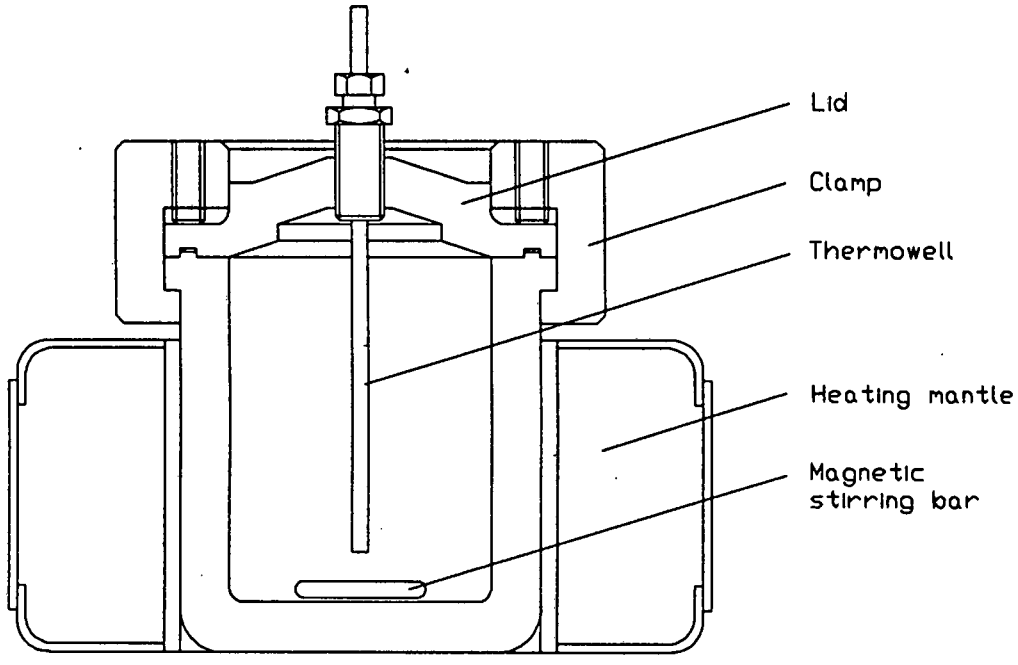

Figure 2.1 : Magnetically stirred autoclave.

2.1.2 MORDENITE

2.1.2.1 Mordenite synthesis

The catalysts used were Zeocat mordenite (ZM), Norton mordenite Z900 (MN) and mordenite synthesized according to the method of Itabashi et al. [1986]. Samples with three different aluminium contents were obtained from Zeocat (Siege Social 154, Rue de L'Universite, Paris) and are referred to as ZM510, ZM760 and ZM980. These samples had been dealuminated by steam treatment followed by acid treatment [Hamon, 1991]. The Norton mordenite (Norton Chemical Co, Ohio, USA) was obtained as 1/16 inch binderless extrudates in the sodium form. In the manufacture of the extrudates it is possible that a viscosity modifier such as hydroxymethylcellulose was used. This would however be removed by combustion during the calcination process. This material was crushed and sieved and particles of less than 75 microns were used in this study. No indication of the presence of any foreign material was found in the calcined ZM and MN samples by either XRD or electron microscopy.

Two batches of mordenite were synthesized according to the method described by Itabashi et al. [1986], in a stainless steel mechanically stirred autoclave (inside dimensions : 90 mm depth and 60 mm diameter) at 190°C under autothermal pressure. The first batch was synthesized at an autoclave impeller speed of 300 RPM (M1) and the second at an impeller speed of 30 RPM (M2). The molar ratios of both synthesis mixtures were $Na_2O/Al_2O_3/SiO_2/H_2O$: 1.7/1/11.5/230, and the synthesis time was 48 hours. The synthesis gel compositions are given in

Synthesis conditions	M1	M2
Temperature (°C)	188	181
Synthesis time (hours)	48	48
Stirring speed (RPM)	300	30
Charged masses (g)		
LUDOX (40%)	104.4	115.4
Sodium aluminate	12.6	12.6
Water	101.4	100.0
Sodium hydroxide	1.4	2.2

Table 2.2 : Synthesis conditions and charged masses for the mordenite catalysts.

Table 2.2. The as-synthesized mordenites were in the sodium form, and were converted to the ammonium form by refluxing 300 g of catalyst in a solution of 2 N NH_4Cl for 12 hours. The catalyst samples were washed in 1 liter of flowing distilled water and dried overnight at 90°C. The sodium, ammonium and hydrogen forms of all the above catalysts are designated -Na, -NH3 and -H, respectively. Hydrogen form catalysts were obtained by calcination of the ammonium forms in air at 400°C for 8 hours or by acid treatment (as described in 2.1.2.2) of the sodium form samples.

2.1.2.2 Mordenite dealumination

The MN, M1 and M2 mordenite samples were dealuminated using a similar procedure to that described by Karge et al. [1984]. Samples designated -A1 and -A2 were prepared by stirring 1.0 g of sodium mordenite in 27 ml of 1 N and 6 N HNO_3 respectively, at room temperature for 4 hours. These samples were washed in 1 liter of flowing distilled water, dried overnight at 90°C and crushed to a particle size of less than 75 microns.

Acid washed samples, designated -2AW, were prepared by stirring 4 g of sodium mordenite in 53 ml of 6 N HNO_3 for 4 hours at room temperature, washing, drying and crushing and repeating these treatments once. More severely dealuminated samples were prepared by multiple cycles of refluxing 4 g of sodium mordenite in 53 ml of 6 N HNO_3 for 4 hours and then washing, drying and crushing as described above. Samples undergoing 2 and 4 such refluxing cycles are designated -2AR and -4AR, respectively.

The M1 samples M1-2AR(NH3) and M1-4AR(NH3) were prepared according to the same procedures as the M1-2AR and M1-4AR samples but the ammonium form of the catalyst was used in place of the sodium form.

2.2 CATALYST CHARACTERIZATION

2.2.1 Catalyst composition

Mordenite aluminium contents were determined by atomic absorption (AA). For this purpose, samples were prepared by dissolving 100 mg of the catalyst in hydrofluoric/hydrochloric acid (5 ml 40% HF, 5 ml 31% HCl) at room temperature. The HCl was added after complete dissolution of all the material in HF. After addition of the HCl, 20 ml of a saturated boric acid solution was added to complex the excess hydrofluoric acid and the resulting solution made up to 50 ml using distilled water. AA standards were prepared using hydrofluoric, hydrochloric and boric acid concentrations corresponding to those used for sample preparation. The mildly and more severely dealuminated ZM510 and ZM760 samples, which were analyzed by XRF at Mintek (Randburg, South Africa), were used as checks in all the mordenite aluminium analyses. The Si, Al, P, Ni and Co contents of the SAPO-34 and MeAPSO-34 were determined at Mintek.

Aluminium co-ordination state was determined from ^{27}Al MAS NMR spectra of the mordenite samples which were recorded at the CSIR (Pretoria, South Africa), using a Bruker AM 300 spectrometer at the following conditions :

Spin rate	5000 Hz
Pulse width	1.5 microseconds
Pulse angle	30°
Relaxation delay	0.1 seconds
External standard	$AlCl_3(H_2O)_6$ at 0 ppm.

Prior to NMR analysis, samples were calcined in air at 400°C for 8 hours and allowed to equilibrate under ambient conditions.

2.2.2 Catalyst acidity

Ammonia temperature programmed desorption (NH_3 TPD) spectra were recorded in the range 100°C to 650°C (10°C/minute temperature ramp, 60 ml/minute helium carrier). The sample masses used were 0.25 g for the SAPO-34 and MeAPSO-34 catalysts and 0.5 g for the mordenite catalysts. Ammonia was pre-adsorbed at

100°C and TPD peak temperatures were reproducible to within 5°C. Calcination was undertaken at 400°C or 500°C in air flowing at 60 ml/minute. The general TPD procedure was as follows :

Ramp to calcination temp.	10°C/minute to 500°C (SAPO-34)
	10°C/minute to 400°C (mordenite)
Maintain temperature	12 hours (SAPO-34)
	4 hours (mordenite)
Cool to 100°C	5°C/minute in helium
Adsorb ammonia	60 minutes
Desorb excess ammonia	60 minutes (mordenite)
	120 minutes (SAPO-34)
Ramp temperature	10°C/minute to 550°C (SAPO-34)
	10°C/minute to 650°C (mordenite)
Maintain temperature	30 minutes

All the TPD spectra displayed two characteristic desorption peaks and for integration purposes these peaks were separated by dropping a perpendicular line from the trough between the two peaks to the baseline of the spectra.

2.2.3 Catalyst structure and morphology

X-ray diffraction (XRD) spectra were obtained using Cu-K alpha radiation. The relative crystallinities of the SAPO-34 and MeAPSO-34 samples were estimated by summing the peak heights of the (100), (-210) and (-310) reflections and normalizing with respect to S3. For mordenite and SAPO-34 catalysts, respectively, relative crystallinity data was obtained under identical instrumental and sample conditions.

The mordenite lattice constants a, b and c were measured from the (200), (020) and (004) reflections, respectively. The relative crystallinities of these samples were estimated by summing the peak heights of the (200), (111), (310), (202), (350) and (402) reflections and normalizing with respect to ZM980.

Infrared spectra were recorded using a Nicolet 5ZDX FTIR spectrometer and are presented as transmittance spectra. The mordenite samples were calcined at

400°C and diluted 1:100 in KBr for viewing the 400-900 cm^{-1} bands and 1:500 for viewing the 1050-1090 cm^{-1} bands.

Temperature programmed reduction (TPR) spectra were recorded in the range 100°C to 650°C (10°C/minute temperature ramp, 60 ml/minute 5.4% hydrogen in a nitrogen carrier, sample mass 0.25 g). Calcination was undertaken at 500°C in air flowing at 60 ml/minute. The general TPR procedure was as follows :

Ramp to calcination temp.	10°C/minute to 500°C
Maintain temperature	12 hours (air)
Cool to 100°C	5°C/minute (air)
Ramp temperature	10°C/minute to 650°C (H_2/N_2)
Maintain temperature	30 minutes (H_2/N_2)

The crystallite sizes were measured from electron micrographs taken at a magnification of 5 500x, using a Cambridge S200 electron microscope. The operating conditions used are as follows :

Accelerating voltage	15 kV (SAPO-34)
	10 kV (mordenite)
Stage tilt	30°
Working distance	9-12 mm
Aperture diameter	30 microns

Catalyst agglomerate sizes were measured using a Malvern 2600/3600 particle sizer.

2.2.4 Catalyst pore volume and surface area

Cyclohexane adsorption levels were determined only for the mordenite samples. Mass and temperature changes were recorded using a Stanton Redcroft STA 780 thermo-gravimetric balance. The cyclohexane partial pressure used was 125 mm Hg, the sample mass 13 mg and the gas flowrates 70 ml/minute. The samples were heated to 400°C at 10°C/minute in air and maintained at this condition for 4 hours. The air stream was replaced by high purity nitrogen and after a further 30 minutes the sample was cooled to the adsorption temperature.

Once the sample reached the adsorption temperature of 70°C, the nitrogen stream was switched through a double-stage saturator and cyclohexane adsorbed on the catalyst sample for 3 hours. The cyclohexane adsorption levels reported are based on the amount of cyclohexane adsorbed per gram of calcined dry catalyst.

Surface areas were measured by nitrogen adsorption using a multipoint Carlo Erba Sorptomatic 1800 surface area analyzer after sample evacuation at 250°C. All SAPO-34 and mordenite samples used for BET analyses were, respectively, precalcined in air at 500°C and 400°C for 8 hours and allowed to cool at ambient conditions overnight.

2.2.5 Coke level determination

Coke levels were calculated as the mass of hydrocarbon burnt off the coked catalyst at 500°C after treating the coked sample at 500°C in flowing nitrogen for 30 minutes. Mass changes were recorded using a Stanton Redcroft STA 780 thermo-gravimetric balance, packing 13 mg of coked sample and using nitrogen and air flowrates of 30 ml/minute. The samples were held at room temperature in flowing nitrogen for 30 minutes before ramping to 500°C at 10°C/minute.

Prior to coke level determination, the SAPO-34 catalysts were deactivated until the oxygenate conversion levels were below 10%. The coke contents reported are based on the amount of coke removed per gram of calcined uncoked catalyst.

2.3 REACTOR CONFIGURATION AND EXPERIMENTAL PROCEDURES

2.3.1 Methanol conversion

Equipment

Unless otherwise stated, all methanol conversion (MTO) reaction studies were carried out in a fixed bed borosilicate glass reactor of 16 mm ID, the catalyst being supported on a glass frit. All the piping used was 1/8 inch stainless steel and was heated to 175°C to eliminate product condensation.

The reactor could be operated in either a fixed or fluidized bed configuration by changing the flow direction using the 3-way valves before and after the reactor (Figure 2.2). When operating in fluidized bed mode with very high flowrates, additional nitrogen could be added to the feed stream after the double stage saturator, this stream being controlled using a needle valve.

For most of the MTO work, high purity nitrogen was used as a carrier for the methanol feed. The nitrogen stream, metered by a mass flow controller, was saturated with methanol using a double stage saturator. When the methanol feed was diluted with water, the feed was metered using 20 ml syringe and a syringe pump.

Conditions and procedures

Unless otherwise stated, the MTO reaction conditions used were as follows :

Reaction temperature	400°C
Methanol space velocity	1.0 g/g/hr
Methanol partial pressure	21 kPa
Methanol diluent	Nitrogen

Prior to the initiation of MTO runs, uncalcined catalysts were calcined in air (30 ml/min) at 550°C for 12-14 hours and cooled to reaction temperature under flowing nitrogen. Catalyst samples which had been previously calcined (eg. the

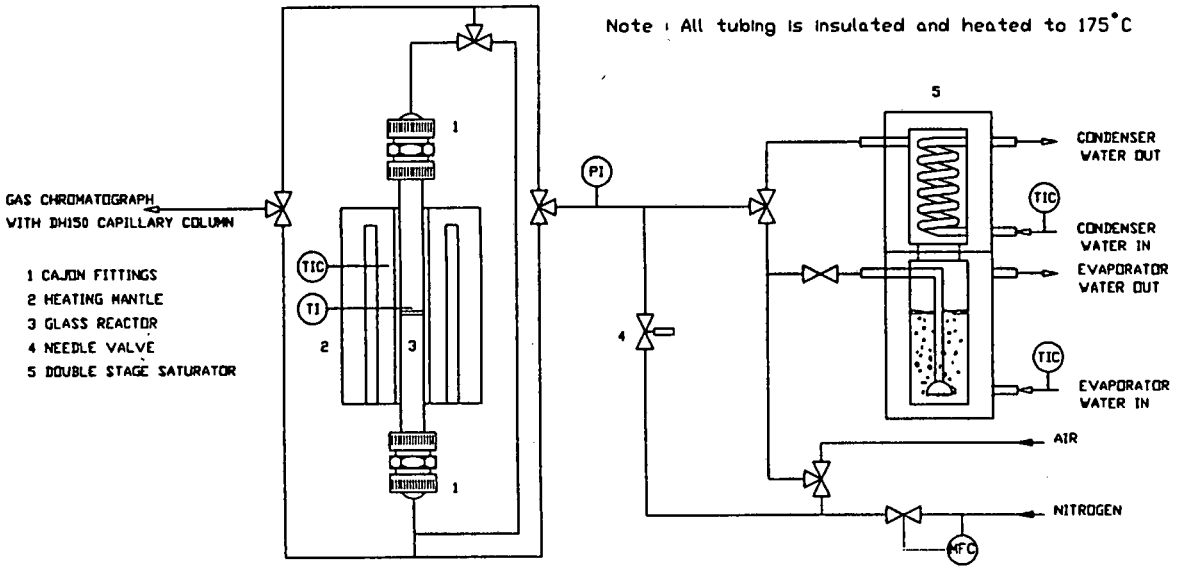

Figure 2.2 : Schematic of atmospheric pressure fixed/fluidized bed MTO rig

S3* samples) were heated to reaction temperature in flowing nitrogen (30 ml/minute) and maintained at that temperature for 15 minutes. The nitrogen stream was switched through the reactor bypass and only then was the nitrogen stream diverted through the double stage saturator. Once the gas flow had stabilized, the feed stream was switched from the reactor bypass back through the reactor and the run was started. The first product sample was taken 10 minutes after the run was commenced and then every 70-100 minutes thereafter.

Product analysis and data work-up

Reaction products were analyzed on-line and were separated on a Supelco DH150 capillary column and detected by flame ionization. Off-line analysis was employed for CO and CO_2 determination, where products were separated on a 25 m Carbosieve SII column and detected by thermal conductivity.

The conversion levels reported refer to conversion of oxygenates (methanol and dimethyl ether) to hydrocarbons because the conversion of methanol to dimethyl ether takes place readily and, therefore, dimethyl ether is considered part of the feed. Product selectivities varied as the catalyst deactivated and, as a result, the

selectivities reported are the average selectivities for oxygenate conversion levels above 90% for the SAPO-34 catalysts and above 50% for the mordenite catalysts (due to the short duration of the mordenite runs).

Conversion levels and hydrocarbon selectivities were calculated as percentages according to :

Oxygenate conversion = $M_{MP}/M_{MF}x100$

M_{MP} = mass of methanol required for the formation of the hydrocarbon product spectrum (i.e. excluding MeOH and DME)

M_{MF} = mass of methanol required for the formation of the entire sample spectrum (i.e. including MeOH and DME)

Individual hydrocarbon selectivity $S_H = M_H/M_{TH}x100$

M_H = mass of hydrocarbon of interest

M_{TH} = total mass of hydrocarbons

C_2/C_3 olefin ratio = S_E/S_P

S_E = selectivity to ethene (wt%)

S_P = selectivity to propene (wt%)

C_2-C_4 olefin selectivity (light olefins) = $S_E+S_P+S_B$

S_E = selectivity to ethene (wt%)

S_P = selectivity to propene (wt%)

S_B = selectivity to butene (wt%)

A typical hydrocarbon product spectrum for the conversion of methanol to olefins over SAPO-34 is as follows (taken from the 2nd sample of Run SG6, data in Appendix V) :

Methane	: 0.5 wt%	$CO+CO_2$	: 0.0 wt%
Ethane	: 0.6 wt%	Ethene	: 34.7 wt%
Propane	: 1.6 wt%	Propene	: 39.6 wt%
Butane	: 0.0 wt%	Butene	: 14.5 wt%
C5 HCs	: 5.7 wt%	C6+ HCs	: 2.8 wt%
C_2-C_4 Ol.	: 88.8 wt%	C_2/C_3 Ol.	: 0.88

Catalyst performance is generally compared as a function of catalyst utilization value (CUV), which, for the MTO reaction, is defined as the mass of methanol converted to hydrocarbons (i.e. excluding dimethyl ether) before the oxygenate conversion level drops below 50% of the maximum oxygenate conversion level for that particular run.

Catalyst lifetime is defined as the time it takes for the oxygenate conversion level to drop below 50% of the maximum oxygenate conversion level for that particular run.

Detailed calculations of the conversion levels, CUVs and selectivities are shown in Appendix I.

2.3.2 Propene oligomerization

Equipment

The reactor in which the oligomerization studies were carried out is shown in Figure 2.3. The system consisted of a high pressure fixed bed stainless steel reactor into which a propene/propane mixture (obtained from SASOL, containing approximately 87% propene) was fed at a weight hourly space velocity (WHSV) of 11-13 h^{-1} using a high pressure diaphragm pump (Lewa type FLM1). The propene/propane feed was fed from a 5 kg gas cylinder through a fixed bed of 3A molecular sieve (in order to remove any water present) and then cooled to below 10°C before reaching the inlet of the diaphragm pump. The product line between the reactor and the back-pressure regulator was heated to 70°C. The liquid product was collected in a glass catchpot maintained at 27°C and the gas product was passed through a gas sampling valve and a wet-gas flowmeter, and then vented to the atmosphere.

Conditions and procedure

The different catalyst samples were run at identical reaction conditions. The mass of catalyst used in each experiment was 1 g and the catalyst samples were calcined in air (60 ml/minute) at 400°C for 8-10 hours. After calcination, the reactor was cooled to 150°C under flowing nitrogen (60 ml/minute) and the reactor system pressurized to 5 MPa. The feed was pumped through the reactor by-pass until a uniform flow rate was obtained, at which time the feed stream was switched from the reactor by-pass back through the reactor. The reactor temperature was slowly ramped to 200°C (approximately 2°C/minute) in order to prevent temperature runaways. The reactor temperature was held at 200°C until the first drop of liquid was collected, this being taken as the beginning of the run. The run procedure used thereafter, was as follows :

Maintain 200°C	(1 hour),	Ramp to 250°C	(1 hour)
Maintain 250°C	(1 hour),	Ramp to 300°C	(1 hour)
Maintain 300°C	(1 hour),	Ramp to 350°C	(1 hour)
Maintain 350°C	(1 hour),	Maintain 350°C	(1 hour)

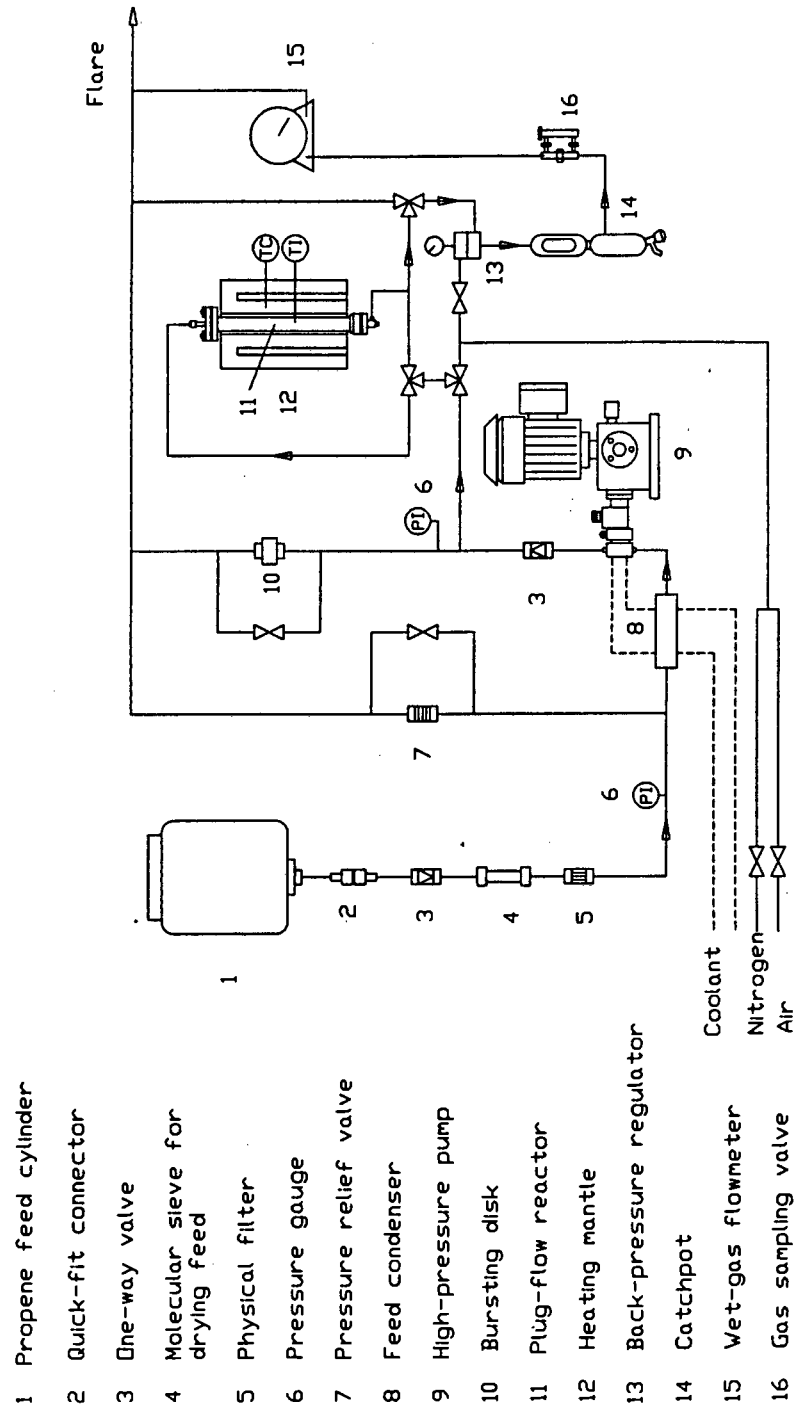

Figure 2.3 : Schematic of high-pressure oligomerization rig.

The liquid products were sampled every hour, the initial sample being the first drop of liquid that was formed and the remaining samples being taken by emptying the catchpot every hour thereafter, thereby obtaining the average liquid product spectrum produced over the preceding hour. The first gas sample was taken 30 minutes after the run was started and then every 60 minutes thereafter.

Product analysis and data work-up

The liquid and gas phase reaction products were analyzed, respectively, using a 30 m megabore column with a DB1 coating and a 2 m stainless steel column with an OV101 packing using a flame ionization detector.

Conversion levels for the propene oligomerization reaction are reported as conversion to liquid product :

% Conversion = $(M_L/M_F)x100$

M_L : mass of liquid product collected over the preceding hour

M_F : mass of feed passing through catalyst bed over the preceding hour

C_{9+} selectivity = $(M_{9+}/M_{HC})x100$

M_{9+} : mass of hydrocarbons containing 9 or more carbon atoms

M_{HC} : mass of liquid hydrocarbon product

C_{12+} selectivity (diesel type product) = $(M_{12+}/M_{HC})x100$

M_{12+} : mass of hydrocarbons containing 12 or more carbon atoms

M_{HC} : mass of liquid hydrocarbon product

A typical liquid propene oligomerization hydrocarbon product spectrum is as follows :

Propane	: 0.0 wt%	Propene	: 0.01 wt%
C_4 HCs	: 4.2 wt%	C_5 HCs	: 0.7 wt%
C_5-C_8 HCs	: 36.1 wt%	C_9-C_{11} HCs	: 30.4 wt%
C_{12}-C_{14} HCs	: 18.3 wt%	C_{15}-C_{20} HCs	: 2.3 wt%
C_{21}+ HCs	: 0.01 wt%		

A commercially obtained diesel fuel was analyzed as being 99% C_{9+} and 95% C_{12+}. The GC spectrum of this product as well as detailed calculations of product selectivities and conversion levels are shown in Appendix II.

Catalyst performance is generally compared as a function of catalyst utilization value (CUV), which, for the propene oligomerization reaction, is defined as the mass of liquid product produced per gram of catalyst during the first three hours of the run (the amount of liquid produced before the reaction temperature is ramped to 350°C).

2.4 ERROR ANALYSIS

Due to the number and length of many of the analysis techniques, a statistical error analysis was not possible. Taking into account the accuracy of the equipment used and the reproducibility of the measurements taken, the error in the various characterization data listed below is a non-statistical estimation made by the author.

Measurement	Units	Technique	%Error
Total Al_2O_3 (SAPO)	wt%	XRF	5
Total SiO_2 (SAPO)	wt%	XRF	5
Total P (SAPO)	wt%	XRF	5
Total Ni, Co (SAPO)	wt%	XRF	10
Total Al (mord.)	wt%	AA	3
Al^{IV} (mord.)	wt%	^{27}Al MAS NMR	10
Al^{IV} peak width (mord.)	ppm	^{27}Al MAS NMR	15
Water content (mord.)	wt%	TGDTA	5
Cyclohex. ads. (mord.)	wt%	TGDTA	5
Crystallinity (SAPO)	ratio	XRD	15
Crystallinity (mord.)	ratio	XRD	5
NH_3 TPD peak temp.	°C	TPD	5°C
NH_3 TPD peak conc.	mmol/g	TPD	7
IR T-O position	1/cm	FTIR	2 cm^{-1}
Unit cell length	Å	XRD	0.01 Å
Unit cell volume	$Å^3$	XRD	5 $Å^3$
Surface area	m^2/g	BET	10

Table 2.3 : %Error in catalyst characterization measurements.

The percentage error in the various MTO reaction data has been estimated as follows :

Measurement	Units	%Error
CUV (SAPO)	g/g cat.	5
CUV (mord.)	g/g cat.	10
Lifetime (SAPO)	hours	5
Lifetime (mord.)	hours	10

Table 2.4 : %Error in MTO activity data.

Considering the initial variation in hydrocarbon selectivities, the percentage error in the various MTO reaction data has been estimated as follows :

Measurement	Units	%Error
Methane (SAPO)	wt%	3
Methane (mord.)	wt%	5
C_2-C_4 olefins (SAPO)	wt%	3
C_2-C_4 olefins (mord.)	wt%	20
C_2/C_3 olefins (SAPO)	ratio	3
C_2/C_3 olefins (mord.)	ratio	10
Coke (SAPO)	g/100 g cat.	10
Coke (mord.)	g/100 g cat.	15

Table 2.5 : %Error in MTO selectivity data.

Taking into account the run reproducibility and the initial variation in hydrocarbon selectivities, the percentage error in the various propene oligomerization reaction data has been estimated as follows :

Measurement	Units	%Error
CUV	g/g cat.	15
C_{9+}	wt%	15
C_{12+}	wt%	15

Table 2.6 : %Error in the oligomerization activity and selectivity data.

Chapter 3

RESULTS

3.1 PHYSICAL AND CHEMICAL CATALYST CHARACTERIZATION

3.1.1 SAPO-34

3.1.1.1 Catalyst composition and morphology

The compositions of the SAPO-34 and MeAPSO-34 materials are presented in Table 3.1. XRD spectra showed that S1 and S2 contained small amounts of SAPO-5, whereas S3, synthesized at 150°C for 133 hours, was essentially pure SAPO-34 (Figure 3.01 (a)) and more crystalline (Table 3.1). The Co1 sample was also highly crystalline and contained no SAPO-5 material (figure 3.01 (b)). The Ni1 catalyst was mostly amorphous, having a relative crystallinity of only 0.33. By increasing the pH of the synthesis gel for Ni2, a product was formed that was completely amorphous, the XRD spectra showing no trace of the SAPO-34 structure or any other crystalline material. By increasing the synthesis time to 133 hours for Ni3, a highly crystalline SAPO-34 product was formed which contained no SAPO-5 material.

The S3* material exhibited a far greater relative crystallinity than the shallow bed calcined S3 (Figure 3.02) and, as a result, all catalyst treatments and modifications were carried out on the S3* catalyst. Generally, there was no difference in the relative crystallinities of the uncalcined and shallow bed calcined material, indicating that shallow bed calcination results in detemplation only and not crystallographic modification. Of the modified samples, the S3*-BRN sample was mostly amorphous and the S3*-ACD and S3*-CAU samples were completely amorphous. S3*-SIL and S3*-STM samples retained the SAPO-34 structure but their relative crystallinities were significantly reduced in comparison to the S3* sample. The relative crystallinity of S3*-AMM was unchanged with respect to that of S3*. XRD patterns of all the SAPO-34 and MeAPSO-34 catalysts are shown in Appendix III.

Electron micrographs showed that the S1 and S2 materials had very similar morphologies (Figure 3.03). Both samples consisted of 5-50 micron agglomerates composed of small angular crystals in the shape of platelets, approximately 0.2 microns thick and 1-2 microns across in the case of the S1 material and approximately 0.1 microns thick and 4-6 microns across in the case of the S2

Catalyst	Relative Crystallinity	HTD NH_3 (mmols/g)	Peak temp. (°C)	Al_2O_3 (wt%)	SiO_2 (wt%)	P (wt%)	Ni/Co (wt%)
% Error	15	7	5°C	5	5	5	10
S1	0.59	0.18	363	27.5	0.4	40.3	-
S2	0.87	0.26	377	35.5	0.5	21.8	-
S3	1.00	0.38	393	36.6	0.4	28.2	-
Co1	1.34	0.21	380	34.9	0.4	31.7	1.7
Ni1	0.33	0.06	357	40.1	1.6	15.9	0.7
Ni2	0.00	0.00	-	33.0	0.4	30.2	2.4
Ni3	1.32	0.37	360	31.1	2.5	41.4	0.5
S3*	1.86	0.46	388	-	-	-	-
S3*-AMM	1.86	0.40	383	-	-	-	-
S3*-SIL	0.68	0.36	388	-	-	-	-
S3*-STM	0.71	0.32	360	-	-	-	-
S3*-BRN	0.24	0.05	-	-	-	-	-
S3*-ACD	0.00	0.00	-	-	-	-	-
S3*-CAU	0.00	0.00	-	-	-	-	-

Table 3.1 : Catalyst crystallinity, acidity and bulk (total) compositions of SAPO-34 catalysts.

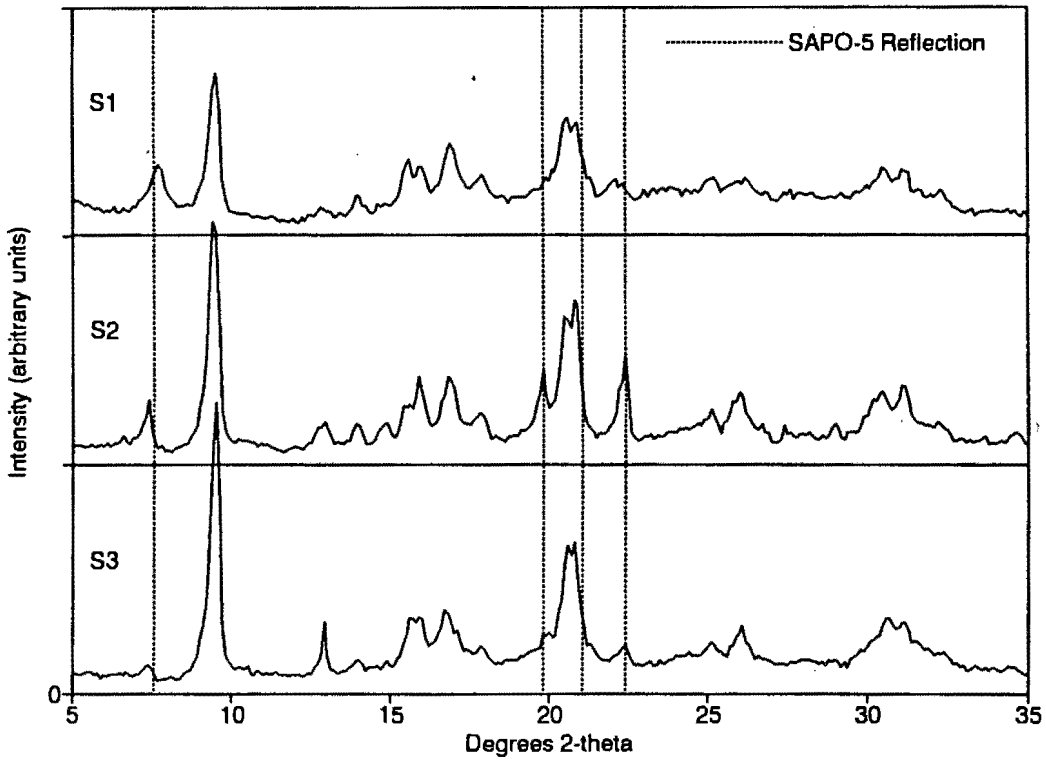

Figure 3.01 (a) : XRD patterns of S1, S2 and S3.

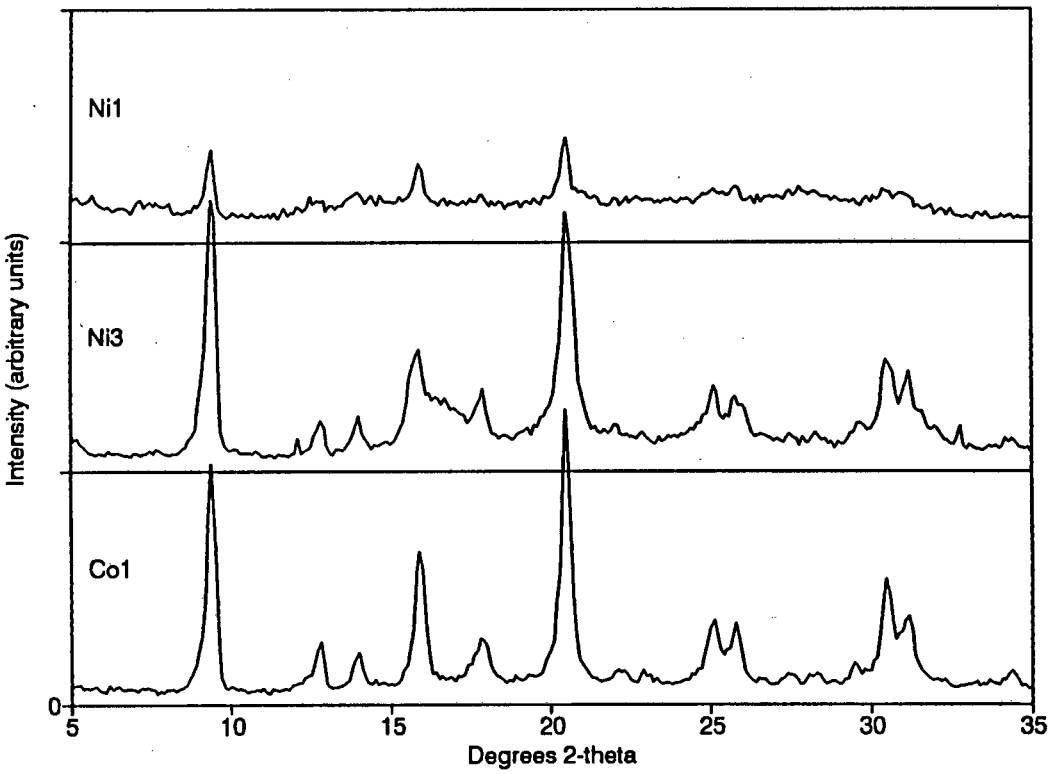

Figure 3.01 (b) : XRD patterns of Ni1, Ni3 and Co1.

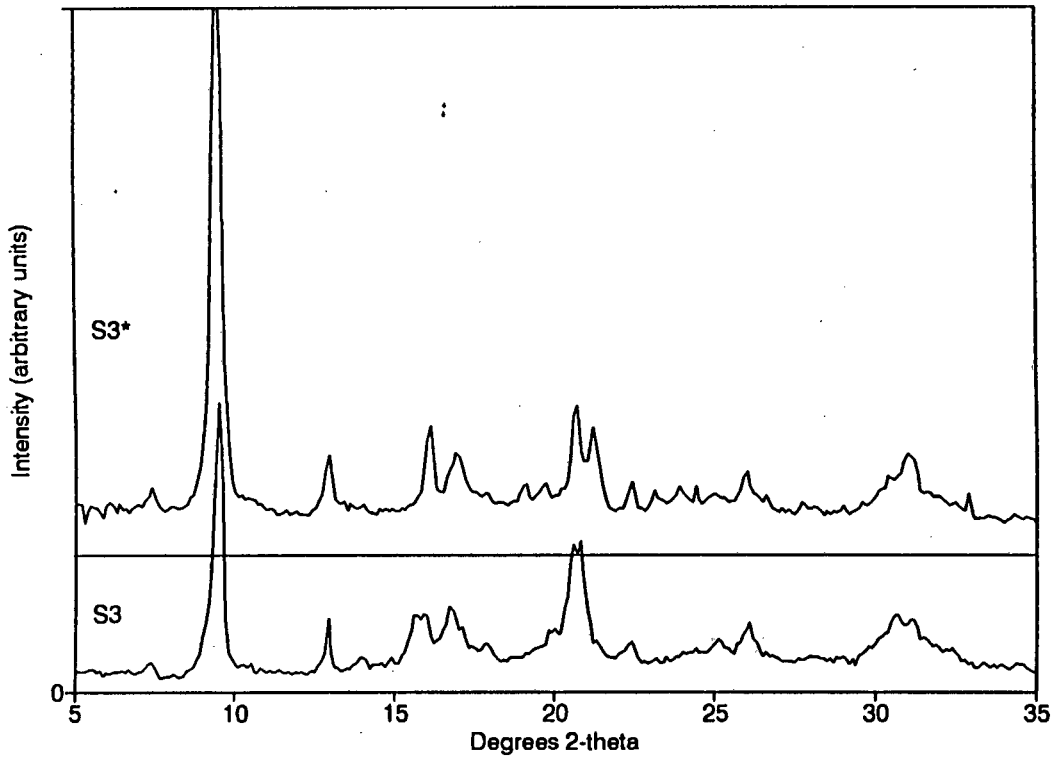

Figure 3.02 : XRD patterns of S3 and S3*.

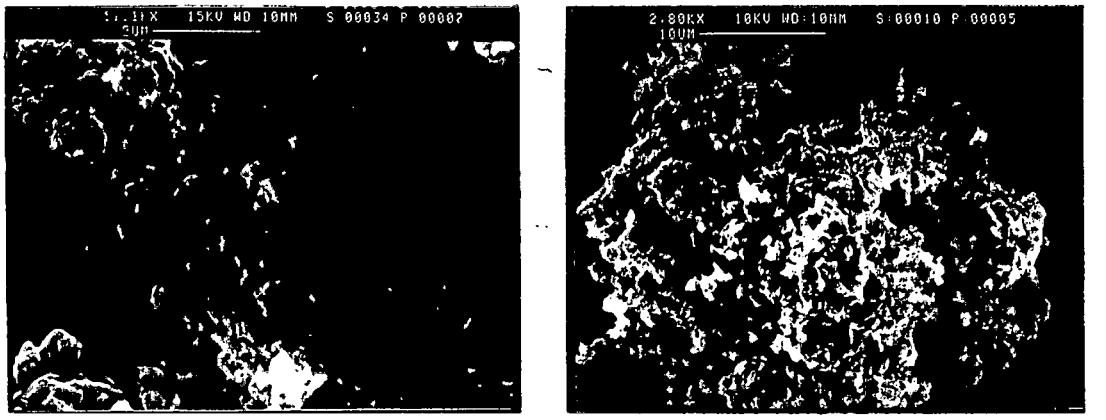

Figure 3.03 (a) : Electron micrographs of S1 and S2.

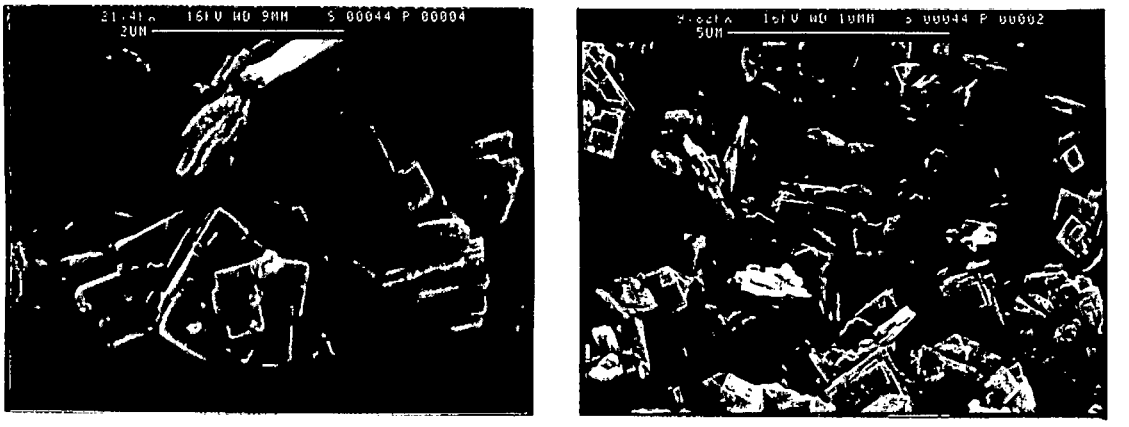

Figure 3.03 (b) : Electron micrographs of S3.

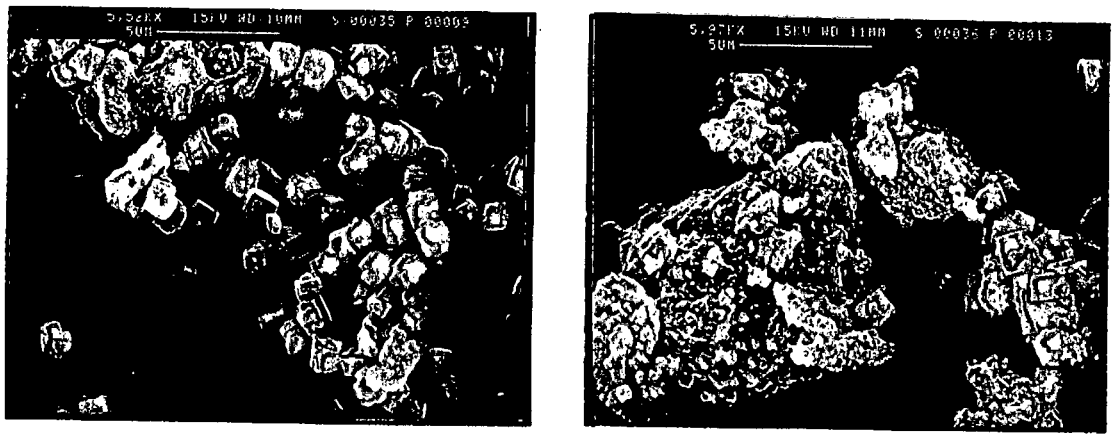

Figure 3.04 (a) : Electron micrographs of Co1 and Ni1.

Figure 3.04 (b) : Electron micrographs of Ni2 and Ni3.

material. The S3 material consisted of 5-50 micron agglomerates composed of small rectangular platelets, 0.2 microns thick with sides 1-2 microns in length, which were often stacked or intergrown. The Co1 crystals were cubic in shape with sides approximately 1 micron in length. Co1 consisted mostly of individual crystals, no large agglomerates being present. Electron micrographs of the Ni1 sample showed mostly amorphous material, throughout which approximately cubic crystals were distributed. These crystals had sides of between 1 micron and 5 microns in length. No crystalline material was seen in the electron micrographs of the Ni2 material (Figure 3.04). The Ni3 material was almost identical to S3 in appearance.

Of the modified S3* samples, the S3*-AMM, S3*-BRN, S3*-STM, S3* and S3*-SIL samples underwent no noticeable morphological change whereas the S3*-ACD and S3*-CAU samples contained no material that was crystalline in appearance.

3.1.1.2 Catalyst acidity

The ammonia TPD spectra of the SAPO-34 and MeAPSO-34 materials generally exhibited two characteristic peaks, a low temperature desorption (LTD) peak between 195°C and 244°C and a high temperature desorption (HTD) peak between 324°C and 380°C. The reproducibility of the concentrations measured for the HTD sites was within 7% of the HTD desorption concentration, and the reproducibility of the peak maximum temperatures was within 5°C. Of the two desorption peaks generated in the NH_3 TPD experiments, only the high temperature desorption (HTD) peak is indicative of strong acidity [Meyers et al., 1988; Sawa et al., 1989]. The size of the low temperature desorption (LTD) peak varies with desorption time prior to the temperature ramp, crystallite size and sample type and is generally indicative of physisorbed NH_3. Almost complete removal of the LTD peak may be achieved by prolonged ammonia desorption prior to the temperature ramp although desorption times in excess of 48 hours are necessary. The three batches of SAPO-34, viz. S1, S2 and S3, exhibited quite different amounts of strong acidity, varying from 0.18 mmols/g to 0.38 mmols/g of catalyst. The Co1 material possessed a similar amount of strong acidity to S1 and the strong acidity of NiAPSO-34 samples varied from 0 mmols/g for Ni2 to 0.36 mmols/g for Ni3.

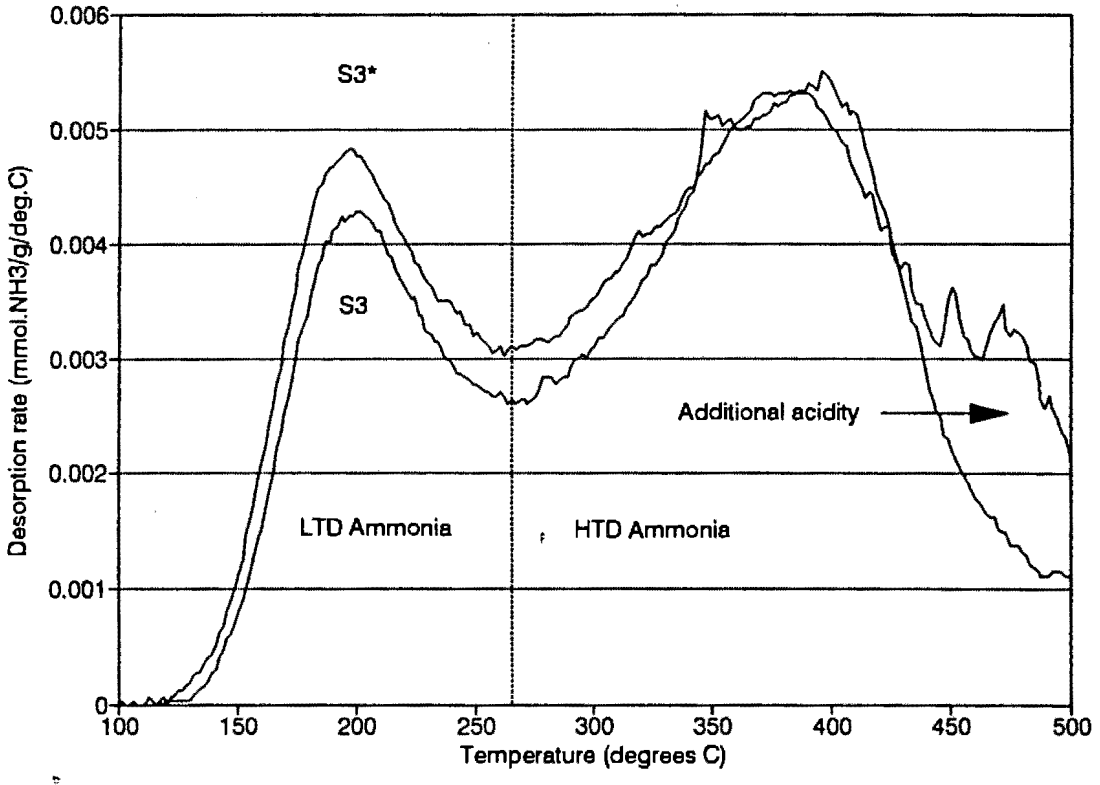

Figure 3.05 : Ammonia TPD spectra of S3 and S3*.

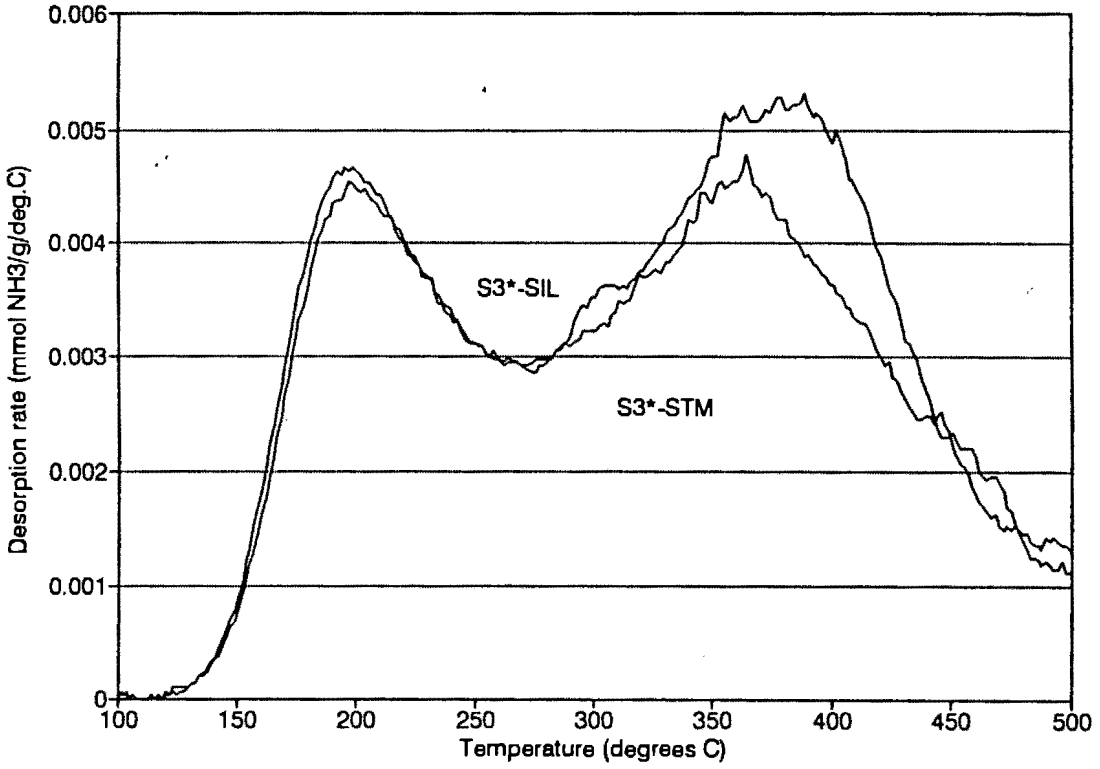

Figure 3.06 : Ammonia TPD spectra of S3*-SIL and S3*-STM.

The S3* sample possessed a greater amount of strong acidity than any of the catalysts investigated (Table 3.1), differing from the unmodified catalyst (S3) by the presence of additional strong acidity from which NH_3 was desorbed at approximately 480°C (Figure 3.05). Further modification (S3*-SIL, S3*-STM, S3*-AMM) gave rise to reduced acidity and the disappearance of the additional strong acidity formed upon deep bed calcination (Figure 3.06). Hydrothermal treatment (S3*-STM) resulted in a large drop in the number of strong acid sites and the S3*-BRN, S3*-ACD and S3*-CAU samples retained no strong acidity whatsoever.

3.1.1.3 Location of transition metals

Back-exchanging the transition metal catalysts with ammonium nitrate for 10 hours at reflux conditions removed 12% of the cobalt from the Co1 material and 33% of the nickel from the Ni3 material (data in Table 3.1 gives MeAPSO-34 compositions before ion exchange). Further back-exchanging removed only traces of cobalt from the Co1 material suggesting that much of the cobalt is non-exchangeable and therefore extremely tightly bound or possibly located in the SAPO-34 framework. The TPR spectra of the non-ion exchanged Co1 sample showed reduction taking place at approximately 600-650°C, the hydrogen consumption being 0.19 mmols/g of catalyst (indicating a reduction of 65% of the total cobalt present). The hydrogen consumption would account for the reduction of all non-framework cobalt and a significant amount of framework cobalt which may be extracted during the detemplation procedure [Goepper et al., 1989] and the remaining cobalt which is unaccounted for is most likely located in the SAPO-34 framework.

There was very little nickel in the Ni3 sample (0.5 wt %) and although the calculated amount of nickel removed was approximately 0.2 wt %, the experimental error of both these measurements is approximately 0.1 wt %. This makes the estimation of the amount of non-exchangeable nickel very difficult. Similar difficulties were encountered with the TPR analyses which showed that all the nickel that was present in the non-ion-exchanged Ni3, was either in the SAPO-34 framework or in the form of nickel metal (unlikely since the catalyst was calcined in air). The nickel content of the sample was so low, however, that it may have been below the detection limits of the atomic absorption equipment.

3.1.2 MORDENITE

3.1.2.1 Catalyst composition and morphology

The sodium forms of the MN, M1 and M2 samples had approximately the same aluminium content. With the exception of M2-2AW (0.3% sodium), only trace quantities of sodium were found in the -2AW, -2AR and -4AR forms of the MN, M1 and M2 samples whereas the -A1 and -A2 samples contained between 0.5% and 1% sodium. After undergoing identical dealumination procedures it was found that the MN, M1 and M2 mordenite materials retained vastly different aluminium contents (Table 3.2). In the case of the M1 mordenite, the aluminium content was reduced by 85% during the first refluxing procedure (M1-2AR) and further refluxing reduced the aluminium content by only an additional 1% of the original amount. In contrast, the MN and M2 materials retained much higher aluminium levels even after 4 acid refluxing cycles. From these results it is apparent that dealumination may reach a limit after removal of approximately 7/8 of the initial aluminium content. Removal of the remaining 1/8 of the aluminium, corresponding to approximately 1 aluminium per unit cell, may require more severe dealumination conditions. It is apparent from the characterization data of the M1-2AR/-4AR and the M1-2AR(NH3)/-4AR(NH3) samples that the type of cation present (Na^+ or NH_4^+) in the mordenite samples did not affect the dealumination characteristics of these samples.

The framework aluminium is generally taken as the tetrahedral aluminium as determined by ^{27}Al MAS NMR [van Geem et al., 1988; Goovaerts et al., 1989; Sawa et al., 1990], the results of which are shown in Table 3.2. Fernandez et al. [1988] found that the ratio of (octahedral aluminium)/(tetrahedral aluminium) ^{27}Al NMR peak intensities increased as the pulse angle was increased and proposed that the relative concentrations of these species should be determined at very low pulse angles. However, for pulse angles up to 30°, the reported variation in the (tetrahedral aluminium)/(total aluminium) ratio for dealuminated mordenite is less than 10% [Fernandez et al., 1988]. Due to the low aluminium content of the severely dealuminated samples, a pulse angle of 30° was required in this study in order to obtain adequate signal intensities. For the above reason, the tetrahedral aluminium contents reported in Tables 3.2 and 3.3 are subject to an error margin of approximately 10%.

Catalyst	Al Cont. (wt%)	Al^{IV} Cont. (wt%)	Al^{IV} Si/Al	^{27}Al NMR Al^{VI} width (ppm)	Water Cont. (wt%)	LTD TPD Peak Temp. (°C)	LTD TPD Peak NH_3 (mmol/g)	HTD TPD Peak Temp. (°C)	HTD TPD Peak NH_3 (mmol/g)
Error *	3%	10%	10%	15%	5%	5°C	7%	5°C	7%
MN-Na	6.17	6.09	-	16.0	0.123	-	-	-	-
MN- H	6.34	6.19	6.2	12.8	0.108	229	0.91	615	1.77
MN-A1	6.32	5.95	6.5	25.4	0.124	231	0.94	590	1.73
MN-A2	6.03	5.52	7.0	23.9	0.125	225	0.94	598	1.92
MN-2AW	5.82	4.19	9.3	14.8	0.152	244	1.05	600	1.65
MN-2AR	4.88	3.02	13.0	5.1	0.140	236	0.80	597	1.14
MN-4AR	3.54	2.30	17.3	4.2	0.130	223	0.67	595	0.87
ZM510	4.01	3.17	12.5	7.9	0.121	226	0.85	622	1.05
ZM760	1.08	0.77	52.7	2.7	0.089	199	0.18	570	0.32
ZM980	0.52	0.43	95.7	4.0	0.059	194	0.09	554	0.12
M1-Na	6.50	6.50	-	-	0.129	-	-	-	-
M1- H	6.73	6.53	5.9	13.1	0.122	236	0.99	626	2.20
M1-A1	6.42	5.88	6.5	17.4	0.130	229	1.06	578	2.07
M1-A2	6.45	5.44	7.1	15.2	0.142	228	0.87	600	2.15
M1-2AW	6.08	3.89	9.9	4.8	0.143	235	1.03	601	1.71
M1-2AR	0.92	0.85	47.8	3.2	0.115	-	-	-	-
M1-4AR	0.87	0.85	47.9	2.7	0.104	203	0.28	590	0.37
M1-2AR(NH3)	0.91	0.89	45.9	3.4	0.095	204	0.28	595	0.35
M1-4AR(NH3)	0.87	0.86	47.7	2.9	0.075	204	0.27	591	0.29
M2-Na	6.41	6.41	-	-	0.116	-	-	-	-
M2- H	6.70	5.89	6.5	13.3	0.118	227	0.63	600	1.66
M2-A1	6.12	5.42	7.1	19.8	0.116	226	0.71	559	1.54
M2-A2	6.09	5.21	7.4	16.6	0.110	228	0.62	580	1.52
M2-2AW	6.40	4.96	8.1	13.0	0.132	223	0.57	587	1.70
M2-2AR	4.17	3.21	12.3	7.8	0.140	233	0.69	606	0.95
M2-4AR	2.77	2.33	17.2	9.3	0.125	215	0.48	590	0.58

Table 3.2 : Mordenite composition and TPD data.

* When listed as %; error is a percentage of the value given in the Table.

MN-H contained 98% tetrahedral aluminium, this value dropping on initial acid refluxing to 62% and then increasing slightly to 65% for MN-4AR. The octahedral resonance of MN-2AW was very broad but narrowed considerably for the refluxed samples (Table 3.2). The ZM samples contained between 72% and 82% of their aluminium in the tetrahedral form. The octahedral resonance of ZM510 was relatively broad, whereas this peak for ZM760 and ZM980 was much sharper. The sodium forms of M1 and M2 contained no octahedral aluminium. After both reflux

Catalyst	Al^{IV} Cont. (wt%)	Infrared T-O band (cm^{-1})	Cyclohexane Adsorbtion (wt%)	Unit cell parameters a	b	c (Angstroms)	Unit Cell Volume ($Å^3$)	Rel. Cryst. (%)	Surface Area (m^2/g)
Error *	3%	2 cm^{-1}	5%	0.01 Angstroms			5$Å^3$	5%	10%
MN-Na	6.09	1044	8.8	18.16	20.54	7.52	2805	91	-
MN- H	6.19	1069	7.6	18.22	20.40	7.50	2787	88	396
MN-A1	5.95	1074	8.5	18.14	20.53	7.50	2792	87	-
MN-A2	5.52	1075	9.1	18.19	20.47	7.49	2789	94	-
MN-2AW	4.19	1080	7.6	18.20	20.35	7.50	2777	86	369
MN-2AR	3.02	1080	7.1	18.16	20.26	7.48	2752	85	372
MN-4AR	2.30	1083	6.7	18.14	20.23	7.47	2741	79	489
ZM510	3.17	1080	6.4	18.18	20.38	7.47	2767	81	410
ZM760	0.77	1086	6.2	18.18	20.40	7.48	2774	97	495
ZM980	0.43	1089	5.6	18.18	20.38	7.48	2771	100	489
M1-Na	6.50	1045	9.3	18.18	20.59	7.54	2822	84	-
M1- H	6.53	1059	9.1	18.24	20.37	7.51	2790	75	450
M1-A1	5.88	1058	9.7	18.23	20.45	7.50	2796	76	-
M1-A2	5.44	1062	10.2	18.26	20.49	7.50	2806	71	-
M1-2AW	3.89	1060	9.2	18.22	20.35	7.51	2784	71	375
M1-2AR	0.85	-	4.9	18.09	20.12	7.42	2700	63	446
M1-4AR	0.85	-	4.1	18.10	20.21	7.44	2721	72	485
M1-2AR(NH3)	0.89	1086	5.0	18.05	20.03	7.41	2679	65	453
M1-4AR(NH3)	0.86	1085	3.5	18.07	20.17	7.43	2708	73	449
M2-Na	6.41	1044	7.0	18.20	20.59	7.53	2821	75	-
M2- H	5.68	1072	6.8	18.17	20.33	7.49	2766	60	-
M2-A1	5.42	1074	7.5	18.20	20.52	7.50	2801	69	-
M2-A2	5.21	1074	7.7	18.20	20.52	7.50	2801	73	-
M2-2AW	4.78	1077	7.3	18.14	20.28	7.49	2755	59	-
M2-2AR	3.21	1083	6.6	18.15	20.26	7.48	2790	51	354
M2-4AR	2.33	1084	6.2	18.12	20.28	7.46	2741	57	378

Table 3.3 : Mordenite crystallographic data, cyclohexane adsorption levels and surface areas.

* When listed as %; error is a percentage of the value given in the Table.

procedures, the percentage aluminium exhibiting tetrahedral co-ordination in the M1 mordenite had increased from 64% for M1-2AW to 98% for M1-4AR whereas in the case of M2-4AR this was only 84%. The octahedral resonances of the acid-treated M1 samples were quite narrow, especially those of the refluxed samples while those of the acid-treated M2 samples were broader.

X-ray diffraction (XRD) patterns of all the samples showed that the catalyst samples

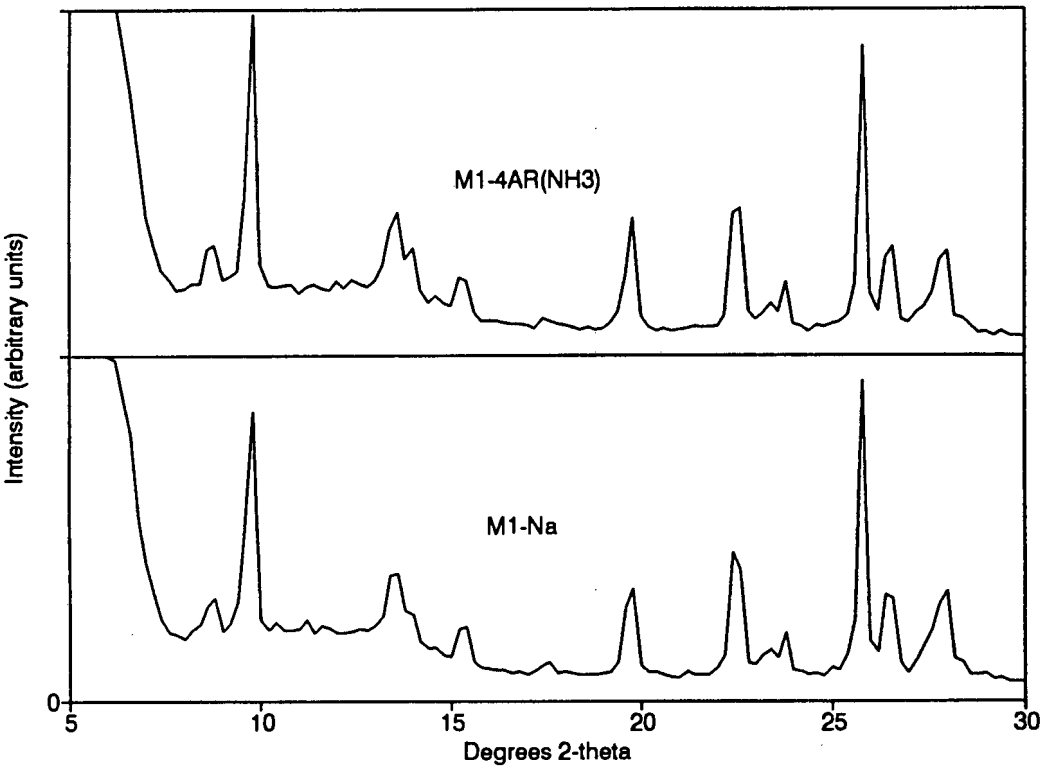

Figure 3.07 : XRD patterns of M1-Na and M1-4AR(NH3).

maintained the mordenite crystal structure throughout all of the acid treatments. This is clearly demonstrated in Figure 3.07 where the XRD pattern of the most severely dealuminated sample, that of M1-4AR(NH3), is compared to the parent sodium form of the M1 catalyst. As can be seen from these XRD patterns, no other crystalline phases are present along with the M1 mordenite material. A computer generated XRD pattern for mordenite is shown in Appendix III along with the XRD patterns of the ZM samples and the parent sodium forms of the MN, M1 and M2 mordenites.

The unit cell volumes listed in Table 3.3 were calculated from the lattice constants a, b and c. Generally, the unit cell volumes of MN, M1 and M2 decreased on dealumination. The unit cell volumes of the ZM samples were essentially the same. The length of the c axis did not vary significantly between catalyst samples, the most significant changes taking place in the direction of the b axis. The one exception to this is the increase in unit cell volume seen for the M1-4AR and M1-4AR(NH3) samples. That this increase was seen for both of these samples

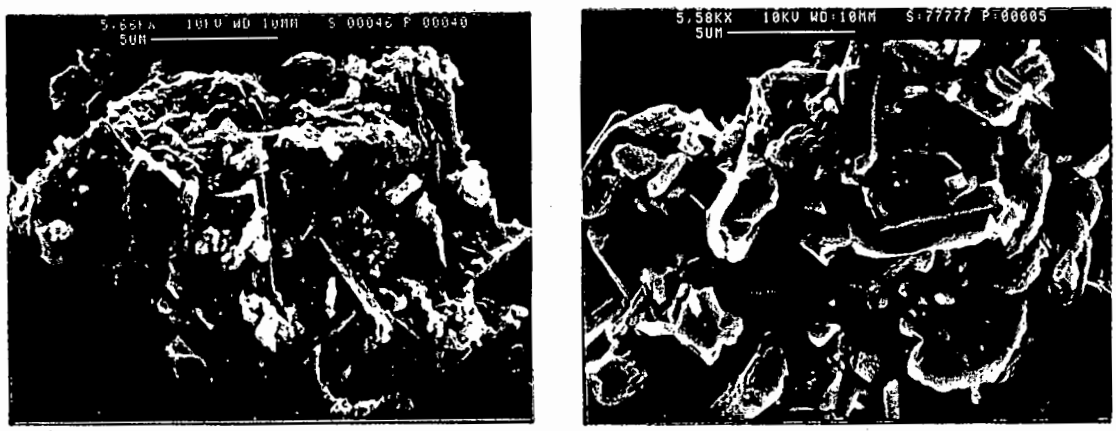

Figure 3.08 (a) : Electron micrographs of MN and ZM mordenites.

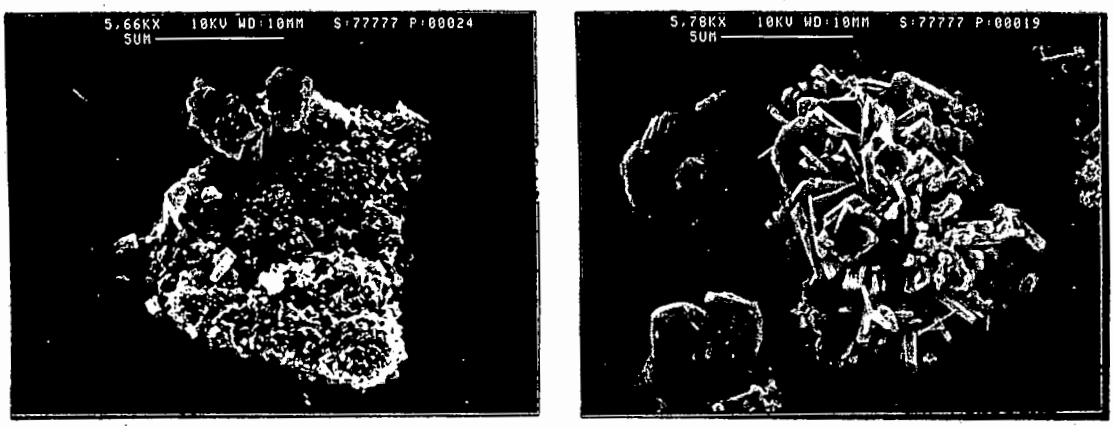

Figure 3.08 (b) : Electron micrographs of M1 and M2 mordenites.

shows that there are definite crystallographic changes taking place during acid treatment even though there is little change in the aluminium content of these samples.

The relative crystallinities of the M2 samples were noticeably lower than those of the other samples (Table 3.3). The ZM samples had the highest percentage crystallinities. The relative crystallinities of the ZM samples increased with decreasing aluminium content whereas those of the MN, M1 and M2 samples generally decreased. As with the unit cell volumes of the M1-4AR and M1-4AR(NH3) samples, the relative crystallinities of both of these samples increased significantly after the second refluxing procedure.

Electron microscopy showed that the catalyst crystallite sizes and morphologies varied considerably from one catalyst to another (Figure 3.08). The MN samples consisted of 10-30 micron intergrown crystals. The ZM samples consisted of 10-50 micron agglomerates of 1-5 micron crystals, some of which are intergrown. The M1 samples consisted of 3-10 micron agglomerates of 0.1-0.5 micron crystals which were uniform in size and shape.

The M2 mordenite consisted of two different types of agglomerates, both of which were made up of long needle-shaped crystals. The first agglomerate type consisted of tightly packed bundles of crystals about 1 micron long and 0.1 microns in diameter. The second agglomerate type, which made up most of the material, consisted of randomly orientated crystals which were about twice the size of those in the agglomerates of the first type.

None of the morphologies, as described above, were observed to change, even after severe dealumination.

3.1.2.2 Catalyst acidity

The ammonia TPD spectra exhibited two characteristic peaks, a low temperature desorption (LTD) peak between 195°C and 244°C and a high temperature desorption (HTD) peak between 554°C and 626°C. The reproducibility of the concentrations measured for the HTD peaks was within 7% of the HTD desorption concentration and the reproducibility of the peak maximum temperatures was

within 5°C. Figure 3.09 shows the concentration-time profiles of a reproducibility test for the M1-4AR catalyst. The LTD peak is a result of physisorbed NH_3 and NH_3 which has not been flushed from the zeolite pores prior to initiation of the temperature ramp. The size and maximum temperature of this peak are not indicative of the acidic nature of the catalyst. The HTD peak is related to the strong acidity resulting from aluminium in the zeolite framework [Sawa et al., 1989, Meyers et al., 1988]. The peak temperatures and desorption concentrations are listed in Table 3.2.

Figure 3.10 shows the existence of a linear relationship between the number of tetrahedral aluminium species generating acid sites (not tetrahedral aluminium species charged balanced by Na^+ ions) and the amount of ammonia desorbing from these sites (HTD peak) for acid dealuminated samples. After initial dealumination, the peak temperatures of both HTD and LTD peaks decreased with decreasing tetrahedral aluminium content. The MN, M1 and M2 samples containing sodium (the -A1 and -A2 samples) had significantly lower HTD peak temperatures than any of the other mordenite samples. The extent to which the

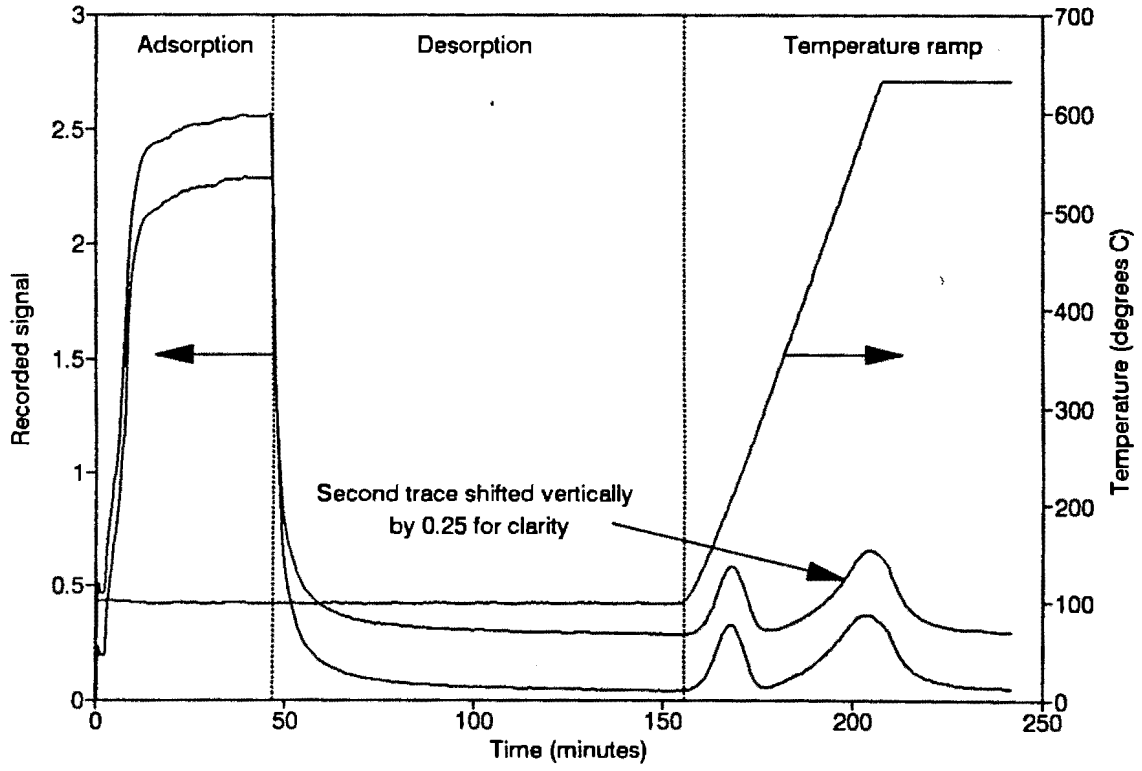

Figure 3.09 : Reproducibility of ammonia TPD profiles for M1-2AR.

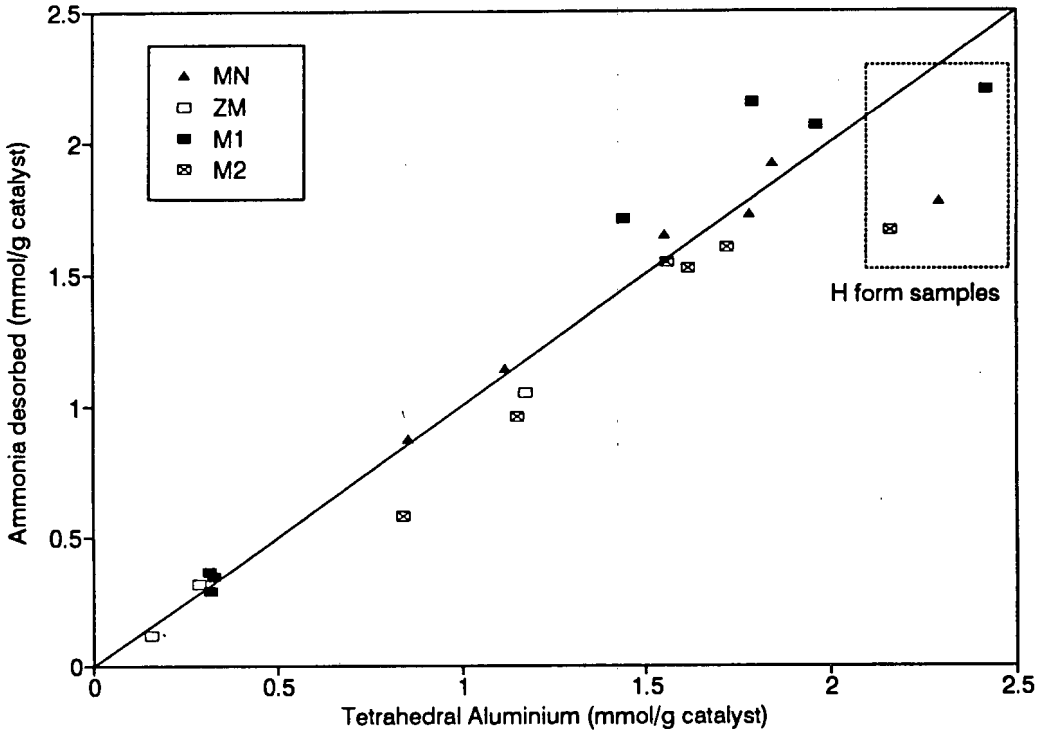

Figure 3.10 : Desorbed ammonia as a function of tetrahedral aluminium concentration.

HTD peak temperature decreased was not the same for the different mordenite samples. The ZM samples showed a large decrease in peak temperature, going from 622°C to 554°C as the framework aluminium content decreased from 3.17 wt% to 0.43 wt%. This was not the case for the MN, M1 or M2 samples where the peak temperature decreased only from 601°C to 591°C as the aluminium content decreased from 3.89 wt% to 0.85 wt%.

3.1.2.3 Catalyst structure

Infrared spectra of the catalyst samples showed that the T-O asymmetric stretching band shifted from 1060 cm^{-1} to 1089 cm^{-1} as the extent of dealumination increased (Table 3.3). The spectra of the ZM samples differed from those of the other mordenites in that the structural bands (400-900 cm^{-1}) were clearly resolved, their resolution increasing as the amount of aluminium in these samples decreased. The 955 cm^{-1} shoulder observed by Dunken and Stephanowitz [1983] and Musa et al. [1987] was not seen in the spectra of any of the ZM samples. This band was not evident in the spectra of the sodium mordenites but did appear as a slight

shoulder in the spectra of the ammonium exchanged MN, M1 and M2 samples. The intensity of this shoulder increased as the framework aluminium content decreased (Figure 3.11). Infrared spectra of all the mordenite samples are shown in Appendix IV. As can be seen in Figure 3.12, there is a direct relationship between the area under the 955 cm^{-1} shoulder of the MN, M1 and M2 samples and the amount of aluminium removed from the mordenite framework. Calcination of the M1-2AR sample at 650°C and 800°C resulted in no significant reduction of the 955 cm^{-1} shoulder and very little shift in any of the band positions.

The peak intensity at 800 cm^{-1} did not increase on dealumination of the mordenite samples but shifted to slightly higher wavenumbers and became more clearly resolved as the intensity of the 710-750 cm^{-1} band decreased (Figure 3.11). This 800-820 cm^{-1} band was particularly sharp for the ZM samples (Figure 3.13) becoming sharper as the extent of dealumination increased.

The 620-630 cm^{-1} band and the broad band between 710 cm^{-1} and 750 cm^{-1} were seen in all the non-dealuminated samples. On dealumination, the 620-630 cm^{-1}

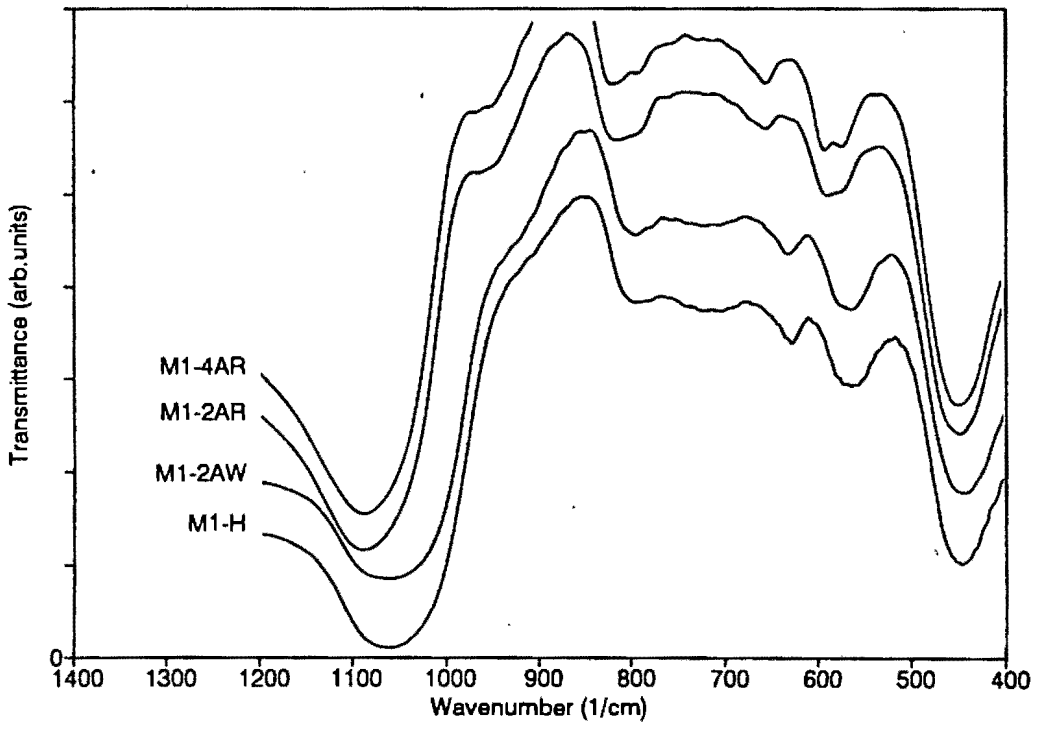

Figure 3.11 : Structural infrared spectra of M1 mordenite at different stages of dealumination.

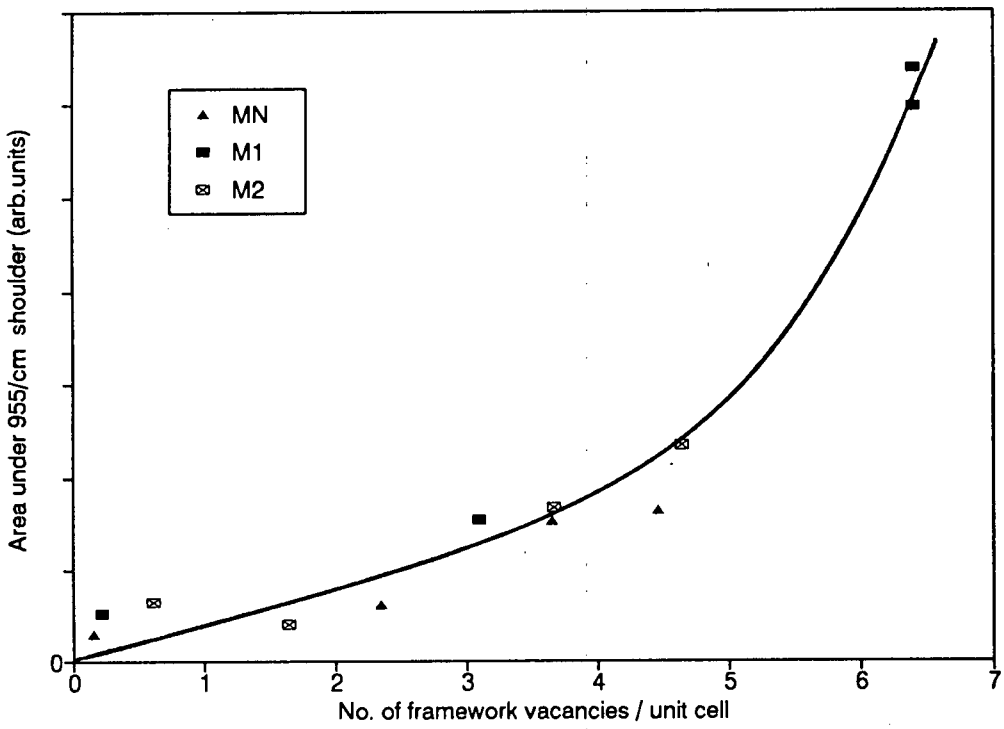

Figure 3.12 : Area of the 955/cm shoulder as a function of the number of framework. vacancies per unit cell.

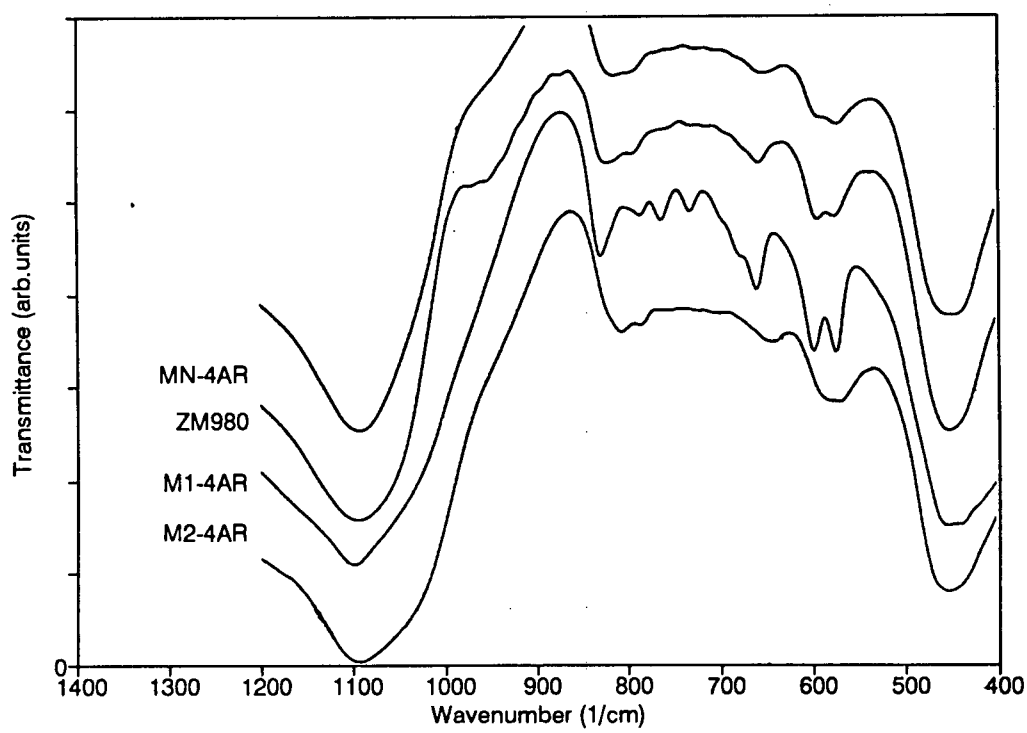

Figure 3.13 : Structural infrared spectra of the most severely dealuminated MN, ZM, M1 and M2 samples.

band shifted to higher wavenumbers but was not significantly reduced whereas the 710-750 cm^{-1} band decreased as the aluminium content of the catalyst samples decreased (Figure 3.11).

3.1.2.4 Porosity and surface area

The cyclohexane adsorption levels that were recorded were reproducible to within 5% (Figure 3.14). It was noted that the sample weight started increasing before the sample had cooled to the adsorption temperature and before the cyclohexane stream replaces the nitrogen stream. This can be seen in Figure 3.14 where the initial slope of the adsorption curve is gradual until the cyclohexane stream replaces the nitrogen stream and the slope becomes sharper. This mass gain is due to the adsorption of cyclohexane which had not been flushed from the system during the catalyst calcination. The resulting cyclohexane adsorption levels were unchanged irrespective of the length of the delay in introducing the cyclohexane stream once the sample had cooled to the adsorption temperature.

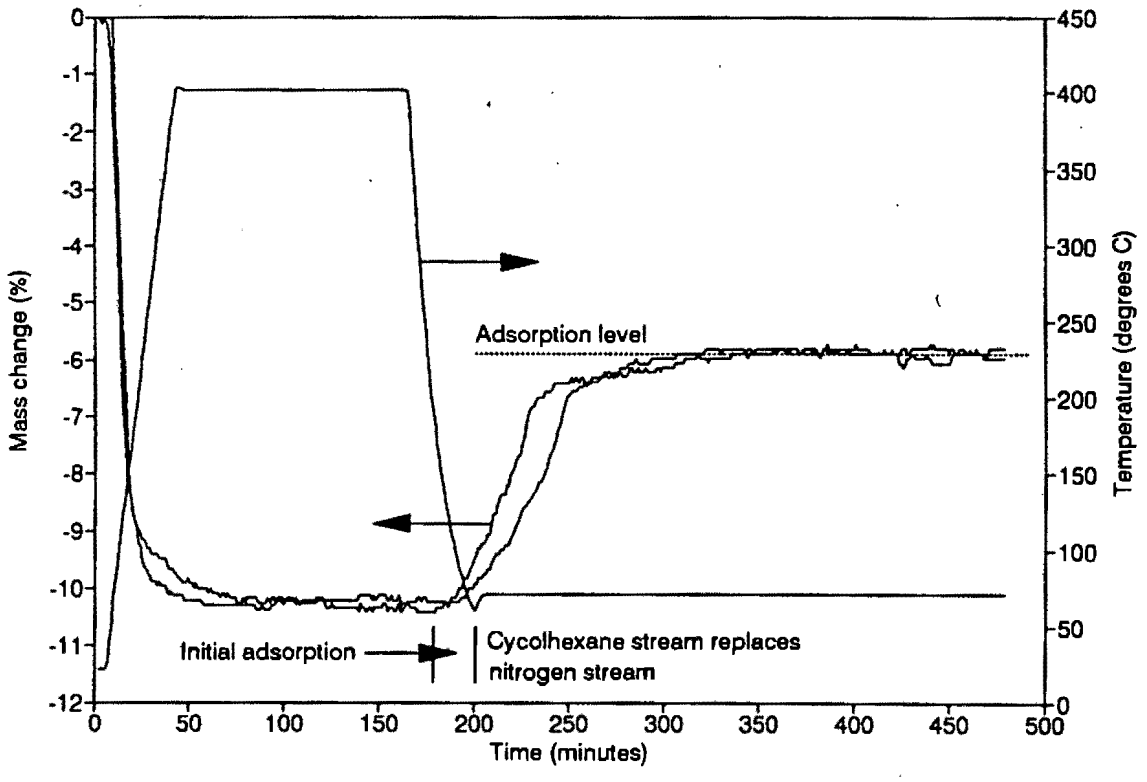

Figure 3.14 : Reproducibility of cyclohexane adsorption level for M1-2AR.

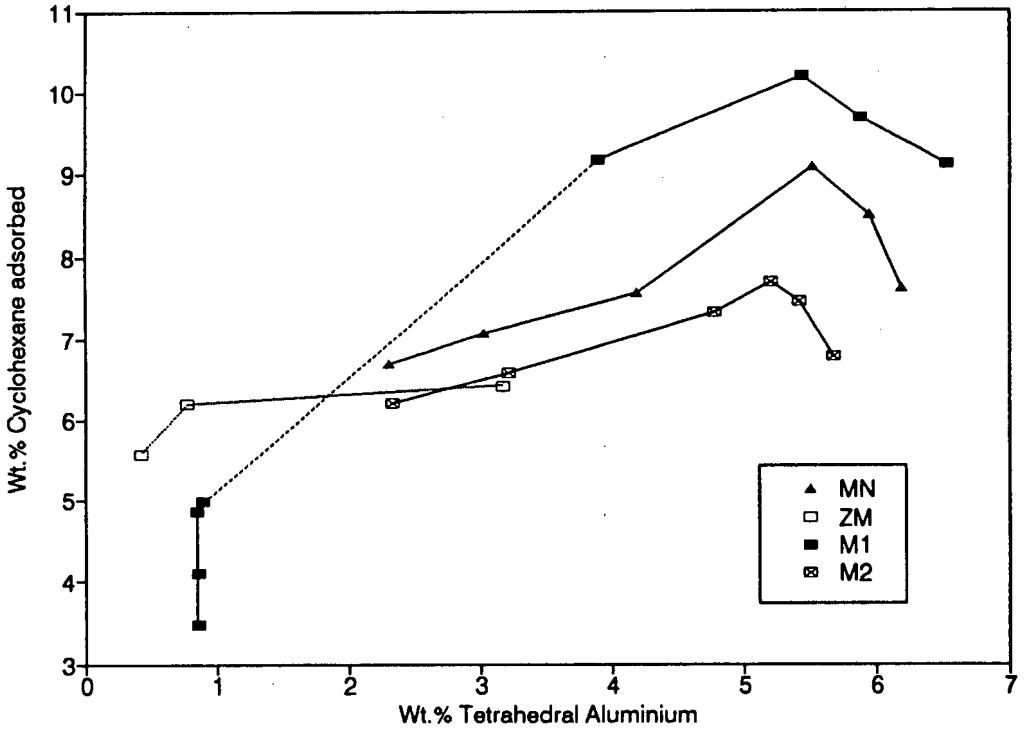

Figure 3.15 : Cyclohexane adsorption levels as a function of tetrahedral aluminium content.

The cyclohexane adsorption levels of the various mordenite samples increased initially and then decreased as the aluminium content of the catalyst decreased due to dealumination (Table 3.3). There are clear differences between the cyclohexane adsorption levels of the MN, M1 and M2 mordenites, the M1 mordenite adsorbing more cyclohexane than the MN and M2 mordenites for equivalent tetrahedral aluminium contents (Figure 3.15). It is also clear that the cyclohexane adsorption levels of the mordenites increase on initial dealumination. The cyclohexane adsorption levels of the M1 samples dropped from 10.2 wt% for M1-6N to 5.1 wt% for M1-2AR. The severely acid-treated sample M1-4AR(NH3) adsorbed only 3.5 wt% cyclohexane although the aluminium content of this catalyst was only slightly less than that of M1-2AR(NH3). A similar trend was seen for the M1-2AR/03 samples. If these adsorption levels were replotted as volume of cyclohexane adsorbed per volume of crystal, backing out the effect of the diminishing unit cell volumes and changes in catalyst density, the trends which are found are the same as those illustrated in Figure 3.15.

The surface areas of all the samples were greater than 350 m^2/g. The surface areas of the mildly acid-treated samples generally decreased from that of the

H-form but increased with progressive acid refluxing (Table 3.3). In all cases the -4AR samples exhibited greater surface areas than the H-forms.

3.2 CATALYTIC ACTIVITY OF SAPO-34

3.2.1 METHANOL CONVERSION OVER SAPO-34

3.2.1.1 Preliminary results

Reactor wall effects

The initial MTO work was done in a stainless steel fixed bed reactor. At reaction temperatures above 400°C reaction of the methanol feed with the stainless steel walls (no catalyst loaded in the reactor) was significant, resulting in the deposition of a black carbonaceous material on the reactor walls. This phenomenon also resulted in the conversion of methanol to methane, the methane yield being of the order of 10%. Insertion of a quartz liner into the reactor decreased the methane yield to approximately 1.5% and the carbonaceous deposits were eliminated. The use of a borosilicate glass tube in which the catalyst was supported, the methanol contacting with stainless steel only at temperatures below 175°C, resulted in an essentially inert reactor. In this case, the methane yield was approximately 0.15%.

MTO reproducibility

The reproducibility of the SAPO-34 oxygenate conversion levels and light olefin selectivity was tested for the S2 material in a quartz lined stainless steel reactor at the following reaction conditions : 400°C, WHSV = 1 hr^{-1}, total pressure = 101 kPa and methanol partial pressure = 21 kPa in nitrogen. As can be seen from Figure 3.16, the reproducibility of both the methanol conversion levels and the light olefin selectivity (C_2-C_4 olefins) is very good.

SAPO-34 regeneration

The regenerability of the S2 material was found to be good. Regeneration in air at 550°C overnight resulted in no significant reduction in the methanol conversion levels (Figure 3.17) or the C_2-C_4 olefin selectivity, even after four regeneration cycles. These findings are similar to those of Liang et al. [1991].

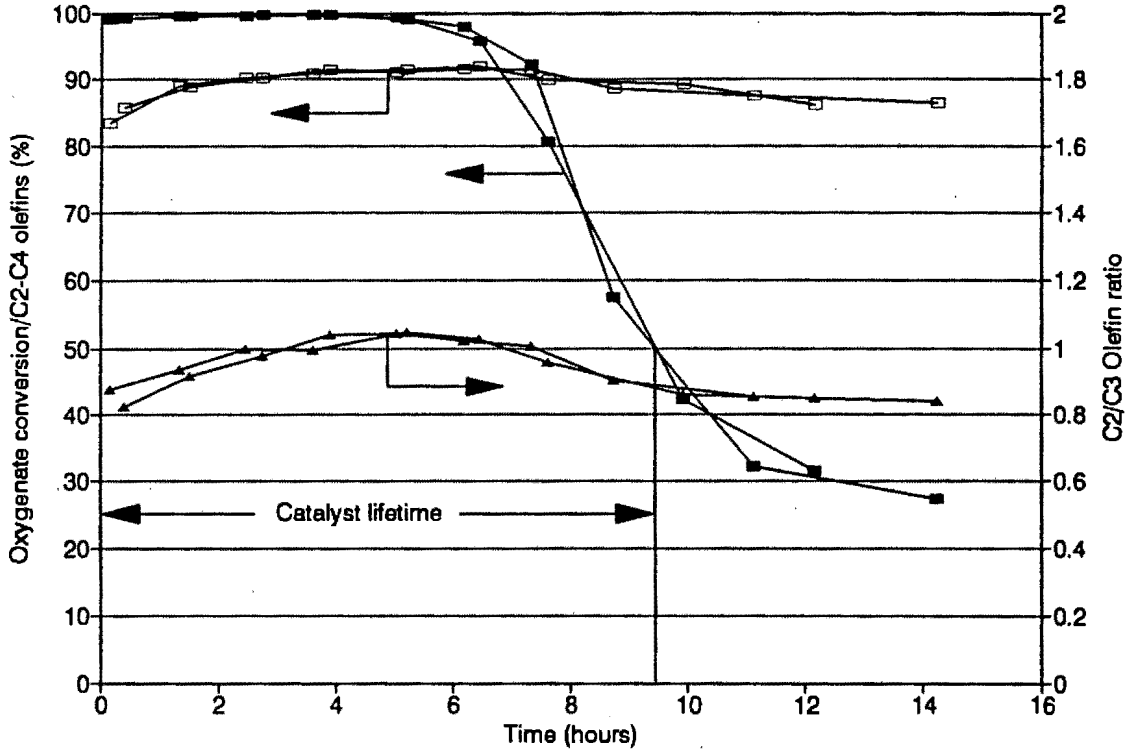

Figure 3.16 : MTO reproducibility of S2 in a fixed bed glass reactor.

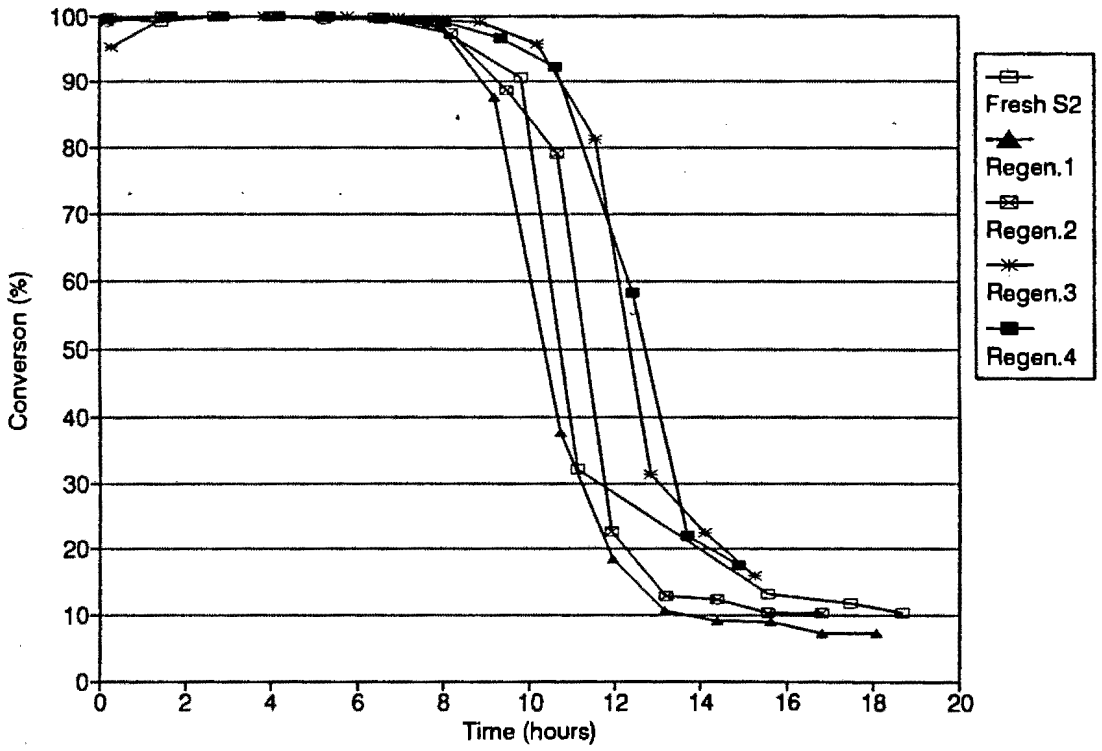

Figure 3.17 : Effect of regeneration on oxygenate conversion of S2 in a quartz lined stainless steel fixed bed reactor.

Fluidized bed studies

Due to the fast deactivation but good regenerability of SAPO-34, this catalyst is well suited for use in a fluidized bed reactor system with continuous regeneration. The SAPO-34 samples containing large amounts of amorphous material (low relative crystallinity) had high bulk densities. The amorphous material acted as a binder for the crystallites and therefore the only material which was mechanically stable under fluidization conditions was the S1 catalyst.

The S1 material was sieved into four size fractions, these being <38 microns, 38-75 microns, 75-106 microns and 106-250 microns. At methanol space velocities between 8 and 30 hr^{-1} (methanol partial pressure 21 kPa), the two smallest size fractions were very difficult to fluidize. This was due to the low density and irregular shape of the agglomerates which led to extensive channeling in the catalyst bed. There was very little channeling in the 106-250 micron material but a high superficial gas rate was needed in comparison to the 75-106 micron material. The porosity of the gas distributor (sintered glass disc) also affected the fluidization characteristics of the catalyst. Four glass sinters were tested and the finest sinter

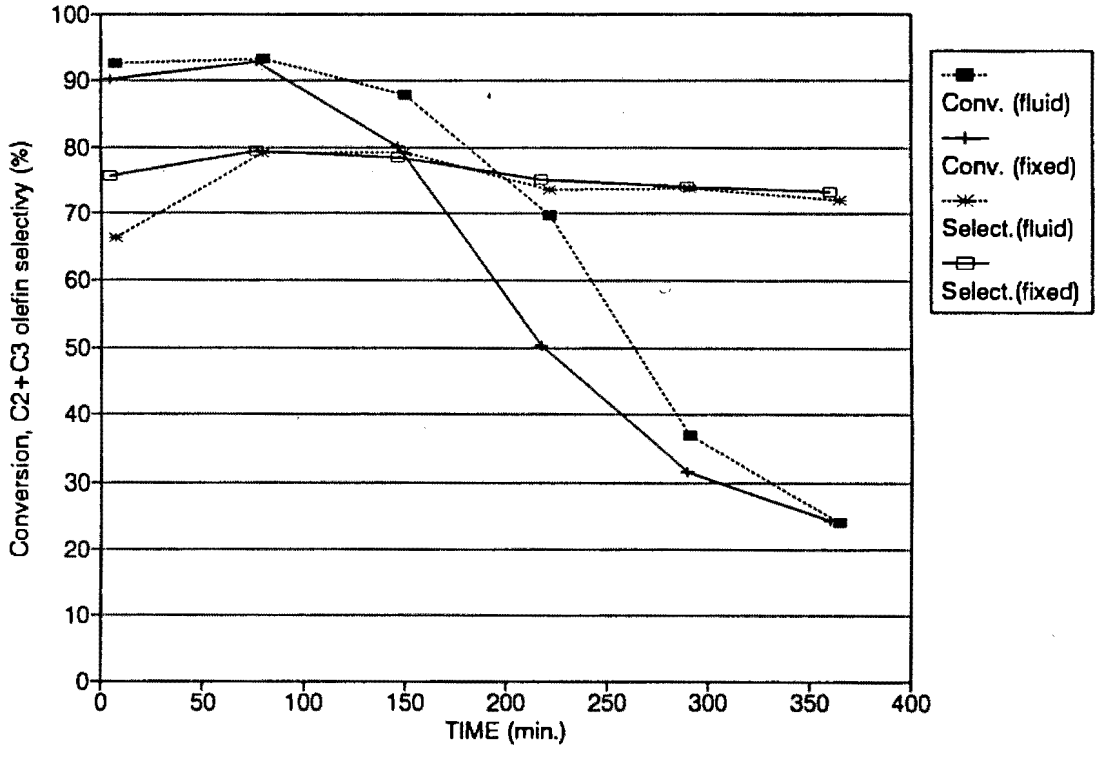

Figure 3.18 : Activity and selectivity of fixed bed vs. fluidized bed reactor.

(5-30 microns) worked best as it produced less channeling in the catalyst bed and did not become blocked with fine particles.

At a reaction temperature of 410°C (WHSV = 14.8, methanol partial pressure = 25 kPa), there was very little difference in the conversion levels and product selectivities of the S1 material in the fixed and the fluidized bed reactors (Figure 3.18). The conversion and selectivity data for these runs is tabulated in Appendix V. As stable operation of the fluidized bed reactor was difficult and there were no substantial differences in catalytic performance, the subsequent MTO studies over SAPO-34 were undertaken in a fixed bed reactor.

3.2.1.2 Synthesis variations

As can be seen from Table 3.4, there were significant differences in the CUVs of the unmodified SAPO-34 catalysts. S3 had the greatest CUV, the oxygenate conversion being above 90% for over 9 hours. The C_2/C_3 olefin ratios were slightly higher for the catalysts with the longer lifetimes.

In spite of the high purity and crystallinity of Co1, the lifetime of this catalyst was half that of S3, although there was little change in the C_2/C_3 olefin ratio. As can be seen from Table 3.4, the CUV of Ni1 was even less than that of Co1 and the C_2/C_3 olefin ratio and the C_2-C_4 olefin selectivity were significantly reduced. Ni2, from the synthesis to which NaOH was added to increase the crystallinity of the catalyst, exhibited negligible MTO activity, the oxygenate conversion being below 1.5%.

The highly crystalline Ni3 was more active than any of the SAPO-34 catalysts synthesized with transition metals, but still had a lower CUV than unmodified S3. As with Ni1, the C_2/C_3 olefin ratio and the C_2-C_4 olefin selectivities were also less than those of the S3 or Co1 catalysts.

3.2.1.3 Post-synthesis modifications

As can be seen from Table 3.4, the S3* sample had a significantly greater CUV than unmodified S3 (shallow bed calcined sample). All further modifications of

Catalyst/ Variable	HTD Ammonia (mmols/g)	MTO Lifetime (hours)	MTO CUV (g/g cat.)	$C_2^=/C_3^=$ (Ratio)	$C_2^=$-$C_4^=$ (Selectivities) (wt%)	CH_4 (wt%)	% Coke Content (wt%)
% Error *	7	5	5	3	3	3	10
Variable	400°C, WHSV 1 hr^{-1}, partial pressure 21 kPa						
S1	0.18	4.8	4.0	0.73	88.2	0.4	3.7
S2	0.26	9.5	9.0	0.98	89.4	0.9	?
S3	0.38	12.3	12.0	1.00	92.2	1.1	14.6
Co1	0.21	5.0	4.4	1.09	86.9	1.5	15.7
Ni1	0.06	2.3	1.8	0.86	72.7	0.7	6.0
Ni2	0.00	2.1	0.0	0.87	33.5	19.8	0.6
Ni3	0.37	8.9	7.9	0.87	91.8	0.6	15.4
S3*	0.46	16.4	15.9	1.01	90.6	1.0	16.6
S3*-AMM	0.40	14.3	13.1	0.84	84.8	0.6	17.4
S3*-SIL	0.36	13.9	13.2	0.84	90.2	0.6	15.5
S3*-STM	0.32	11.0	10.4	0.81	91.5	0.6	18.1
S3*-BRN	0.00	1.3	0.2	1.41	8.2	0.6	-
S3*-ACD	0.00	0.0	-	-	-	-	-
S3*-CAU	0.00	0.0	-	-	-	-	-
Variable Temperature	Reaction conditions (S3*)						
350°C	0.46	26.5	23.5	0.69	90.8	0.5	16.5
400°C	0.46	16.4	15.9	1.01	90.6	1.0	16.6
450°C	0.46	7.2	7.1	1.58	87.5	3.1	15.9
WHSV							
0.5 g/g/hr	0.46	25.0	12.3	1.14	89.7	1.3	17.7
1 g/g/hr	0.46	16.4	15.9	1.01	90.6	1.0	16.6
2 g/g/hr	0.46	11.3	21.4	0.92	91.0	0.9	18.5
P.Pressure							
11 kPa	0.46	21.2	20.2	1.08	91.5	1.2	15.5
21 kPa	0.46	16.4	15.9	1.01	90.6	1.0	16.6
42 kPa	0.46	12.9	12.1	0.98	89.3	1.0	17.3
Water	Influence of temperature for runs with a MeOH/water feed						
350°C	0.46	41.2	36.0	0.52	88.3	0.4	15.0
400°C	0.46	51.5	45.8	0.79	89.7	0.5	19.8
450°C	0.46	13.5	12.1	1.35	91.2	1.2	17.1

Table 3.4 : MTO activity and selectivity for modified and unmodified SAPO-34.

* Error data is given as a percentage of the value listed in the Table

the S3* sample yielded catalysts which had lower CUVs. The S3*-SIL and S3*-AMM samples had similar CUVs although the CUV of the S3*-STM catalyst was less than that of the unmodified S3. The S3*-BRN catalyst showed only slight MTO activity, the initial conversion being less than 15% whereas that of all the other modified samples was above 99%. The S3*-ACD and S3*-CAU samples were totally inactive.

Excluding the S3*-BRN/ACD/CAU catalysts, the S3* material had a slightly higher C_2/C_3 olefin ratio than the other modified samples. Also excluding the S3*-BRN/ACD/CAU catalysts, the methane and C_2-C_4 olefin selectivities were similar for all the modified samples. The only exception was the C_2-C_4 olefin selectivity of the S3*-AMM sample which was lower than that of the other samples.

3.2.1.4 Reaction temperature

In the temperature range 350-450°C, it is clear that for S3*, increased reaction temperatures result in reduced CUVs (Table 3.4) and increased rates of deactivation (Figure 3.19). In all cases, the initial conversion of oxygenates was above 99%. This was not the case for the less acidic S2, where the catalyst was most active at 400°C, although the rate of deactivation still increased as the reaction temperature was increased.

For all the reaction conditions investigated, a steady increase in the C_2/C_3 olefin ratio was seen with time-on-stream while methanol conversion levels were at 100%. As conversion levels dropped below 100%, the C_2/C_3 olefin ratio leveled out and, whereas this ratio remained constant thereafter at the reaction temperature of 350°C, it increased with the continued drop in conversion levels at 400°C and 450°C. There was a significant increase in the C_2/C_3 olefin ratio as the reaction temperature was increased (Table 3.4). It is clear that this increase was accompanied by an increase in the methane selectivity at the expense of the C_2-C_4 olefin selectivity. The amount of coke deposited on the catalyst samples did not vary significantly as the reaction temperature was varied, being between 0.159 g/g and 0.166 g/g of clean catalyst (for catalysts deactivated until the oxygenate conversion levels were approximately 10%).

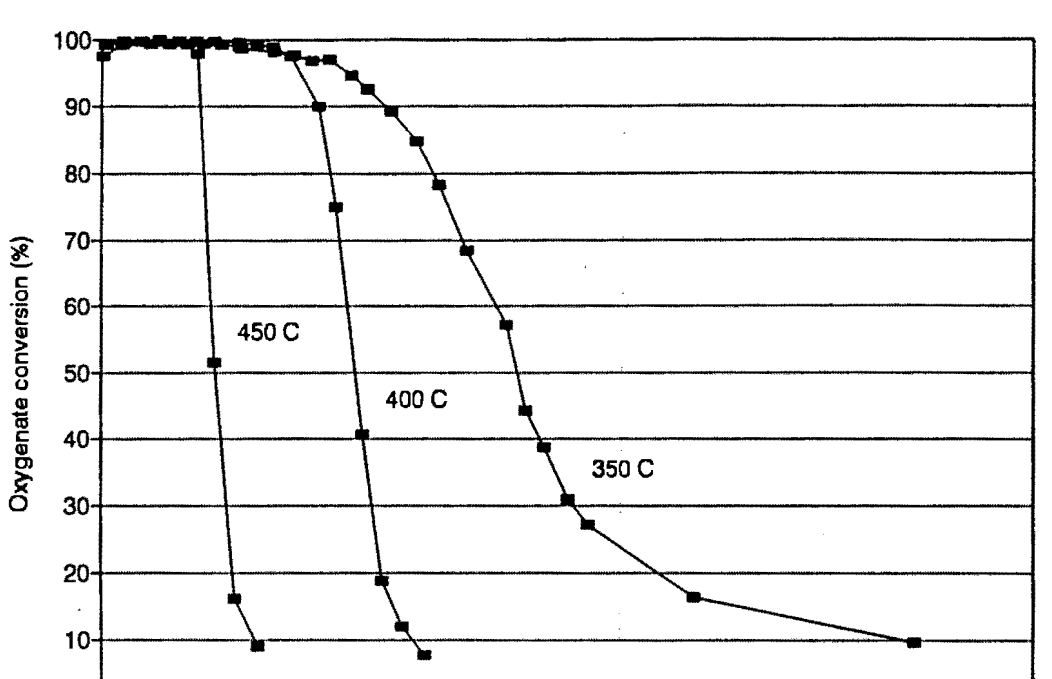

Figure 3.19 : Effect of reaction temperature on oxygenate conversion (catalyst : S3*).

3.2.1.5 Methanol space velocity

For the methanol weight hourly space velocities investigated, the methanol partial pressures were kept constant resulting in different feed and product residence times in the catalyst bed. The initial conversion levels were always 100%. From Table 3.4, it may be seen that increased space velocities resulted in increased CUVs for the S3* material although the lifetime decreased as the space velocity was increased (Figure 3.20). Similar trends were found for the S2 catalyst. The C_2/C_3 olefin ratio decreased as the space velocity was increased although this variation was less marked than that obtained when the reaction temperature was decreased. A similar effect was seen for the methane selectivity, which decreased slightly as the space velocity was increased.

The amount of coke deposited on the catalyst samples varied between 0.166 and 0.185 g/g of clean catalyst. Comparison of the coke contents for these runs is difficult because these runs did not end at equivalent oxygenate conversion levels (4.3% for WHSV = 2 and 11.9% for WHSV = 0.5).

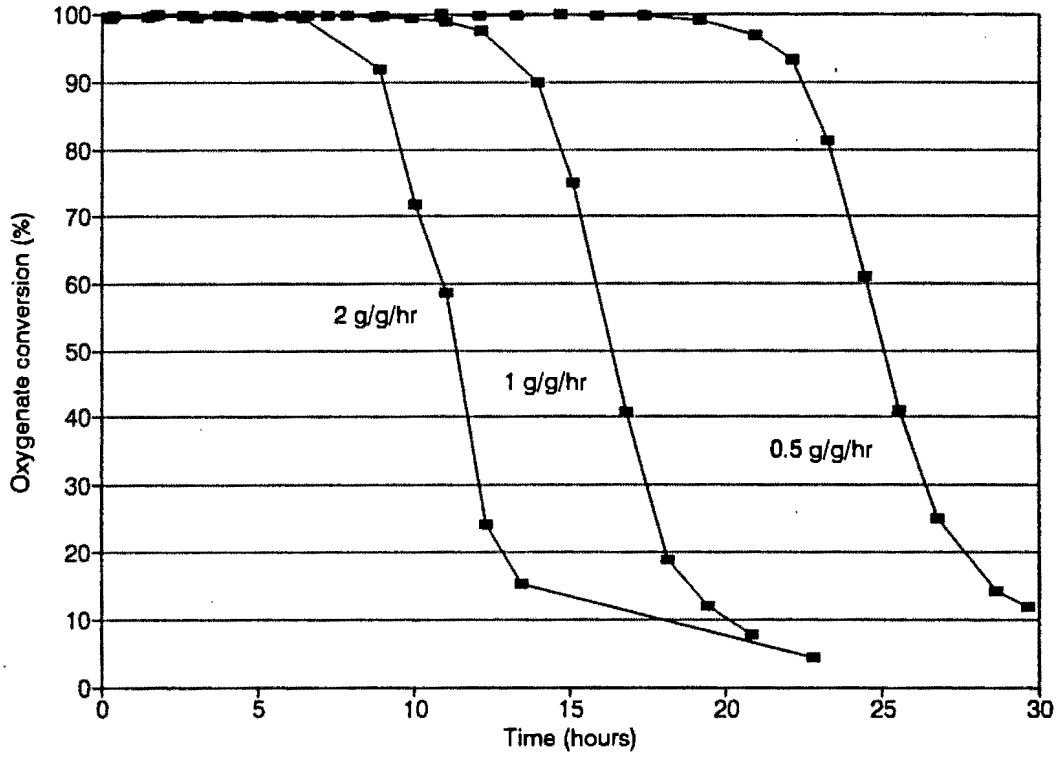

Figure 3.20 : Effect of methanol space velocity on oxygenate conversion (catalyst : S3*).

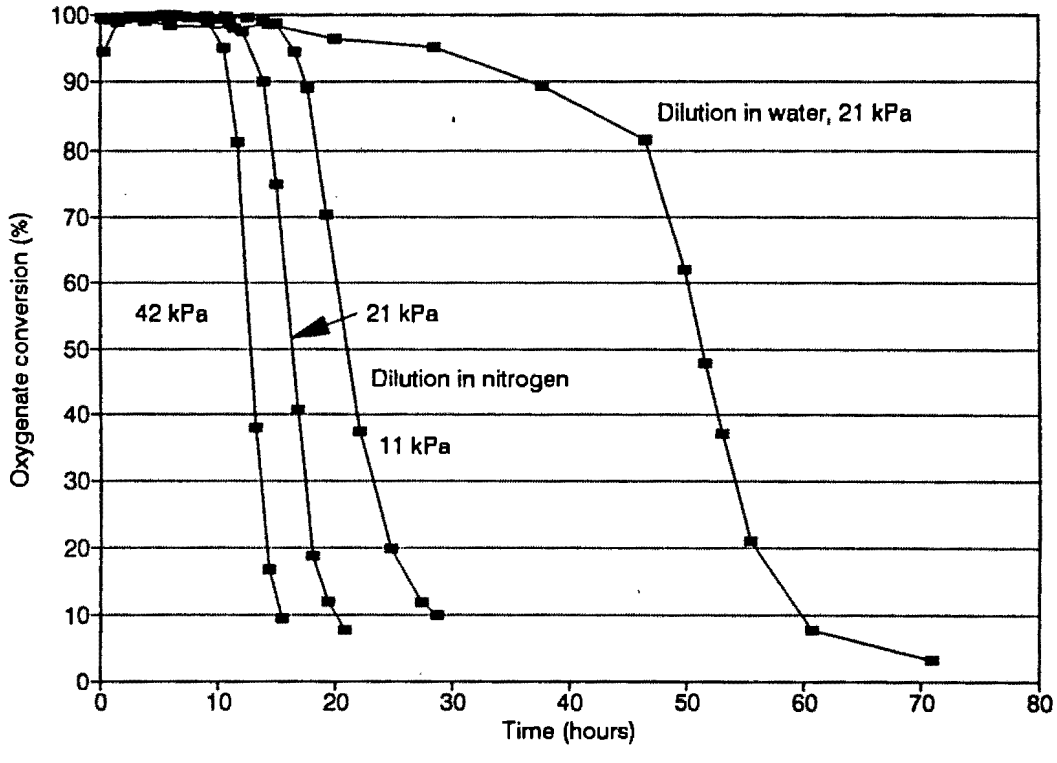

Figure 3.21 : Effect of methanol dilution on oxygenate conversion (catalyst : S3*).

3.2.1.6 Methanol partial pressure and methanol diluent

For the partial pressures investigated, the methanol space velocity was kept constant resulting in different reactant and product residence times in the catalyst bed. Nitrogen was used as a diluent because it would not interact with acid sites as would water, which would be used as a diluent industrially. As can be seen from Table 3.4, catalyst CUVs decreased as the partial pressure was increased. There was a slight decrease in the C_2/C_3 olefin ratio for the catalyst samples run at higher partial pressures although the methane selectivity was essentially unchanged. The amount of coke deposited on the catalyst samples increased slightly for the catalysts run at higher methanol partial pressures, increasing from 0.155 g/g to 0.173 g/g of clean catalyst.

A methanol partial pressure of 21 kPa was maintained when water was used as a diluent. As can be seen from Figure 3.21, at a reaction temperature of 400°C there was a three fold increase in catalyst time-on-stream when water was used as a diluent instead of nitrogen. The C_2/C_3 olefin ratio was consistently lower when water was used as a diluent. There was very little variation in the olefin ratio, which only started increasing once the conversion dropped below 20%. Although the C_2-C_4 olefin selectivity was essentially unchanged, the methane selectivity was slightly reduced when water was used as a diluent. It was also noticeable that there was no increase in the methane selectivity as the catalyst deactivated. The amount of coke deposited on the catalyst samples was increased when water was used as a diluent instead of nitrogen.

It is clear from Table 3.4 that the magnitude of the CUV enhancement is strongly dependent on reaction temperature, the enhancement being greatest at 400°C. The increase in the C_2/C_3 olefin ratio with increasing reaction temperature was far less marked when water was used as a diluent. This was also the case with the C_2-C_4 olefin selectivity and the methane selectivity, the methane selectivity being significantly lower at 450°C when water was used as a diluent instead of nitrogen.

3.2.2 PROPENE OLIGOMERIZATION OVER SAPO-34

The activity and selectivity data for the S2, Co1 and Ni3 samples is shown in Table 3.5. None of the catalysts were active at the initial reaction temperature of 220°C and even when the reaction temperature was ramped to 280°C, the conversion to liquid product remained below 1%. The liquid produced consisted of mostly propene oligomers and was free of cracked products. The C_9+ and C_{12}+ selectivities were similar to those obtained from the mordenite catalysts, except for the Co1 sample, which produced a C_{12}+ fraction of over 80%.

No further oligomerization was done over the SAPO-34 or MeSAPO-34 catalysts due to their very low activity.

Catalyst	Oligomeriz. CUV (g/g cat.)	Oligomeriz. C_9+ Sel. (wt%)	Oligomeriz. C_{12}+ Sel. (wt%)
% Error *	-	15	15
S2	-	85.0	46
Co1	-	98.0	83
Ni3	-	88.0	50

Table 3.5 : Oligomerization performance of SAPO-34 catalysts.

* Error data is given as a percentage of the value listed in the Table.

3.3 CATALYTIC ACTIVITY OF MORDENITE

3.3.1 METHANOL CONVERSION OVER MORDENITE

3.3.1.1 Preliminary results

Reproducibility

The reproducibility of the MTO oxygenate conversion levels was tested for the ZM760 material in a fixed bed reactor at standard MTO reaction conditions (400°C, WHSV 1 hr^{-1}, methanol partial pressure 21 kPa in nitrogen). As can be seen in Figure 3.22, the conversion levels do not vary by more than 10 percentage points throughout the length of the run.

Mordenite regeneration

The regenerability of the mordenite was found to be reasonably good and, as can be seen for the M1-2AR material (Figure 3.23) the CUV was virtually unchanged although the regenerated sample was slightly less active once the conversion levels dropped below 40%.

Fluidized bed studies

The effect of fluidization on the activity and selectivity of mordenite for the MTO reaction was investigated using the ZM760 catalyst. The ZM760 material was mechanically stable under the fluidization conditions used, the amount of fine material lost during 10 hours of fluidization being less than 2%.

The ZM760 material was sieved into three size fractions, these being <38 microns, 38-75 microns and 75-106 microns. The 75-106 micron size fraction was used in the MTO experiments because the two finer size fractions were difficult to fluidize due to channeling and slugging of the catalyst bed. As with the SAPO-34, use of the 5-30 micron sintered glass distributor produced less channeling.

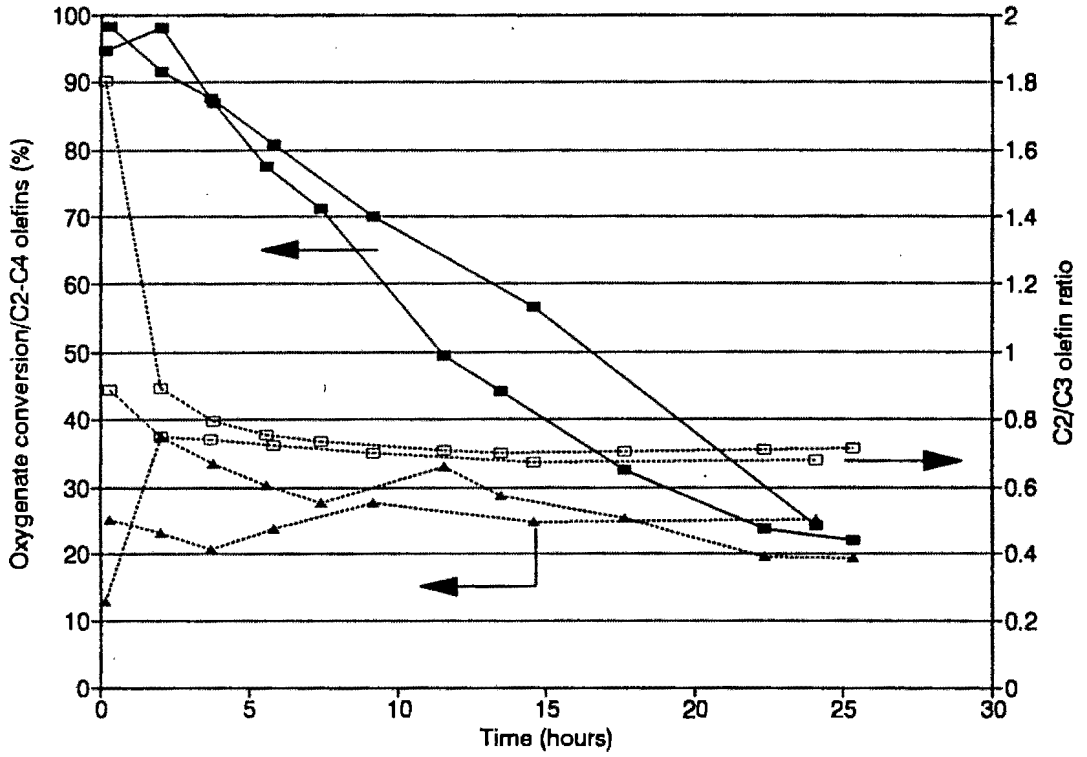

Figure 3.22 : MTO reproducibility for ZM760.

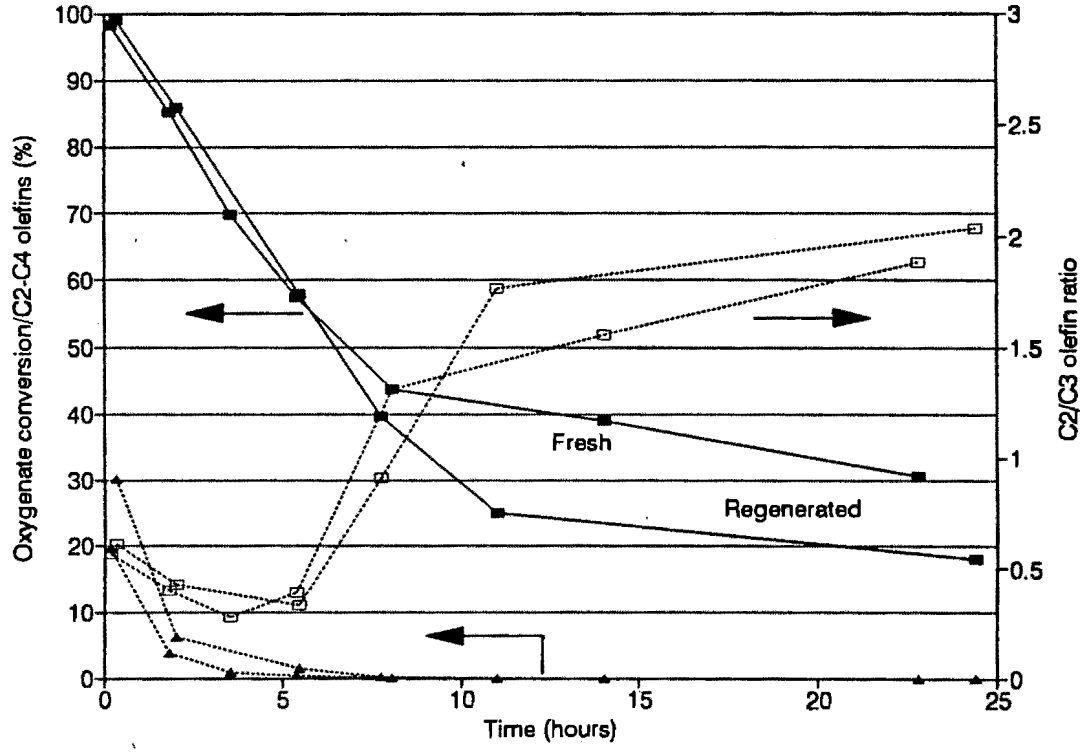

Figure 3.23 : Regeneration of M1-2AR.

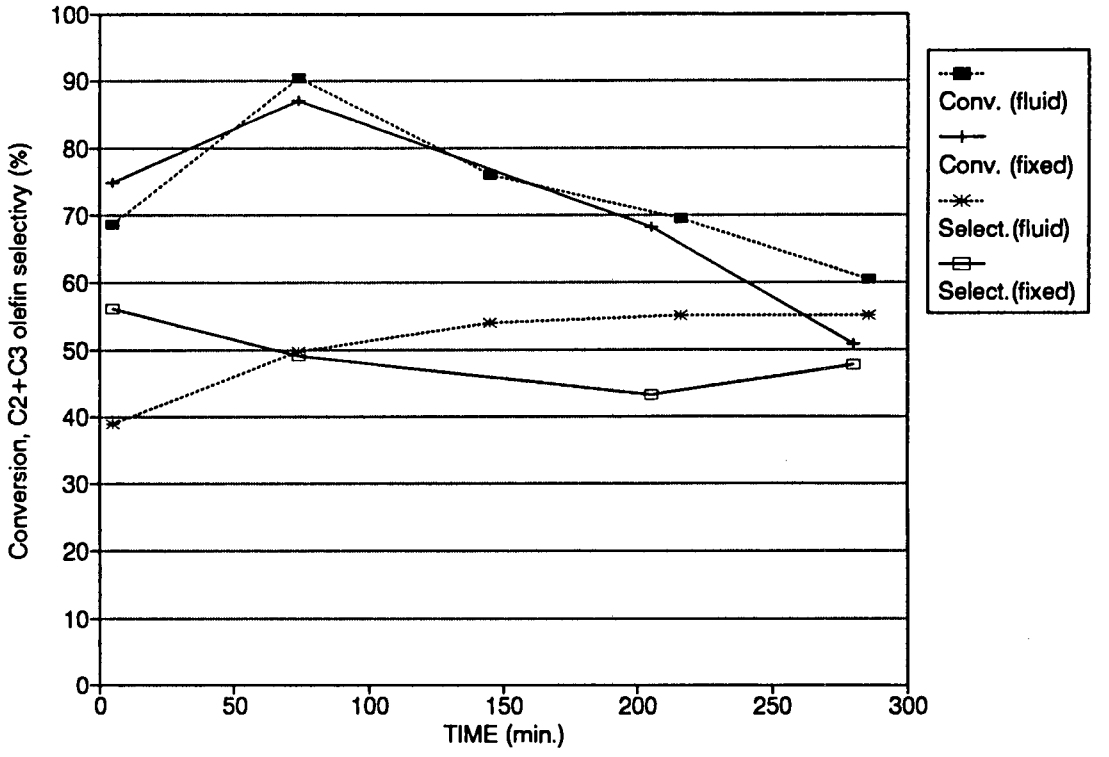

Figure 3.24 : MTO performance of fixed bed vs. fluidized bed reactor.

At a reaction temperature of 410°C (WHSV = 14.8, methanol partial pressure = 25 kPa), the conversion levels of the ZM760 material in the fixed and the fluidized bed reactors did not vary significantly (Figure 3.24). There were slight differences in the product selectivities however, the average C_2-C_3 olefin selectivity and C_2/C_3 olefin ratio being higher in the fluidized bed reactor. The conversion and selectivity data for these runs is tabulated in Appendix VI. Stable operation of the fluidized bed reactor was difficult to maintain, and as no major activity or selectivity advantages were observed when using the fluidized bed reactor, the remaining MTO work with mordenite was done in a fixed bed reactor.

3.3.1.2 Catalyst acidity and acid site accessibility

The initial methanol conversion levels of all the samples were above 95%. The MTO performance of the M1 and M2 series of catalysts were similar in that the CUVs of the mildly dealuminated samples were less than those of the untreated samples (Figure 3.25). The severely dealuminated samples had greater CUVs than any of the other samples and the CUV trends of the MN, M1 and

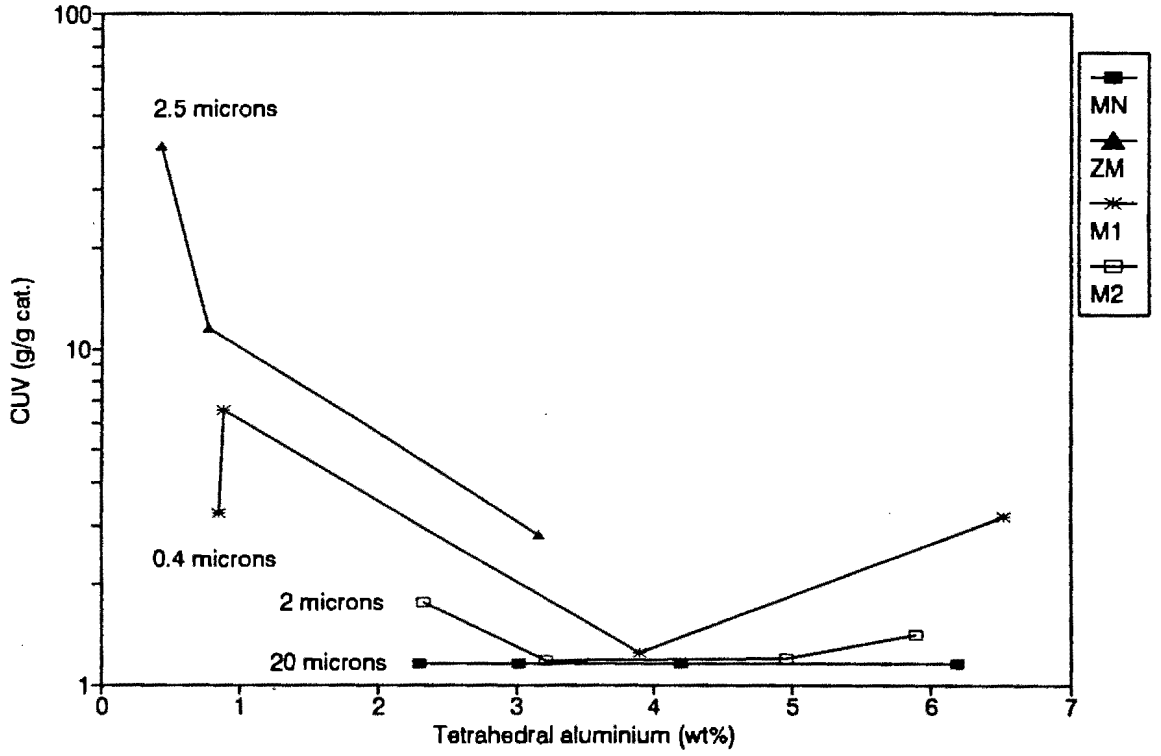

Figure 3.25 : CUV as a function of tetrahedral aluminium for dealuminated mordenites (400 C).

M2 mordenites, when plotted as a function of tetrahedral aluminium, were strongly influenced by mordenite type (Figure 3.25). None of the MN samples showed significant MTO activity after the first product sample was taken. Of all the mordenites investigated, the ZM samples were the most active, their MTO CUV increasing with increasing dealumination.

The product selectivities of the catalysts changed significantly as the samples deactivated. The initial MTO reaction products at complete oxygenate conversion consisted of mostly C_1-C_4 paraffins. As the catalyst samples deactivated and the oxygenate conversion dropped, the selectivity shifted to mostly C_2-C_4 olefins. The most active samples (ZM and M1-2AR/03) produced far more high molecular weight hydrocarbons, the combined C_9+ and aromatic selectivity rising to as much as 34% (Table 3.6).

The amount of coke deposited on the catalyst samples varied between 9% and 16.5%. The catalyst coke contents increased with increasing run-times (same catalyst and reaction conditions). This is clearly seen with conversion data of runs M8 and M11 (Appendix VI), M8 being on-line for 31 hours (13.1% coke) and M11

Catalyst/ Variable	Tetrahedral Aluminium (wt%)	MTO Lifetime (hours)	MTO CUV (g/g cat.)	$C_2^=/C_3^=$ (Ratio)	$C_2^=$-$C_4^=$ (Selectivities) (wt%)	CH_4 (wt%)	MTO C_9+ Sel. (wt%)	% Coke Content (wt%)
% Error *	10	10	10	10	20	5	15	15
Catalyst	Dealuminated mordenite (400 deg.C, 1g/g/hr, 21 kPa)							
MN								
MN- H	6.19	1.2	0.9	4.33	9.5	7.3	3	7.4
MN-2AW	4.19	1.2	0.9	4.07	5.7	3.7	7	8.5
MN-2AR	3.02	1.2	0.9	5.89	5.1	3.6	4	9.1
MN-4AR	2.30	1.2	0.9	3.08	9.1	3.1	5	10.0
ZM								
ZM510	3.17	2.8	2.6	1.78	27.6	6.5	16	11.5
ZM760	0.77	11.4	8.9	1.00	28.4	3.8	28	15.0
ZM980	0.43	40.4	32.9	0.31	28.2	1.3	23	3.6
M1								
M1- H	6.53	1.7	1.3	1.26	43.7	5.0	4	9.1
M1-2AW	3.89	1.3	1.0	2.79	9.3	9.3	4	9.2
M1-2AR	0.89	6.5	4.9	0.81	16.5	1.6	34	11.0
M1-4AR	0.86	3.3	2.7	1.12	15.8	3.0	32	11.6
M2								
M2- H	5.89	1.4	1.1	1.72	17.3	13.3	4	6.1
M2-2AW	4.96	1.2	0.9	1.74	19.5	11.0	3	6.4
M2-2AR	3.21	1.2	0.9	2.87	12.6	3.8	3	7.2
M2-4AR	2.33	1.8	1.3	4.07	19.3	3.0	4	9.0
	Reaction conditions (ZM760)							
Variable								
Temp.	(WHSV 1g/g/hr, p.pres. 21 kPa)							
350 C	0.74	34.6	25.1	1.07	32.2	2.2	-	10.4
400 C	0.74	11.4	8.9	1.00	28.4	3.8	-	15.0
450 C	0.74	1.3	1.1	1.25	22.8	15.1	-	13.5
WHSV	(temperature 400°C, p.pres. 21 kPa)							
0.5 g/g/hr	0.74	12.3	4.7	1.07	44.1	7.0	-	11.1
1 g/g/hr	0.74	11.4	8.9	1.00	28.4	3.8	-	15.0
2 g/g/hr	0.74	8.3	12.8	0.68	36.0	3.4	-	14.5
P.Pres.	(WHSV 1g/g/hr, temperature 400°C)							
11 kPa	0.74	10.1	7.0	0.70	14.5	1.6	-	13.8
21 kPa	0.74	11.4	8.9	1.00	28.4	3.8	-	15.0
42 kPa	0.74	13.2	9.8	1.08	32.7	4.7	-	13.3
Water	0.74	75.0	54.1	0.86	44.8	3.0	-	16.5

Table 3.6 : MTO performance of dealuminated mordenites.

* Error data is given as a percentage of the value listed in the Table.

for 43 hours (17.4% coke). Additional coking trends were difficult to ascertain as these runs were on-line for different lengths of time and were stopped while at different conversion levels.

3.3.1.3 Reaction temperature

The ZM760 mordenite was used in the investigation of the various reaction conditions due to the large amount of material available and the intermediate activity of this catalyst compared to the ZM510 and ZM980 samples. As can be seen from Figure 3.26, reducing the reaction temperature resulted in a significant increase in catalyst lifetime and a large reduction in the rate of catalyst deactivation.

The light olefin selectivity (C_2-C_4 olefins) decreased and the methane selectivity and C_2/C_3 olefin ratio increased as the reaction temperature was increased. The conversion and selectivity data for these runs is tabulated in Appendix IV and

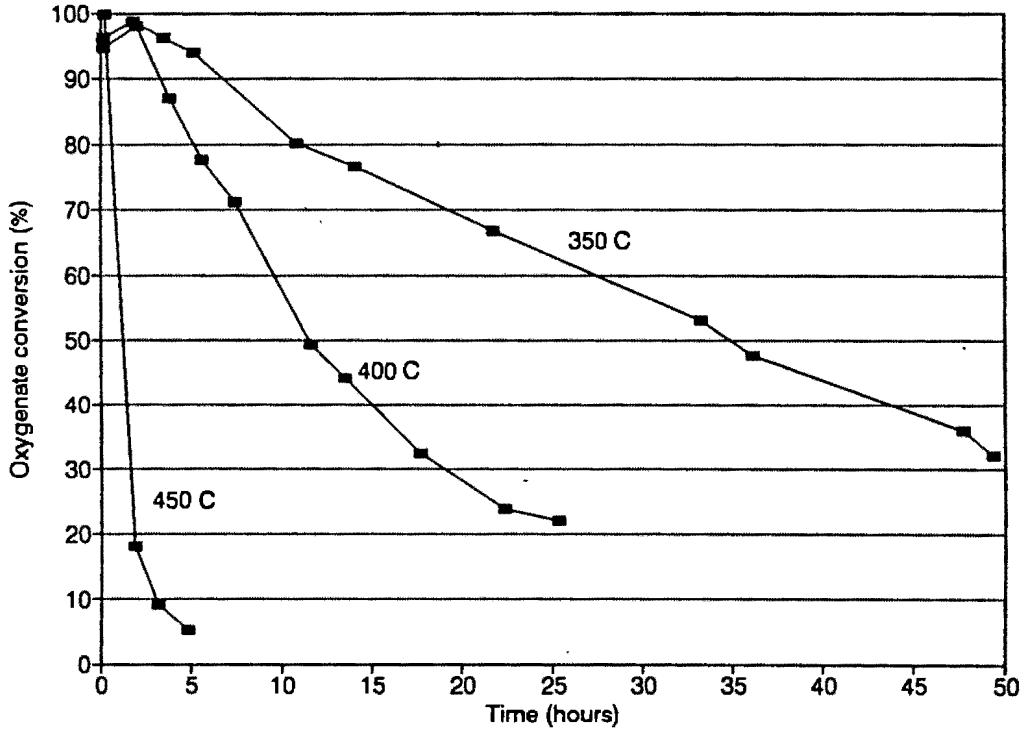

Figure 3.26 : Effect of reaction temperature on oxygenate conversion (ZM760, WHSV 1, 21 kPa)

CUVs and product selectivities are summarized in Table 3.6. The amount of coke removed from the spent catalyst also increased as the reaction temperature was increased.

3.3.1.4 Methanol space velocity

The initial oxygenate conversion was above 95% for all the space velocities investigated. As can be seen from Figure 3.27, increasing the space velocity of the methanol feed resulted in very little reduction in the oxygenate conversion levels of the ZM760 catalyst. Although there was very little change in the C_2/C_3 olefin ratio, the methane selectivity decreased as the methanol space velocity was increased (Table 3.6).

The amount of coke deposited on the catalyst samples varied from between 0.111 g/g and 0.150 g/g of clean catalyst, even though the conversion-time profiles for these runs were very similar.

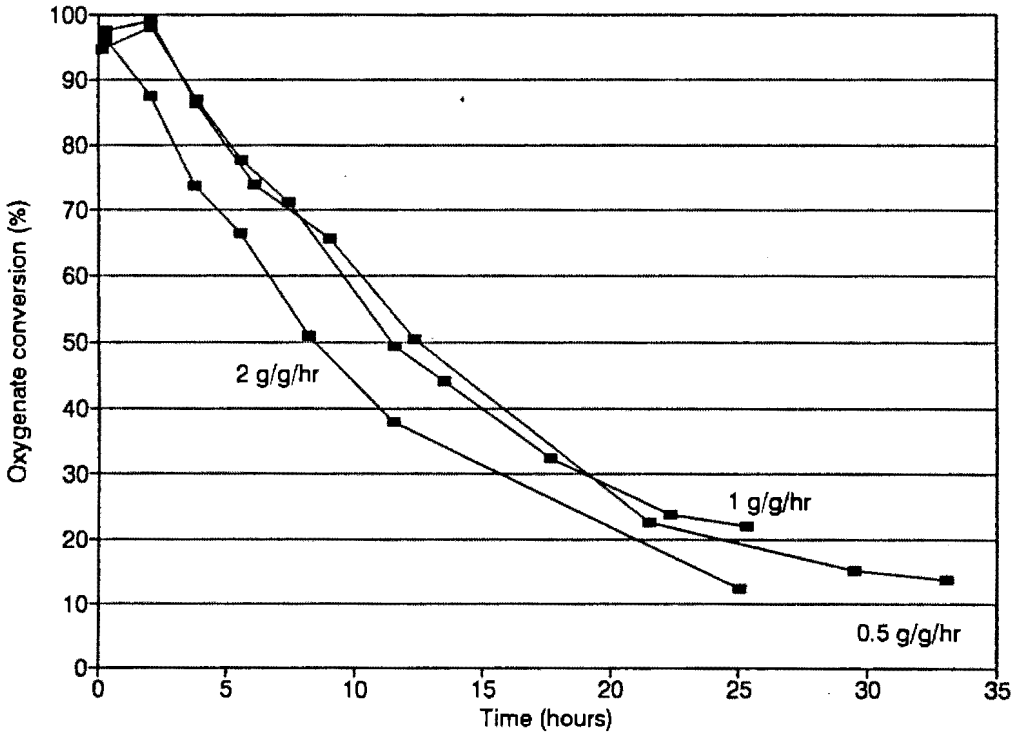

Figure 3.27 : Effect of methanol space velocity on oxygenate conversion (ZM760, 400 C, 21 kPa).

3.3.1.5 Methanol partial pressure and methanol diluent

As with the variation of space velocity, variation of methanol partial pressure resulted in very little change in the oxygenate conversion levels of the ZM760 catalyst (Figure 3.28). As the methanol partial pressure was increased, the methane and light olefin selectivities increased and there was a slight reduction in the C_2/C_3 ratio. The amount of coke deposited on the catalyst samples varied between 0.130 g/g and 0.150 g/g of clean catalyst.

Dilution of the methanol feed with water instead of nitrogen resulted in a large decrease in the rate of deactivation of the ZM760 catalyst (Figure 3.28). When water is used as a diluent, the methane selectivity is slightly reduced and the light olefin selectivity is significantly increased (Table 3.6). The amount of coke deposited on the catalyst samples was increased when water was used as a diluent instead of nitrogen (even though the run where water was used as a diluent was stopped at a significantly higher oxygenate conversion level).

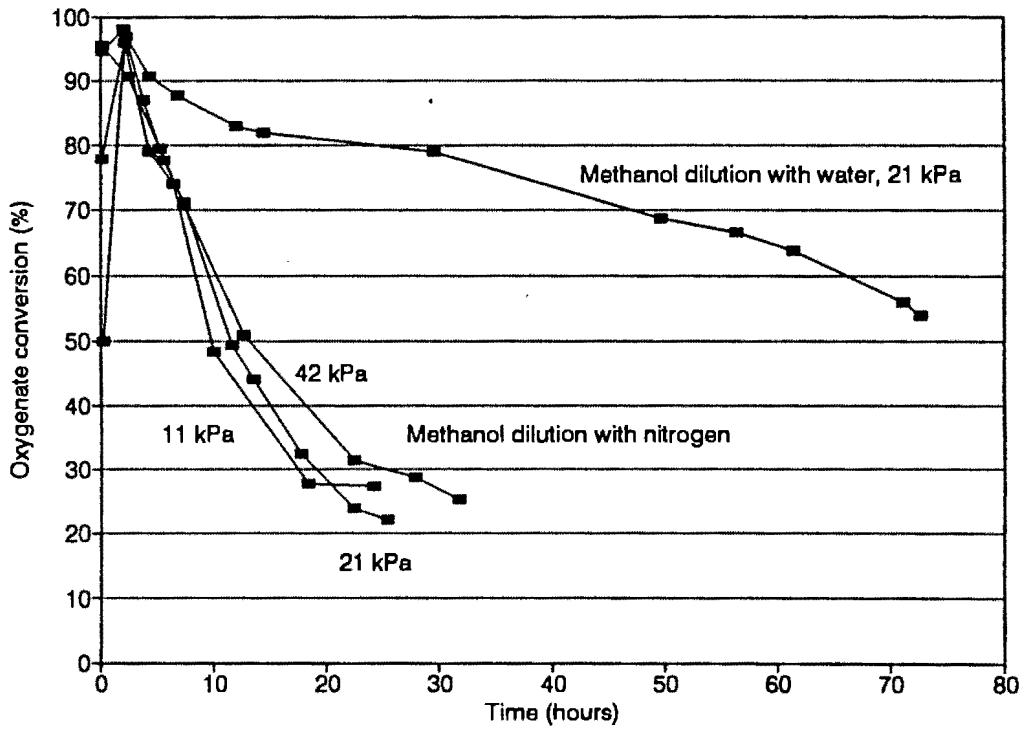

Figure 3.28 : Effect of diluent and methanol partial pressure on oxygenate conversion (ZM760, 400 C, WHSV 1).

3.3.2 PROPENE OLIGOMERIZATION OVER MORDENITE

The catalyst utilization values (CUVs) of the various mordenite catalysts are reported in Table 3.7 and the conversion levels obtained at the different temperature stages are reported in Appendix VI. As can be seen in Figure 3.29, the conversion levels at the different temperature steps are reproducible.

The mildly dealuminated MN, M1 and M2 samples were generally less active than the unmodified catalysts, and the more severely dealuminated samples were the most active of the mordenite samples investigated (Figure 3.30). The severely

Catalyst	Tetrahedral Aluminium (wt%)	Al^{VI}/ Pore	Oligomeriz. CUV (g/g cat.)	Oligomeriz. C_{12}+ Sel. (wt%)	Coke Content (g/100g cat.)
% Error *	10	40	15	15	5
MN					
MN- H	6.19	4159	2.3	57	12.3
MN-2AW	4.19	45860	0.0	-	7.1
MN-2AR	3.02	50929	0.0	-	7.4
MN-4AR	2.30	32991	0.5	-	8.1
ZM					
ZM510	3.17	2815	2.0	60	14.1
ZM760	0.77	939	2.8	64	18.1
ZM980	0.43	294	3.9	58	12.8
M1					
M1- H	6.53	115	2.7	49	17.6
M1-2AW	3.89	1228	1.7	63	8.5
M1-2AR	0.85	35	6.2	47	12.3
M1-4AR	0.85	9	5.7	56	11.0
M1-2AR(NH3)	0.89	11	6.1	-	11.8
M1-4AR(NH3)	0.86	7	5.5	-	10.9
M2					
M2- H	5.89	2313	2.5	-	4.9
M2-2AW	4.96	4080	0.3	-	3.7
M2-2AR	3.21	2569	0.0	-	5.3
M2-4AR	2.33	1146	3.2	80	8.8

Table 3.7 : Oligomerization performance of dealuminated mordenites.

* Error data is given as a percentage of the value listed in the Table

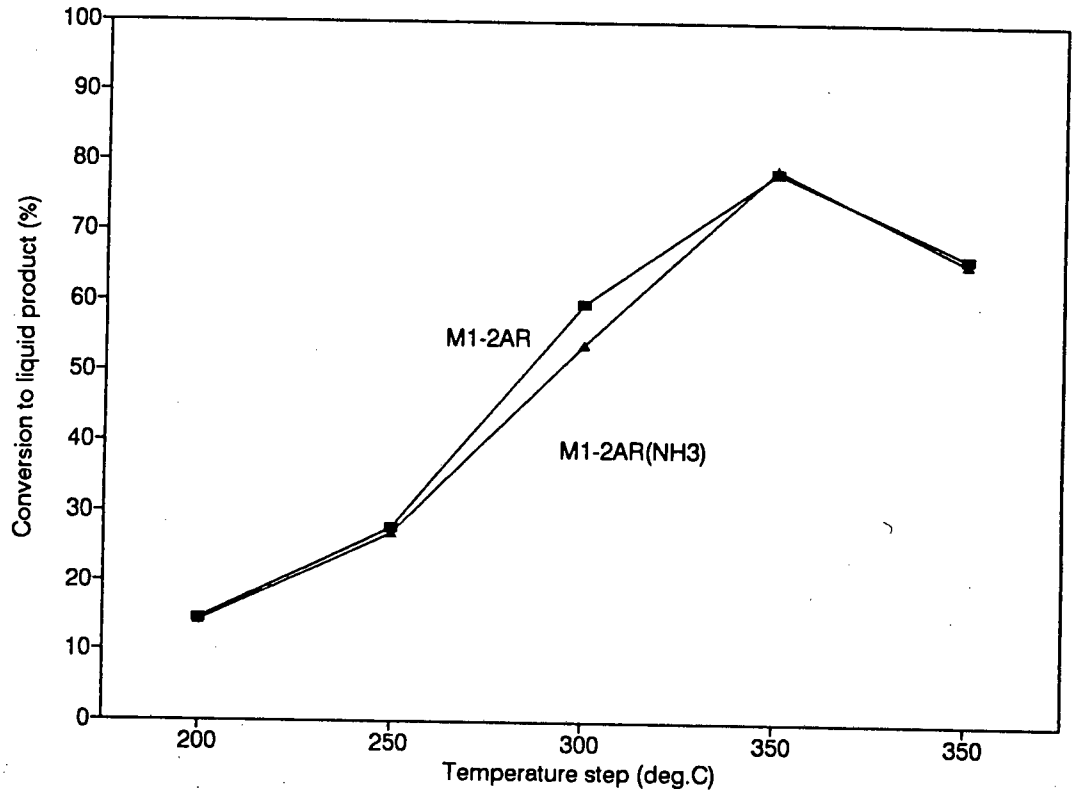

Figure 3.29 : Reproducibilityof propene oligomerization for M1-2AR/-2AR(NH3).

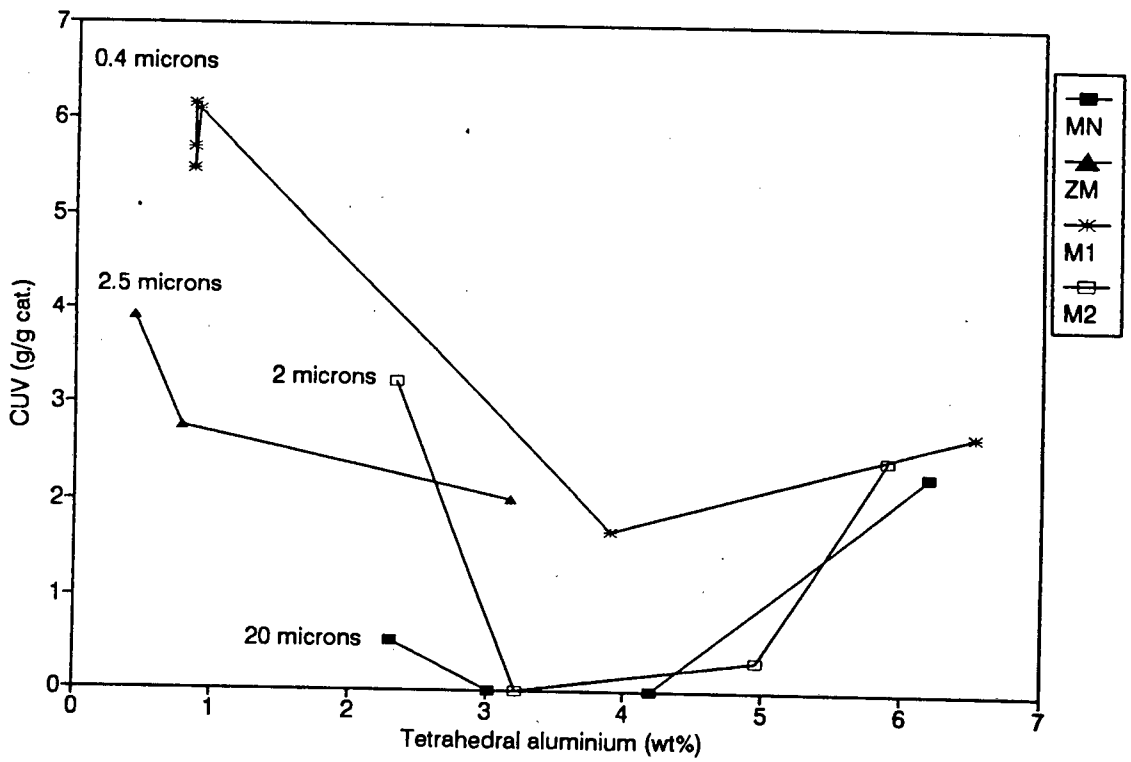

Figure 3.30 : CUV as a function of tetrahedral aluminium for dealuminated mordenites.

dealuminated M1 samples had significantly higher initial activities than the other mordenite samples investigated, some of which produced no liquid product until the reaction temperature was raised as high as 350°C.

The oligomer product spectra of most of the catalysts followed a general trend. At low temperatures (200-250°C) the liquid product had a high fraction of typical distillate hydrocarbons (C_{12}+ fraction) and the oligomer groupings could be clearly seen in the GC traces. By 300°C the C_{12}+ fraction had decreased and the oligomer groupings had become indistinct. There were no significant differences in the C_{12}+ selectivities between the different types of mordenite except for the M2-2AR sample, which produced an 80% C_{12}+ fraction. The amount of graphitic coke formed on the various samples varied between 0.037 g/g and 0.181 g coke/g fresh catalyst.

Chapter 4

DISCUSSION

4.1 CATALYTIC ACTIVITY OF SAPO-34

4.1.1 CONVERSION OF METHANOL TO LIGHT OLEFINS OVER SAPO-34

4.1.1.1 Synthesis variations

CUV as a function of HTD acidity

A general trend was found where the CUV and lifetime of the various SAPO-34 and MeAPSO-34 catalysts were dependent on the amount of HTD acidity as determined by NH_3 TPD (Figure 4.1). This result does not reflect a particular mode of catalyst deactivation (i.e. pore blockage or acid site poisoning, which is dealt with in more detail in Section 4.1.1.3).

The CUVs of the various SAPO/MeAPSO-34 catalysts differ considerably. The SAPO-34 catalysts with the longer MTO lifetimes and higher CUVs also have higher relative crystallinities and greater amounts of HTD acidity (Table 3.4). When the MeAPSO-34 catalysts are studied alongside these catalysts it can be seen that even though the Co1 and Ni3 catalysts have far higher relative crystallinities than the S3 catalyst, the latter still has the highest CUV. It can however be seen that the Co1 and Ni3 catalysts have less HTD acidity than the S3 catalyst and there is a general trend whereby the CUV of the catalyst increases as the amount of HTD acidity of the catalyst increases.

This observation is limited to samples which are predominantly SAPO-34 as it was seen that samples containing large fractions of SAPO-5 (SAPO-5 > 30%) had greater amounts of HTD acidity yet yielded reduced CUVs. It is unlikely that SAPO-5 would have a greater MTO activity than SAPO-34 as the catalytic activity of SAPO-5 has been found to be negligible in comparison to that of SAPO-34 for vapor phase propene oligomerization [Pellet et al., 1988]. Marchi and Froment [1991] found that changes in the amount of Brønsted acidity, as measured by changes in the infrared Al-OH stretching band, had no effect on the MTO activity of SAPO-34. These results are not conclusive as TPD techniques probe accessible acidity and would not necessarily correlate with the amount of acidity as measured by infrared spectroscopy, which reflects total acidity, including acid sites which may not be readily reached by TPD probe molecules. Acid sites which are not

easily reached by NH_3 probe molecules may arise as a result of pore mouth blockage by amorphous material or by defects in crystal structure.

It is difficult to predict the amount of acidity that a particular SAPO-34 or MeAPSO-34 will exhibit from the catalyst composition. Although acid sites are generated by silicon incorporation in the place of phosphorus, and cobalt and nickel incorporation in the place of aluminium, these elements are always incorporated in small amounts and therefore the relative amounts of these materials in the SAPO-34 crystals and other phases is difficult to quantify. In addition, it has been noted that the silicon dispersion in SAPO materials is often not homogeneous and silicon may be incorporated into the crystalline material as "silicon islands" [Mertens et al., 1990]. As a result, only silicon molecules at the interface between these islands and the crystalline aluminium/phosphorus material will be able to exhibit net negative framework charges and hence be able to function as acid sites. From the various SAPO-34 and MeAPSO-34 syntheses it can be seen that within a particular group of these materials (eg. NiAPSO-34) the HTD acidity is generally a function of catalyst crystallinity and that the crystallinity of these materials is often increased by the use of longer synthesis times.

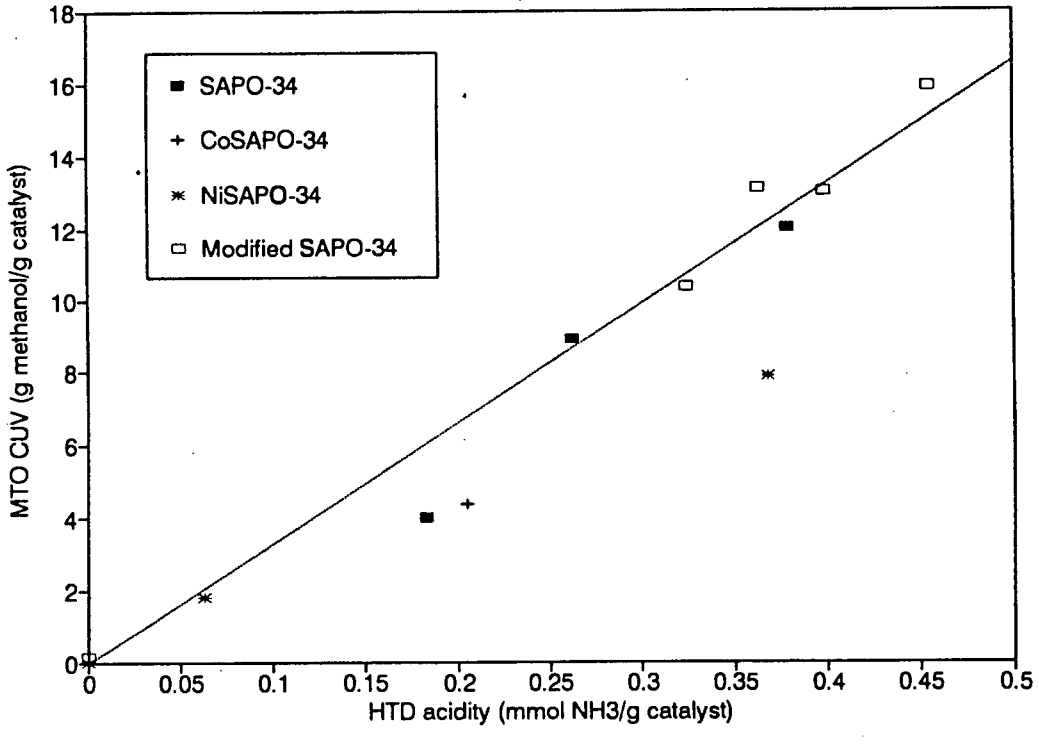

Figure 4.1 : Catalyst utilization value as a function of catalyst HTD acidity.

Of the various SAPO-34 and MeAPSO-34 catalysts only the Ni1 material had a significantly reduced light olefin selectivity. This catalyst was essentially inactive however and the average selectivity reported in Table 3.4 was taken from the first product sample only. Marchi and Froment [1991] found similar results for methanol conversion over SAPO-34 catalysts of different Si/Al ratios, the C_2-C_4 olefin selectivity remaining virtually unchanged for these catalysts.

Shape selectivity

An indication of shape selectivity may be obtained from the C_2/C_3 olefin ratio. Propene and higher molecular weight hydrocarbons have greater critical diameters than that of ethene and thus their diffusivities will be more strongly influenced by changes in pore diameter. Reporting diffusivities of *n*-paraffins in H-chabazite (an isomorph of SAPO-34), Chen [1988] showed that the diffusivities of ethane and propane differed by nearly one order of magnitude. The C_2/C_3 olefin ratio (shape selectivity) of the S1 material was reduced in comparison to the other catalysts, the reason for this being the presence of a significant quantity of SAPO-5 material (10-20%) which would not have the shape selectivity of SAPO-34 material due to its considerably larger pore diameter (SAPO-5 : 0.8 Å; SAPO-34 : 0.43 Å). The shape selectivities of the Ni1 and Ni2 catalysts were reduced and that of the Co1 increased in comparison to the S2 and S3 materials.

The increased C_2/C_3 olefin ratio (shape selectivity) of the Co1 catalyst may be due to framework distortion as a result of cobalt incorporation into a tetrahedral position as suggested by Bennett and Marcus [1988]. Unlike cobalt which is frequently found in a tetrahedral environment, four coordinate nickel is usually square-planar in structure although it may be forced into a tetrahedral configuration by ligand-ligand steric restrictions [Purcell and Kotz, 1977]. A more severe framework distortion might therefore be expected if nickel were incorporated into a tetrahedral framework position. No significant framework distortions were indicated by the XRD spectra of the Ni1 or Ni3 materials suggesting that nickel may in fact not have been incorporated into the SAPO-34 framework of these samples. The reduced ethene selectivity of the Ni1 and Ni3 catalysts (in comparison to the S2 and S3* materials) may be due to the ethene dimerization activity of nickel oxide species which are most likely present in these materials. This explanation is supported by the drop in ethene selectivity of the Ni1 and Ni3 materials

(Ni3 : 35.5%; S3* : 39.0%) which is accompanied by an increase in butene selectivity (Ni3 : 15.2%; S3* : 13.2%).

Inui et al. [1990] reported that ethene selectivities could be increased to as high as 90% (C_2/C_3 olefin ratio of approximately 17) by incorporating nickel into the SAPO-34 synthesis and proposed that this change in selectivity was due to a reduction in acid site strength. These authors proposed that the weaker acidity of the NiAPSO-34 catalyst was sufficient for the dehydration of DME only, thus limiting the hydrocarbon formation to that of ethene. This explanation is questionable however, since the NH_3 TPD spectra of these NiAPSO-34 catalysts [Inui, 1991] which did indeed demonstrate a reduction in the amount of HTD acidity showed no significant reduction in the HTD peak temperature (in comparison to SAPO-34), indicating no reduction in acid site strength.

SAPO-11 (pore diameter : 0.6 Å), which has a significantly reduced acid site strength in comparison to that of SAPO-34 (pore diameter : 0.43 Å) exhibits a reduced MTO C_2/C_3 olefin ratio of 0.77 and an increased C_5+ selectivity of approximately 30% [Vaughan, 1991] compared to a C_2/C_3 olefin ratio of 1.01 and a C_5+ selectivity of 6.7% for SAPO-34. These results show that reduced acid site strength alone cannot account for the increased ethene and light olefin selectivities reported by Inui [1991].

It is possible that the high ethene selectivities reported by Inui [1991] may be explained by a distortion in a SAPO framework structure containing nickel (as proposed by Bennet and Marcus [1988] for cobalt incorporation). Framework distortion could alter the pore shape or diameter and hence the diffusivities of MTO product molecules within these pores. Although it may also be possible that the increase in selectivity seen by Inui was due to the deposition of Ni species within the SAPO-34 pore structure, this is unlikely, since during the catalyst synthesis the pore structure is filled with template, leaving little or no space for the nickel species to accumulate or deposit.

4.1.1.2 Post-synthesis modifications

Of all the modifications investigated, only deep bed calcination (S3*) resulted in an increase in catalyst CUV (Table 3.4). The appearance of additional strong HTD acidity in the S3* sample (Figure 3.05) is quite possibly due to the presence of "super" acid sites which were formed during the mild steaming which is likely to take place under deep bed calcination conditions. The formation of these super acid sites under steaming conditions has been observed with various zeolites [Beyerlein et al., 1988; Lago et al., 1986] although there is some uncertainty regarding the exact nature of these sites.

The increased crystallinity of the S3* sample may also be a result of the mild steaming which could facilitate aluminium, phosphorus or silicon migration. Silicon migration has been found to take place in zeolites under steaming conditions [Beyer et al., 1984], resulting in the formation of a uniformly structured material which is highly crystalline [Musa et al., 1987]. It is most likely that the additional HTD acidity formed in the S3* sample led to the increased MTO activity of this catalyst because, when these acid sites were selectively poisoned using ammonia, the activity of the catalyst was significantly reduced even though no structural changes took place. It is possible that the high strength of these new HTD acid sites contributed to the increased CUV of the S3* catalyst although this effect is difficult to quantify.

It is also clear that the additional strong acid sites are relatively unstable because all further modifications (S3*-SIL, S3*-STM, S3*-ACD, S3*-CAU, S3*-BRN) of the S3* catalyst resulted in almost complete elimination of these sites as measured by the additional high temperature NH_3 HTD peak (Table 3.4). This loss in acidity is reflected in the reduced CUVs and lifetimes of the various modified catalysts.

The TPD spectra of the S3*-SIL sample was very similar to that of the S3* sample with the exception of the disappearance of the additional strong acid site desorption peak (Figure 3.05 and Figure 3.06). This indicates that the additional strong acidity may be formed mostly on the outside of the catalyst, a likely possibility since steaming would be more severe on exterior of the crystallites. The tetraethoxysilane molecules are too large to enter the pores and the deposition of a silica layer on the exterior of the crystallites will cover and thus eliminate any of the acid sites which are located there.

The further reduction in the HTD acidity of the S3*-STM sample (Figure 3.06), which is also reflected in the MTO activity of this catalyst, shows that the formation of the additional strong acid sites occurs only for the very mild hydrothermal conditions of deep bed calcination (S3*) and that the SAPO-34 structure is unstable under the steaming conditions (S3*-STM) used in this study, even though these steaming conditions are considered mild for ZSM-5. Further evidence of the chemical instability of the SAPO-34 structure is seen with the S3*-BRN, S3*-CAU and the S3*-ACD samples. These samples were almost completely XRD amorphous, had very little HTD acidity and exhibited negligible MTO activity.

In summary, while post-synthesis modifications of the S3* catalyst resulted in changes in MTO activity, these modifications caused no significant changes in product selectivity. Furthermore, irrespective of the synthesis method or post-synthesis modifications, the CUV and lifetime of all the SAPO-34 catalysts tested in this study are directly related to the amount of HTD acidity of the catalysts. This trend is clearly illustrated in Figure 4.1.

4.1.1.3 Reaction conditions

Changes in CUV may be more easily understood bearing in mind the series nature of the coke formation reaction:

Oxygenates ⟶	short chain linear HCs ⟶	long chain branched HCs
	↓	↓
	(desorption)	(no desorption)
	hydrocarbon product	pore blockage (coke)

Differences in product selectivity brought about by variation of reaction conditions are largely a result of hydrocarbon cracking :

Oxygenates ⟶	short chain HCs ⟶	long chain branched HCs
	↓	↓
	cracking	cracking
	↓	↓
	(desorption)	(desorption)
	methane, ethene	short chain hydrocarbons

Reaction temperature

Changes in reaction temperature had a greater effect on the MTO activity and selectivity of the S3* catalyst than changes in space velocity or feed partial pressure. Murakami et al. [1968] investigated the effect of the Thiele modulus (ratio of chemical reaction resistance to intraparticle diffusional resistance) on series coking by varying reaction temperature. At high reaction temperatures (diffusional resistance controlled) coke deposits were concentrated on the outer layers of the catalyst pellets, the feed being converted to coke precursors almost immediately on entering the pore system. At low temperatures (reaction rate controlled) coke concentrations were highest at the center of the catalyst pellets, the feed diffusing throughout the pore system before being converted to coke precursors.

The CUV of the more acidic S3* material was significantly reduced at the higher reaction temperatures (450°C). This is to be expected considering the explanation of Murakami et al. [1968] that the coked outer layers of the catalyst pellets (and crystallites) block access to the undeactivated interior of the pellets (crystallites). This explanation is substantiated by the reduced coke content of the S3* sample run at 450°C even though the color of the spent catalyst was far darker (indicating a higher coke content, at least in the outer layers of the pellets) than that run at lower reaction temperatures. The fast coking rates at high reaction temperatures will be aggravated by direct coke formation as described by Schulz et al. [1991] :

$$2\,CH_3OH \longrightarrow C_{coke} + CH_4 + 2\,H_2O$$

The increased methane selectivity that would be expected from such a coking reaction was indeed seen for the S3* catalyst run at higher reaction temperatures, notably at 450°C.

At lower reaction temperatures (350°C) the coke concentration is highest at the center of the catalyst pellet (crystallite), allowing far better utilization of the interior of the catalyst pellet and hence an increased CUV. At the intermediate reaction temperature (400°C) it is possible that coke will form on the outer layers of the pellets and crystallites but this coke layer will be far less concentrated than at higher temperatures and will not result in blockage of the catalyst interior.

Reaction temperature required for maximum CUV

Variations in CUV, brought about by changes in reaction temperature are also affected by catalyst acidity. On materials with significantly reduced amounts of HTD acidity the formation of a coke band in the outer layer of the catalyst pellet or crystallite is inhibited at high reaction temperatures (reduced reaction rates of both coke and coke precursors allowing the feed to diffuse further into the catalyst pellet or crystallite before reacting). In this situation the interior of the catalyst pellets and crystallites may be more efficiently utilized at high reaction temperatures, and this in combination with the increased methanol conversion rate will result in increased CUVs. At low reaction temperatures, the combination of a reduced acid site concentration and a reduced reaction rate results in reduced methanol conversion rates and hence reduced CUVs.

Marchi and Froment [1991] found that increasing the reaction temperature from 380°C to 480°C increased the MTO activity of the SAPO-34 catalyst. It is possible that this trend is due to their catalyst being far less acidic than the samples used in this study, a reasonable assumption when it is noted that at similar methanol/water partial pressures, the S3* sample is 10 times more active than the more acidic of the two samples used in their study. This being the case, the effect found for the S2 sample (having a maximum activity at a higher reaction temperature) would be significantly magnified. Consequently, the findings of this study are not necessarily in disagreement with those of Marchi and Froment.

Catalysts containing an intermediate amount of acidity will be expected to have maximum CUVs at intermediate reaction temperatures. The methanol conversion reaction rate will increase with increasing reaction temperature but CUV will decrease at high reaction temperatures due to the formation of coke band in the outer layers of the catalyst pellets and/or crystallites. This situation is seen for the S2 catalyst having 66% of the acidity of the S3* material and producing a maximum CUV at 400°C.

Product selectivities as a function of reaction temperature

The increase in the C_2/C_3 olefin ratio at higher reaction temperatures (450°C), also found by Liang et al. [1990], may be due to an increase in the rate of thermal and

catalytic cracking reactions. This is supported by the associated drop in the C_2-C_4 olefin selectivity at the higher reaction temperatures.

It is likely that the increase in the C_2/C_3 olefin ratio and the decrease in the butene selectivity, as the catalyst deactivates, is due to an increase in the shape selectivity of the catalyst brought about by a reduction in the pore diameter resulting from coke deposition. The deposition of coke in the chabazite cavities may also place steric restrictions on the formation of the longer chain hydrocarbons, thereby increasing the selectivity towards the production of ethene.

Liang et al. [1990] found an increase in the C_2-C_4 olefin selectivity when the reaction temperature was increased but only reported initial selectivities. As can be seen from this study (Table 3.5), although the trend in initial selectivities is similar to that of Liang et al., these selectivities change significantly as the catalyst deactivates, especially at high temperatures. The lower initial olefin selectivities at lower reaction temperatures may be due to the longer initiation phase found for the MTO reaction at low temperatures (Prinz and Riekert, 1988).

The effect of product residence times on CUV and selectivity

Changes in CUV and selectivity as a function of space velocity, feed partial pressure and feed diluent may all be attributed to reaction product residence times within the catalyst. The series nature of coke formation in the MTO reaction ensures that CUVs are reduced when coking rates are high. As a result, a reduction in the residence times of coke precursors (MTO olefin reaction products) leads to an increase in CUV, brought about by a reduction in the rate of coke formation. Similarly, short reaction product residence times lead to decreased cracking and decomposition rates which, in turn, ensure an increased light olefin selectivity and reduced methane formation.

The above phenomena are seen at high space velocities and low methanol partial pressures where the volumetric flowrate through the catalyst bed is increased, resulting in reduced external mass transfer resistance. Reduced external mass transfer resistance results in increased product desorption and hence decreased hydrocarbon product residence times within the catalyst. Using high space velocities is advantageous from a process engineering point of view, especially

since they also result in increased catalyst utilization. The use of low methanol partial pressures will however, necessitate larger and hence more expensive process equipment.

In contrast to the above findings, Marchi and Froment [1991] found that changing the WHSV from 1 to 2.7, produced very little difference in the CUV of the SAPO-34 catalyst for the MTO reaction. This may be partially due to water being used as a diluent for the methanol feed whereas in this study, the diluent used was nitrogen. The competitive adsorption of the water diluent on the acid sites would also reduce the residence times of the light olefins on the catalyst and thereby limit coke precursor formation.

The increase in the C_2-C_4 olefin selectivity with increasing space velocity, as found for both the S2 and S3* catalysts, was also reported by Liang et al. [1990]. Marchi and Froment [1991] found no change in product selectivity with increasing space velocity. These authors did however report a slight decrease in light olefin selectivity with increasing methanol partial pressure, as was found in this study.

The use of water as a feed diluent also results in reduced reaction product residence times and hence reduced coke formation and cracking and enhanced CUV. Water is a stronger base than the methanol feed or the olefin reaction products [Xu et al., 1990] and will displace these species from the acid sites (competitive chemisorption). By reducing the residence times of the olefin reaction products (coke precursors) on the acid sites, the rate of coke formation is reduced. It has also been proposed that water inhibits the cyclization of free radical coke precursors thus reducing the formation of bulky cyclic species which may block the catalyst pore structure. The enhancement of catalyst CUV and light olefin selectivity when diluting the methanol feed with water, was also found by Marchi and Froment [1991] and Xu et al. [1990].

The best catalytic activity achieved in this study, was attained at 400°C using a highly acidic S3* catalyst and diluting the methanol feed in water, giving a catalyst lifetime of more than 50 hours. The magnitude of this lifetime and CUV enhancement depends on the reaction temperature (Table 3.4) and probably also on the catalyst acidity. As was seen in this study, at lower temperatures the magnitude of the CUV enhancement (when diluting the methanol with water) was reduced, competitive chemisorption reducing the MTO reaction rate significantly.

Although competitive chemisorption of water will reduce the residence time of a particular olefin species on an acid site, at the higher reaction temperatures the rate of the coke formation reaction is so high that the coke molecules are formed before the hydrocarbon species can desorb.

4.1.2 PROPENE OLIGOMERIZATION OVER SAPO-34

From the S2, Co1 and Ni1 samples which were tested for propene oligomerization activity it can be seen that SAPO-34 type material is not suitable for production of gasoline and distillate fuel via light olefin oligomerization. This is as expected considering the small-pore channel structure and low acid strength (in comparison to zeolites) of SAPO-34.

The channel structure of SAPO-34 is small enough to limit the formation of butenes in the MTO reaction and it is clear that the formation of even the primary propene oligomerization products, notably 2-methyl pentenes, will be restricted to a far greater extent. The coke levels of the spent catalysts were similar to those obtained for the MTO reaction indicating that propene conversion does take place within the SAPO-34 channel structure; probably within the chabazite cages. Much of the dimer and probably any of the higher oligomer reaction products (which would be highly branched) formed within the SAPO-34 channels would be trapped within the chabazite cages.

Most of the liquid product, containing mainly C_9 and C_{12} oligomers and even oligomer groupings up to C_{21}, would have had to be formed on the external surface of the SAPO-34 crystallites. These findings are similar to those of Durgakumari et al. [1990] who studied phenol alkylation over various SAPO materials. These authors found no shape selectivity for the SAPO-34 catalyst. The product spectrum included p-cresols and other aromatics, suggesting that reaction took place on the exterior surface of the catalyst.

In the case of the S2 material, oligomerization may have taken place within the SAPO-5 phase present, since the SAPO-5 channel diameter is large enough to accommodate the oligomerization products. In view of propene oligomerization studies over various SAPO materials [Pellet et al., 1986] where the oligomerization activity of SAPO-5 was found to be negligible in comparison to that of SAPO-34 this, however, seems unlikely. In addition, the propene conversion levels and product selectivities of the Co1 and Ni3 catalysts, which contained no SAPO-5 material, were similar to those of the S2 catalyst.

4.1.3 THE CATALYTIC ACTIVITY OF SAPO-34

The suitability of SAPO-34 for catalyzing methanol conversion is determined predominantly by the restrictions imposed by the catalyst pore structure. From the high MTO activity and selectivity and the low propene oligomerization activity of the catalyst it can be seen that reaction over SAPO-34 material takes place mostly within the catalyst pores. The diameter of the pores, mild acid strength and the dimensions of the chabazite cages are such that the production of C_5+ hydrocarbons is severely limited which results in a catalyst which exhibits a very high selectivity towards light hydrocarbons. Consequently, SAPO-34 is totally unsuitable for reactions involving reactants or products of more than 5 carbon atoms, unless the molecules are linear.

The small pore diameter of the SAPO-34 catalyst is not the only shape selective feature influencing the light olefin selectivity. It has been shown that the diffusivity of *n*-decane in H-chabazite (SAPO-34 isomorph) is as high as that of ethane [Chen et al., 1988]. Due to a "cage" or "window" effect the diffusivity of *n*-pentane is more than one order of magnitude less than that of *n*-decane. This cage effect arises where the dimensions of the diffusing molecule (*n*-pentane) are similar to the internal dimensions of the chabazite cage. The "caged" molecule is stabilized and will therefore, in addition to having a reduced diffusivity, also have a lower reactivity as was seen between the relative *n*-octane cracking rate constant and reduced diffusivity of *n*-octane (due to the "cage" effect) in erionite [Chen, 1988]. The mild acid strength of SAPO-34 further adds to the reduced reactivity of the "caged" molecule.

In support of this proposal, Anderson et al. [1990] showed that whereas the MTO product spectrum of SAPO-34 contained less than 1% C_5 hydrocarbons, the concentration of C_5 hydrocarbons in the intracrystalline space of the catalyst was high (approximately 25%). Thus, although the chabazite cages are largely responsible for the reduced lifetimes of the SAPO-34 catalysts, partial filling of these cages in order to reduce coking (boron impregnation) may well result in a reduction in the light olefin selectivity of the SAPO-34 catalyst by eliminating the "cage" effect.

The catalyst utilization value (CUV) of the SAPO-34 catalysts for both methanol conversion and propene oligomerization is directly related to the amount of HTD

acidity. Post-synthesis modification of the SAPO-34 catalyst by "deep bed" calcination resulted in increased HTD acidity and a greater CUV. Further modification of this deep bed calcined catalyst resulted in a reduction in catalyst acidity, yielding an associated decrease in lifetime and CUV.

Small increases in ethene selectivity were obtained on the incorporation of cobalt into the SAPO-34 framework although these were negligible in comparison to those reported by Inui [1991] for NiAPSO-34. The NiAPSO-34 samples synthesized in this study had reduced ethene selectivities, most likely due to ethene dimerization over nickel oxide species expected to be present. No significant changes in product selectivity were obtained for any of the post-synthesis modified catalysts.

The performance of the SAPO-34 catalyst at various reaction conditions is controlled by reactant and product residence times. As the formation of coke is a series reaction, shorter residence times limit the formation of coke precursors and thus increase the catalyst CUV. In a similar manner, short residence times limit the formation of methane and ethene by reducing the extent of methanol decomposition and olefin cracking.

ZSM-5, the catalyst used in the Mobil MTO process, has a far greater CUV and lifetime than that of SAPO-34 but the high light olefin selectivities produced by the latter catalyst are unrivalled. The extremely good regeneration characteristics of the SAPO-34 catalyst makes the industrial use of this catalyst viable. The cost of incorporating frequent catalyst regeneration into the process design may be somewhat offset by reduced costs of minimal downstream product separation.

4.2 CATALYTIC ACTIVITY OF MORDENITE

4.2.1 PHYSICAL AND CHEMICAL CATALYST CHARACTERIZATION

Catalyst dealumination

The increasing extent of framework dealumination with successive leaching cycles of the M1 mordenite compared with that of the MN and M2 materials (Table 3.2) can be ascribed to the differences in crystallite sizes of these materials. The smaller M1 crystallites present less intracrystalline diffusional restrictions to the leaching process than do the larger crystallites of the MN and M2 materials. These diffusional restrictions would be increased by the presence of extra-framework silicon species deposited during the catalyst synthesis. The differing dealumination rates cannot be ascribed to varying amounts of 2-D channel structure material (Cmmm point group - lower diffusional resistance) and the more common 1-D channel structure material (Cmcm point group - higher diffusional resistance) as described by Musa et al. [1987]. XRD spectra show no evidence for the presence of the Cmmm space group variant (absence of a reflection at 2-theta = 15.31°) nor is the appearance of significant amounts of amorphous material (resulting from the decomposition of the less thermally stable Cmmm material [Musa et al., 1987]) seen in any of the electron micrographs. The amount of tetrahedral aluminium remaining in the M1-2AR and M1-4AR samples was approximately 1/8 of the aluminium initially present. There are approximately 8 aluminium atoms per unit cell in unmodified mordenite and, thus, under the leach conditions used, one aluminium atom appears to be more stably bound in the crystal structure.

This effect of crystallite size is not expected to be limited to the extent of framework dealumination, but should also influence the extent of removal of the resulting extra-framework aluminium species from the crystallites. Thus, the significantly higher octahedral content of the MN and M2 samples, versus that of the M1 material, can also be explained by the smaller M1 crystallites from which the extra-framework aluminium species can diffuse more easily. Furthermore, the relative sharpness of the M1 and ZM octahedral aluminium resonances indicate these octahedral species to be highly mobile, hydrated and located in the main 12-ring channels [Goovaerts et al., 1989]. In contrast, the broad resonances observed for the refluxed MN and M2 samples suggest that a large fraction of the octahedral aluminium species located in these materials is located in the 8-ring side channels.

A sequence of dealumination events is proposed in which framework dealumination takes place simultaneously in the main channels and the side pockets. Extra-framework aluminium species in the main channels are hydrated oxy-hydroxy species which readily diffuse out of the crystallite into the bulk leaching medium. Extra-framework aluminium species within the side pockets are partially hydrated [Goovaerts et al., 1989]. As the main channel species diffuse out of the crystallites, the side pocket extra-framework species migrate into the main channels where they become fully hydrated and, in turn, diffuse out of the crystallites.

Catalyst acidity

The NH_3 desorption temperatures, especially those of the HTD peaks, are higher than those previously reported [Sawa et al., 1990; Meyers et al., 1988; Hidalgo et al., 1984; Miradatos et al., 1980]. This is due to NH_3 readsorption which was caused by the low carrier/sample ratio employed for the purpose of increasing the NH_3 concentration levels in the thermal conductivity detector.

On dealumination the number of acid sites available for NH_3 readsorption decreases and the reduced readsorption results in a lower peak maximum temperature. Thus, the results of this study, viz. the decrease in the HTD peak maximum temperature with increasing dealumination (Table 3.2), do not necessarily imply a decrease in the acid site strength as dealumination proceeds. Indeed, other workers [Karge and Dondur, 1990], using a vacuum TPD system in which the influence of readsorption is negligible, observed an increase in the strength of strong Brønsted acid sites with increasing severity of dealumination.

The initial increase in the peak temperatures of the acid treated samples is only seen where incomplete Na exchange has taken place, again reducing the number of acid sites available for readsorption and thus the HTD peak temperature maxima. This result is also to be expected since it is not unreasonable to assume that the stronger acid sites are more difficult to ion exchange than the weaker sites and hence the lower HTD peak temperature maxima for incompletely ion exchanged samples. This is clearly seen for the M2 samples and to a lesser extent the MN and M1 samples. Similar results were reported by Hidalgo et al. [1984] for potassium exchanged mordenites. The M2-2AW sample was the only -2AW

sample of the MN, M1 and M2 mordenites that still contained Na charge balancing ions and this is the most likely reason for this sample having a HTD peak temperature maxima lower than that of the M2-2AR sample.

The HTD peak maximum temperatures of all of the -H samples which had been ion exchanged and not acid treated, were significantly higher than those of the mildly acid treated -A1 and -A2 samples and in the case of the MN and M1 samples, higher than any of the peak maxima reported. Similar results were reported by Sawa et al. [1989] and Hidalgo et al. [1984]. It is likely that NH_3 readsorption is largely responsible for this in that these samples have no charge balancing Na ions present and thus all the acid sites are involved in NH_3 readsorption. Furthermore, as these samples have not been exposed to any acid, acid soluble non-structural species on the crystallite surface and in the pores would not have been removed as may be the case for the acid treated samples, resulting in reduced NH_3 diffusivity out of the crystallites and thus higher HTD peak temperature maxima.

Regardless of the difficulties introduced due to NH_3 readsorption in this study, the total acidity of the samples as measured by the total HTD NH_3 is still correctly determined by these measurements. There is a good 1:1 relationship between the amount of HTD NH_3 and the tetrahedral aluminium content of all the -2AW, -2AR and -4AR samples. As the -A1 and -A2 samples still contained significant amounts of sodium, the tetrahedral aluminium contents plotted in Figure 4.1 reflect aluminium species generating acid sites and not aluminium species which are charge balanced by Na^+ ions. The slight reduction in the amount of HTD NH_3 for the -H samples is ascribed to reduced accessibility of framework aluminium due to the presence of non-structural species deposited on the crystallite surface or in the channel structure during synthesis. The reduced accessibility of the zeolite channels of the -H samples is also seen in the cyclohexane adsorption levels of these samples (Table 3.3) indicating that acid treatment facilitates the removal of these species resulting in a more accessible pore volume, as was also reported by Chen [1976].

Sawa et al. [1990] found that, for mordenites with aluminium contents of greater than 1.65 mmol/g, the amount of HTD NH_3 decreased with increasing framework aluminium content. As the only samples in their work for which the HTD NH_3 / framework aluminium ratio was found to decrease, were unmodified, it is suggested that the accessibility to aluminium in these samples may have been

similarly restricted due to the presence of non-structural species in the zeolite channels.

Structural characterization

The shift in the asymmetric stretching T-O band with reduction in aluminium content has been reported by other workers [Musa et al., 1987; Bremer et al., 1983] and their data is compared with that obtained in this study in Figure 4.2. The results of this study are similar to those reported by Musa et al. [1987] in which the band frequency is observed to shift in the range 1060-1090 cm^{-1} as dealumination proceeds to completion. The shift of the asymmetric stretching T-O band and most of the structural bands to higher frequencies is the result of removal of aluminium from the zeolite framework. Aluminium extraction results in a reduction in the variation in the T-O bond lengths as silicon becomes the prevalent T atom in the framework. The infrared bands move to higher frequencies due to the shortening of the average T-O bond length (Si-O bond is shorter than the Al-O bond). The trend of the asymmetric stretching T-O band as a function of the

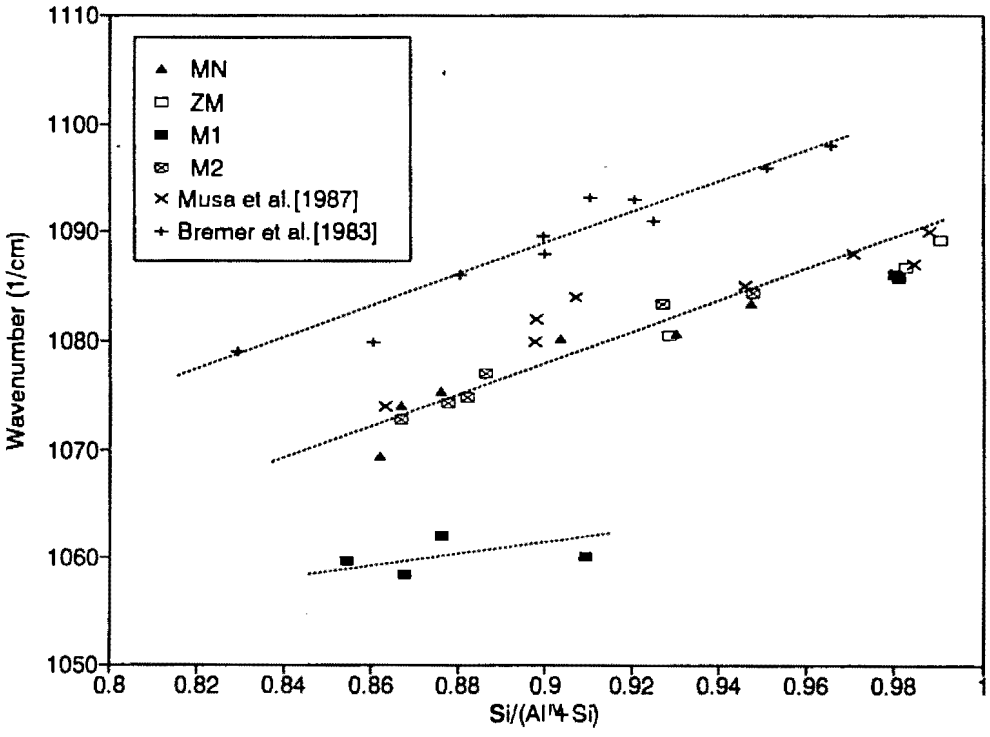

Figure 4.2 : Frequency of assymetric streching vibration as a function of Si/(tet.Al+Si).

tetrahedral aluminium content of the mildly dealuminated M1 samples lies below that of the other mordenites. The data presented by Bremer et al. [1983] indicate that the Si/(Al+Si) ratio of mordenites may be monitored by the shift in the position of the asymmetric stretching T-O band. From the results obtained in this study (Table 3.3) as well as those obtained by Musa et al., it would appear that infrared spectroscopy is an unreliable method for monitoring this Si/(Al+Si) ratio.

Several workers [Fejes et al., 1984; Dunken and Stephanowitz, 1983; Musa et al., 1987] have postulated that, when dealumination occurs without silicon substituting for extracted aluminium, new $O_3Si\text{-}O\text{-}SiO_3$ bonds may be formed between SiO_4 tetrahedra previously linked via AlO_4 tetrahedra. Ha et al. [1979] attributed an increase in the 820 cm^{-1} band to the formation of these new $O_3Si\text{-}O\text{-}SiO_3$ bonds. In the present study, however, no relationship was found between the magnitude of the 820 cm^{-1} band and the amount of framework aluminium removed.

Beyer et al. [1984] attributed the 955 cm^{-1} peak to the presence of hydroxyl nests formed on the removal of aluminium from the zeolite framework. Fejes et al. [1985] suggested that such hydroxyl nests would have a low thermal stability and should decompose at low temperatures. As no reduction in the 955 cm^{-1} band was seen in the spectra of the M1-2AR(NH3) samples calcined at 650°C and 800°C, it seems unlikely that such nests can be associated with the 955 cm^{-1} band. The inability to incorporate silicon into such nests [Barrer, 1978] is further evidence against the presence of these nests in calcined samples.

From the results of this study it can be seen that the 955 cm^{-1} band was the only structural infrared band which increased in intensity as the number of T-vacancies resulting from aluminium extraction in the mordenite structure increased (Figure 4.3). The above findings confirm that the 955 cm^{-1} band, noticeably present in the acid treated M1 and M2 samples, results from the formation of new $O_3Si\text{-}O\text{-}SiO_3$ bonds. These bonds would be longer than the normal T-O bonds since they stretch across vacancies formed by the extracted aluminium and, hence the appearance of this new band at lower frequencies than that of the undistorted T-O bonds.

The infrared spectra of the ZM samples exhibit no band at 955 cm^{-1} (Figure 3.13). This is to be expected since the dealumination procedure employed for these samples is conducive for the replacement of extracted aluminium by silicon [Pichat

et al., 1974] and, consequently, new O_3Si-O-SiO_3 bonds responsible for the 955 cm^{-1} band are not formed. The various structural bands and the asymmetric stretching T-O band are, however, narrower than those of the MN, M1 and M2 samples as would be expected since silicon has replaced aluminium (which has a longer bond length with oxygen) and thus the average variation in the T-O bond length of the ZM samples is less.

Given this assignment of the 955 cm^{-1} band to new O_3Si-O-SiO_3 bonds formed upon dealumination, it is likely that the assignment of the 820 cm^{-1} band to external symmetric stretching vibrations is correct [Flanigen, 1976; Breck, 1974]. The results shown in Figure 3.3 show the frequency of this vibration to shift from 800 cm^{-1} to 818 cm^{-1} as dealumination approaches completion, in the same manner that the asymmetric stretching vibration shifts from 1060 cm^{-1} to 1086 cm^{-1}.

As found by other workers [Musa et al., 1987; Pichat et al., 1974], the intensity of the broad band in the region 710-750 cm^{-1} decreased with decreasing framework aluminium content (Figure 3.3). This result is consistent with the previously reported association of a band at 720 cm^{-1} to framework aluminium in mordenite [Ha et al., 1979; Pichat et al., 1974].

Upon dealumination, the band in the 620-630 cm^{-1} region is observed to shift to higher wavenumbers without any accompanying loss in intensity (Figure 3.3). This band is also present at similar intensities in the highly dealuminated ZM980 sample (Figure 3.5). The assignment of this band to isolated AlO_4 tetrahedra [van Geem et al., 1988] or alternating SiO_4 and AlO_4 tetrahedra [Ha et al., 1979] is therefore not supported by these results and it is more likely that the correct assignment is that proposed by Coudurier et al. [1982] to single 4-ring vibrations. The shift in this band upon dealumination is, therefore, analogous to the shifts in the 1060-1090 cm^{-1} and 800-818 cm^{-1} regions as described above.

For the acid leached samples (MN, M1, M2) the unit cell parameters and the relative crystallinities are generally observed to decrease with decreasing aluminium content. In contrast, the unit cell parameters of the ZM samples are essentially identical, irrespective of aluminium content, and the relative crystallinity was observed to increase with decreasing aluminium content (Table 3.1). These

results are in accordance with expected trends given the removal of aluminium T-atoms in the acid leached samples and their replacement by silicon in the ZM samples. Extraction of aluminium results in a reduced unit cell size and a distorted framework structure brought about by the new bonds between $SiO_{4/2}$ tetrahedra previously linked to $AlO_{4/2}$ tetrahedra. Replacement of lost aluminium by silicon results in an increasingly crystalline framework structure formed when $SiO_{4/2}$ tetrahedra replace $AlO_{4/2}$ tetrahedra and the deviation in the T-O bond lengths becomes less.

Cyclohexane adsorption and surface areas

Cyclohexane adsorption levels (Table 3.3) indicate that all unmodified catalyst samples were large port mordenite since the adsorption levels of small port mordenites are about 1% [Raatz et al., 1983]. Upon initial dealumination, the quantity of cyclohexane adsorbed increased from that of the -H and -Na form samples. This trend was also found by Chen [1976] who ascribed this initial increase in cyclohexane adsorption levels to the removal of extraneous materials from the mordenite channels. The cyclohexane adsorption levels of the more severely dealuminated samples decreased and it is likely that this decrease is due to the simultaneous progressive decrease in channel diameter, thereby limiting the capacity for cyclohexane adsorption. That such a decrease in channel diameter occurs with dealumination may be deduced from the observed reduction in unit cell parameters (Table 3.3). In contrast to the MN, M1 and M2 materials, the cyclohexane adsorption capacities of the ZM samples are essentially constant with decreasing aluminium content as are their unit cell parameters. This result is consistent with the dealumination procedure employed for the ZM catalysts in which the extracted aluminium is replaced by silicon, thereby stabilizing the zeolite framework. The initial increase in cyclohexane adsorption capacity from that of the -H and -Na forms, is ascribed to the removal of acid-soluble non-structural species deposited in the channels or on the crystallite surface during synthesis. It is likely that the non-structural species are silicon based as there is very little extra-framework aluminium in the channels of the M1-H and M2-H samples as indicated by ^{27}Al MAS NMR. Furthermore, all organic material is removed by combustion during calcination.

The surface areas of the acid-leached samples decreased after initial dealumination (samples designated -2AW) but increased with further dealumination. These results are consistent with the sequence of dealumination steps proposed above (Section 4.2.1, Catalyst dealumination) in that the initial decrease in surface area is most likely due to partial blocking of the side pockets. Further dealumination and subsequent removal of leached aluminium species from the side pockets would result in the observed increase in surface area. The surface areas of the severely dealuminated samples exceeded those of the H-form of the catalyst. This suggests that severe dealumination may result in the linking of side pockets of adjacent main channels as described by Barrer and Petersen [1964]. Such a linking of side pockets provides both additional virgin surface area and possible accessibility to previously inaccessible channel volume. For the severely dealuminated samples, cyclohexane adsorption levels are low while the BET surface areas exceed those of the starting materials. These results are to be expected as the side pockets are accessible to nitrogen but not cyclohexane.

4.2.2 METHANOL CONVERSION OVER MORDENITE

4.2.2.1 Mordenite dealumination

From the data presented in Figure 3.25, it can be seen that the MTO CUV of the mordenite samples is not simply a function of the amount of catalyst acidity. Due to the effects of incomplete ion exchange and NH_3 readsorption in the TPD experiments, very little may be said concerning the role of acid site strength and its effect on CUV. Although several authors [Karge and Dondur, 1990; Ghosh and Curthoys, 198; Kiovsky et al., 1978; Scherzer, 1983] have reported increased acid site strength on dealumination, the rate of coke formation for several reactions is found to decrease with reduction in aluminium content [Karge et al., 1985; Karge and Boldingh, 1988; Itoh et al., 1982; Moscou and Mone, 1973; Haas et al., 1985], indicating that coke formation is possibly also dependent on acid site concentration. In agreement with these findings, several authors have found increasing MTO lifetimes with increasing dealumination [Bandiera et al., 1984; Sawa et al., 1989; Meyers et al., 1988].

The dependence of coking on acid concentration does not explain the differences in CUV trends (as a function of tetrahedral aluminium content) of the MN, M1 and M3 materials as shown in Figure 3.25. These differences are brought about by differences in crystallite size, the small crystallite M1 (0.4 microns) material being more active than the M2 material (2 microns) which is more active than the MN material (20 microns). The ZM material does not fit into the above trend due to the different dealumination procedure employed for this catalyst. The hydrothermal treatment conditions used in the dealumination of the ZM samples are conducive to silicon migration, resulting in the replacement of lost aluminium by silicon. This phenomena stops the unit cell contraction which is seen for the MN, M1 and M2 samples, thus limiting reduction of the pore diameters and ensuring increased reactant and product diffusivities, resulting in reduced reactant and product residence times and thus ensuring reduced coking and increased CUVs.

As may be expected, the diffusivity of hydrocarbon molecules within the pores of a zeolite crystal is unaffected by crystallite size [Post, 1991]. The rate of hydrocarbon adsorption/desorption, however, has been found to increase with decreasing crystallite size [Lin et al., 1989; Ruthven et al., 1988; Shah et al., 1988; Chon and Park, 1988]. Herrmann et al. [1987] found decreased conversion with

increasing crystallite size of ZSM-5 for methanol amination, methanol conversion to olefins and hexane cracking and ascribed this phenomena to under-utilization of the interior regions of the larger crystallites. Similar findings were reported by Schwarz et al. [1991] for propene oligomerization over ZSM-5.

Although the influence of crystallite size may be used to explain the differences in activity between the MN, M1 and M2 samples, the reduced CUVs of the samples containing between 3% and 5% tetrahedral aluminium require a different explanation. Samples in this range all contain significant amounts of octahedral aluminium within the channel structure. These aluminium species would reduce the effective channel diameter and therefore reduce reactant and product diffusivities which would result in increased reactant and product residence times within the catalyst pores. This increase in hydrocarbon residence time increases the amount of reaction products which are converted to coke (coke formation is a series reaction), thereby reducing the catalyst CUV and lifetime.

Configurational diffusion occurs in situations where the structural dimensions of the pores approach those of the molecules [Weisz, 1973]. Under such conditions, small changes in pore diameter may result in changes in diffusivity of several orders of magnitude [Chen et al., 1988]. That small changes in the size of pore openings strongly affect the catalytic performance of mordenite was shown by Niwa et al. [1988] who demonstrated that reduction of the pore mouth opening of mordenite (6x7 Å reduced to between 5 and 6 Å) results in large reductions in the cracking rates of various C_8 paraffins. Similar results were reported by Peeters et al. [1980] regarding the sorption capacity of various gases (Xe, Kr, Ar, N_2, O_2, H_2).

In the light of these results it is reasonable to assume that the deposition of extra-framework aluminium within the mordenite pores would result in reduced reaction product (and thus coke precursor) diffusivities (as also suggested by Scherzer [1984]) and therefore longer residence times of these products within the catalyst pores. The ionic diameter of Al^{3+} is 1.06 Å and depending on its position in the mordenite pore, could reduce the pore diameter by as much as 17%. This calculation is made using only the ionic radius of the aluminium ion and does not take into account the contribution of any of the oxygen atoms which would be bonded to the aluminium atom. In addition, Sawa et al. [1992] suggested that extra-framework aluminium species may be occluded as blocks or clusters in the zeolite crystal, a situation which would result in a further reduction in reactant and

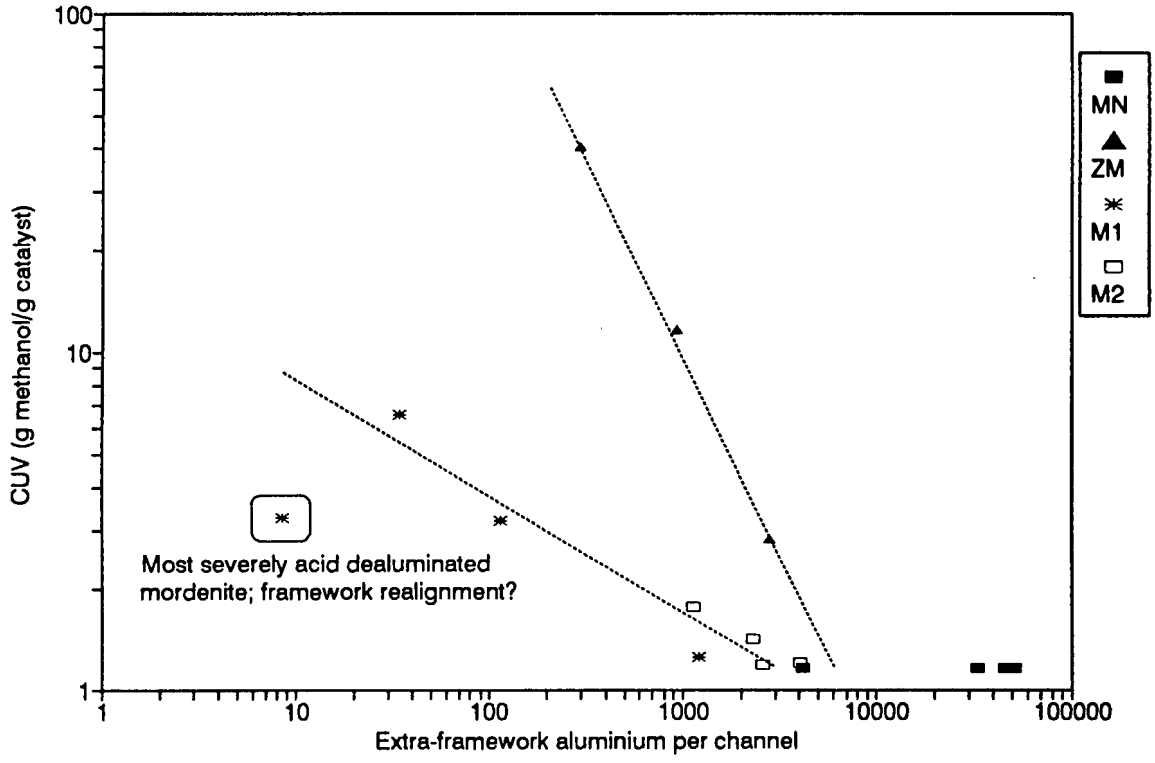

Figure 4.3 : CUV as a function of extra-framework aluminium per channel.

product diffusivities. As is the case with different crystallite sizes, samples which have physical characteristics which cause increased product residence times, have increased rates of coke formation (series nature of coking reaction) and therefore have reduced catalytic lifetimes and CUVs.

The approximate amount of extra-framework aluminium per channel may be calculated using the average crystallite size (side length for cubic crystals and length for needle shaped crystals, see Appendix VII) and the ratio of octahedral to tetrahedral aluminium (Table 3.7). The use of this parameter, viz. number of extra-framework aluminium per channel, includes the effect of extra-framework material as well as that of crystallite size (Figure 4.3), both of which increase the reactant and product residence times within the mordenite pores and thus the coking rates of these samples (coke formed by a series reaction). The more active samples containing less aluminium per channel had increased selectivities toward the higher molecular weight hydrocarbons, indicating that the reduced hydrocarbon residence times in these samples allowed the escape of these larger molecules before they could be converted to coke.

Samples containing above approximately 4 000 extra-framework aluminium atoms per channel had very close to the minimum possible lifetime (the initial conversion being 100% at the first product sampling and drastically reduced at the second product sampling). For MN, M1 and M2 samples containing less than approximately 4 000 aluminium atoms per channel, the MTO lifetime and CUV increased with decreasing number of extra-framework aluminium atoms per channel. The only exception to this was the M1-4AR(NH3) sample which had a shorter lifetime. This may be expected as this was the most severely acid dealuminated sample studied and as can be seen from the reduced unit cell size and severely reduced cyclohexane adsorption levels of this sample, it is likely that the channels have collapsed to an extent where the rates of diffusion of reactants and products through the zeolite pores are severely limited, once again resulting in an increased coking rate and hence a reduced CUV. It has also been suggested that in the so-called "T-jump" mechanism for filling of vacancies following dealumination, whole cages may collapse, the residual amorphous material creating severe diffusional restrictions within the pores.

4.2.2.2 Reaction conditions

Effect of reaction temperature

The decrease in CUV with increasing reaction temperature was marked, and similar to that found with SAPO-34. As with the SAPO-34, increasing the reaction temperature results in an increased Thiele modulus (diffusion controlled) resulting in the conversion of methanol feed into coke precursors almost immediately on entering the pore system. The coke build-up near the pore mouths makes the undeactivated crystallite interior inaccessible to the methanol feed resulting in shorter lifetimes and reduced CUVs. This explanation is supported by the relatively low coke contents of the ZM760 material (relatively uncoked crystallite interior) run at 450°C (Table 3.6) even though the final oxygenate conversion (5.3%) was lower than that of the catalyst run at 400°C (22.1%). In addition the color of the deactivated catalyst run at 450°C was far darker than that run at the lower reaction temperatures indicating increased coking, especially on the catalyst surface. The formation of this coke band on the exterior of the crystallite may be reduced by using a catalyst with a low acid site concentrations or a small crystallite material.

The very high methane selectivities obtained from the catalyst run at 450°C is an indication that direct coke formation (as described by Schulz et al., 1991) may be taking place. This phenomenon in combination with the effects arising from the elevated Thiele modulus (coking taking place close to the pore mouths) explains the very short lifetime of the catalyst run at 450°C. Hydrogen transfer and cracking rates are also increased at higher reaction temperatures as is seen by the reduction in the C_2-C_4 olefin selectivity.

Space velocity

As with the SAPO-34 catalyst, increases in space velocity resulted in reduced lifetimes and increased CUVs. The most likely reason for this trend being the reduced external mass transfer resistance at higher space velocities (due to increased volumetric flowrates; partial pressure kept constant) resulting in shorter coke precursor residence times within the crystallites and hence reduced coke formation, especially in the pore mouths. At the lowest space velocity investigated, the increased residence times near the pore mouths may result in increased coke formation which could reduce access to the crystallite interior, thereby explaining the low coke content of the catalyst run at this reaction condition.

Partial pressure

The change in CUV and lifetime with increasing methanol partial pressure is different from that observed for the SAPO-34 catalyst. Increasing partial pressures resulted in slight increases in CUV but it can be seen that the initial oxygenate conversion levels were reduced for the catalyst run at the lowest partial pressure. Taking into account the auto-catalytic nature of the methanol conversion reaction, it is possible that the reduced feed concentration resulted in a reduced initial reaction rate hence reduced initial product formation. After the initial stages of the reaction, the oxygenate conversion levels were quite similar showing that the rate of mordenite deactivation is less dependent on feed concentration than that of SAPO-34.

As with SAPO-34, dilution of the methanol feed with water resulted in a large increase in catalyst lifetime and CUV. Competitive chemisorption of water reduces

the residence times of the reaction products (coke precursors) on the active sites, thus reducing the rate of coke formation and increasing catalyst lifetime and CUV. The catalyst tested with water as a feed diluent had a CUV six times that tested using nitrogen as a diluent and yet had only a slightly higher coke content, supporting the competitive chemisorption/reduced residence time explanation as described above.

4.2.3 PROPENE OLIGOMERIZATION OVER MORDENITE

As with the MTO reaction, it can be seen from Figure 3.30 that the CUV of dealuminated mordenites for propene oligomerization is not simply a function of catalyst acidity. Once again the initial activity of these samples is influenced by the presence of extra-framework aluminium and by the crystallite size, both of which would affect the residence time of the reactants and products in the mordenite pores. This is shown in Figure 4.4 where the amount of extra-framework aluminium per channel, a combination of these two parameters, is plotted against the initial CUV of the catalyst samples. As with the MTO reaction, the propene oligomerization CUV of the M1-4AR sample is less than that of the M1-2AR which had a very similar aluminum content. This is most likely due to partial crystal collapse (as seen by the reduction in unit cell size and cyclohexane adsorption levels) or channel realignment as a result of removing too much aluminium from the mordenite framework.

Unlike with the MTO reaction, the CUV trend of the ZM samples was similar to that of the MN, M1 and M2 samples when plotted as a function of the amount of extra-

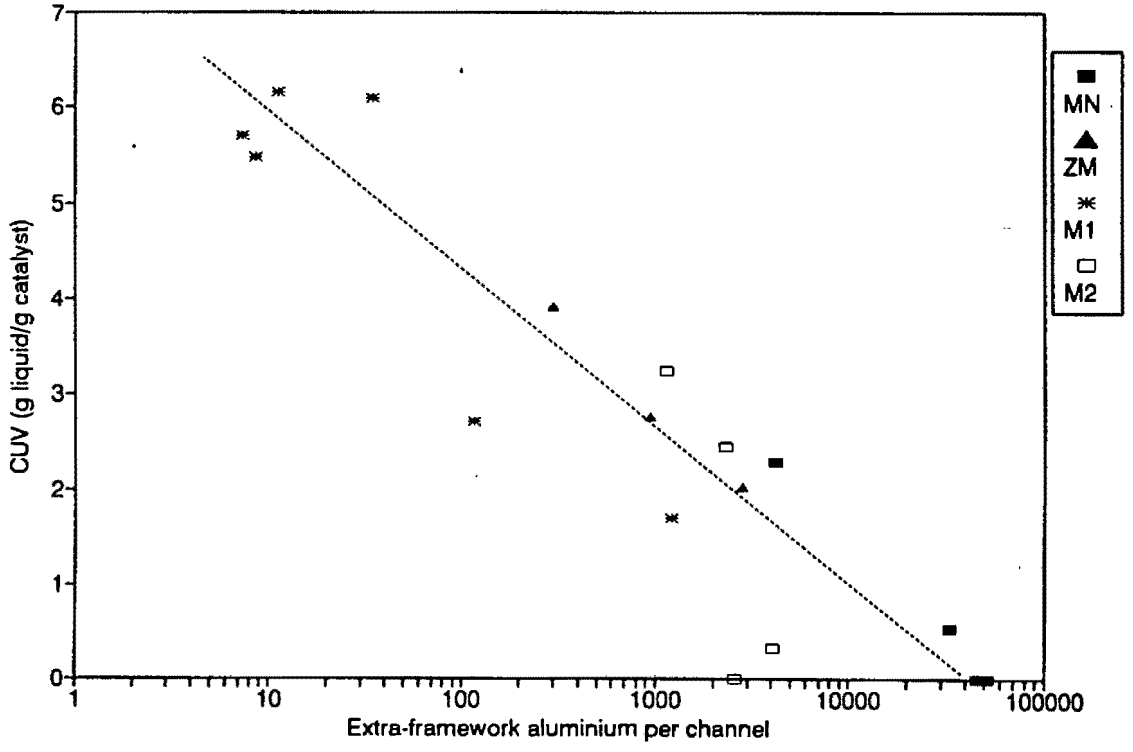

Figure 4.4 : CUV as a function of extra-framework aluminium per channel.

framework aluminium per channel. The increased CUVs of the ZM samples for the MTO reaction was ascribed to increased reactant and product diffusivities which were a result of the manner in which these samples were dealuminated. For the propene oligomerization reaction, the reaction temperature was much lower than that used for methanol conversion (200°C as apposed to 400°C) resulting in a reduced Thiele modulus. Under these conditions, the diffusional restrictions are of less importance than the reaction rate and hence the reduced diffusional restrictions imposed by the pore system of the ZM samples do not have the marked effect that they would have at the higher temperature MTO reaction conditions.

4.2.4 THE CATALYTIC ACTIVITY OF DEALUMINATED MORDENITE

The catalytic activity of the mordenite samples is severely affected by the nature and extent of dealumination. Due to the dominance of 5-rings in its structure, mordenite is unique in comparison to many other zeolites where the extraction of aluminium from the crystal framework is concerned. Unlike zeolite X or Y (three 4-rings attached to every T atom), mordenite has between zero and one 4-ring attached to every T atom [Meier, 198]. In the case of mordenite, extraction of a T atom which is connected to 5-rings may, due to the formation of new Si-O-Si bonds, result in the formation of two new 4-rings. Extraction of a mordenite T-atom connected to a 4-ring followed by the formation of new Si-O-Si bonds will result in the formation of a new 4-ring (from a 5-ring) and a new 7-ring (from a previous 8-ring).

In the case of zeolite Y, the extraction of aluminium followed by the formation of new Si-O-Si bonds can only result in the formation of new 3-rings. No new Si-O-Si bond formation has been reported for zeolite Y and it is reasonable to assume that the formation of 3-rings is difficult (lovradite is the only zeolite structure which has 3-rings) and as a result, the extraction of aluminium from zeolite Y is characterized by the formation of hydroxyl nests [Szostak, 1991].

The importance of the type of dealumination procedure employed is seen for the ZM samples; the hydrothermal treatment results in aluminium replacement by silicon and the formation of a highly stable and crystalline material as opposed to the unit cell collapse caused by acid dealumination alone. Extreme dealumination (M1-4AR) by acid treatment results in a reduction in the unit cell size and hydrocarbon sorption capacity. Sawa et al. [1992] also reported reduced sorption properties for mordenite samples dealuminated under very severe conditions.

From the study of various reaction conditions it may be seen that the rate of catalyst deactivation and CUV are severely affected by reaction temperature. Increasing the reactant space velocity or partial pressure results in little reduction in the MTO CUV indicating that, within the range investigated, catalyst deactivation is unaffected by feed space velocities and partial pressures. This means that for the MTO reaction, increased feed space velocities and partial pressures should be selected to give improved CUVs.

The trends in catalytic activity of the dealuminated mordenites were the same for both methanol conversion and propene oligomerization. It is clear that crystallite size has a significant effect on the catalytic activity of the various mordenite samples. This is not surprising when it is considered that the adsorption and desorption rates in solids are inversely proportional to the square of the diffusion path length [Chon and Park, 1988; Shah et al., 1988].

The dominant factor affecting the catalytic activity of the various mordenite samples seems to be the reactant and product residence times within the zeolite pores. Increased residence times allow for higher coking rates due to the series nature of the coking reaction. Residence times are affected by both crystallite size and occlusion by extra-framework material, within the zeolite pores. This material may be silicon species deposited during synthesis or extra-framework aluminium species deposited during the dealumination process. Using the results of this study, the selection of a mordenite catalyst for either methanol conversion or propene oligomerization should be guided by the following points :

- Small crystallite size, preferably below 1 micron in diameter
- Minimization of extra-framework species deposited during synthesis or by dealumination, possibly by acid refluxing dealuminated material with a dilute acid solution or by extensive dealumination

Minimization of the amount of extra-framework aluminium may be difficult if only mild catalyst dealumination is required unless a dilute acid solution is used in the dealumination procedure. In comparison to ZSM-5, the commercially favoured catalyst for the MTO and MOGD processes, even the highly dealuminated ZM samples exhibit severely reduced lifetimes and CUVs, the mordenite catalysts being far more susceptible to coke formation than ZSM-5.

Chapter 5

CONCLUDING REMARKS AND RECOMMENDATIONS

parent materials; most likely due to additional surface area created by the linking of side pockets of adjacent main channels.

For acid dealuminated mordenites, the area under the NH_3 TPD HTD peak may be used to determine framework aluminium content, irrespective of the presence of extra-framework aluminium. In view of conflicting results reported by other workers as well as results obtained in this study, it can be seen that infrared spectroscopy is not a reliable tool for determining the tetrahedral aluminium content of mordenites. In agreement with other authors, the 955 cm^{-1} infrared band is assigned to vibrations from new $O_3Si\text{-}O\text{-}SiO_3$ bonds formed upon framework aluminium extraction during the dealumination process. The formation of these new bonds only takes place under dealumination conditions which inhibit silicon migration (eg. non-hydrothermal conditions) and may be restricted to mordenite which has an abundance of 5-rings and, in addition, has no more than one 4-ring attached to a T-atom.

Consistent with the findings of this study, it is proposed that nitric acid dealumination of mordenites takes place in accordance with the following process:

(i) Framework dealumination occurs simultaneously in the main channels and the side pockets;
(ii) Extra-framework aluminium species in the main channels are hydrated oxy-hydroxy species which readily diffuse out of the crystallite into the bulk leaching medium;
(iii) As the main channel species diffuse out of the crystallites, partially hydrated extra-framework species within the side pockets migrate into the main channels where they become fully hydrated and, in turn, diffuse out of the crystallites.

The activity of dealuminated mordenites for methanol conversion to olefins and the oligomerization of propene is not a simple function of catalyst acidity but is significantly influenced by crystallite size and the amount of extra-framework aluminium present in the zeolite pores. The presence of extra-framework material increases reactant and product residence times within the crystallites thus increasing the probability of these species being converted to coke. If dealumination is accomplished using mineral acid treatment only, extreme dealumination is not desirable as this results in crystal collapse, which leads to a

reduced MTO and propene oligomerization catalytic activity. Dealumination accomplished using hydrothermal treatment, which facilitates the replacement of extracted aluminium by silicon, is desirable as catalysts prepared in this way have increased MTO activities.

It has been widely accepted that ZSM-5 is the preferred catalyst for the commercial MTO and MOGD processes. In this regard, neither the SAPO-34 nor the mordenite catalysts have MTO lifetimes which are comparable to that of ZSM-5. Whereas the SAPO-34 catalysts produce a significantly improved light olefin selectivity in comparison to ZSM-5, the strong acid site strength with its accompanying hydrogen transfer ability and wide pore diameter of mordenite results in a low light olefin and high paraffin selectivity. With regard to the use of these catalysts for propene oligomerization, the lifetime and CUV of the mordenite catalysts are significantly less than those obtained using ZSM-5. SAPO-34 catalysts, as a result of their low acidity and small pore diameter, exhibit almost no propene oligomerization activity.

APPENDICES

APPENDIX I : Sample calculation of conversion and selectivity for the MTO reaction

As specified in Chapter 2, conversion levels reported refer to conversion of oxygenates (methanol and dimetylether) to hydrocarbons. Product selectivities varied as the catalyst deactivated and, as a result, the selectivities reported are the average selectivities for oxygenate conversion levels above 90% for the SAPO-34 catalysts and above 50% for the mordenite catalysts (due to the short duration of the mordenite runs).

Conversion levels and hydrocarbon selectivities were calculated as percentages according to :

Oxygenate conversion = M_{MP} / M_{MF} x 100

M_{MP} = mass of methanol required for the formation of the hydrocarbon product spectrum (ie. excluding MeOH and DME)

M_{MF} = mass of methanol required for the formation of the entire sample spectrum (ie. including MeOH and DME)

Individual hydrocarbon selectivity $S_H = M_H / M_{TH} \times 100$

M_H = mass of hydrocarbon of interest

M_{TH} = total mass of hydrocarbons

C_2/C_3 olefin ratio = S_E / S_P

S_E = selectivity to ethene (wt%)

S_P = selectivity to propene (wt%)

C_2-C_4 olefin selectivity (light olefins) = $S_E + S_P + S_B$

S_E = selectivity to ethene (wt%)

S_P = selectivity to propene (wt%)

S_B = selectivity to butene (wt%)

A typical hydrocarbon product spectrum for the conversion of methanol to olefins over SAPO-34 is as follows (taken from the 2nd sample of Run SG6, data in Appendix V) :

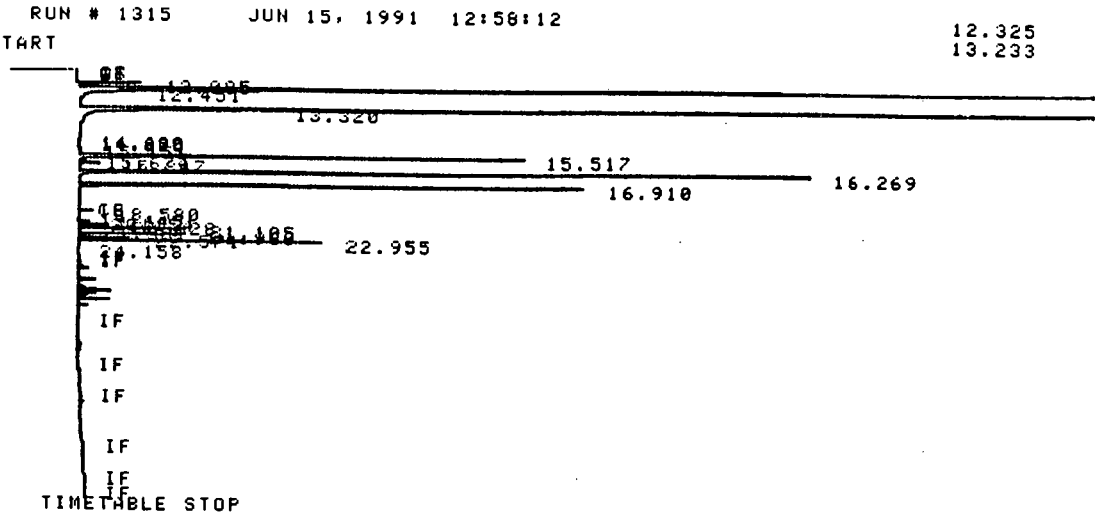

Error storing signal to M:SIGNAL .BNC
ATTEMPTED WRITE PAST END OF FILE

RUN# 1315 JUN 15, 1991 12:58:12

SAMPLE NAME: METH 1

NORM-AREA

RT	TYPE	AREA	WIDTH	HEIGHT
12.085	PB	21917	.044	8339
12.325	PV	1585401	.042	626238
12.451	VB	28965	.069	7045
13.233	BV	1807976	.042	716151
13.320	VB	71825	.049	24212
14.680	BP	529	.046	191
14.825	PP	628	.054	193
15.151	PP	2165	.070	513
15.517	PB	196554	.058	56366
15.674	PP	1577	.041	641
15.847	PB	8371	.049	2826
16.269	PB	272878	.049	92458
16.910	PB	195060	.051	63891
21.500	++	261220	.058	75257
29.500	++	99140	.063	26029
37.250	++	15208	.062	4073
42.750	++	4353	.074	975
48.500	++	7100	.087	1360
54.250	++	1001	.088	189

TOTAL AREA=4581869
MUL FACTOR=1.0000E+00

GC spectrum of on-line MTO product sample from SAPO-34.

Peak allocations for SG6 are as follows :

Peak R.Time	Component Name	Area	Response Factor	Component wt %
12.085	Methane	21917	1	0.47
12.325	Ethene	1585401	1	34.11
12.451	Ethane	28965	1	0.62
13.233	Propene	1807979	1	38.90
13.320	Propane	71825	1	1.55
14.680	DME	529	3	0.03
14.825	*i*-Butane	628	1	0.01
15.151	Methanol	2165	3	0.14
15.517	*1*-Butene	196554	1	4.23
15.674	*n*-Butane	1577	1	0.03
15.847	MEE	8371	3	0.54
16.269	*c-2*-Butene	272878	1	5.87
16.910	*t-2*-Butene	195060	1	4.20
21.500	C-5	261220	1	5.62
29.500	C-6	99140	1	2.13
37.250	C-7	15208	1	0.33
42.750	C-8	4353	1	0.09
48.500	C-9	7100	1	0.15
54.250	C-10	1001	1	0.02
Total		4581869		

$CO + CO_2$ analysis : Nothing detected.

1 g DME is formed from 1.39 g of methanol
1 g MEE is formed from 1.60 g of methanol
1 g of methane is formed from 2.0 g of methanol
1 g of olefin is formed from 2.28 g of methanol
1 g of paraffin is formed from 2.13 g of methanol

From the above, the mass of methanol needed to form all the oxygenates in the product (including methanol) is :

0.03 g x 1.39 = 0.04 g (DME)
0.54 g x 1.60 = 0.86 g (DME)
0.14 g (methanol)
Total methanol needed = 0.98 g

The mass of methanol needed to form the methane is :

0.47 g x 2.00 = 0.94 g

The mass of methanol needed to form the C_2-C_4 paraffins is :

(0.62 + 1.55 + 0.01 + 0.03) g x 2.13 = 4.71 g

The mass of methanol needed to form the C_2-C_4 olefins is :

(34.11 + 38.90 + 4.23 + 5.87 + 4.20) g x 2.28 = 199.07 g

Assuming the remaining product to be mostly olefinic, the mass of methanol needed to form the remaining hydrocarbons is :

(5.62 + 2.13 + 0.33 + 0.09 + 0.15 + 0.02) g x 2.28 = 19.02 g

Thus, the mass of methanol needed to form the hydrocarbon product is :

0.94 g + 4.71 g + 199.07 g + 19.02 g = 223.74 g

The oxygenate conversion in therefore :

223.74/(223.74 + 0.98) x 100 = 99.56%

For the hydrocarbon selectivities, the component area, as shown above, is divided by cumulative area of the hydrocarbon product :

Methane 21917/(4 581 869-529-2165-8371) x 100 = 0.48

The remaining selectivities may be calculated in a similar manner :

Methane	: 0.5 wt%	$CO+CO_2$	: 0.0 wt%
Ethane	: 0.6 wt%	Ethene	: 34.7 wt%
Propane	: 1.6 wt%	Propene	: 39.6 wt%
Butane	: 0.0 wt%	Butene	: 14.5 wt%
C_5 HCs	: 5.7 wt%	C_6+ HCs	: 2.8 wt%
C_2-C_4 Ol.	: 88.8 wt%	C_2/C_3 Ol.	: 0.88

The above values are those that are displayed in Section 2.3.1.

APPENDIX II : Sample calculation of conversion and selectivity for the oligomerization reaction

As shown in Chapter 2, conversions and selectivities for the oligomerization are calculated as follows :

% Conversion = $(M_L / M_F) \times 100$

M_L : mass of liquid product collected over the preceding hour

M_F : mass of feed passing through catalyst bed over the preceding hour

C_{9+} selectivity = $(M_{9+} / M_{HC}) \times 100$

M_{9+} : mass of hydrocarbons containing 9 or more carbon atoms

M_{HC} : mass of liquid hydrocarbon product

C_{12+} selectivity (diesel type product) = $(M_{12+} / M_{HC}) \times 100$

M_{12+} : mass of hydrocarbons containing 12 or more carbon atoms

M_{HC} : mass of liquid hydrocarbon product

The mass of liquid product is obtained by weighing the contents of the catchpot. The feed rate through the catalyst bed is a combination of the liquid and gas product rates, the latter being calculated as follows :

$$\text{Mass of gas} = n \times MW_{av}$$

The average molecular weight (MW_{av}) is calculated from the GC analysis of the gas product taken during the preceding hour. The number of moles (n) is calculated as follows :

$$n = P \times V / (R \times T \times z)$$

P : Absolute gas pressure

V : WGF_2-WGF_1, the change in wet-gas-flowmeter readings over the previous hour.

R : Molar gas constant

T : Absolute temperature

z : Compressibility factor (0.98 for an average gas product at ambient conditions)

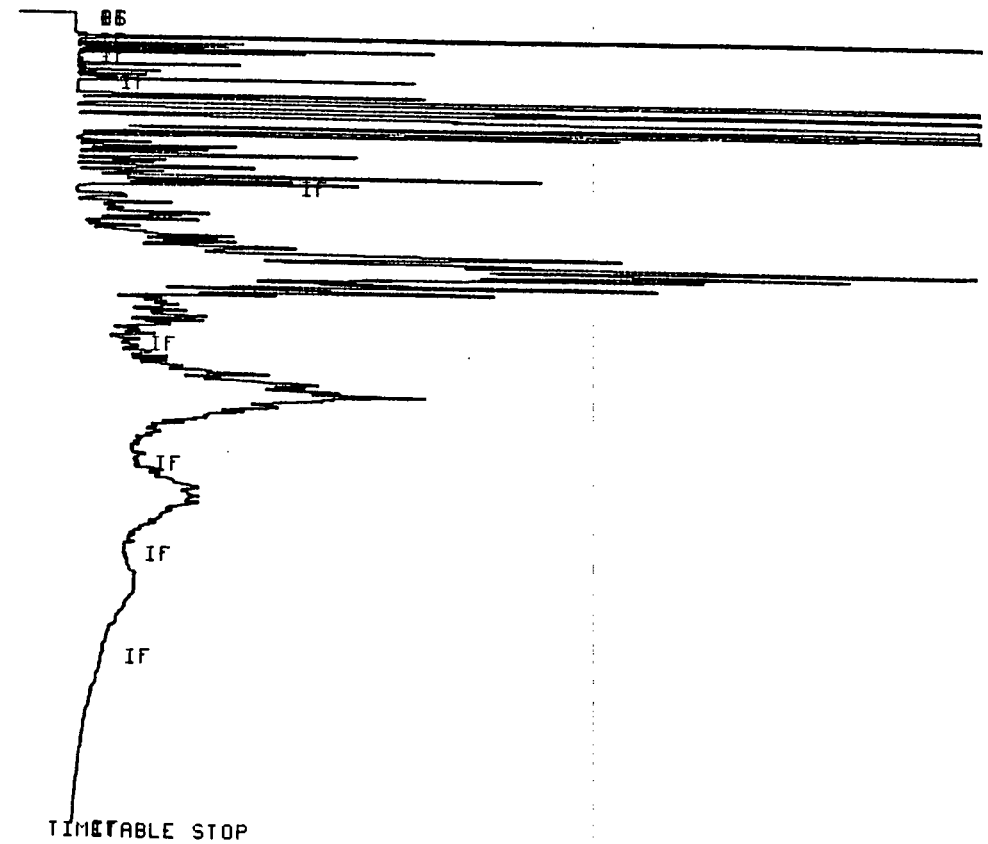


```
Closing signal file M:SIGNAL   .BNC
Storing report to M:Q4B47B49.RPT

RUN#     98            JUN 15, 1992  14:55:04

METHOD NAME: M:SAPO.MET

SIGNAL FILE: M:SIGNAL.BNC
REPORT FILE: M:Q4B47B49.RPT
NORM-AREA
      RT TYPE        AREA  WIDTH CAL#      AMOUNT  NAME
   2.545   PB        3025   .017   1R        .007  C3
   2.850   ++     1896924   .027   2        4.227  C4
   3.525   ++      310710   .029   3         .692  C5
   5.575   ++    16220840   .067   4       36.142  C6/C7/C8
   9.750   ++    13622640   .091   5       30.353  C9/C10/C11
  14.275   ++     8218064   .104   6       18.311  C12/C13/C14
  17.675   ++     3554949   .124   7        7.921  C15/C16/C17
  20.750   ++     1048615   .077   8        2.336  C18/C19/C20
  25.200   ++        4967   .049   9         .011  C21+

TOTAL AREA=4.4881E+07
MUL FACTOR=1.0000E+00
```

An example of a propene oligomerization liquid product spectrum with peak allocations.

The C_{9+} and C_{12+} selectivities for this sample are as follows :

$$C_{9+} = 30.353 + 18.311 + 7.921 + 2.336 + .011 = 58.93\%$$
$$C_{12+} = 18.311 + 7.921 + 2.336 + .011 = 40.62\%$$

A commercially obtained diesel fuel was analyzed as being 99% C_{9+} and 95% C_{12+} as shown below using the same GC program as was used for the liquid product analysis :

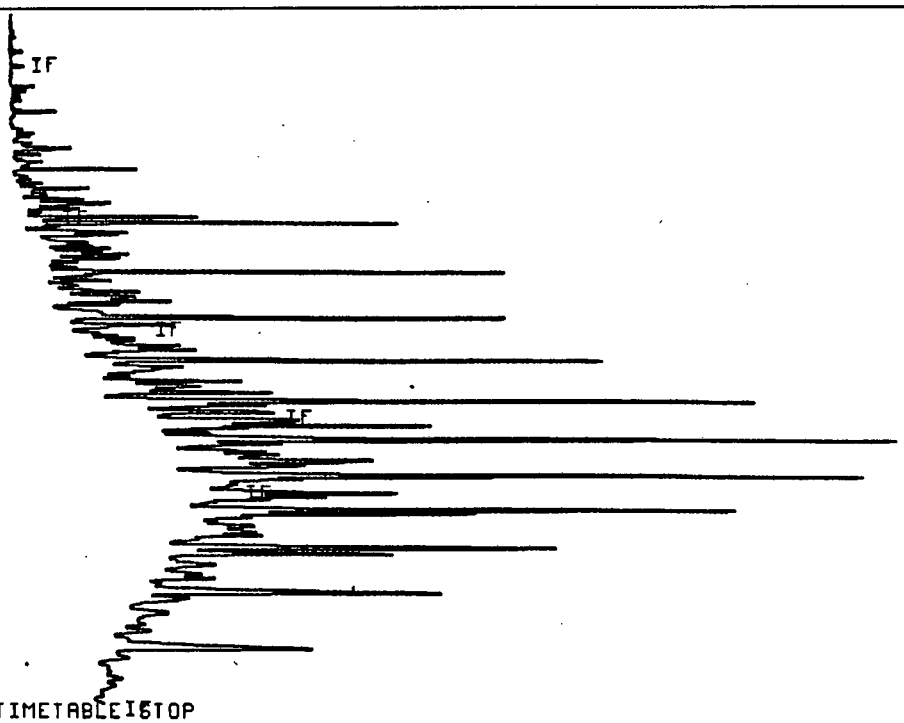


```
Closing signal file M:SIGNAL   .BNC
Storing report to M:Q4D2ABF4.RPT

RUN#   131          JUL  7, 1992  12:30:42

METHOD NAME: M*SAPO.MET

SIGNAL FILE: M:SIGNAL.BNC
REPORT FILE: M:Q4D2ABF4.RPT
NORM-AREA
      RT TYPE        AREA  WIDTH CAL#      AMOUNT  NAME
   2.900   ++        1241   .025   2         .005  C4
   3.650   ++        9627   .035   3         .036  C5
   5.750   ++       63010   .054   4         .236  C6/C7/C8
   9.725   ++     1095551   .068   5        4.096  C9/C10/C11
  13.925   ++     3478862   .071   6       13.008  C12/C13/C14
  17.125   ++     3646005   .081   7       13.633  C15/C16/C17
  19.775   ++     7571139   .098   8       28.309  C18/C19/C20
  24.500 I ++    10879064   .121           40.678

TOTAL AREA=2.6744E+07
MUL FACTOR=1.0000E+00
```

APPENDIX III : XRD patterns of SAPO-34 and mordenite catalysts

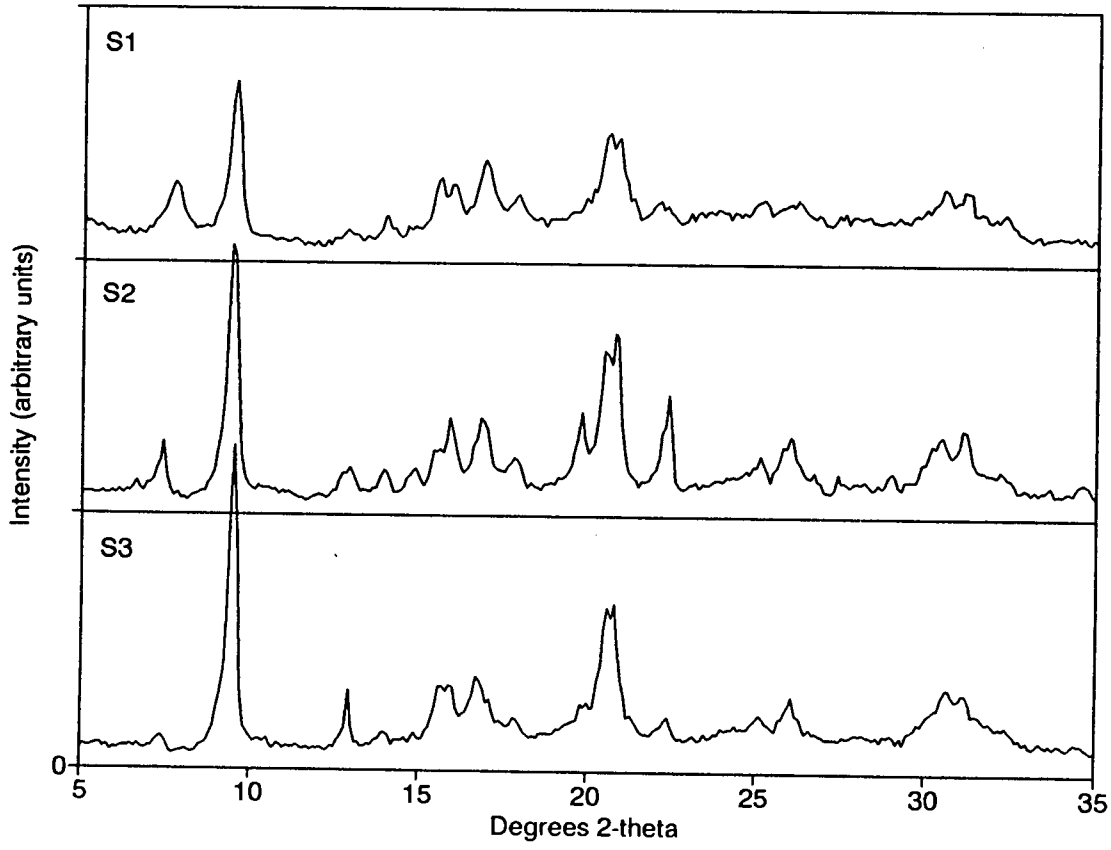

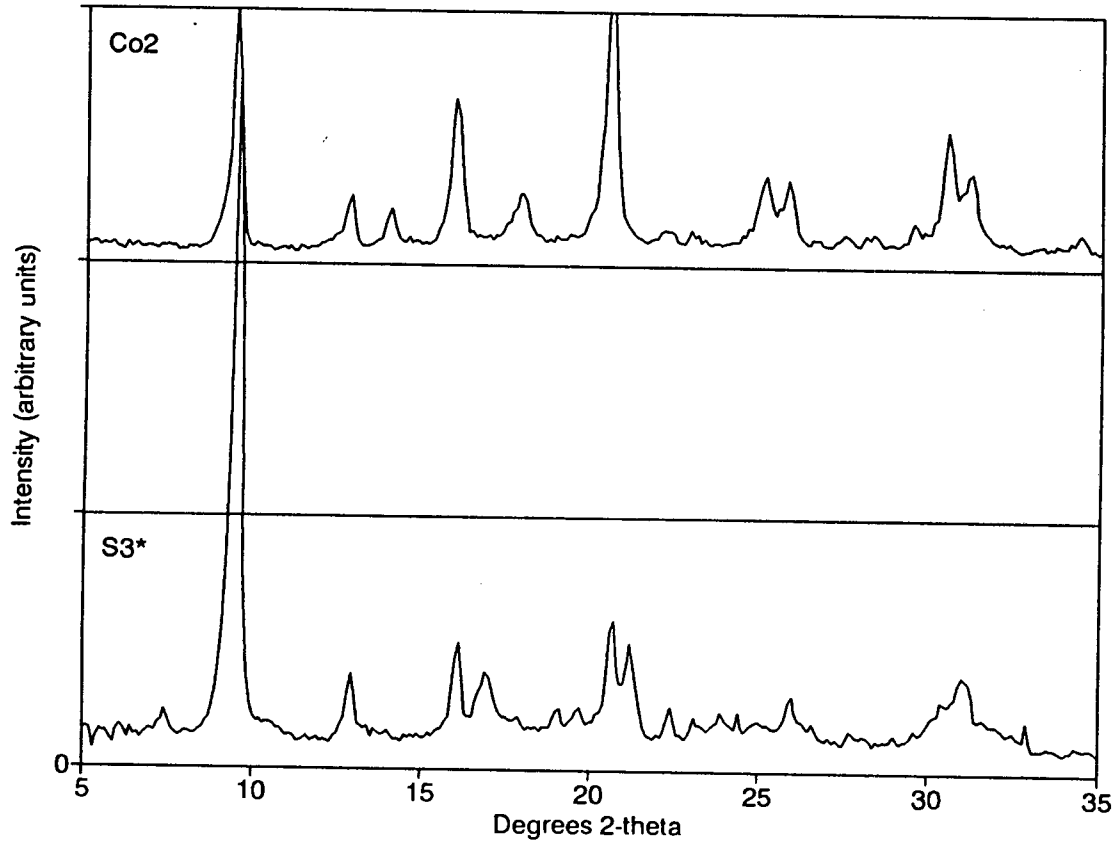

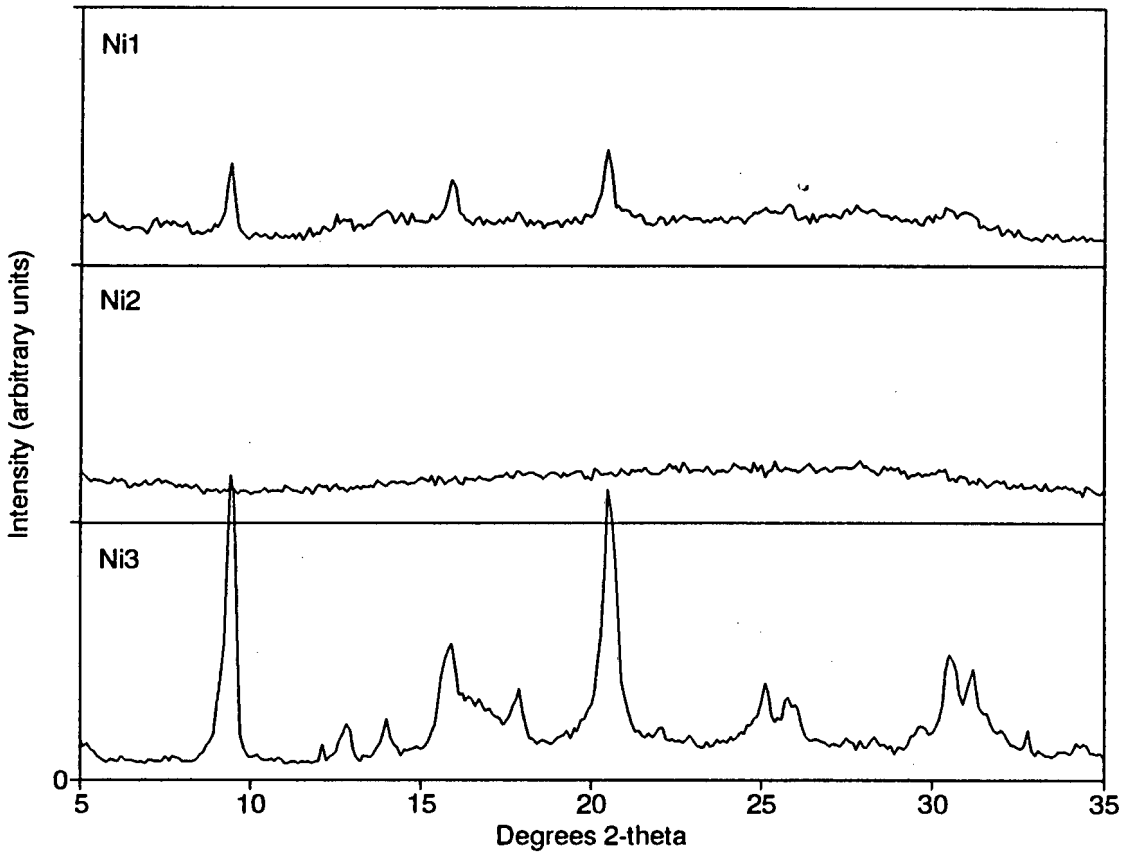
Ni1
Ni2
Ni3
Intensity (arbitrary units)
0
5
10
15
20
25
30
35
Degrees 2-theta

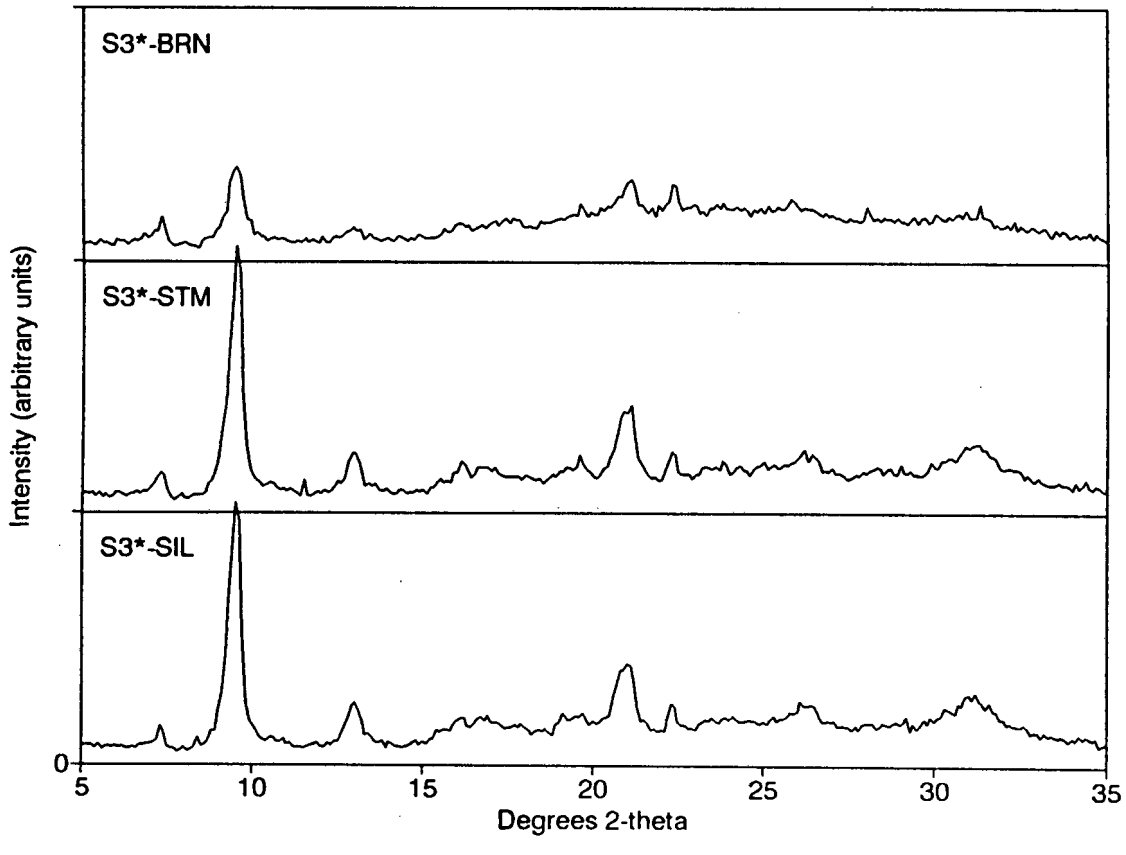
S3*-BRN
S3*-STM
S3*-SIL
Intensity (arbitrary units)
0
5
10
15
20
25
30
35
Degrees 2-theta

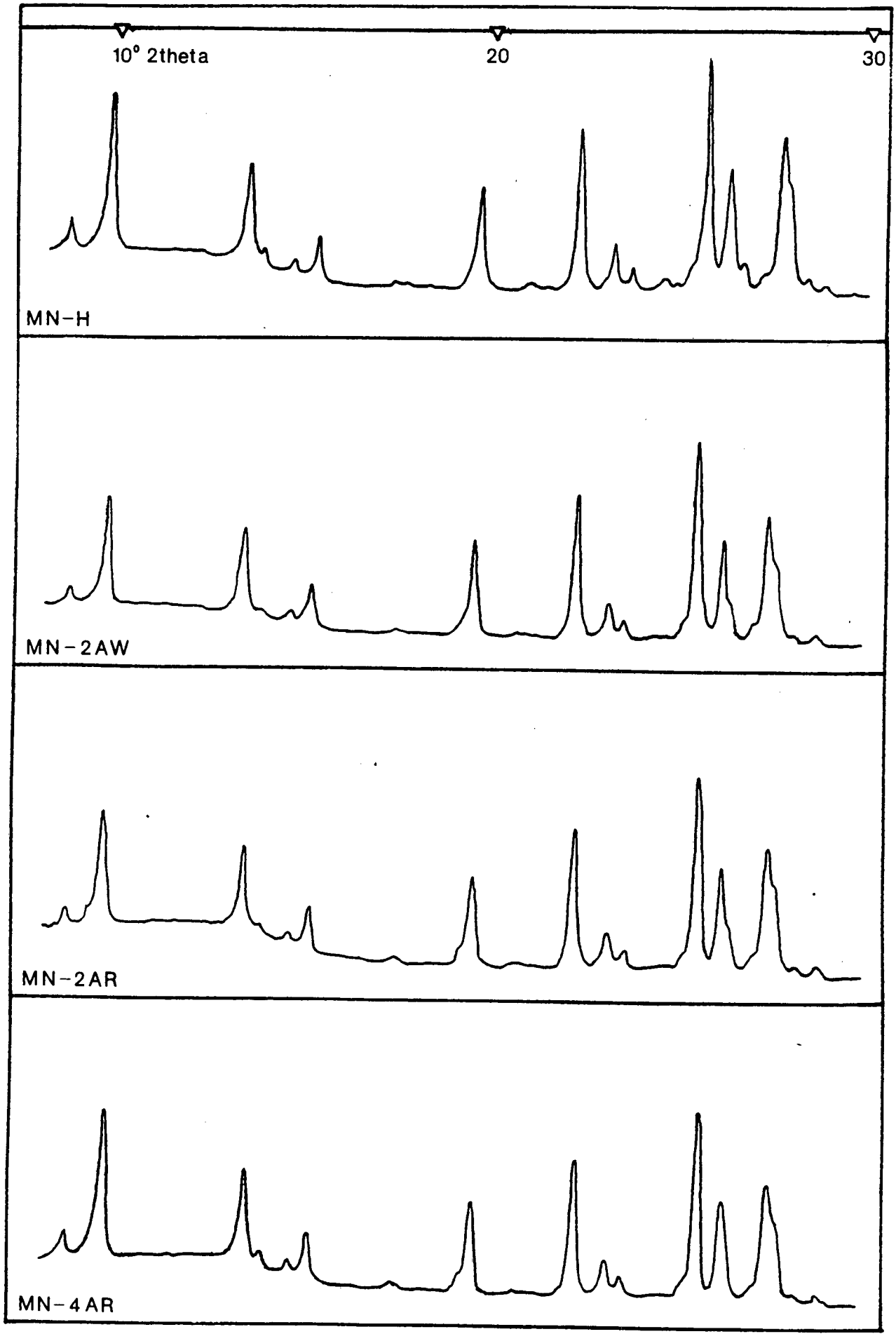
10° 2theta
20
30
MN-H
MN-2AW
MN-2AR
MN-4AR

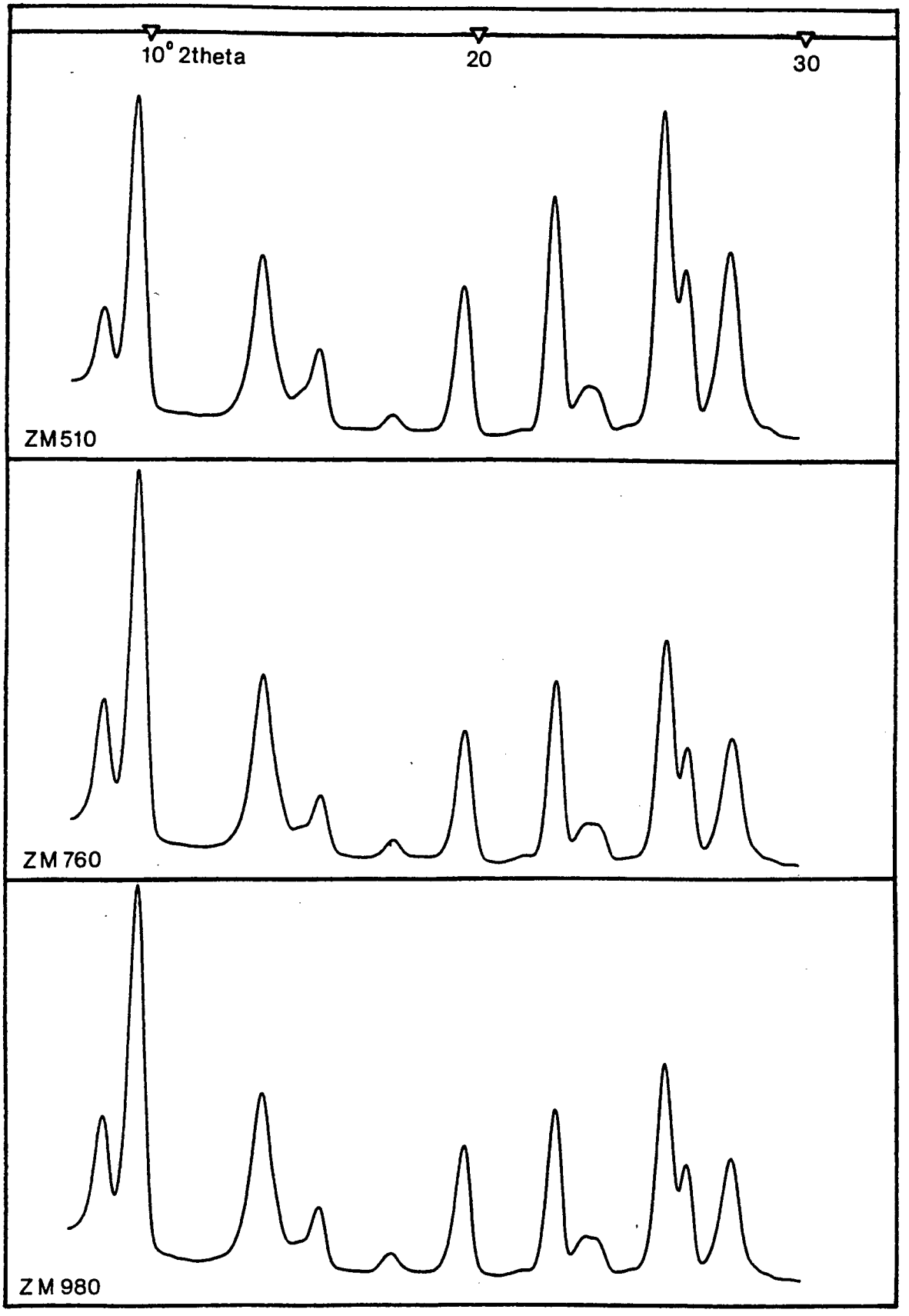
10° 2theta
20
30
ZM510
ZM760
ZM980

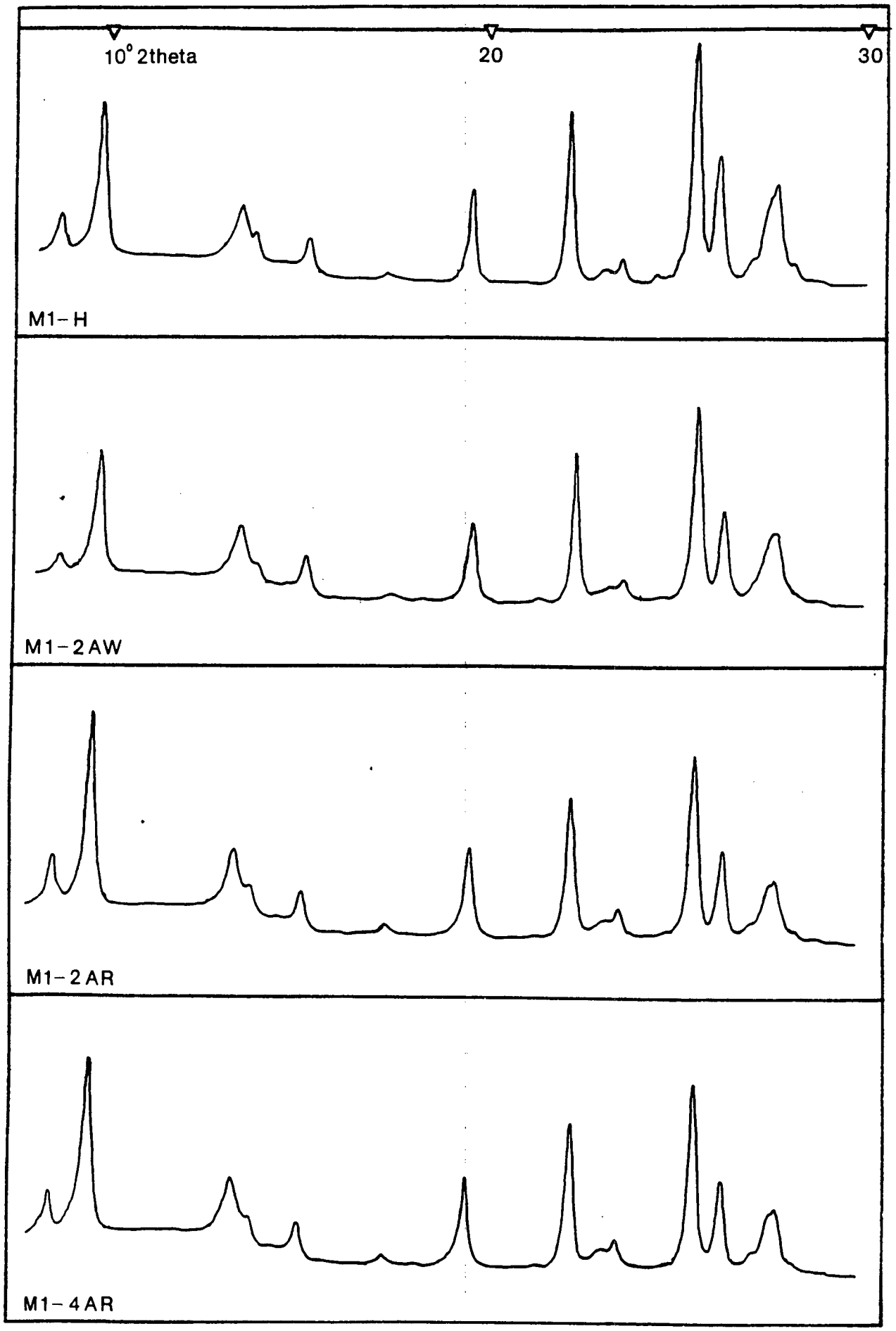
10° 2theta
20
30
M1-H
M1-2AW
M1-2AR
M1-4AR

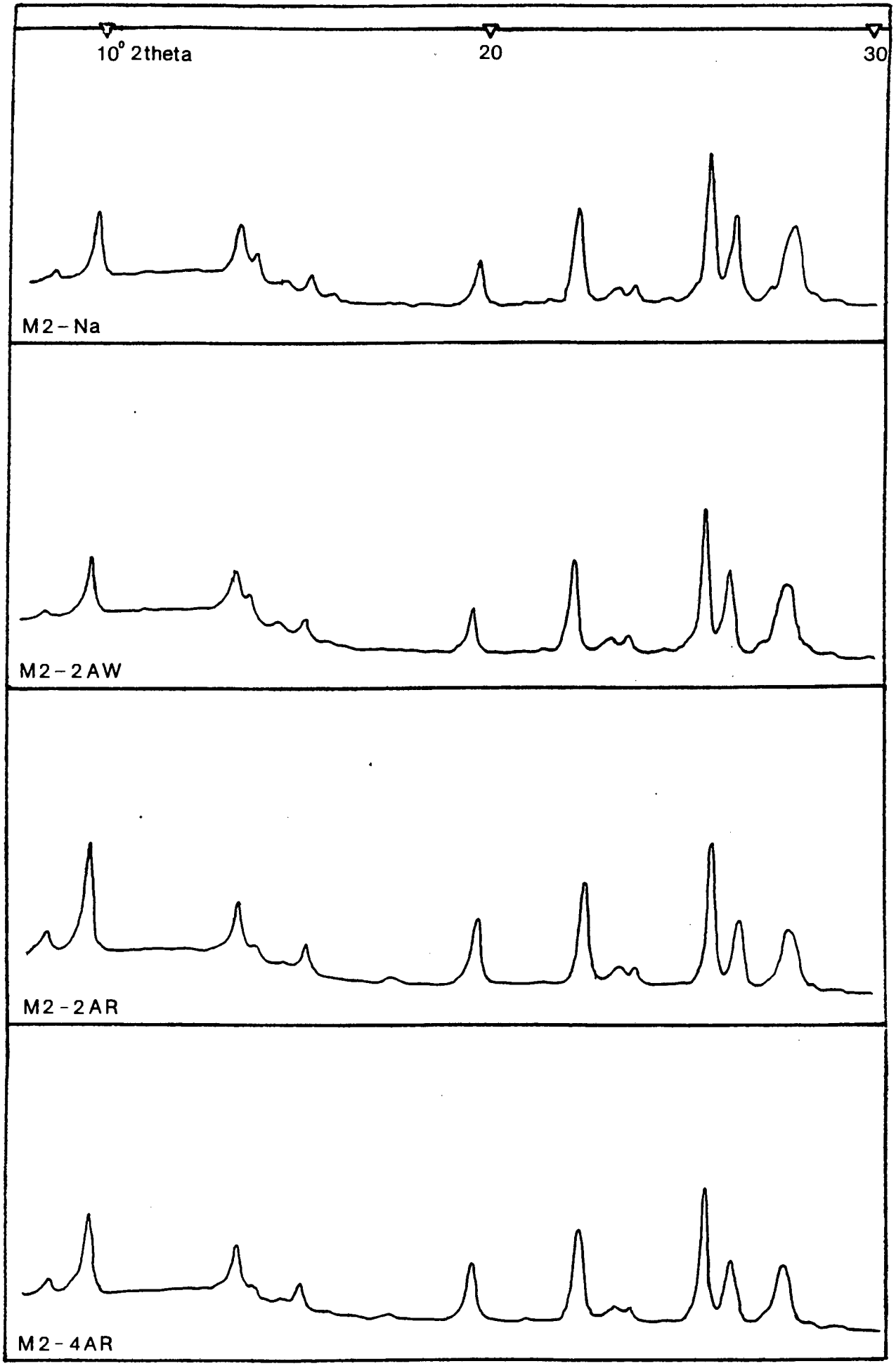
10° 2theta
20
30
M2-Na
M2-2AW
M2-2AR
M2-4AR

APPENDIX IV : Infrared spectra of the mordenite catalysts

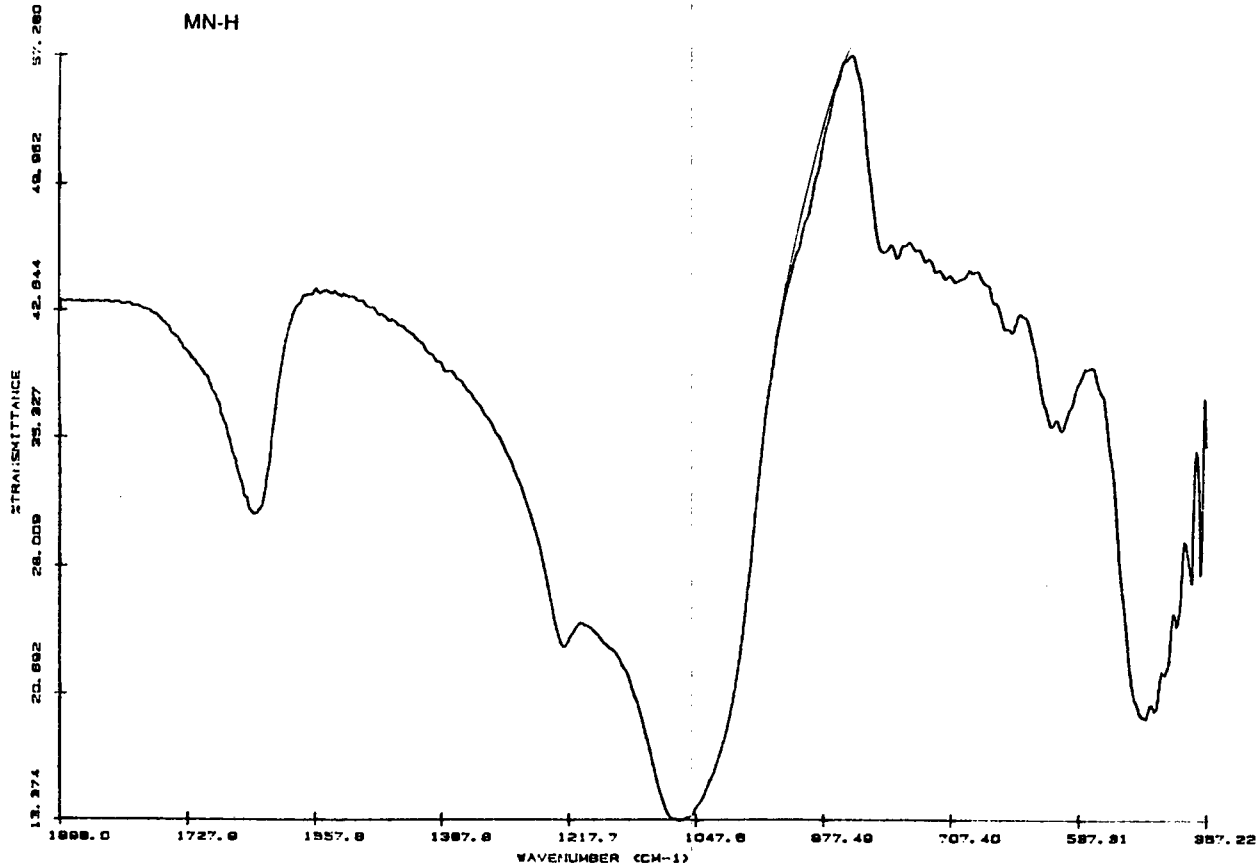

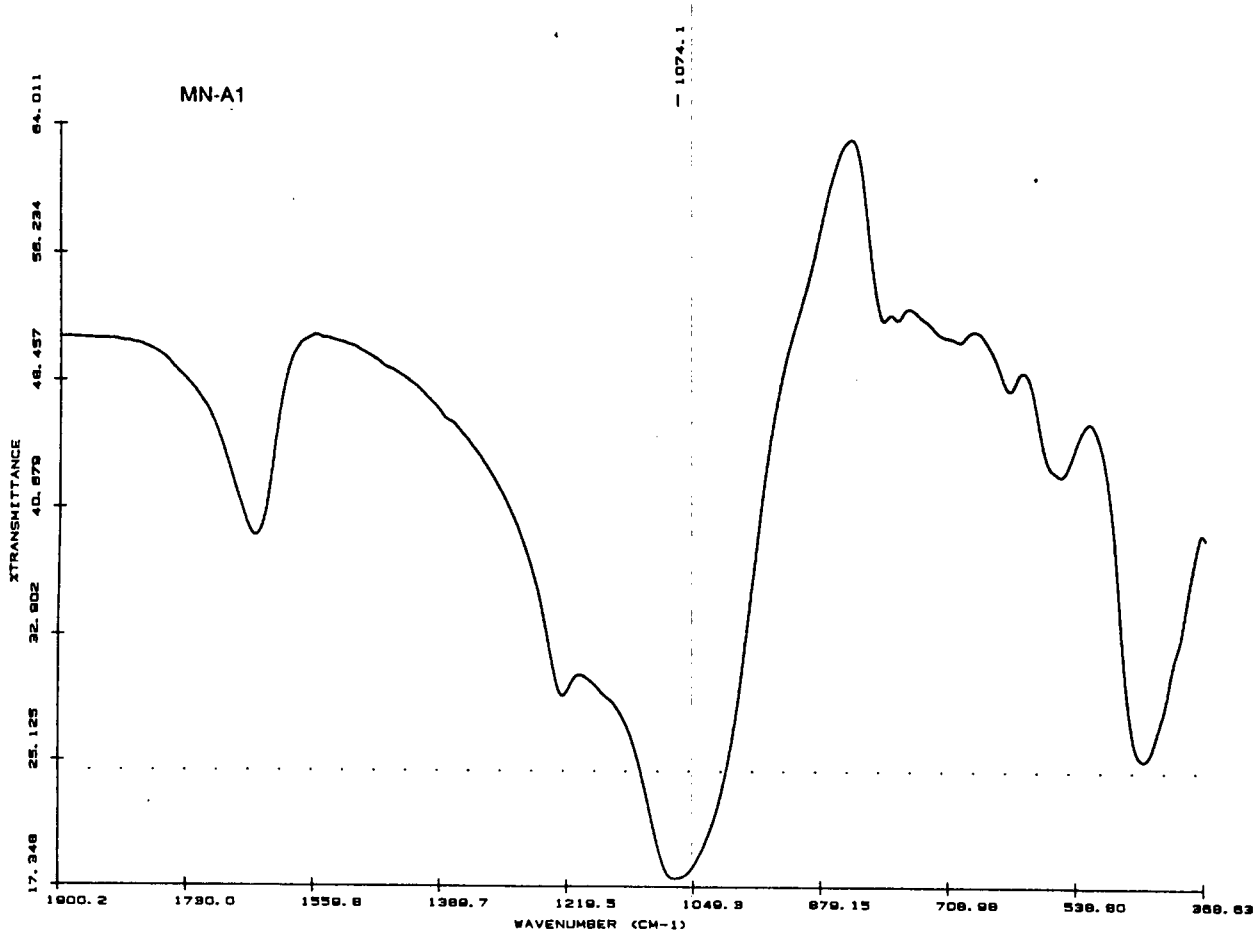

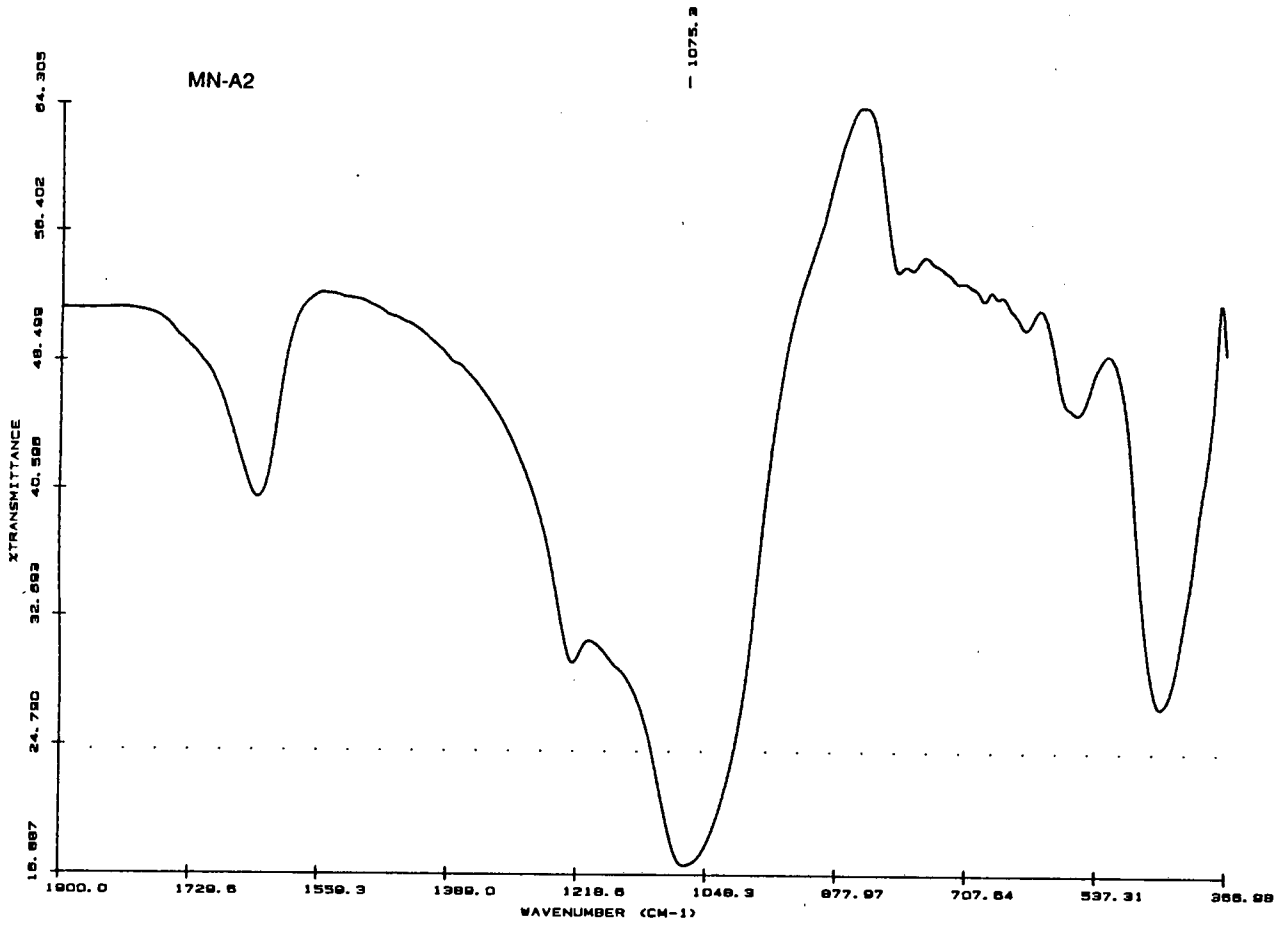
MN-A2
1075.2
64.305
56.402
48.498
40.595
32.693
24.790
16.887
%TRANSMITTANCE
1900.0
1729.6
1559.3
1389.0
1218.6
1048.3
877.97
707.64
537.31
366.98
WAVENUMBER (CM-1)

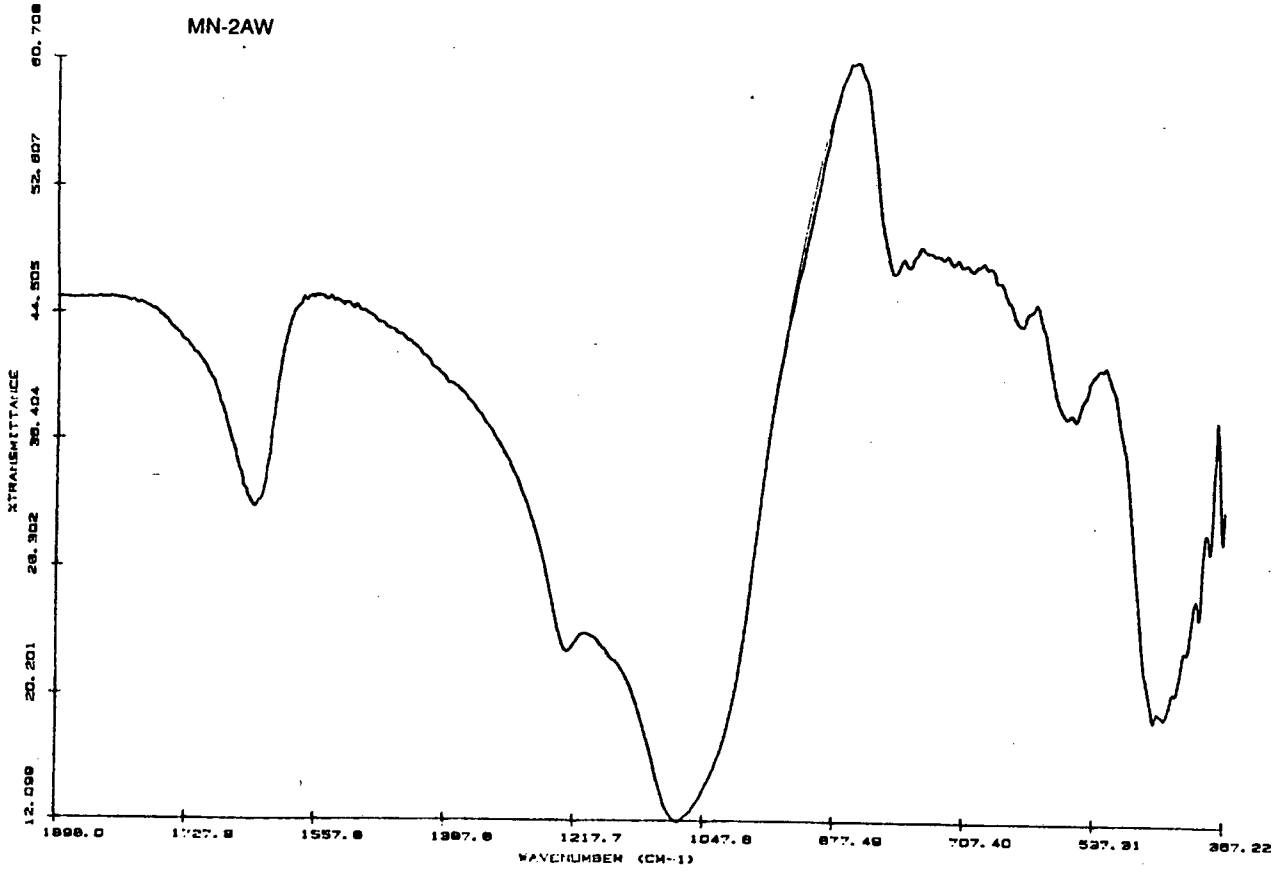
MN-2AW
60.708
52.807
44.905
37.004
29.102
21.201
13.299
%TRANSMITTANCE
1898.0
1727.8
1557.6
1387.6
1217.7
1047.8
877.49
707.40
537.31
367.22
WAVENUMBER (CM-1)

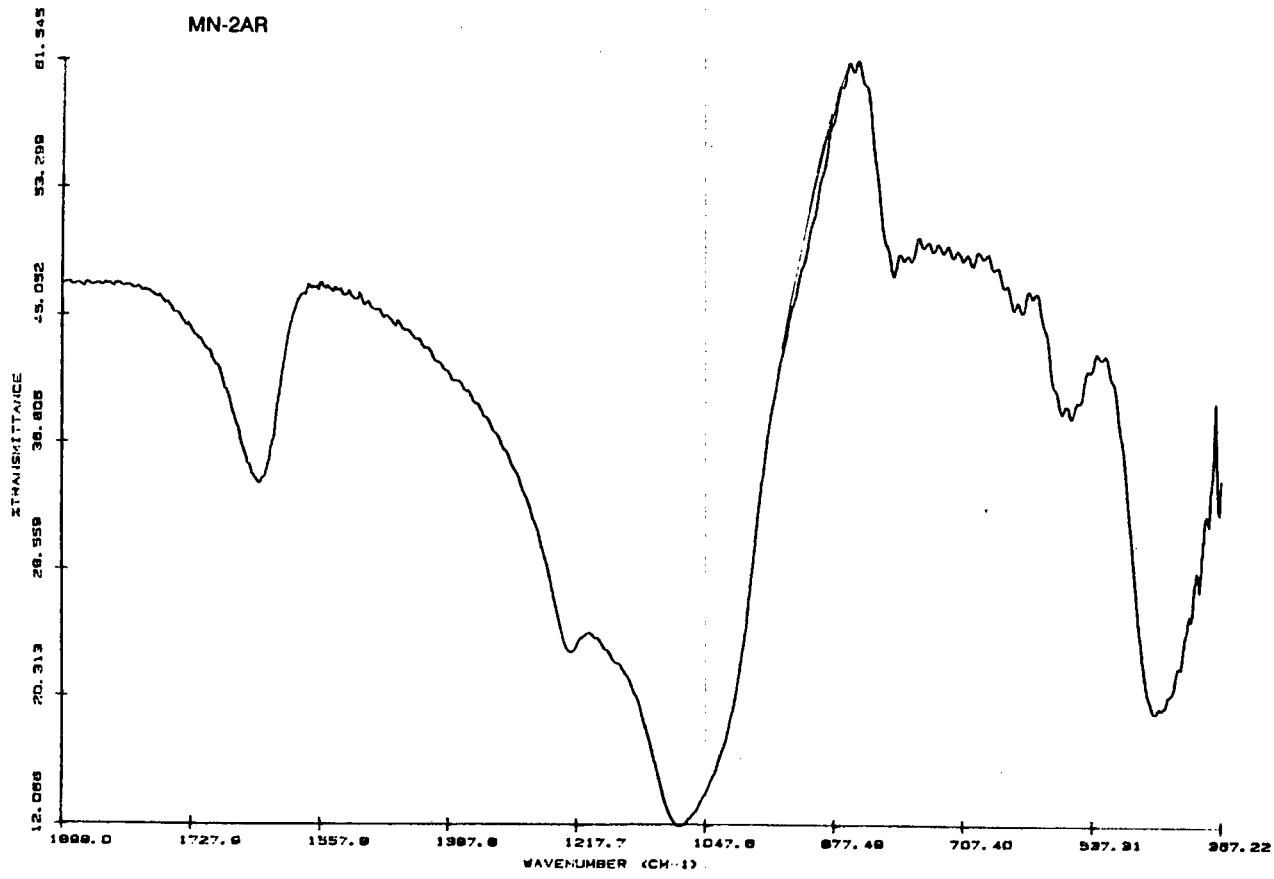
MN-2AR
%TRANSMITTANCE
61.345
53.299
45.252
38.806
28.559
20.313
12.066
1898.0
1727.9
1557.9
1387.8
1217.7
1047.6
877.49
707.40
537.31
367.22
WAVENUMBER (CM-1)

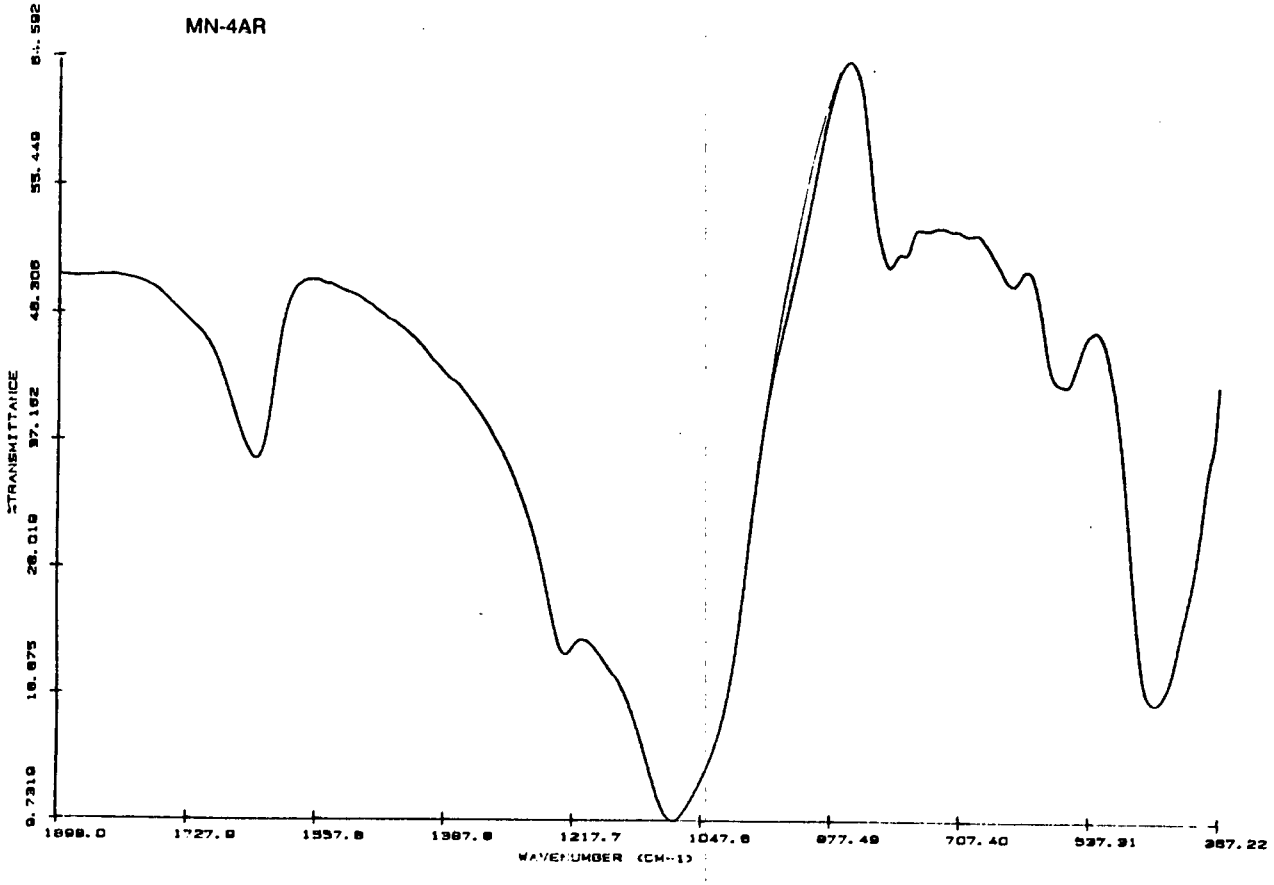
MN-4AR
%TRANSMITTANCE
64.592
55.449
46.306
37.162
28.019
18.875
9.7319
1898.0
1727.9
1557.8
1387.8
1217.7
1047.6
877.49
707.40
537.31
367.22
WAVENUMBER (CM-1)

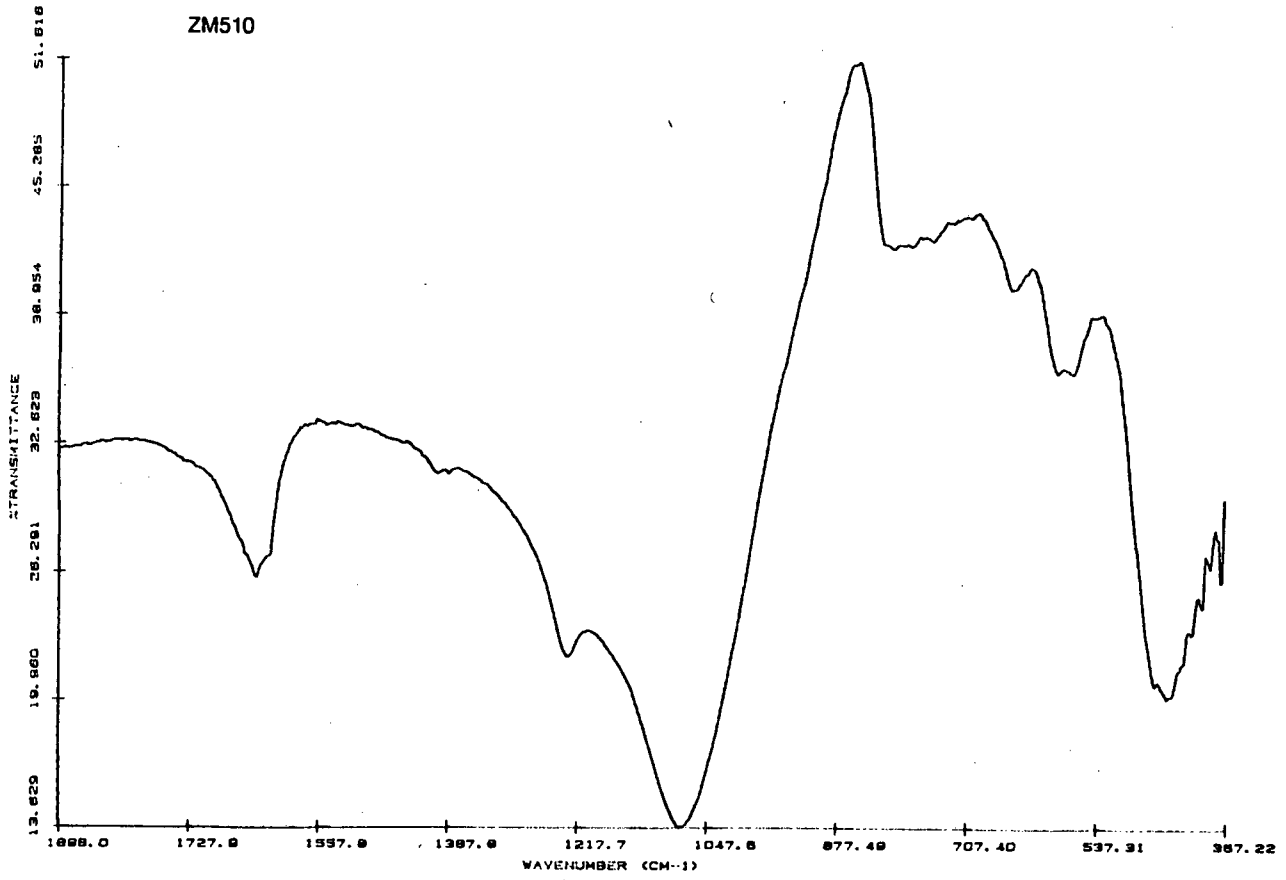
ZM510
TRANSMITTANCE
51.818
45.285
38.954
32.623
26.291
19.960
13.629
1888.0
1727.9
1567.8
1387.6
1217.7
1047.6
877.49
707.40
537.31
367.22
WAVENUMBER (CM-1)

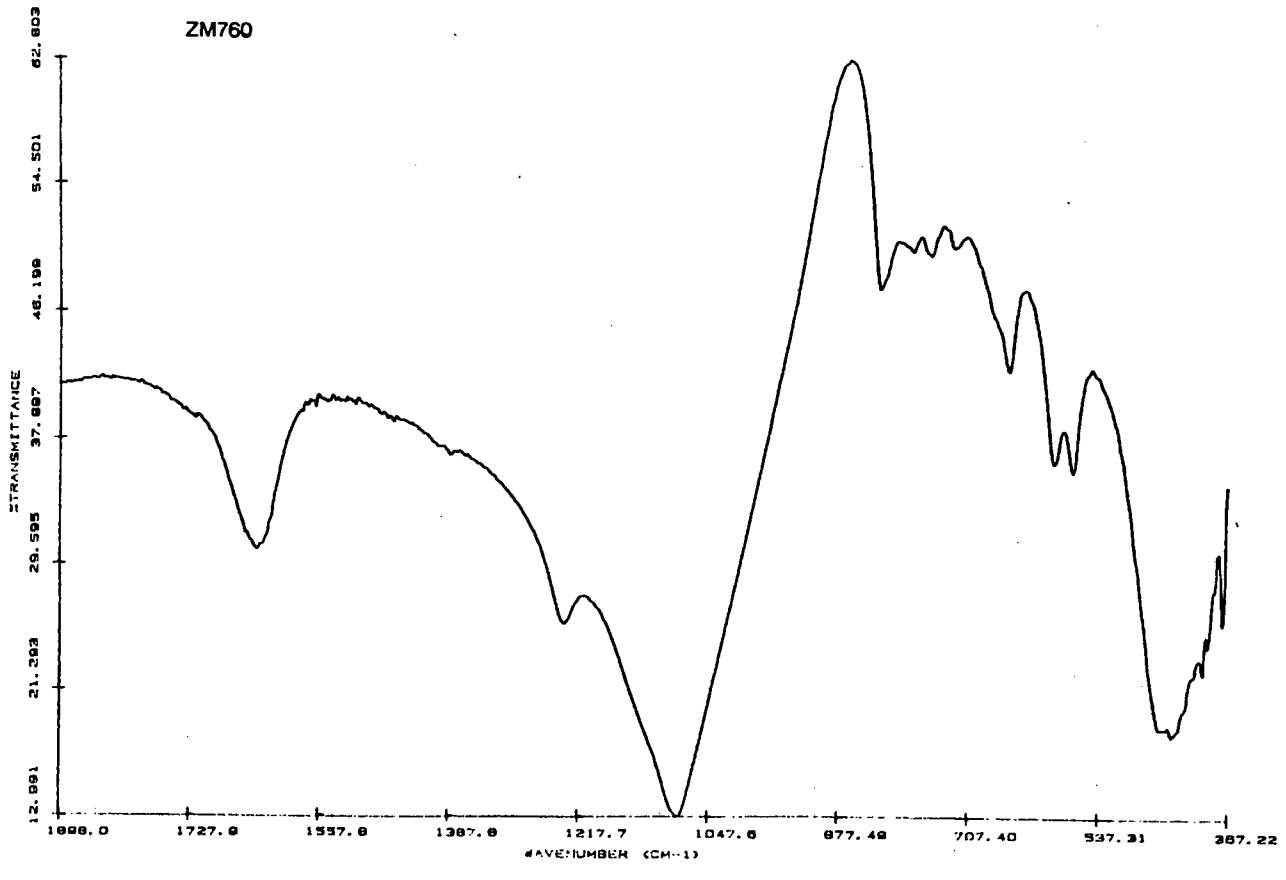
ZM760
TRANSMITTANCE
62.803
54.501
46.198
37.897
29.595
21.293
12.991
1888.0
1727.9
1567.8
1387.6
1217.7
1047.6
877.49
707.40
537.31
367.22
WAVENUMBER (CM-1)

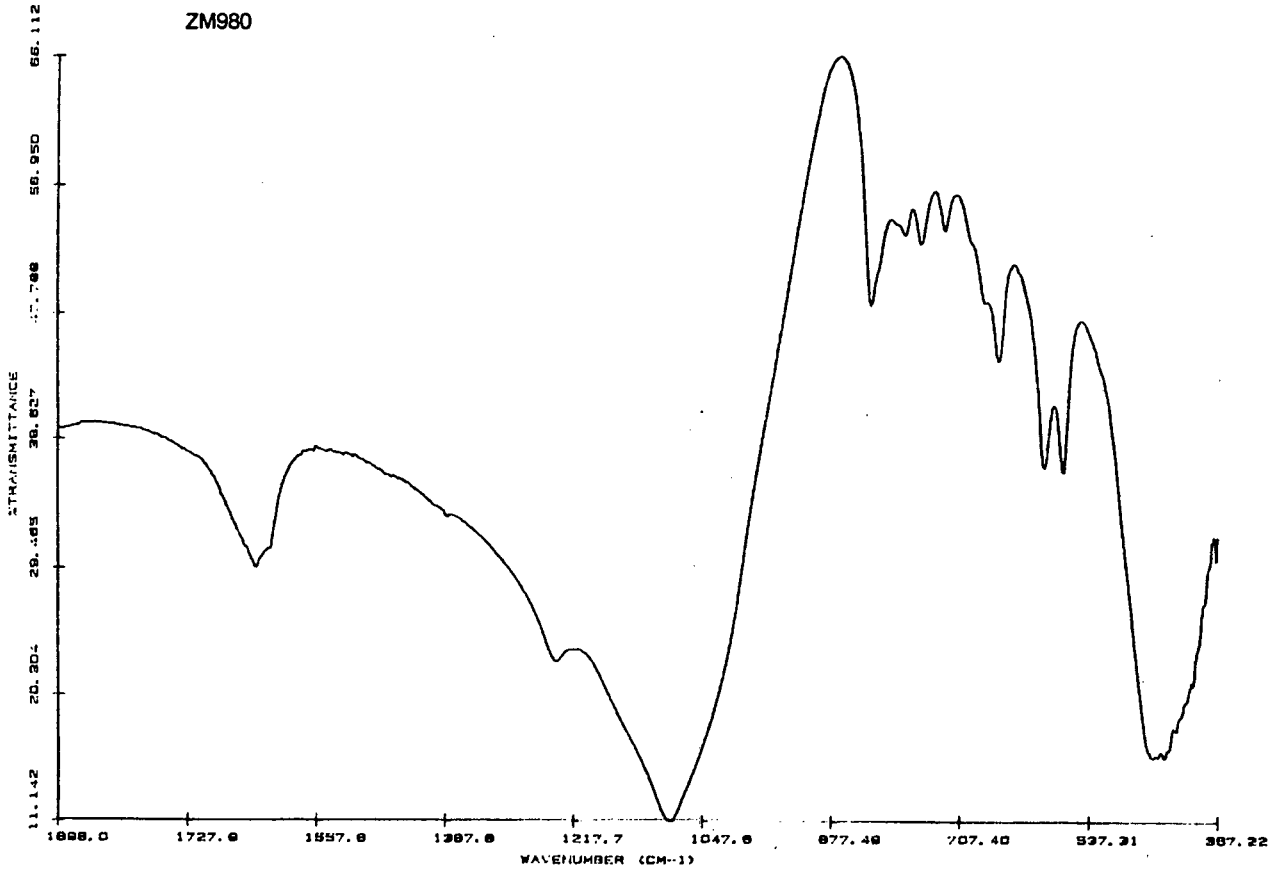
ZM980
%TRANSMITTANCE
66.112
56.950
38.627
29.485
20.304
11.142
1898.0
1727.9
1557.8
1387.8
1217.7
1047.6
877.49
707.40
537.31
367.22
WAVENUMBER (CM-1)

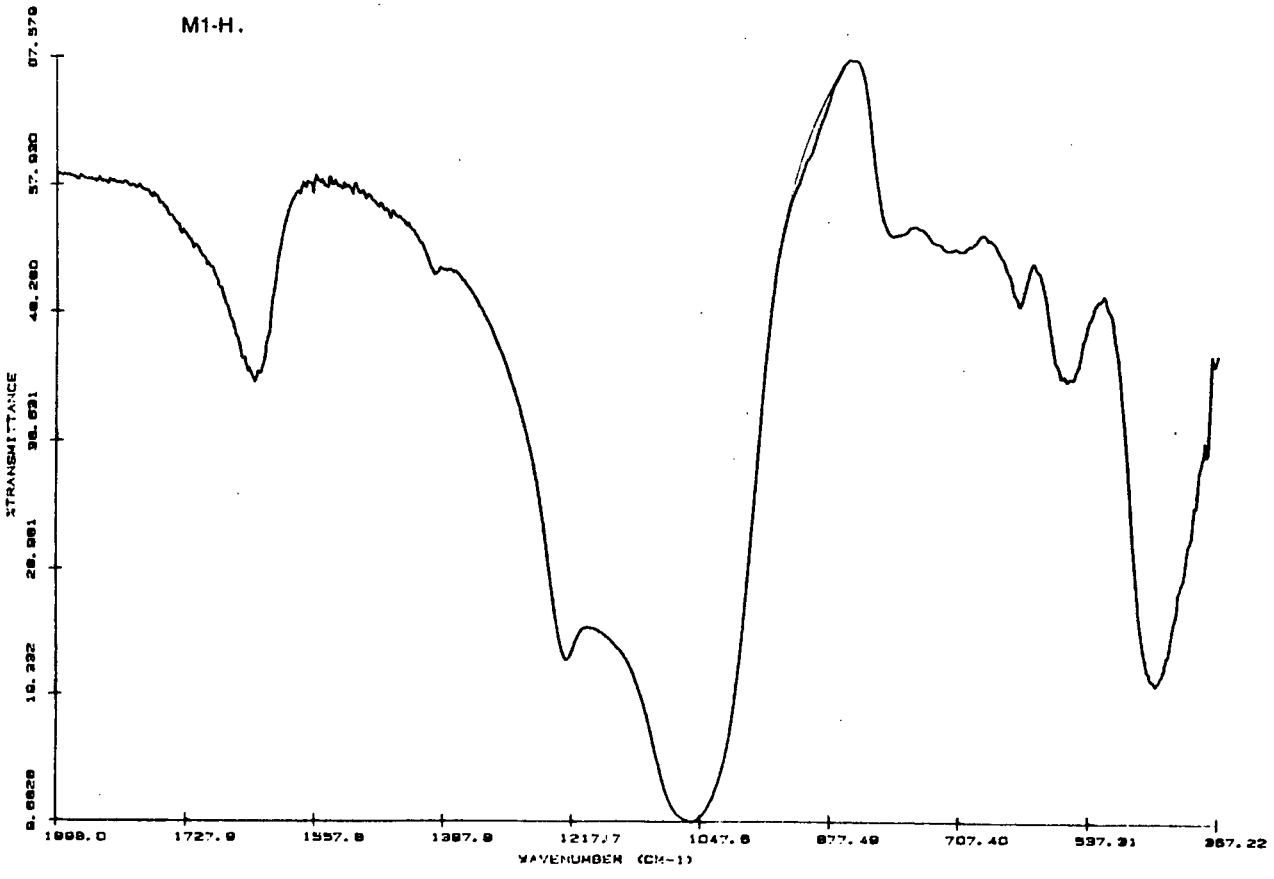
M1-H.
%TRANSMITTANCE
67.579
57.930
48.280
38.631
28.981
19.332
9.6828
1898.0
1727.9
1557.8
1387.8
1217.7
1047.6
877.49
707.40
537.31
367.22
WAVENUMBER (CM-1)

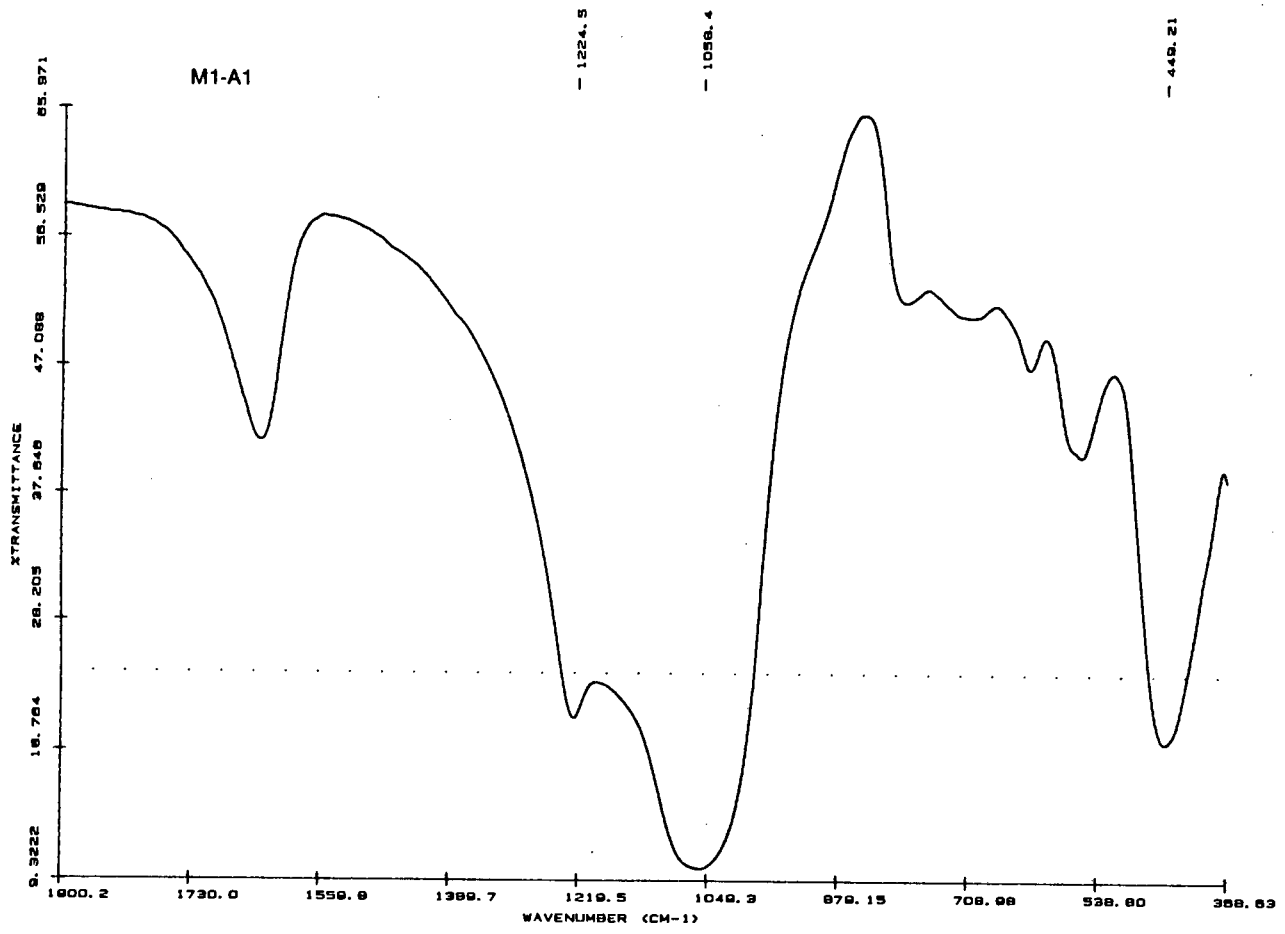
M1-A1
1224.5
1058.4
449.21
%TRANSMITTANCE
85.971
56.529
47.088
37.646
28.205
18.764
9.3222
1900.2
1730.0
1559.8
1389.7
1219.5
1049.3
879.15
708.98
538.80
388.63
WAVENUMBER (CM-1)

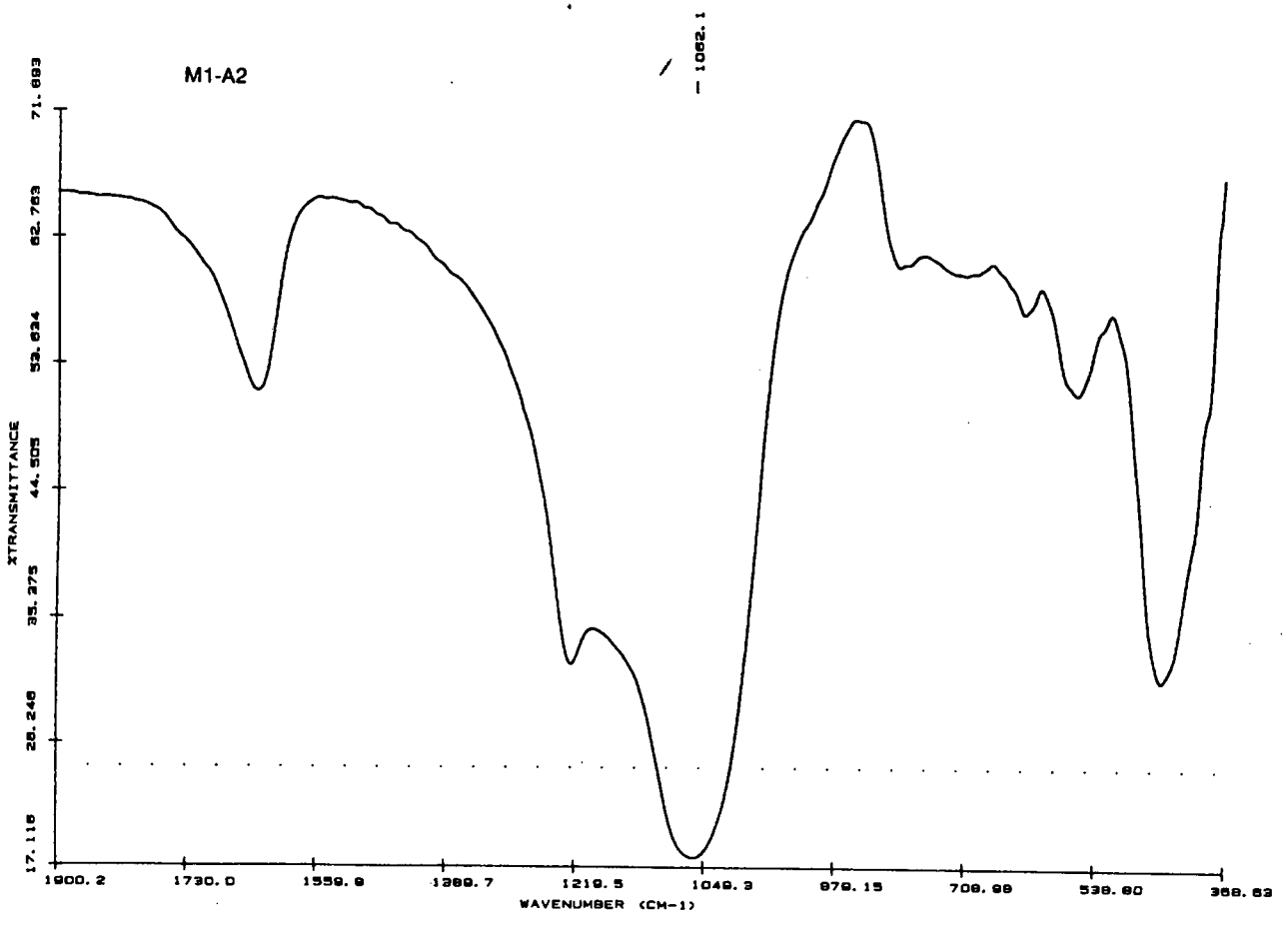
M1-A2
1082.1
%TRANSMITTANCE
71.683
62.783
53.834
44.905
35.975
26.246
17.116
1900.2
1730.0
1559.8
1389.7
1219.5
1049.3
879.15
708.98
538.80
388.63
WAVENUMBER (CM-1)

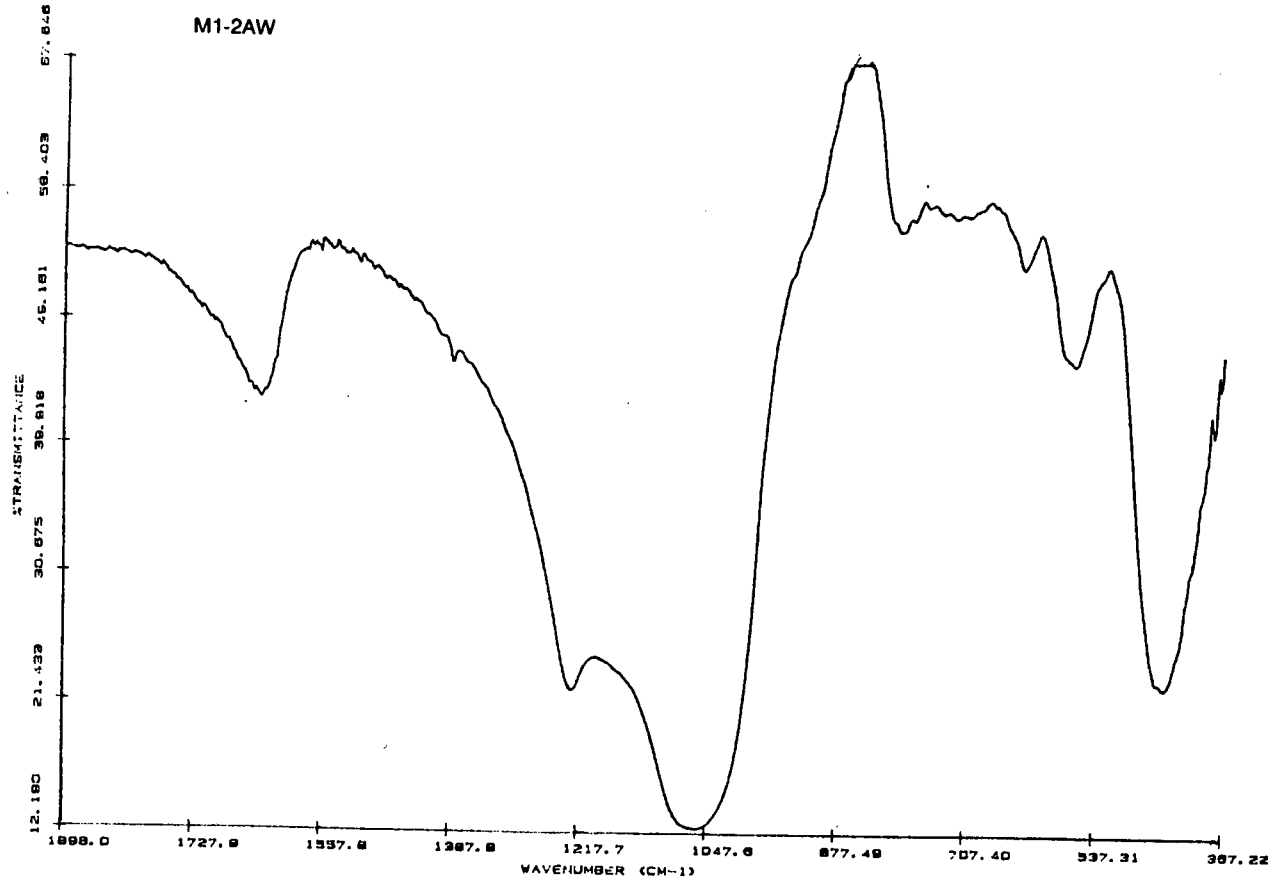
M1-2AW
%TRANSMITTANCE
67.648
58.403
46.181
38.818
30.675
21.433
12.180
1898.0
1727.9
1557.8
1387.8
1217.7
1047.6
877.49
707.40
537.31
367.22
WAVENUMBER (CM-1)

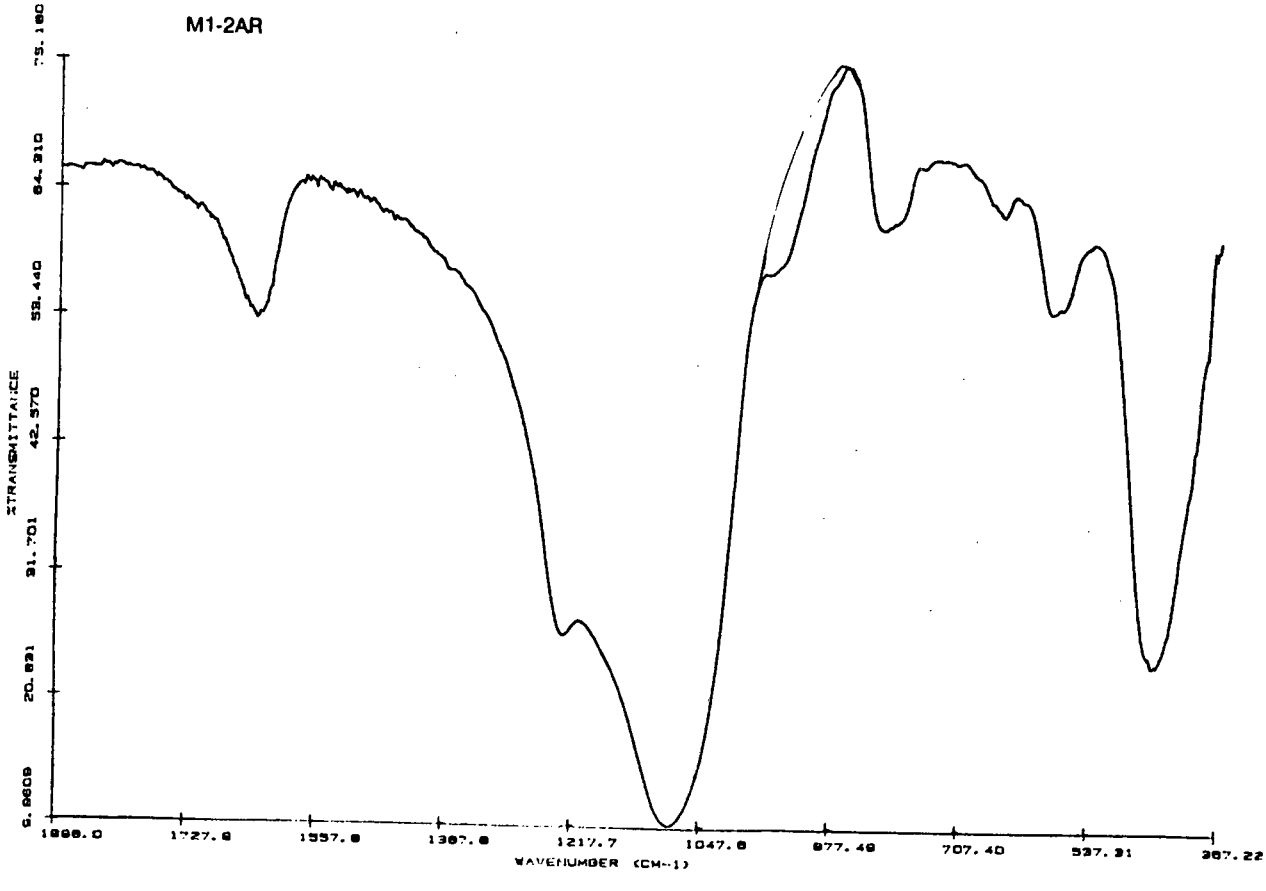
M1-2AR
%TRANSMITTANCE
75.180
64.310
53.440
42.570
31.701
20.831
9.8609
1898.0
1727.9
1557.8
1387.8
1217.7
1047.6
877.49
707.40
537.31
367.22
WAVENUMBER (CM-1)

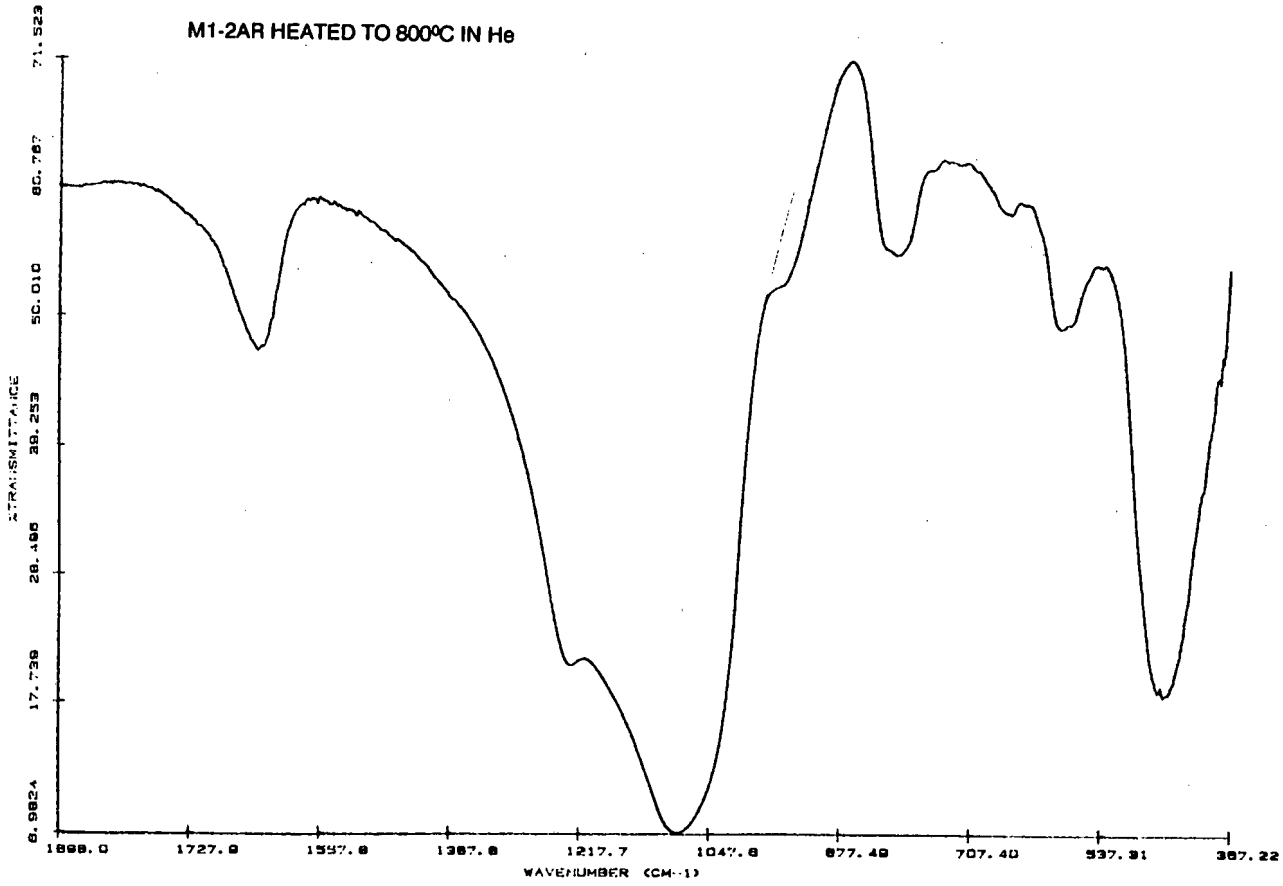
M1-2AR HEATED TO 800°C IN He
%TRANSMITTANCE
71.523
60.767
50.010
39.253
28.495
17.739
6.9824
1888.0
1727.9
1567.8
1387.8
1217.7
1047.6
877.49
707.40
537.31
387.22
WAVENUMBER (CM-1)

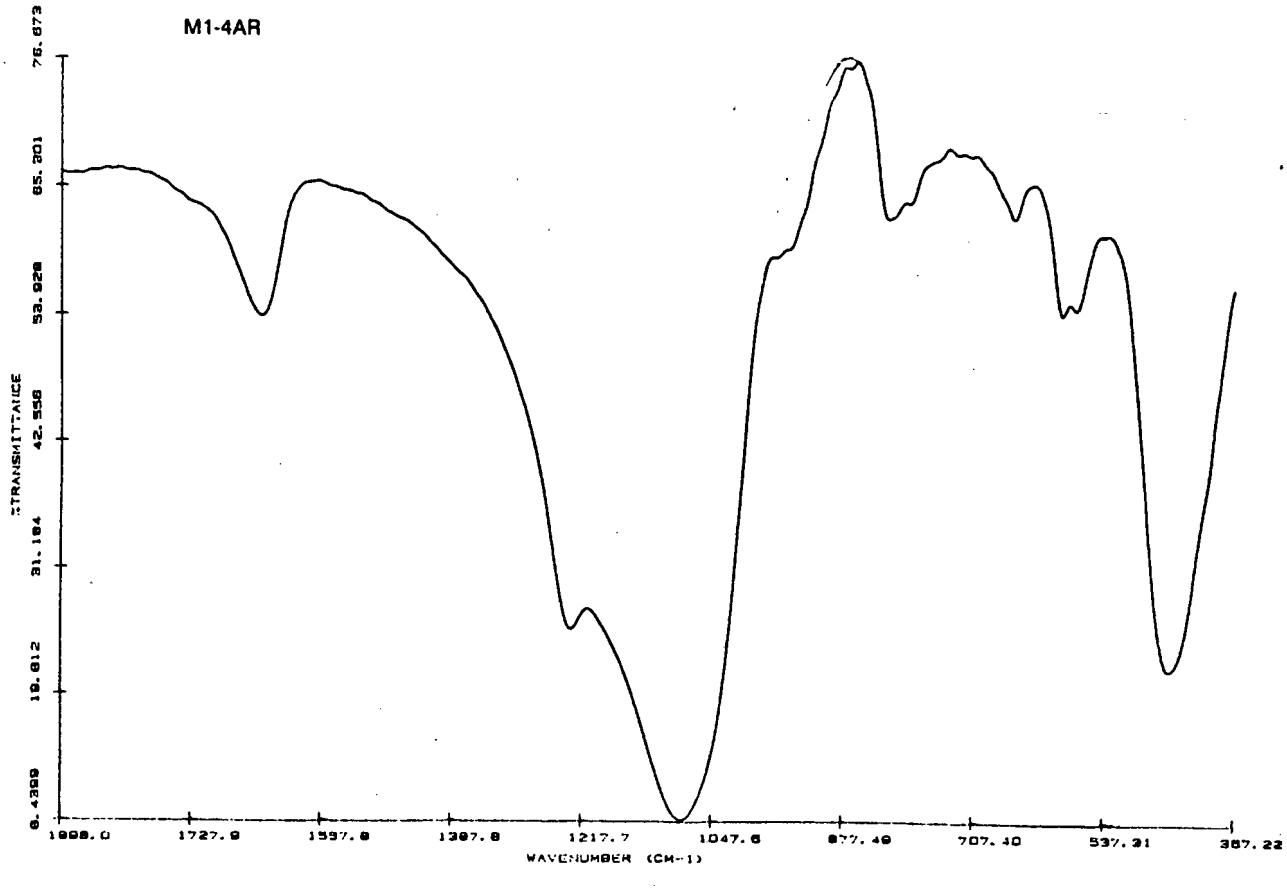
M1-4AR
%TRANSMITTANCE
76.673
65.201
53.928
42.656
31.184
19.812
8.4399
1888.0
1727.9
1567.8
1387.8
1217.7
1047.6
877.49
707.40
537.31
387.22
WAVENUMBER (CM-1)

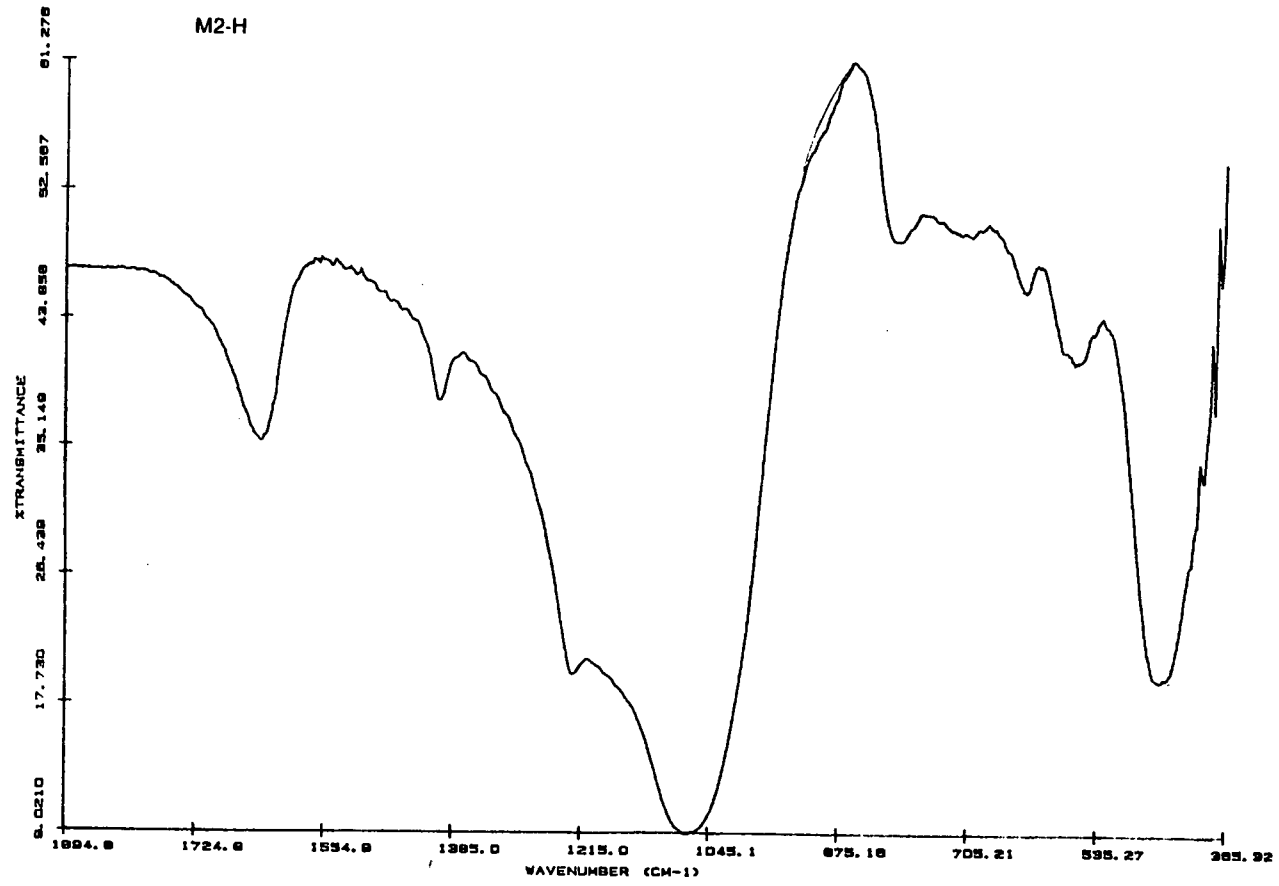
M2-H
%TRANSMITTANCE
61.278
52.567
43.856
35.145
26.433
17.720
9.0210
1894.9
1724.9
1554.9
1385.0
1215.0
1045.1
875.18
705.21
535.27
365.32
WAVENUMBER (CM-1)

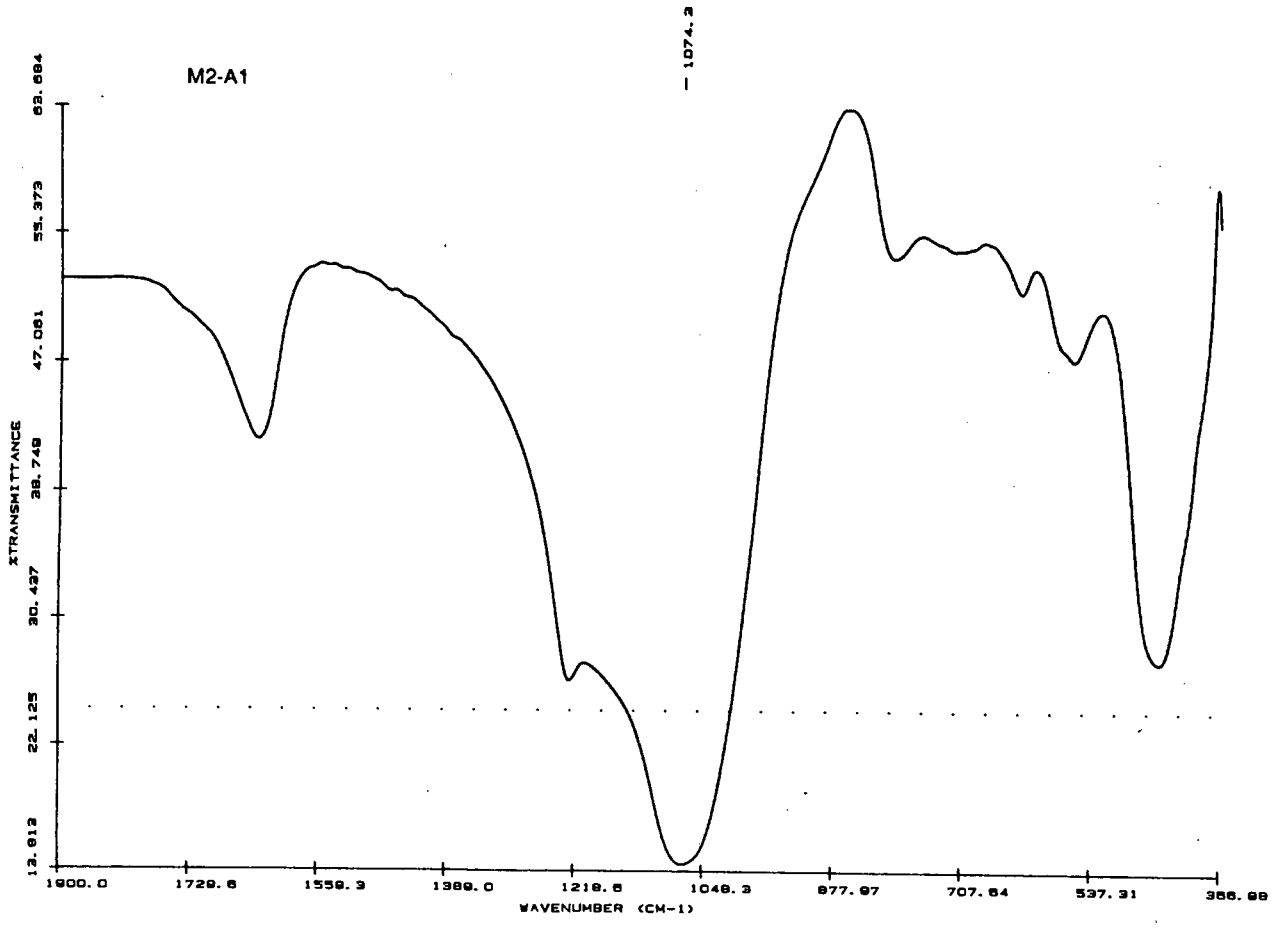
M2-A1
1074.3
%TRANSMITTANCE
63.684
55.373
47.061
38.749
30.437
22.125
13.813
1900.0
1729.6
1559.3
1389.0
1218.6
1048.3
877.97
707.64
537.31
366.98
WAVENUMBER (CM-1)

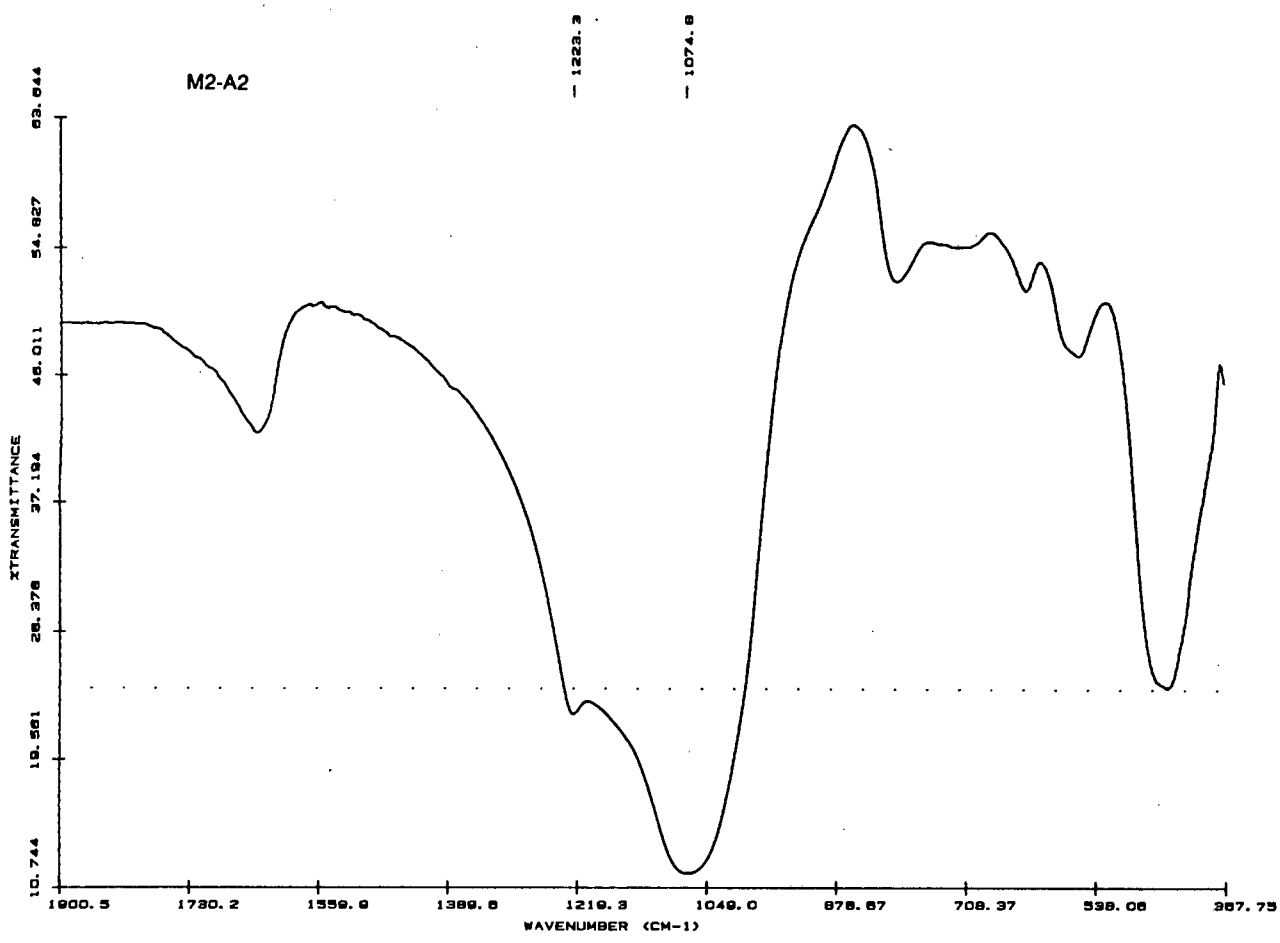
M2-A2
1223.3
1074.8
%TRANSMITTANCE
63.644
54.827
46.011
37.194
28.378
19.561
10.744
1900.5
1730.2
1559.9
1389.6
1219.3
1049.0
878.67
708.37
538.08
367.75
WAVENUMBER (CM-1)

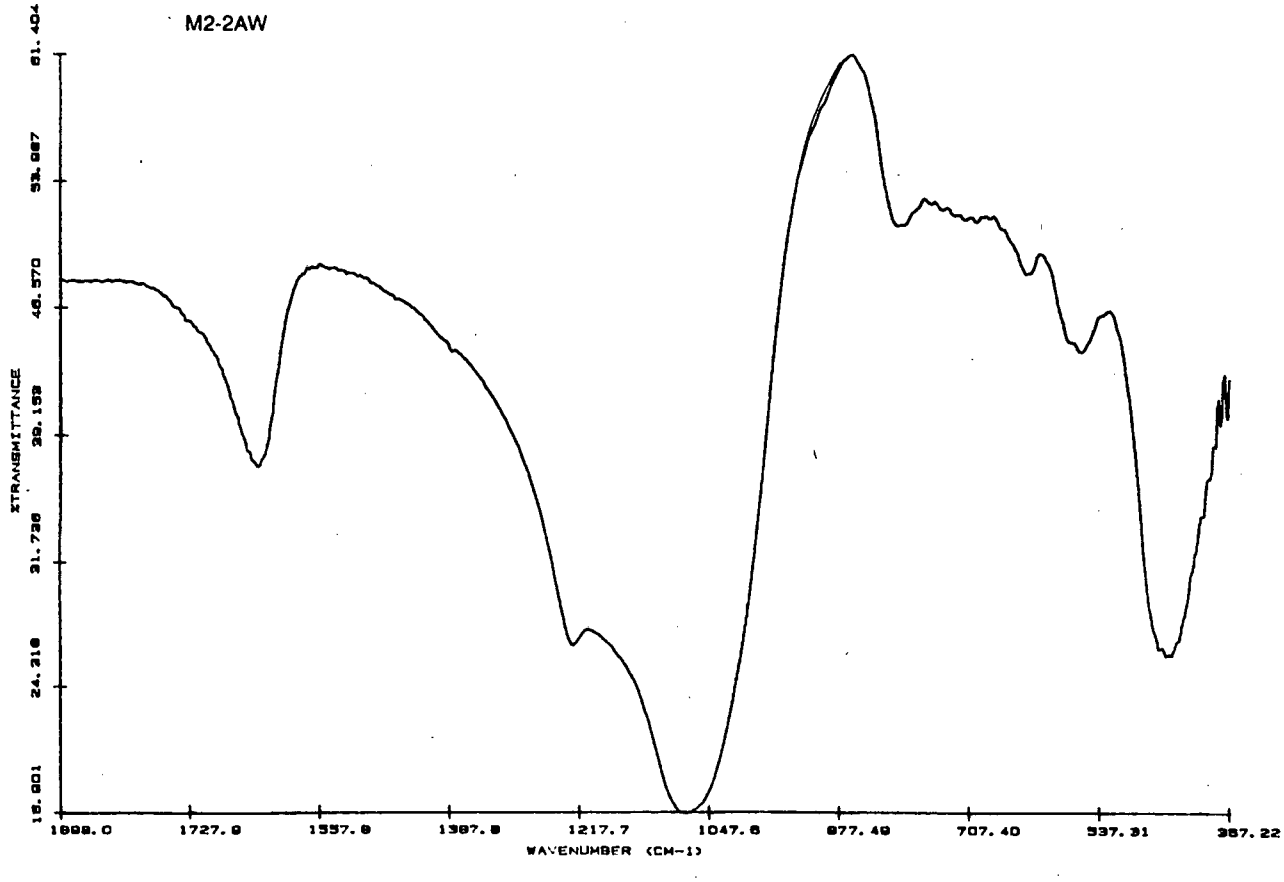
M2-2AW
%TRANSMITTANCE
61.404
53.987
46.570
39.152
31.736
24.319
16.901
1898.0
1727.9
1557.9
1387.8
1217.7
1047.6
877.49
707.40
537.31
367.22
WAVENUMBER (CM-1)

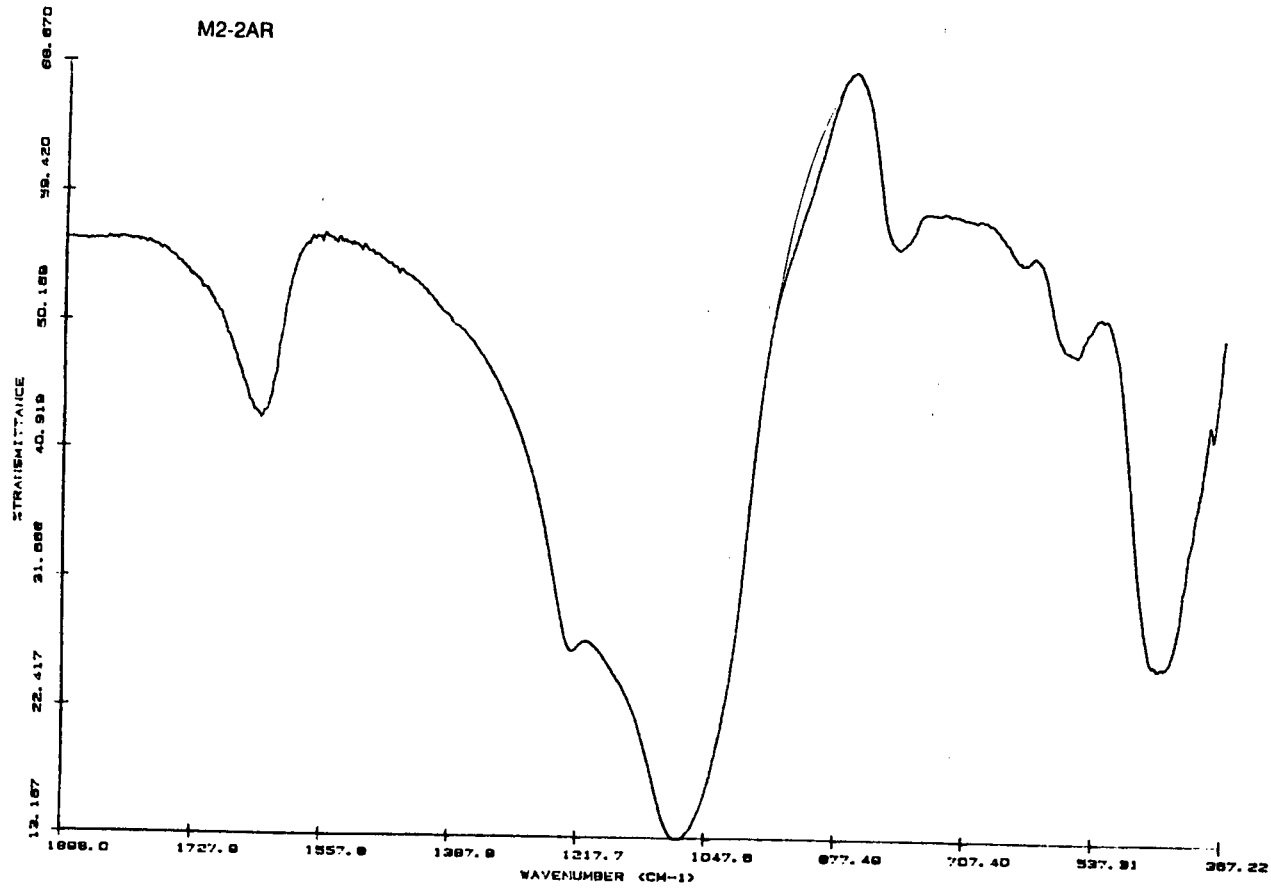
M2-2AR
%TRANSMITTANCE
68.670
59.420
50.169
40.919
31.668
22.417
13.167
1898.0
1727.9
1557.8
1387.9
1217.7
1047.6
877.49
707.40
537.31
387.22
WAVENUMBER (CM-1)

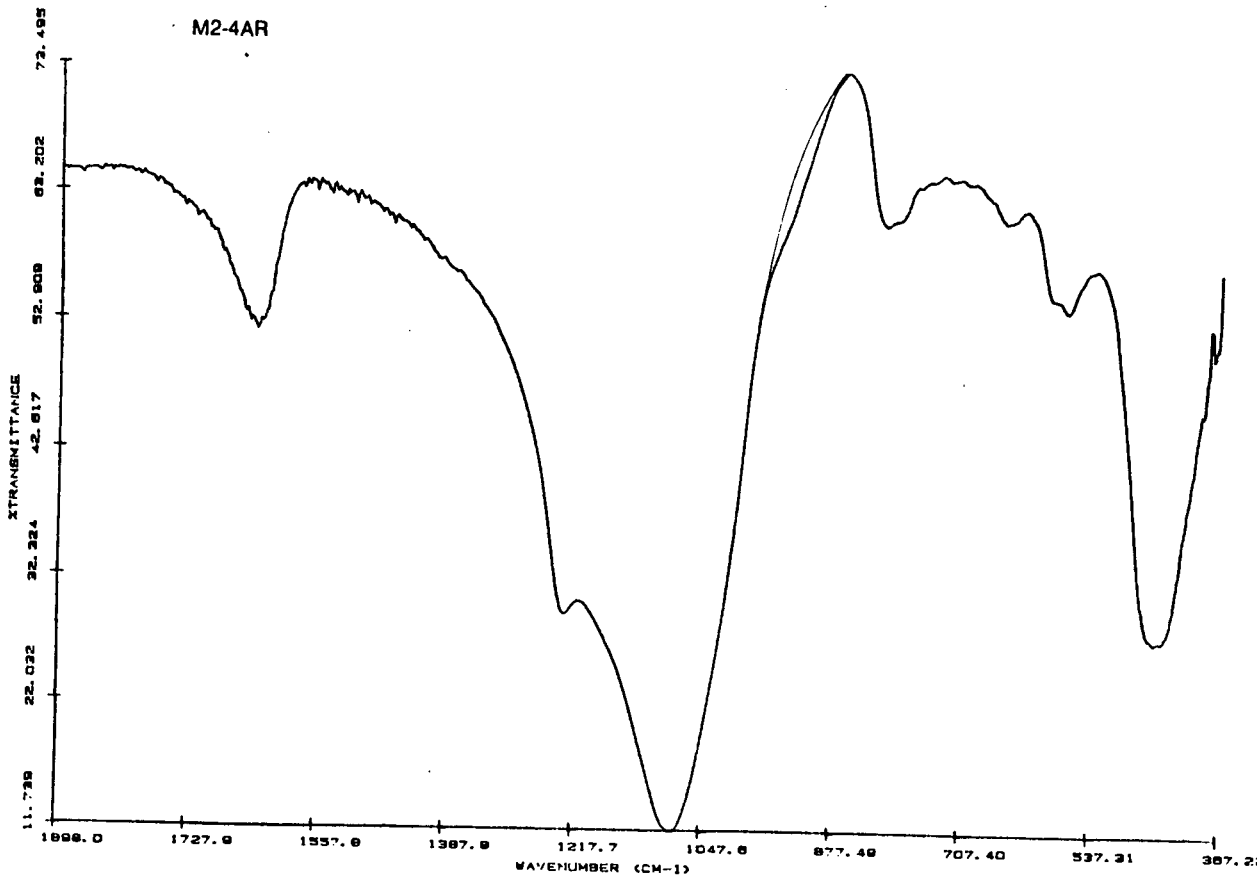
M2-4AR
%TRANSMITTANCE
72.495
62.202
52.908
42.617
32.324
22.032
11.739
1898.0
1727.9
1557.8
1387.9
1217.7
1047.6
877.49
707.40
537.31
387.22
WAVENUMBER (CM-1)

APPENDIX V : Reaction data for the SAPO-34 catalysts

Run Number	Reaction	Catalyst	Aim of experiment
SG0	MTO	S2	Act. Sel.
SG1	MTO	S2	Reprod. S2
SG2	MTO	S1	Act. Sel.
SG3	MTO	S3	Shallow bed calcination
SG4	MTO	S3*	WHSV 0.5 hr^{-1} (DBC)
SG5	MTO	S3*	WHSV 2 hr^{-1} (DBC)
SG6	MTO	S3*	Standard conditions (DBC)
SG7	MTO	S3*	P.Press. 42 kPa (DBC)
SG8	MTO	S3*	P.Press. 11 kPa (DBC)
SG9	MTO	S3*	R.Temp. 350°C (DBC)
SG10	MTO	S3*	R.Temp. 450°C (DBC)
SG11	MTO	Ni2	Act. Sel.
SG12	MTO	Co1	Act. Sel.
SG13	MTO	S1	Regen. SG2
SG14	MTO	S3*-STM	Act. Sel.
SG15	MTO	Ni3	Act. Sel.
SG16	MTO	S3*-SIL	Act. Sel.
SG17	MTO	Ni4 (cont.SAPO-5)	Act. Sel.
SG18	MTO	S3*-BRN	Act. Sel.
SG19	MTO	S3*-AMM	Act. Sel.
SG20	MTO	Ni1	Act. Sel.
57	$C3^=$ Olig.	Co1	Act. Sel.
58	$C3^=$ Olig.	S2	Act. Sel.
59	$C3^=$ Olig.	Ni3	Act. Sel.

Run No.	WG1	WHSV (g/g/hr)	1	Calcination Temp.	550
Catalyst	S3*	Temp. (deg.C)	400	Sat.Temp. (C)	Syringe
Mass (g)	0.5	Part.press. (kPa)	21	MFC Setting	0
Date	27-08-1991	Calcination	Deep bed	GC Trace Nos.	1482-1512

Time (hours)	Ox.Conv. (%)	Methane	Ethene	Ethane	Propene	Propane	Butene	Butane	C5	C6+	C2-C4	C2/C3	% Paraf. C2-C4
		(Hydrocarbon selectivities : wt%)									(olefin selectivities)		
0.4	94.5	0.9	26.9	0.3	31.6	6.9	16.8	0.5	10.3	4.4	75.4	0.85	9.2
1.6	98.9	0.4	28.3	0.0	40.8	2.7	17.5	0.5	7.3	2.4	86.6	0.69	3.6
2.8	99.6	0.3	26.9	0.0	41.4	3.1	18.0	0.4	6.3	1.6	86.2	0.65	4.0
3.9	99.1	0.3	29.6	0.2	42.8	2.1	17.6	0.4	5.5	1.4	90.1	0.69	2.9
6.0	98.4	0.3	32.1	0.0	44.9	0.8	15.6	0.3	5.3	0.7	92.5	0.71	1.2
11.5	98.0	0.4	35.9	0.3	42.3	1.7	14.5	0.1	3.9	0.7	92.6	0.85	2.2
14.4	98.6	0.5	39.3	0.2	42.0	1.5	12.8	0.2	3.0	0.3	94.1	0.94	2.0
20.1	96.4	0.6	38.5	0.1	42.5	0.0	13.7	0.3	3.6	0.6	94.7	0.91	0.5
28.6	95.1	0.7	36.8	0.1	43.2	0.0	14.9	0.4	3.7	0.2	94.8	0.85	0.5
37.8	89.3	0.8	34.7	0.1	43.1	0.0	16.6	0.4	6.7	0.9	94.4	0.81	0.5
46.6	81.6	1.0	35.9	0.0	42.8	0.0	16.0	0.6	3.4	0.2	94.7	0.84	0.7
49.9	62.1	1.2	35.8	0.0	42.5	0.0	16.1	0.7	3.5	0.1	94.4	0.84	0.8
51.6	47.9	1.4	35.5	0.0	42.7	0.0	16.1	0.8	3.4	0.1	94.3	0.83	0.8
53.1	37.2	1.8	35.3	0.1	42.3	0.0	16.1	0.8	3.6	0.1	93.7	0.84	0.9
55.5	21.1	2.4	35.2	0.1	41.4	0.0	16.1	1.0	3.7	0.1	92.7	0.85	1.1
60.8	7.7	5.5	41.3	0.0	37.3	0.0	13.1	0.0	1.8	0.0	91.7	1.11	0.0
71.0	3.2	9.9	44.9	0.3	32.4	0.0	10.9	0.6	1.1	0.0	88.1	1.39	0.9
Selectivities		0.5	32.7	0.1	41.3	2.1	15.7	0.4	5.4	1.4	89.7	0.79	2.9

Run No.	WG2	WHSV (g/g/hr)	1	Calcination Temp.	550
Catalyst	S3*	Temp. (deg.C)	450	Sat.Temp. (C)	Syringe
Mass (g)	0.5	Part.press. (kPa)	21	MFC Setting	0
Date	02-09-1991	Calcination	Deep bed	GC Trace Nos.	1513-1526

Time (hours)	Ox.Conv. (%)	Methane	Ethene	Ethane	Propene	Propane	Butene	Butane	C5	C6+	C2-C4	C2/C3	% Paraf. C2-C4
		(Hydrocarbon selectivities : wt%)									(olefin selectivities)		
1.6	98.5	0.6	36.8	0.2	38.4	1.6	12.7	0.2	7.1	2.4	87.8	0.96	2.3
3.3	97.6	0.9	44.6	0.5	35.2	1.4	10.6	0.2	4.7	1.7	90.5	1.27	2.4
4.7	99.4	1.1	48.9	0.4	34.7	0.5	8.8	0.2	5.9	1.0	92.3	1.41	1.2
6.3	99.0	1.6	51.7	0.4	32.9	1.0	8.1	0.3	2.8	0.8	92.7	1.57	1.9
7.5	96.1	1.8	51.1	0.3	33.3	1.0	8.1	0.4	5.3	1.0	92.4	1.54	1.9
13.2	58.7	7.5	48.6	0.3	31.7	0.0	7.4	1.0	2.4	1.0	87.7	1.53	1.5
14.9	17.9	15.4	49.2	0.5	24.8	0.0	5.7	0.8	1.3	2.6	79.6	1.98	1.5
18.6	5.2	27.6	51.5	1.0	16.6	0.0	2.9	0.4	0.0	0.0	71.0	3.11	2.0
Selectivities		1.2	46.6	0.4	34.9	1.1	9.7	0.3	5.2	1.4	91.2	1.35	1.9

Run No.	WG3			WHSV (g/g/hr)	1			Calcination Temp.	550					
Catalyst	S3*			Temp. (deg.C)	350			Sat.Temp. (C)	Syringe					
Mass (g)	0.5			Part.press. (kPa)	21			MFC Setting	0					
Date	09-09-1991			Calcination	Deep bed			GC Trace Nos.	1541-1573					
Time (hours)	Ox.Conv. (%)	Methane	Ethene	Ethane	Propene	Propane	Butene	Butane	C5	C6+	C2-C4	C2/C3	% Paraf. C2-C4	
		(Hydrocarbon selectivities : wt%)									(olefin selectivities)			
2.7	97.2	0.5	22.8	0.0	42.2	2.9	19.2	0.9	7.5	3.9	84.2	0.54	4.3	
4.0	96.6	0.4	21.1	0.0	43.1	2.0	21.6	0.7	7.4	3.7	85.8	0.49	3.1	
5.2	98.9	0.4	22.1	0.1	43.6	1.8	21.0	0.1	7.0	3.4	86.7	0.51	2.2	
8.2	97.2	0.3	24.0	0.0	45.6	1.7	20.1	0.3	6.2	1.6	89.7	0.53	2.2	
11.0	96.6	0.3	24.3	0.0	46.6	1.1	20.1	0.2	5.9	1.2	91.0	0.52	1.4	
13.0	96.7	0.4	21.5	0.1	43.8	2.0	22.2	0.4	7.5	2.1	87.5	0.49	2.7	
14.1	96.8	0.4	23.5	0.1	44.8	0.6	21.5	0.1	6.8	1.9	89.8	0.52	0.9	
21.4	92.6	0.5	24.7	0.1	44.9	1.4	20.5	0.2	6.5	1.0	90.1	0.55	1.8	
24.0	91.3	0.4	24.9	0.0	44.9	1.2	20.4	0.3	6.7	0.9	90.2	0.55	1.7	
29.9	85.4	0.5	25.5	0.0	45.3	1.1	20.1	0.3	6.2	0.7	90.9	0.56	1.6	
35.0	76.2	0.6	25.8	0.0	45.5	0.7	20.3	0.4	5.9	0.5	91.7	0.57	1.2	
39.8	53.2	0.8	25.9	0.0	44.9	0.0	20.4	0.7	6.2	0.9	91.1	0.58	0.8	
42.4	44.3	1.0	26.8	0.1	45.2	0.0	20.0	0.8	5.4	0.5	92.0	0.59	0.9	
47.8	24.5	1.1	26.3	0.1	45.1	0.0	20.2	1.0	5.5	0.6	91.5	0.58	1.1	
56.3	15.4	1.3	25.8	0.1	45.3	0.0	20.2	0.9	5.2	1.2	91.2	0.57	1.0	
Selectivities		0.4	23.2	0.0	44.4	1.6	20.7	0.4	6.8	2.2	88.3	0.52	2.2	

Run No.	WG4			WHSV (g/g/hr)	1			Calcination Temp.	500					
Catalyst	ZM760			Temp. (deg.C)	400			Sat.Temp. (C)	Syringe					
Mass (g)	0.5			Part.press. (kPa)	21			MFC Setting	0					
Date	18-02-1992			Calcination	Shallow bed			GC Trace Nos.	1911-1931					
Time (hours)	Ox.Conv. (%)	Methane	Ethene	Ethane	Propene	Propane	Butene	Butane	C5	C6+	C2-C4	C2/C3	% Paraf. C2-C4	
		(Hydrocarbon selectivities : wt%)									(olefin selectivities)			
0.2	77.8	1.2	8.6	0.3	8.1	14.2	3.9	39.8	10.4	13.6	20.5	1.06	72.6	
2.3	96.9	2.4	15.8	0.4	13.9	17.6	7.5	24.1	8.9	9.4	37.2	1.14	53.1	
4.4	90.7	3.2	17.9	0.5	16.4	19.9	8.0	13.9	4.8	15.3	42.4	1.09	44.7	
6.9	87.6	3.5	19.8	0.4	22.7	17.1	8.6	12.3	4.6	11.1	51.1	0.87	36.8	
12.0	82.9	3.6	19.9	0.4	23.9	17.5	8.2	13.2	4.3	9.0	52.1	0.83	37.4	
14.4	81.8	3.5	18.6	0.4	21.8	16.6	7.4	12.6	4.1	15.0	47.8	0.85	38.3	
29.6	78.9	3.5	19.7	0.4	25.2	17.3	8.4	14.5	4.4	6.7	53.3	0.78	37.7	
49.7	68.8	3.5	18.7	0.0	24.4	14.4	7.8	13.3	4.2	13.7	50.9	0.77	35.2	
56.4	66.6	2.7	14.8	0.3	19.9	10.6	5.9	10.3	3.2	32.2	40.7	0.74	34.2	
61.5	63.8	3.0	16.6	0.3	22.9	12.3	6.9	12.3	3.8	22.0	46.4	0.73	34.9	
71.1	55.9	3.1	16.7	0.3	22.0	11.4	6.5	11.5	3.5	24.9	45.3	0.76	33.9	
72.7	53.9	3.2	17.9	0.3	24.9	12.7	7.5	13.0	4.0	16.4	50.3	0.72	34.1	
Selectivities (>50%)		3.0	17.1	0.3	20.5	15.1	7.2	15.9	5.0	15.8	44.8	0.86	41.1	

Run No.	SG0			WHSV (g/g/hr)	1			Calcination Temp.	550				
Catalyst	S2			Temp. (deg.C)	400			Sat.Temp. (C)	30				
Mass (g)	0.5			Part.press. (kPa)	21			MFC Setting	22				
Date	24-05-1991			Calcination	Regeneretion			GC Trace Nos.	1232-1241				
Time (hours)	Ox.Conv. (%)	Methane	Ethene	Ethane	Propene	Propane	Butene	Butane	C5	C6+	C2-C4 (olefin selectivities)	C2/C3	% Paraf. C2-C4
		(Hydrocarbon selectivities : wt%)											
0.2	99.1	0.7	31.9	0.7	36.4	2.4	15.1	0.1	7.1	5.1	83.4	0.88	3.7
1.3	99.5	0.6	36.0	0.7	38.4	1.9	14.6	0.1	5.1	2.6	89.0	0.94	2.9
2.5	99.6	0.8	38.1	0.8	38.1	0.0	14.1	0.1	4.6	3.3	90.2	1.00	0.9
3.6	99.7	1.0	38.6	0.0	38.8	1.2	13.3	0.1	4.4	2.5	90.8	1.00	1.4
5.2	99.0	1.2	40.1	0.7	38.4	0.0	12.9	0.2	4.1	2.3	91.4	1.04	1.0
6.5	95.9	1.4	40.0	0.8	39.0	0.0	12.9	0.3	3.9	1.7	91.9	1.02	1.1
7.6	80.6	1.9	37.3	0.7	38.9	0.0	13.6	0.4	4.1	3.0	89.8	0.96	1.3
9.9	42.4	2.7	34.2	0.7	39.7	0.0	15.3	0.6	4.7	2.1	89.1	0.86	1.4
12.2	31.4	2.8	32.8	0.7	38.5	0.0	14.9	0.6	4.5	5.1	86.1	0.85	1.6
Selectivities		1.0	37.4	0.6	38.2	0.9	13.8	0.1	4.9	2.9	89.4	0.98	1.8

Run No.	SG1			WHSV (g/g/hr)	1			Calcination Temp.	550				
Catalyst	S2			Temp. (deg.C)	400			Sat.Temp. (C)	30				
Mass (g)	0.5			Part.press. (kPa)	21			MFC Setting	22				
Date	27-05-1991			Calcination	Regeneration			GC Trace Nos.	1242-1252				
Time (hours)	Ox.Conv. (%)	Methane	Ethene	Ethane	Propene	Propane	Butene	Butane	C5	C6+	C2-C4 (olefin selectivities)	C2/C3	% Paraf. C2-C4
		(Hydrocarbon selectivities : wt%)											
0.4	99.3	0.5	31.3	0.6	37.9	2.2	16.6	0.1	7.2	3.6	85.8	0.83	3.2
1.5	99.5	0.6	35.3	0.6	38.6	1.7	15.0	0.0	5.2	3.0	88.9	0.92	2.6
2.8	99.7	0.8	37.7	0.7	38.6	0.0	14.0	0.1	5.1	2.6	90.2	0.98	0.9
3.9	99.7	0.9	39.5	0.8	38.0	0.0	13.9	0.1	4.5	2.3	91.3	1.04	1.0
5.0	99.5	1.1	39.6	0.8	37.9	0.0	13.6	0.2	4.4	1.6	91.1	1.04	1.0
6.2	97.9	1.2	39.5	0.7	38.6	0.0	13.4	0.2	4.2	0.8	91.6	1.02	1.0
7.3	92.2	1.5	39.0	0.7	38.8	0.0	13.6	0.3	4.0	2.0	91.4	1.00	1.1
8.8	57.5	2.2	34.7	0.7	38.4	0.0	15.4	0.4	4.7	3.4	88.5	0.90	1.2
11.1	32.2	2.6	32.7	0.7	38.3	0.0	16.4	0.1	5.1	3.5	87.5	0.85	0.9
14.3	27.5	2.9	31.7	0.7	37.6	0.0	17.1	0.5	5.3	4.0	86.4	0.84	1.4
Selectivities		0.9	37.4	0.7	38.3	0.6	14.3	0.2	4.9	2.3	90.0	0.98	1.6

Run No.	SG2	WHSV (g/g/hr)	1	Calcination Temp.	550
Catalyst	S1	Temp. (deg.C)	400	Sat.Temp. (C)	30
Mass (g)	0.5	Part.press. (kPa)	21	MFC Setting	22
Date	29-05-1991	Calcination	Shallow bed	GC Trace Nos.	1406-1405

Time (hours)	Ox.Conv. (%)	Methane	Ethene	Ethane	Propene	Propane	Butene	Butane	C5	C6+	C2-C4	C2/C3	% Paraf. C2-C4
		(Hydrocarbon selectivities : wt%)									(olefin selectivities)		
0.2	97.2	0.5	32.1	0.0	38.9	1.2	13.8	0.3	9.0	4.2	84.8	0.82	1.7
2.1	93.4	1.0	36.6	0.0	41.7	0.0	15.4	0.1	4.2	0.9	93.7	0.88	0.1
3.4	77.6	1.7	35.0	0.7	41.8	0.0	15.6	0.1	4.2	0.9	92.4	0.84	0.9
4.5	53.5	2.8	33.0	0.7	42.3	0.0	16.1	0.1	4.2	0.8	91.4	0.78	0.9
5.8	32.3	3.9	32.5	0.8	42.3	0.0	15.9	0.0	4.0	0.5	90.7	0.77	0.9
7.2	19.4	5.2	32.3	0.8	41.7	0.1	15.6	0.0	3.9	0.4	89.7	0.77	0.9
8.9	13.3	6.6	31.7	0.8	41.3	0.1	15.2	0.0	4.0	0.1	88.2	0.77	1.0
Selectivities		0.8	34.3	0.0	40.3	0.6	14.6	0.2	6.6	2.6	89.2	0.85	0.9

Run No.	SG3	WHSV (g/g/hr)	1	Calcination Temp.	550
Catalyst	S3	Temp. (deg.C)	400	Sat.Temp. (C)	30
Mass (g)	0.5	Part.press. (kPa)	21	MFC Setting	22
Date	07-06-1991	Calcination	Shallow bed	GC Trace Nos.	1261-1274

Time (hours)	Ox.Conv. (%)	Methane	Ethene	Ethane	Propene	Propane	Butene	Butane	C5	C6+	C2-C4	C2/C3	% Paraf. C2-C4
		(Hydrocarbon selectivities : wt%)									(olefin selectivities)		
0.3	99.6	0.6	37.1	0.0	39.2	1.4	13.0	0.2	5.7	3.0	89.4	0.95	1.7
1.6	99.6	1.0	37.5	0.7	39.3	1.3	13.6	0.1	4.4	2.1	90.4	0.95	2.3
2.8	99.7	1.0	38.3	0.7	39.5	1.2	13.6	0.1	4.1	1.5	91.3	0.97	2.2
3.8	99.7	1.1	39.5	0.8	39.6	0.0	13.6	0.2	3.9	1.4	92.7	1.00	1.0
5.0	99.7	1.1	40.0	0.7	39.2	0.0	13.8	0.2	3.8	1.3	93.0	1.02	1.0
6.8	99.1	1.3	41.2	0.0	39.8	0.0	13.0	0.4	3.5	0.8	94.0	1.04	0.4
8.0	97.5	1.4	41.4	0.7	39.4	0.0	12.6	0.5	3.4	0.7	93.3	1.05	1.2
9.1	94.2	1.6	41.3	0.7	39.4	0.0	12.5	0.6	3.3	0.6	93.2	1.05	1.4
10.3	86.5	1.9	40.5	0.0	39.3	0.0	12.9	0.7	3.6	0.8	92.7	1.03	0.7
12.2	51.9	2.5	41.0	0.6	39.1	0.0	12.4	0.8	3.0	0.5	92.5	1.05	1.5
13.7	30.9	4.0	42.4	0.0	37.7	0.0	12.1	0.8	2.8	0.2	92.2	1.13	0.8
15.2	13.9	6.0	44.6	0.8	34.5	0.0	10.6	0.7	2.3	0.4	89.7	1.29	1.6
16.3	13.0	7.4	45.2	0.8	33.1	0.0	10.4	0.7	2.4	0.0	88.7	1.36	1.7
Selectivities		1.1	39.5	0.5	39.4	0.5	13.2	0.3	4.0	1.4	92.2	1.00	1.4

Run No.	SG4	WHSV (g/g/hr)	0.5	Calcination Temp.	550
Catalyst	S3*	Temp. (deg.C)	400	Sat.Temp. (C)	30
Mass (g)	0.5	Part.press. (kPa)	21	MFC Setting	11
Date	11-06-1991	Calcination	Deep bed	GC Trace Nos.	1275-1298

Time (hours)	Ox.Conv. (%)	Methane	Ethene	Ethane	Propene	Propane	Butene	Butane	C5	C6+	C2-C4 (olefin selectivities)	C2/C3	% Paraf. C2-C4
		(Hydrocarbon selectivities : wt%)											
0.4	99.7	0.6	28.7	0.6	36.2	3.0	16.4	0.4	9.8	4.3	81.2	0.79	4.7
1.8	100.0	0.5	34.0	0.7	37.4	2.2	15.0	0.3	6.7	3.2	86.4	0.91	3.6
3.1	99.5	0.5	37.1	0.8	37.1	2.0	13.9	0.1	5.6	3.1	88.1	1.00	3.1
4.3	99.6	0.7	39.7	0.8	36.5	1.7	12.9	0.0	7.3	2.7	89.1	1.09	2.8
5.4	99.6	0.8	40.5	0.9	36.1	1.8	12.5	0.1	4.8	2.6	89.1	1.12	3.0
6.6	99.7	0.9	40.4	0.8	36.3	1.5	12.6	0.1	4.8	2.6	89.3	1.11	2.6
7.9	99.8	1.0	40.6	0.8	36.6	1.3	12.5	0.0	4.6	2.5	89.7	1.11	2.3
9.0	99.7	1.0	40.2	0.9	36.5	1.4	12.7	0.1	4.6	2.6	89.4	1.10	2.6
10.9	99.8	1.2	40.7	0.8	36.4	1.4	12.6	0.1	4.3	2.5	89.6	1.12	2.5
12.1	99.8	1.2	41.7	0.8	36.9	1.2	12.1	0.1	3.9	2.1	90.7	1.13	2.2
13.3	99.8	1.4	43.0	0.9	36.5	0.0	12.1	0.1	3.8	2.2	91.6	1.18	1.1
14.7	99.8	1.5	44.1	0.9	36.1	0.0	11.7	0.2	3.6	1.9	92.0	1.22	1.1
15.9	99.8	1.7	44.7	0.9	35.8	0.0	11.3	0.3	3.5	1.8	91.9	1.25	1.2
17.4	99.7	1.9	45.6	0.9	35.6	0.0	10.9	0.3	3.4	1.6	92.0	1.28	1.3
19.2	99.1	2.1	46.3	0.8	35.1	0.0	10.4	0.4	3.2	1.5	91.8	1.32	1.3
21.0	96.9	2.5	46.1	0.0	35.5	0.0	10.4	0.6	3.2	1.5	92.1	1.30	0.7
22.1	93.2	2.9	45.2	0.9	34.9	0.0	10.4	0.7	3.3	1.7	90.6	1.29	1.7
23.3	81.4	3.4	44.5	0.8	35.2	0.0	10.1	0.8	3.2	2.1	89.7	1.26	1.8
24.5	61.1	4.4	44.7	0.8	34.6	0.0	9.8	0.8	3.1	1.8	89.0	1.29	1.8
25.6	41.1	6.0	45.1	0.9	32.2	0.0	9.3	0.8	2.9	2.9	86.5	1.40	1.9
26.8	25.0	8.5	46.8	0.9	29.1	0.0	8.4	0.7	2.4	3.2	84.3	1.61	1.9
28.7	14.3	12.0	48.1	1.0	24.8	0.0	7.0	0.6	1.8	4.8	79.9	1.94	1.9
29.7	11.9	13.6	48.4	1.1	23.0	0.0	6.4	0.5	1.9	5.2	77.8	2.11	2.0
Selectivities		1.3	41.1	0.8	36.2	1.0	12.4	0.2	4.7	2.4	89.7	1.14	2.2

Run No.	SG5	WHSV (g/g/hr)	2	Calcination Temp.	550
Catalyst	S3*	Temp. (deg.C)	400	Sat.Temp. (C)	30
Mass (g)	0.5	Part.press. (kPa)	21	MFC Setting	44.1
Date	13-06-1991	Calcination	Deep bed	GC Trace Nos.	1299-1312

Time (hours)	Ox.Conv. (%)	Methane	Ethene	Ethane	Propene	Propane	Butene	Butane	C5	C6+	C2-C4 (olefin selectivities)	C2/C3	% Paraf. C2-C4
		(Hydrocarbon selectivities : wt%)											
0.2	99.6	0.5	29.7	0.0	40.3	1.8	16.3	0.2	7.6	3.6	86.3	0.74	2.3
1.7	99.7	0.7	35.3	0.6	39.9	1.2	14.6	0.1	5.2	2.5	89.8	0.89	2.0
2.9	99.7	0.9	36.5	0.7	39.5	1.1	14.3	0.1	4.7	2.1	90.4	0.93	2.0
4.2	99.7	0.9	38.0	0.6	39.9	0.0	14.3	0.2	4.4	1.6	92.3	0.95	0.8
5.3	99.7	0.9	38.8	0.6	40.3	0.0	13.8	0.2	4.0	1.3	92.9	0.96	0.9
6.5	99.5	1.1	39.4	0.7	39.5	0.0	13.8	0.3	3.9	1.2	92.8	1.00	1.0
8.9	91.8	1.5	39.1	0.0	39.7	0.0	14.0	0.6	4.0	1.1	92.7	0.98	0.7
10.1	71.7	1.6	39.0	0.6	40.4	0.0	13.3	0.7	3.5	1.1	92.7	0.96	1.4
11.1	58.5	2.1	38.6	0.6	39.2	0.0	13.7	0.7	3.6	1.4	91.5	0.98	1.4
12.3	24.2	3.0	40.1	0.0	39.0	0.0	13.2	0.7	3.2	0.7	92.3	1.03	0.8
13.5	15.2	3.9	40.7	0.6	37.5	0.0	12.7	0.7	3.1	0.6	91.0	1.08	1.4
22.8	4.3	11.6	44.5	0.0	30.2	0.0	8.7	1.9	3.2	0.8	83.4	1.48	2.3
Selectivities		0.9	36.7	0.4	39.9	0.6	14.5	0.2	4.8	1.9	91.0	0.92	1.4

Run No.	SG6	WHSV (g/g/hr)	1	Calcination Temp.	550
Catalyst	S3*	Temp. (deg.C)	400	Sat.Temp. (C)	30
Mass (g)	0.5	Part.press. (kPa)	21	MFC Setting	21
Date	15-06-1991	Calcination	Deep bed	GC Trace Nos.	1313-1330

Time (hours)	Ox.Conv. (%)	Methane	Ethene	Ethane	Propene	Propane	Butene	Butane	C5	C6+	C2-C4 (olefin selectivities)	C2/C3	% Paraf. C2-C4
		(Hydrocarbon selectivities : wt%)											
0.3	99.4	0.6	31.2	0.5	38.3	2.1	15.0	0.0	8.5	3.7	84.5	0.82	3.0
1.5	99.6	0.5	34.7	0.6	39.6	1.6	14.5	0.0	5.7	2.8	88.8	0.88	2.5
2.6	99.7	0.6	37.0	0.6	39.1	1.3	13.9	0.1	5.0	2.4	90.0	0.95	2.2
3.8	99.7	0.8	38.5	0.7	38.9	0.0	13.7	0.1	4.9	2.3	91.2	0.99	0.9
5.0	99.7	0.9	38.9	0.7	38.9	0.0	13.9	0.1	4.7	2.1	91.7	1.00	0.9
6.1	99.7	0.9	38.8	0.0	39.3	0.8	13.5	0.1	4.4	2.0	91.7	0.99	1.0
7.3	99.7	1.0	39.8	0.0	39.6	0.0	13.5	0.1	4.2	1.8	92.8	1.00	0.2
8.8	99.6	1.1	41.1	0.7	38.4	0.0	12.9	0.2	3.9	1.6	92.5	1.07	1.0
9.9	99.4	1.2	41.7	0.7	38.2	0.0	12.6	0.3	3.8	1.4	92.5	1.09	1.1
11.0	98.9	1.3	42.3	0.7	38.0	0.0	12.2	0.4	3.7	1.3	92.6	1.11	1.2
12.2	97.5	1.5	42.7	0.7	37.7	0.0	12.0	0.5	3.6	1.3	92.3	1.13	1.3
14.0	90.0	1.9	42.3	0.7	37.6	0.0	11.8	0.7	3.6	1.4	91.7	1.13	1.5
15.1	75.0	2.3	41.4	0.6	37.5	0.0	11.6	0.8	3.5	2.3	90.5	1.10	1.5
16.9	40.8	4.0	43.0	0.7	35.6	0.0	11.4	0.8	3.3	1.3	89.9	1.21	1.7
18.2	18.8	6.1	44.6	0.0	33.3	0.0	10.7	0.7	3.1	1.5	88.6	1.34	0.8
19.5	12.0	8.2	45.9	0.8	30.3	0.0	9.7	0.7	2.8	1.6	85.9	1.52	1.7
20.9	7.7	10.7	47.1	0.0	28.5	0.0	8.9	0.6	2.6	1.6	84.5	1.65	0.7
Selectivities		1.0	39.1	0.6	38.6	0.5	13.3	0.2	4.7	2.0	90.6	1.01	1.4

Run No.	SG7	WHSV (g/g/hr)	1	Calcination Temp.	550
Catalyst	S3*	Temp. (deg.C)	400	Sat.Temp. (C)	45.5
Mass (g)	0.5	Part.press. (kPa)	42	MFC Setting	8.8
Date	20-06-1991	Calcination	Deep bed	GC Trace Nos.	1334-1348

Time (hours)	Ox.Conv. (%)	Methane	Ethene	Ethane	Propene	Propane	Butene	Butane	C5	C6+	C2-C4 (olefin selectivities)	C2/C3	% Paraf. C2-C4
		(Hydrocarbon selectivities : wt%)											
0.9	99.2	0.5	29.7	0.7	36.5	3.1	16.7	0.1	7.3	5.1	83.0	0.81	4.5
2.2	99.4	0.6	34.2	0.8	36.9	2.2	15.1	0.1	5.7	4.3	86.2	0.93	3.4
3.5	99.6	0.8	36.1	0.8	38.1	1.7	14.2	0.1	4.9	3.4	88.4	0.95	2.8
4.7	99.7	0.8	36.9	0.8	39.0	1.3	14.0	0.1	4.4	2.8	89.9	0.94	2.3
5.9	99.7	0.9	38.4	0.8	39.1	0.0	14.0	0.1	4.1	2.6	91.5	0.98	1.0
7.6	99.6	1.1	39.7	0.8	38.8	0.0	13.4	0.2	3.8	2.1	91.9	1.02	1.1
9.2	98.9	1.5	41.3	0.8	38.2	0.0	12.6	0.5	3.5	1.4	92.2	1.08	1.3
10.6	95.0	1.9	41.5	0.8	38.0	0.0	12.2	0.7	3.5	1.6	91.6	1.09	1.5
11.8	81.1	2.5	40.7	0.7	38.0	0.0	12.2	0.8	3.6	1.4	90.9	1.07	1.6
13.2	37.9	4.4	40.9	0.7	34.9	0.0	12.0	0.8	3.7	2.2	87.8	1.17	1.7
14.4	16.9	7.7	44.1	0.8	31.5	0.0	10.4	0.8	3.2	1.5	86.0	1.40	1.9
15.5	9.5	10.5	45.2	0.9	28.2	0.0	8.9	0.7	2.7	2.8	82.3	1.60	1.9
Selectivities		1.0	37.2	0.8	38.1	1.0	14.0	0.2	4.6	2.9	89.3	0.98	2.2

Run No.	SG8	WHSV (g/g/hr)	1	Calcination Temp.	550
Catalyst	S3*	Temp. (deg.C)	400	Sat.Temp. (C)	16
Mass (g)	0.5	Part.press. (kPa)	11	MFC Setting	50.9
Date	25-06-1991	Calcination	Deep bed	GC Trace Nos.	1349-1371

Time (hours)	Ox.Conv. (%)	Methane	Ethene	Ethane	Propene	Propane	Butene	Butane	C5	C6+	C2-C4 (olefin selectivities)	C2/C3	% Paraf. C2-C4
		(Hydrocarbon selectivities : wt%)											
0.2	99.5	0.9	28.0	0.0	41.2	1.5	14.4	0.1	9.4	4.4	83.6	0.68	1.9
1.5	99.6	0.6	35.9	0.6	40.2	0.0	14.2	0.1	6.3	2.1	90.3	0.89	0.8
2.9	99.8	0.7	38.3	0.0	40.0	0.0	13.7	0.2	5.3	4.0	91.9	0.96	0.2
4.0	99.8	0.9	40.3	0.7	37.6	0.0	13.1	0.1	5.3	1.9	91.0	1.07	0.9
5.4	99.9	1.0	40.9	0.0	38.7	0.0	12.9	0.2	4.9	1.4	92.5	1.06	0.2
6.6	99.9	1.1	41.9	0.7	37.1	0.0	12.8	0.7	4.9	1.3	91.8	1.13	1.5
9.2	99.8	1.1	42.1	0.7	38.1	0.0	12.3	0.2	4.3	1.2	92.5	1.11	0.9
10.7	99.7	1.3	43.2	0.0	37.3	0.0	12.5	0.2	4.5	1.1	92.9	1.16	0.3
12.6	99.6	1.4	44.2	0.7	36.3	0.0	11.9	0.3	4.1	1.0	92.4	1.22	1.2
13.9	99.3	1.5	44.4	0.0	37.1	0.0	11.6	0.4	3.9	0.9	93.1	1.20	0.5
15.0	98.8	1.6	44.9	0.8	36.2	0.0	11.3	0.5	3.8	1.0	92.3	1.24	1.3
16.6	94.4	1.7	44.6	0.0	37.3	0.0	11.1	0.6	3.8	0.8	93.0	1.20	0.7
17.8	89.0	1.9	44.6	0.7	36.7	0.0	10.9	0.7	3.6	0.7	92.3	1.21	1.5
19.3	70.4	2.3	44.4	0.0	37.3	0.0	10.9	0.8	3.5	0.7	92.6	1.19	0.9
22.1	37.5	3.8	46.5	0.0	35.5	0.0	9.7	0.8	3.1	0.7	91.7	1.31	0.8
24.7	19.9	5.7	48.3	0.0	33.5	0.0	9.1	0.6	2.6	0.3	90.8	1.44	0.6
27.5	11.9	7.9	50.3	0.0	31.2	0.0	8.1	0.0	1.9	0.6	89.6	1.61	0.0
28.7	10.0	9.5	51.4	0.0	30.0	0.0	7.6	0.0	1.5	0.5	89.0	1.71	0.0
Selectivities		1.2	40.7	0.4	38.1	0.1	12.6	0.3	5.0	1.8	91.5	1.08	0.9

Run No.	SG9	WHSV (g/g/hr)	1	Calcination Temp.	550
Catalyst	S3*	Temp. (deg.C)	350	Sat.Temp. (C)	30
Mass (g)	0.5	Part.press. (kPa)	21	MFC Setting	22
Date	03-07-1991	Calcination	Deep bed	GC Trace Nos.	1372-1405

Time (hours)	Ox.Conv. (%)	Methane	Ethene	Ethane	Propene	Propane	Butene	Butane	C5	C6+	C2-C4 (olefin selectivities)	C2/C3	% Paraf. C2-C4
		(Hydrocarbon selectivities : wt%)											
0.1	97.5	1.1	23.5	0.4	36.8	2.9	16.2	0.1	10.6	8.3	76.6	0.64	4.3
1.3	99.2	0.3	24.6	0.0	40.7	2.2	20.4	0.0	7.1	4.6	85.7	0.60	2.6
3.1	99.4	0.4	27.2	0.5	42.8	0.0	19.8	0.0	6.1	3.2	89.8	0.64	0.6
4.3	99.5	0.4	27.9	0.0	43.4	0.0	19.7	0.1	5.8	2.7	91.0	0.64	0.1
5.5	99.4	0.4	28.9	0.5	43.2	0.0	19.2	0.1	5.5	2.2	91.3	0.67	0.6
6.6	99.4	0.4	29.2	0.6	43.2	0.0	19.0	0.1	5.3	2.1	91.5	0.68	0.7
7.7	99.2	0.4	29.9	0.5	43.6	0.0	18.6	0.1	5.1	1.6	92.1	0.68	0.8
8.8	99.0	0.5	30.4	0.5	43.6	0.0	18.3	0.2	5.0	1.5	92.4	0.70	0.8
9.0	98.6	0.5	31.0	0.4	43.7	0.0	17.9	0.2	4.8	1.3	92.7	0.71	0.7
11.1	98.3	0.5	31.5	0.5	43.8	0.0	17.8	0.2	4.7	1.0	93.1	0.72	0.8
12.4	97.8	0.5	31.8	0.5	43.7	0.0	17.6	0.3	4.7	0.9	93.1	0.73	0.8
13.5	96.9	0.5	32.0	0.5	43.9	0.0	17.3	0.3	4.6	0.9	93.2	0.73	0.9
14.7	96.9	0.5	31.9	0.5	43.4	0.0	17.6	0.3	4.7	1.0	92.9	0.74	0.9
16.1	94.7	0.5	32.3	0.5	43.6	0.0	17.2	0.4	4.6	0.9	93.1	0.74	0.9
17.2	92.5	0.5	32.0	0.5	43.8	0.0	17.2	0.4	4.6	0.9	93.1	0.73	0.9
18.7	89.2	0.6	31.8	0.0	44.2	0.0	17.5	0.4	4.7	0.8	93.5	0.72	0.5
20.3	84.8	0.6	31.4	0.0	44.2	0.0	17.8	0.5	4.8	0.8	93.3	0.71	0.5
21.8	78.3	0.6	31.1	0.0	44.3	0.0	18.0	0.5	4.9	0.7	93.3	0.70	0.5
23.6	68.6	0.7	30.8	0.0	44.2	0.0	18.1	0.5	4.8	0.8	93.1	0.70	0.6
26.2	57.1	0.8	30.4	0.0	43.6	0.0	18.3	0.6	5.8	1.0	92.2	0.70	0.7
27.4	44.3	0.9	30.3	0.0	44.2	0.0	18.2	0.8	6.7	1.2	92.7	0.69	0.8
28.6	38.8	1.0	30.2	0.0	44.1	0.0	18.2	0.7	4.9	1.0	92.5	0.68	0.7
30.2	30.9	1.0	30.2	0.0	43.7	0.0	18.3	0.6	4.9	0.9	92.1	0.69	0.7
31.5	27.2	1.1	30.0	0.0	44.1	0.0	18.3	0.7	5.0	0.8	92.3	0.68	0.7
38.3	16.5	1.4	29.8	0.0	43.3	0.0	18.3	0.7	4.7	1.2	91.4	0.69	0.7
52.5	9.7	1.7	29.9	0.0	43.7	0.0	18.8	0.6	5.0	0.3	92.3	0.68	0.7
Selectivities		0.5	29.6	0.4	42.9	0.3	18.3	0.2	5.6	2.2	90.8	0.69	1.1

Run No.	SG10	WHSV (g/g/hr)	1	Calcination Temp.	550	
Catalyst	S3*	Temp. (deg.C)	450	Sat.Temp. (C)	30	
Mass (g)	0.5	Part.press. (kPa)	21	MFC Setting	22	
Date	05-07-1991	Calcination	Deep bed	GC Trace Nos.	1406-1405	

Time (hours)	Ox.Conv. (%)	Methane	Ethene	Ethane	Propene	Propane	Butene	Butane	C5	C6+	C2-C4 (olefin selectivities)	C2/C3	% Paraf. C2-C4
		(Hydrocarbon selectivities : wt%)											
0.3	99.3	0.9	33.6	0.7	37.5	2.1	13.2	0.1	9.2	2.4	84.4	0.90	3.3
1.4	99.7	1.5	46.8	1.0	33.0	0.0	10.1	0.1	5.9	1.6	89.9	1.42	1.3
2.6	99.7	2.5	49.1	1.0	30.9	0.0	9.3	0.2	5.3	1.6	89.3	1.59	1.4
3.7	99.8	3.1	50.1	1.0	29.7	0.0	8.7	0.3	5.2	2.0	88.5	1.68	1.4
5.0	99.7	4.5	52.0	1.1	27.2	0.0	8.0	0.4	4.6	2.1	87.2	1.91	1.7
6.1	97.8	5.9	52.0	1.1	25.9	0.0	7.5	0.8	4.2	2.6	85.4	2.01	2.1
7.3	51.4	13.0	48.8	1.1	23.8	0.0	6.4	0.9	3.0	2.9	79.0	2.05	2.5
8.6	16.2	27.7	44.4	1.9	16.2	0.0	4.2	0.5	1.9	3.1	64.9	2.74	3.6
10.1	8.9	36.5	39.0	2.6	11.5	0.0	2.5	0.3	0.9	6.2	53.0	3.40	5.1
Selectivities		3.1	47.3	1.0	30.7	0.3	9.5	0.3	5.7	2.1	87.5	1.58	1.9

Run No.	SG11	WHSV (g/g/hr)	1	Calcination Temp.	500	
Catalyst	Ni2	Temp. (deg.C)	400	Sat.Temp. (C)	30	
Mass (g)	0.5	Part.press. (kPa)	21	MFC Setting	22	
Date	08-07-1991	Calcination	Shallow bed	GC Trace Nos.	1516-1422	

Time (hours)	Ox.Conv. (%)	Methane	Ethene	Ethane	Propene	Propane	Butene	Butane	C5	C6+	C2-C4 (olefin selectivities)	C2/C3	% Paraf. C2-C4
		(Hydrocarbon selectivities : wt%)											
0.2	1.3	18.6	18.9	0.8	21.8	0.0	4.6	0.0	0.8	34.3	45.3	0.87	1.8
1.3	1.3	20.9	9.2	0.7	10.5	0.0	2.0	0.0	36.7	19.9	21.7	0.87	2.9
2.6	0.5	35.1	10.5	0.0	10.2	0.0	0.0	0.0	44.2	0.0	20.7	1.03	0.0
3.6	0.3	52.0	13.4	0.0	12.5	0.0	0.0	0.0	0.0	0.0	25.9	1.07	0.0
4.2	0.2	71.7	15.0	0.0	13.3	0.0	0.0	0.0	0.0	0.0	28.3	1.12	0.0
4.6	0.2	61.6	11.6	0.0	9.1	0.0	0.0	0.0	0.0	0.0	20.7	1.27	0.0
Selectivities		19.8	14.1	0.7	16.1	0.0	3.3	0.0	18.7	27.1	33.5	0.87	2.4

Run No.	SG12			WHSV (g/g/hr)	1			Calcination Temp.	500					
Catalyst	Co1			Temp. (deg.C)	400			Sat.Temp. (C)	30					
Mass (g)	0.5			Part.press. (kPa)	21			MFC Setting	22					
Date	09-07-1991			Calcination	Shallow bed			GC Trace Nos.	1423-1432					
Time (hours)	Ox.Conv. (%)	Methane	Ethene	Ethane	Propene	Propane	Butene	Butane	C5	C6+	C2-C4	C2/C3	% Paraf. C2-C4	
		(Hydrocarbon selectivities : wt%)									(olefin selectivities)			
0.2	96.3	1.1	29.6	1.2	35.4	10.4	16.1	0.0	4.9	1.3	81.1	0.84	12.6	
1.3	99.0	1.5	39.4	1.1	35.6	3.0	12.7	0.1	3.7	2.8	87.6	1.11	4.6	
2.6	97.1	2.0	47.1	0.9	35.5	0.0	9.4	0.4	3.1	1.6	92.0	1.33	1.4	
4.0	60.9	3.6	46.0	0.9	37.2	0.0	8.6	0.6	2.2	0.9	91.8	1.24	1.6	
5.6	37.1	5.9	46.0	1.1	36.4	0.0	7.6	0.4	1.2	1.3	90.0	1.26	1.6	
6.3	15.5	8.2	48.7	1.1	33.8	0.0	6.2	0.3	0.7	0.8	88.7	1.44	1.5	
7.5	8.3	10.1	49.9	1.1	32.2	0.0	5.8	0.2	0.4	0.1	87.9	1.55	1.5	
8.7	5.7	11.7	50.4	1.1	30.4	0.0	5.1	0.2	0.3	0.8	85.9	1.66	1.5	
9.9	4.4	13.6	51.9	1.2	28.7	0.0	4.3	0.0	0.3	0.0	84.9	1.81	1.4	
Selectivities		1.5	38.7	1.1	35.5	4.5	12.7	0.2	3.9	1.9	86.9	1.09	6.2	

Run No.	SG13			WHSV (g/g/hr)	1			Calcination Temp.	550					
Catalyst	S1			Temp. (deg.C)	400			Sat.Temp. (C)	30					
Mass (g)	0.5			Part.press. (kPa)	21			MFC Setting	22					
Date	23-07-1991			Calcination	Shallow bed			GC Trace Nos.	1474-1481					
Time (hours)	Ox.Conv. (%)	Methane	Ethene	Ethane	Propene	Propane	Butene	Butane	C5	C6+	C2-C4	C2/C3	% Paraf. C2-C4	
		(Hydrocarbon selectivities : wt%)									(olefin selectivities)			
0.1	96.2	0.4	27.8	0.0	38.6	1.6	16.7	0.3	9.2	5.0	83.2	0.72	2.2	
1.6	95.6	0.5	32.2	0.0	43.1	0.0	17.9	0.5	5.0	1.0	93.2	0.75	0.6	
2.7	74.7	0.8	31.0	0.0	44.1	0.0	17.8	0.6	4.8	0.7	92.8	0.70	0.6	
3.9	40.3	1.7	29.3	0.1	44.6	0.0	18.1	0.6	4.9	0.7	91.9	0.66	0.8	
5.0	20.6	2.3	28.4	0.1	44.7	0.0	18.2	0.6	4.8	0.6	91.3	0.64	0.8	
6.2	12.1	2.9	28.3	0.0	44.5	0.0	17.9	0.7	4.8	0.2	90.8	0.64	0.8	
7.4	6.2	3.4	28.1	0.2	44.3	0.0	17.6	0.2	4.9	0.0	90.1	0.63	0.4	
Selectivities		0.4	30.0	0.0	40.9	0.8	17.3	0.4	7.1	3.0	88.2	0.73	1.4	

Run No.	SG14	WHSV (g/g/hr)	1	Calcination Temp.	400
Catalyst	S3*	Temp. (deg.C)	400	Sat.Temp. (C)	30
Mass (g)	0.5	Part.press. (kPa)	21	MFC Setting	22
Date	05-09-1991	Calcination	Dehydration	GC Trace Nos.	1528-1540

Time (hours)	Ox.Conv. (%)	Methane	Ethene	Ethane	Propene	Propane	Butene	Butane	C5	C6+	C2-C4	C2/C3	% Paraf. C2-C4
		(Hydrocarbon selectivities : wt%)									(olefin selectivities)		
0.1	97.1	0.5	27.8	0.1	40.6	2.5	18.3	0.0	7.0	3.1	86.7	0.68	2.9
1.4	99.4	0.4	31.1	0.1	42.2	1.8	16.9	0.0	5.1	2.2	90.3	0.74	2.2
2.6	99.5	0.5	33.6	0.1	42.5	1.6	15.7	0.1	4.6	1.3	91.8	0.79	1.9
4.2	99.4	0.6	35.5	0.1	42.6	0.9	14.9	0.2	4.2	1.0	92.9	0.83	1.4
5.5	98.9	0.7	37.0	0.1	42.1	0.0	14.7	0.4	4.1	0.9	93.8	0.88	0.5
7.0	96.9	0.8	37.7	0.1	40.8	0.0	14.8	0.6	4.2	0.9	93.3	0.92	0.7
8.7	85.8	1.0	37.4	0.0	42.0	0.0	14.0	0.8	3.9	0.9	93.4	0.89	0.8
10.1	67.6	1.3	37.5	0.1	42.0	0.0	14.0	0.8	3.7	0.6	93.6	0.89	0.9
11.7	38.6	1.9	38.7	0.1	41.2	0.0	13.6	0.8	3.2	0.5	93.5	0.94	1.0
12.9	25.2	2.6	39.2	0.1	40.2	0.0	13.5	0.9	3.2	0.3	92.9	0.98	1.1
14.0	13.6	3.5	40.9	0.1	39.2	0.0	12.5	0.9	3.0	0.0	92.6	1.04	1.0
24.4	2.2	8.3	46.1	0.0	34.5	0.0	9.6	0.2	1.3	0.0	90.2	1.34	0.2
Selectivities		0.6	33.8	0.1	41.8	1.1	15.9	0.2	4.8	1.6	91.5	0.81	1.6

Run No.	SG15	WHSV (g/g/hr)	1	Calcination Temp.	525
Catalyst	Ni3	Temp. (deg.C)	400	Sat.Temp. (C)	30
Mass (g)	0.5	Part.press. (kPa)	21	MFC Setting	22
Date	13-09-1991	Calcination	Shallow bed	GC Trace Nos.	1574-1584

Time (hours)	Ox.Conv. (%)	Methane	Ethene	Ethane	Propene	Propane	Butene	Butane	C5	C6+	C2-C4	C2/C3	% Paraf. C2-C4
		(Hydrocarbon selectivities : wt%)									(olefin selectivities)		
0.2	99.0	0.6	30.3	0.2	39.2	2.2	17.4	0.1	7.3	2.7	86.9	0.77	2.8
1.8	99.5	0.5	35.4	0.1	41.5	1.3	15.1	0.1	4.5	1.4	92.0	0.85	1.6
3.1	99.3	0.5	36.0	0.1	41.7	1.4	14.6	0.2	4.3	1.1	92.3	0.86	1.9
4.2	98.0	0.6	37.3	0.0	41.9	0.0	14.6	0.5	4.1	1.0	93.8	0.89	0.6
5.4	95.6	0.8	38.5	0.1	40.9	0.0	14.4	0.6	3.9	0.7	93.9	0.94	0.7
6.5	88.4	0.8	38.0	0.0	41.8	0.0	14.0	0.8	3.7	0.8	93.8	0.91	0.8
7.7	73.7	1.1	37.5	0.0	42.1	0.0	14.1	0.9	3.6	0.8	93.6	0.89	0.9
9.1	44.2	1.6	36.3	0.0	42.7	0.0	14.5	0.8	3.6	0.4	93.5	0.85	0.9
10.5	26.8	2.2	35.7	0.1	42.4	0.0	15.0	0.9	3.3	0.3	93.1	0.84	1.1
13.3	12.4	3.0	35.4	0.1	41.9	0.0	15.1	0.8	3.7	0.0	92.4	0.84	1.0
Selectivities		0.6	35.5	0.1	41.0	1.0	15.2	0.3	4.8	1.4	91.8	0.87	1.5

Run No.	SG16			WHSV (g/g/hr)	1				Calcination Temp.	550					
Catalyst	S3*-SIL			Temp. (deg.C)	400				Sat.Temp. (C)	30					
Mass (g)	0.5			Part.press. (kPa)	21				MFC Setting	22					
Date	17-09-1991			Calcination	Shallow bed				GC Trace Nos.	2585-1599					
Time (hours)	Ox.Conv. (%)	Methane	Ethene	Ethane	Propene	Propane	Butene	Butane	C5	C6+	C2-C4	C2/C3	% Paraf. C2-C4		
		(Hydrocarbon selectivities : wt%)									(olefin selectivities)				
0.2	97.4	0.5	25.8	0.1	37.4	3.1	18.2	0.0	9.7	5.1	81.4	0.69	3.9		
1.3	99.4	0.4	30.0	0.1	40.9	2.1	16.7	0.0	6.2	3.5	87.6	0.73	2.5		
2.5	99.6	0.5	32.6	0.1	41.0	1.8	15.6	0.1	5.4	3.0	89.3	0.80	2.1		
3.7	99.7	0.5	34.1	0.1	40.9	1.4	15.2	0.1	5.0	2.6	90.3	0.83	1.8		
4.8	99.8	0.5	35.1	0.1	41.6	1.3	14.9	0.1	4.6	1.9	91.5	0.84	1.6		
7.1	99.4	0.6	36.8	0.1	41.7	0.8	14.3	0.2	4.2	1.3	92.7	0.88	1.2		
8.3	99.0	0.7	38.0	0.0	41.3	0.0	14.2	0.4	4.1	1.3	93.4	0.92	0.4		
10.0	96.6	0.9	37.5	0.1	41.1	0.0	14.3	0.5	4.2	1.3	92.9	0.91	0.7		
11.2	90.0	1.0	37.6	0.1	40.7	0.0	14.5	0.7	4.2	1.2	92.7	0.92	0.8		
12.5	76.4	1.2	37.4	0.0	40.9	0.0	14.4	0.8	4.1	1.1	92.7	0.92	0.9		
14.5	39.1	1.8	38.0	0.1	40.3	0.0	13.6	0.8	3.6	1.7	91.9	0.94	1.0		
15.8	21.3	2.6	38.7	0.1	38.7	0.0	13.0	0.9	3.6	2.4	90.4	1.00	1.1		
17.0	13.4	3.3	40.0	0.1	38.0	0.0	12.7	0.9	3.3	1.7	90.7	1.05	1.1		
18.1	12.2	3.8	40.0	0.0	37.9	0.0	12.9	0.9	3.7	0.8	90.7	1.06	1.0		
Selectivities		0.6	34.2	0.1	40.7	1.2	15.3	0.2	5.3	2.4	90.2	0.84	1.7		

Run No.	SG17			WHSV (g/g/hr)	1				Calcination Temp.	500					
Catalyst	Ni4 (contains SAPO-			Temp. (deg.C)	400				Sat.Temp. (C)	30					
Mass (g)	0.5			Part.press. (kPa)	21				MFC Setting	22					
Date	31-09-1991			Calcination	Shallow bed				GC Trace Nos.	1646-1653					
Time (hours)	Ox.Conv. (%)	Methane	Ethene	Ethane	Propene	Propane	Butene	Butane	C5	C6+	C2-C4	C2/C3	% Paraf. C2-C4		
		(Hydrocarbon selectivities : wt%)									(olefin selectivities)				
0.1	83.3	0.4	27.8	0.0	22.5	0.0	4.5	0.8	2.5	41.2	54.8	1.24	1.5		
1.3	73.8	1.0	34.6	0.0	36.3	0.0	10.0	1.0	3.1	13.9	80.9	0.95	1.2		
3.9	52.3	1.5	31.2	0.0	33.8	0.0	8.9	0.3	2.6	21.6	73.9	0.92	0.4		
5.7	40.4	2.1	29.2	0.0	31.2	0.0	8.7	0.0	2.6	26.1	69.1	0.93	0.0		
7.5	15.8	3.1	35.5	0.0	37.7	0.0	9.4	0.0	2.9	11.4	82.6	0.94	0.0		
9.2	13.4	4.0	37.5	0.0	38.8	0.0	10.1	0.0	3.0	6.3	86.5	0.97	0.0		
Selectivities		0.9	31.2	0.0	30.9	0.0	7.8	0.7	2.8	25.6	69.9	1.0	1.0		

Run No.	SG18	WHSV (g/g/hr)	1	Calcination Temp.	500
Catalyst	S3*-BRN	Temp. (deg.C)	400	Sat.Temp. (C)	30
Mass (g)	0.5	Part.press. (kPa)	21	MFC Setting	22
Date	04-11-1991	Calcination	Shallow bed	GC Trace Nos.	1654-1660

Time (hours)	Ox.Conv. (%)	Methane	Ethene	Ethane	Propene	Propane	Butene	Butane	C5	C6+	C2-C4 (olefin selectivities)	C2/C3	% Paraf. C2-C4
		(Hydrocarbon selectivities : wt%)											
0.2	14.4	0.6	4.7	0.0	3.4	0.0	0.1	0.0	0.8	91.0	8.2	1.41	0.0
1.7	4.9	2.6	24.6	0.0	26.0	0.0	4.8	0.0	1.7	42.9	55.4	0.94	0.0
2.9	3.3	2.0	34.6	0.0	40.2	0.0	5.9	0.0	1.8	17.5	80.7	0.86	0.0
4.3	4.3	0.0	35.8	0.0	39.3	0.0	6.4	0.0	1.4	17.1	81.5	0.91	0.0
Selectivities		0.6	4.7	0.0	3.4	0.0	0.1	0.0	0.8	91.0	8.2	1.41	0.0

Run No.	SG19	WHSV (g/g/hr)	1	Calcination Temp.	400
Catalyst	S3*-AMM	Temp. (deg.C)	400	Sat.Temp. (C)	30
Mass (g)	0.5	Part.press. (kPa)	21	MFC Setting	22
Date	29-11-1991	Calcination	Shallow bed	GC Trace Nos.	1696-1707

Time (hours)	Ox.Conv. (%)	Methane	Ethene	Ethane	Propene	Propane	Butene	Butane	C5	C6+	C2-C4 (olefin selectivities)	C2/C3	% Paraf. C2-C4
		(Hydrocarbon selectivities : wt%)											
0.2	98.9	0.6	27.6	0.3	39.9	2.1	17.3	0.1	8.2	4.4	84.9	0.69	2.8
1.5	99.6	0.5	29.1	0.4	38.3	2.0	15.9	0.0	4.6	9.7	83.3	0.76	2.8
2.7	99.7	0.5	31.6	0.4	38.7	1.4	14.5	0.1	4.1	9.1	84.8	0.82	2.2
4.2	99.8	0.5	32.4	0.3	38.0	0.9	13.4	0.1	3.7	11.2	83.7	0.85	1.6
5.5	99.7	0.6	33.4	0.0	37.5	0.0	13.1	0.2	3.6	12.2	84.0	0.89	0.3
6.6	99.7	0.6	34.7	0.4	37.9	0.0	13.0	0.2	3.4	10.4	85.7	0.92	0.7
10.8	92.6	1.0	36.3	0.3	38.6	0.0	12.6	0.5	3.4	8.2	87.5	0.94	0.9
13.1	64.0	1.4	36.3	0.3	38.9	0.0	12.8	0.7	3.3	7.6	88.1	0.93	1.2
15.5	31.7	2.5	36.8	0.0	36.3	0.0	12.0	0.7	3.0	11.2	85.1	1.02	0.9
16.8	19.0	3.2	35.6	0.5	32.9	0.0	10.5	0.7	2.7	17.1	79.0	1.08	1.5
19.6	11.3	3.9	30.0	0.4	24.1	0.0	7.5	0.3	2.1	35.5	61.7	1.24	1.1
24.4	6.7	5.6	32.4	0.1	23.7	0.0	7.5	0.2	2.4	33.8	63.6	1.37	0.4
Selectivities		0.6	32.2	0.3	38.4	0.9	14.3	0.2	4.4	9.3	84.8	0.84	1.6

Run No.	SG20	WHSV (g/g/hr)	1	Calcination Temp.	500
Catalyst	Ni1	Temp. (deg.C)	400	Sat.Temp. (C)	30
Mass (g)	0.5	Part.press. (kPa)	21	MFC Setting	22
Date	16-12-1991	Calcination	Shallow bed	GC Trace Nos.	1746-1750

Time (hours)	Ox.Conv. (%)	Methane	Ethene	Ethane	Propene	Propane	Butene	Butane	C5	C6+	C2-C4 (olefin selectivities)	C2/C3	% Paral. C2-C4
		(Hydrocarbon selectivities : wt%)											
0.2	95.3	0.7	26.8	0.2	31.1	2.6	14.9	0.1	8.0	16.3	72.7	0.86	3.9
2.0	69.6	1.9	35.9	0.5	40.2	1.6	12.4	0.2	3.2	5.9	88.5	0.89	2.6
3.1	11.1	7.9	31.4	1.2	33.0	2.4	12.2	0.3	3.8	15.8	76.5	0.95	4.8
4.4	4.9	9.5	21.4	1.2	20.7	1.7	7.1	0.3	1.9	45.9	49.1	1.03	5.9
Selectivities		0.7	26.8	0.2	31.1	2.6	14.9	0.1	8.0	16.3	72.7	0.86	3.9

Catalyst : S2 (58) Calc. Temp. (C) : 500
Date : 08-05-1991 Calc. Time (hr) : 48

Conditions	Period	Gas Product g/g cat/hr	Liquid Product g/g cat/hr	WHSV g/g cat/hr	Total Conversion %	Propene Conversion %	Cumulative Liquid product g/g cat/hr
220 deg.C	1	11.50	0.00	11.50	0.00	0.00	0.00
280 deg.C	2	10.07	0.00	10.07	0.00	0.00	0.00

Catalyst : Co1 (57) Calc. Temp. (C) : 500
Date : 07-05-1991 Calc. Time (hr) : 16

Conditions	Period	Gas Product g/g cat/hr	Liquid Product g/g cat/hr	WHSV g/g cat/hr	Total Conversion %	Propene Conversion %	Cumulative Liquid product g/g cat/hr
220 deg.C	1	9.50	0.00	9.50	0.00	0.00	0.00
250 deg.C	1	9.22	0.07	9.29	0.75	0.86	0.07
280 deg.C	1	8.10	0.04	8.14	0.49	0.56	0.11

Catalyst : Ni3 Calc. Temp. (C) : 500
Date : 25-09-1991 Calc. Time (hr) : 10

Conditions	Period	Gas Product g/g cat/hr	Liquid Product g/g cat/hr	WHSV g/g cat/hr	Total Conversion %	Propene Conversion %	Cumulative Liquid product g/g cat/hr
250 deg.C	1	ca.10	0.00	10.00	0.00	0.00	0.00
280 deg.C	1	ca.10	0.00	10.00	0.00	0.00	0.00
315 deg.C	1	ca.10	0.00	10.00	0.00	0.00	0.00

APPENDIX VI : Reaction data for the mordenite catalysts

Run Number	Reaction	Catalyst	Aim of experiment
M1	MTO	ZM980	Act. Sel.
M2	MTO	ZM510	Act. Sel.
M3	MTO	ZM760	Standard conditions
M4	MTO	ZM760	R.Temp. 450°C
M5	MTO	ZM760	R.Temp. 350°C
M6	MTO	ZM760	WHSV 0.5 hr^{-1}
M7	MTO	ZM760	P.Press. 10.5 kPa
M8	MTO	ZM760	P.Press. 42 kPa
M9	MTO	ZM760	WHSV 2 hr^{-1}
M10	MTO	ZM760	Standard conditions
M11	MTO	ZM760	P.Press. 42 kPa Reprod.
M12	MTO	ZM760	Dehyd. Catalyst loaded
M13	MTO	M1-4AR	Act. Sel.
M14	MTO	M1-2AR	Act. Sel.
M15	MTO	M1-2AR	Act. Sel. for regen.
M16	MTO	M1-H	Act. Sel.
M17	MTO	M1-2AW	Act. Sel.
M18	MTO	M2-H	Act. Sel.
M19	MTO	M2-4AR	Act. Sel.
M20	MTO	M2-2AR	Act. Sel.
M21	MTO	M2-2AW	Act. Sel.
M22	MTO	M1-4AR	Dehyd. Catalyst loaded
M23	MTO	MN-4AR	Act. Sel.
M24	MTO	MN-2AR	Act. Sel.
M25	MTO	MN-H	Act. Sel.
M26	MTO	MN-2AW	Act. Sel.

Run No.	M1	WHSV (g/g/hr)	1	Calcination Temp.	500
Catalyst	ZM980	Temp. (deg.C)	400	Sat.Temp. (C)	30
Mass (g)	0.5	Part.press. (kPa)	21	MFC Setting	22
Date	28-11-1991	Calcination	Shallow bed	GC Trace Nos.	1661-1694

Time (hours)	Ox.Conv. (%)	Methane	Ethene	Ethane	Propene	Propane	Butene	Butane	C5	C6+	C2-C4 (olefin selectivities)	C2/C3	% Paraf. C2-C4
		(Hydrocarbon selectivities : wt%)											
0.4	97.1	1.0	3.4	0.1	14.3	6.5	1.5	8.9	7.5	56.9	19.2	0.24	44.7
2.0	99.5	1.2	4.9	0.1	11.8	4.6	5.1	21.6	7.0	43.7	21.7	0.41	54.9
3.7	99.7	1.2	4.9	0.1	13.2	4.5	6.4	23.5	8.5	37.5	24.5	0.37	53.5
5.5	99.5	1.6	5.4	0.1	14.9	4.8	7.4	24.9	9.4	31.4	27.8	0.36	51.7
10.1	98.0	1.8	5.2	0.1	19.2	3.5	10.3	20.2	10.2	29.3	34.7	0.27	40.7
16.4	85.9	1.4	8.3	0.0	30.6	0.0	0.0	22.8	15.2	21.8	38.9	0.27	36.9
22.5	81.8	1.5	7.4	0.0	31.4	0.0	0.0	7.0	13.8	38.9	38.8	0.24	15.3
25.6	73.6	1.4	7.4	0.0	30.0	0.0	0.0	4.3	14.4	42.4	37.4	0.25	10.4
30.3	65.3	0.6	3.2	0.0	7.7	0.0	0.0	0.0	24.1	64.4	11.0	0.42	0.0
50.9	35.4	0.5	1.6	0.0	1.5	0.0	0.0	0.0	39.3	57.1	3.1	1.04	0.0
Selectivities (>50%)		1.3	5.6	0.1	19.2	2.7	3.4	14.8	12.2	40.7	28.2	0.31	61.6

Run No.	M2	WHSV (g/g/hr)	1	Calcination Temp.	500
Catalyst	ZM510	Temp. (deg.C)	400	Sat.Temp. (C)	30
Mass (g)	0.5	Part.press. (kPa)	21	MFC Setting	22
Date	02-12-1991	Calcination	Shallow bed	GC Trace Nos.	1708-1712

Time (hours)	Ox.Conv. (%)	Methane	Ethene	Ethane	Propene	Propane	Butene	Butane	C5	C6+	C2-C4 (olefin selectivities)	C2/C3	% Paraf. C2-C4
		(Hydrocarbon selectivities : wt%)											
0.2	97.5	3.6	7.9	2.3	3.7	42.8	1.7	22.0	3.6	12.6	13.2	2.15	83.6
2.1	96.5	9.4	20.8	1.8	14.8	15.4	6.4	4.3	2.9	24.1	42.0	1.40	33.9
3.5	2.0	47.9	17.4	1.3	17.0	2.7	6.9	1.9	2.8	1.4	41.3	1.03	12.4
4.7	0.7	70.0	12.6	1.4	9.5	0.0	0.0	0.0	8.7	0.0	22.1	1.32	6.0
Selectivities (>50%)		6.5	14.3	2.0	9.2	29.1	4.1	13.1	3.3	18.4	27.6	1.78	58.7

Run No.	M3			WHSV (g/g/hr)	1			Calcination Temp.	500				
Catalyst	ZM760			Temp. (deg.C)	400			Sat.Temp. (C)	30				
Mass (g)	0.5			Part.press. (kPa)	21			MFC Setting	22				
Date	10-12-1991			Calcination	Shallow bed			GC Trace Nos.	1715-1724				

Time (hours)	Ox.Conv. (%)	Methane	Ethene	Ethane	Propene	Propane	Butene	Butane	C5	C6+	C2-C4	C2/C3	% Paraf. C2-C4
		(Hydrocarbon selectivities : wt%)									(olefin selectivities)		
0.1	99.2	1.8	10.8	0.3	9.4	18.1	4.0	36.7	8.9	10.0	24.2	1.15	69.5
2.0	83.7	5.9	16.9	0.4	21.9	9.8	9.6	7.6	5.1	22.8	48.4	0.77	26.9
3.6	74.9	5.7	16.6	0.4	20.9	11.4	8.3	8.5	4.8	23.4	45.8	0.80	30.7
5.5	61.9	5.5	16.7	0.3	22.2	10.5	8.2	8.9	4.7	23.0	47.0	0.75	29.6
7.3	50.1	5.5	16.9	0.3	23.3	10.4	8.2	9.4	4.7	21.4	48.3	0.73	29.4
9.7	37.9	5.5	17.1	0.3	24.4	9.9	8.3	9.8	4.6	20.1	49.8	0.70	28.7
11.1	32.7	5.5	16.9	0.4	24.3	9.6	8.1	9.6	4.3	21.4	49.3	0.70	28.4
16.2	17.2	5.5	14.7	0.3	21.2	7.1	10.6	3.3	3.3	34.0	46.5	0.69	16.7
22.5	11.6	4.4	10.6	0.2	15.4	4.7	7.2	2.5	2.4	52.4	33.3	0.69	18.3
Selectivities (>50%)		4.9	15.6	0.4	19.5	12.1	7.7	14.2	5.7	20.1	42.8	0.84	37.2

Run No.	M4			WHSV (g/g/hr)	1			Calcination Temp.	500				
Catalyst	ZM760			Temp. (deg.C)	450			Sat.Temp. (C)	30				
Mass (g)	0.5			Part.press. (kPa)	21			MFC Setting	22				
Date	12-12-1991			Calcination	Shallow bed			GC Trace Nos.	1728-1732				

Time (hours)	Ox.Conv. (%)	Methane	Ethene	Ethane	Propene	Propane	Butene	Butane	C5	C6+	C2-C4	C2/C3	% Paraf. C2-C4
		(Hydrocarbon selectivities : wt%)									(olefin selectivities)		
0.2	99.7	3.7	12.0	0.7	8.2	23.6	2.7	23.5	4.7	21.1	22.8	1.47	67.7
1.9	18.0	37.9	16.0	1.5	19.8	2.3	8.6	2.0	4.3	7.6	44.4	0.81	11.7
3.2	9.1	26.7	4.9	0.9	4.5	0.6	1.1	0.2	4.9	56.0	10.6	1.09	14.4
4.9	5.3	30.7	3.8	0.0	1.0	0.2	0.3	0.0	0.5	63.6	5.0	3.76	3.1
Selectivities (>50%)		15.1	13.3	1.0	12.1	16.5	4.6	16.3	4.6	16.6	30.0	1.25	49.0

Run No.	M5				WHSV (g/g/hr)	1			Calcination Temp.	500				
Catalyst	ZM760				Temp. (deg.C)	350			Sat.Temp. (C)	30				
Mass (g)	0.5				Part.press. (kPa)	21			MFC Setting	22				
Date	13-12-1991				Calcination	Shallow bed			GC Trace Nos.	1733-1745				
Time (hours)	Ox.Conv. (%)	Methane	Ethene	Ethane	Propene	Propane	Butene	Butane	C5	C6+	C2-C4 (olefin selectivities)	C2/C3	% Paraf. C2-C4	
		(Hydrocarbon selectivities : wt%)												
0.2	96.2	1.0	6.9	0.2	2.9	13.1	1.0	48.1	10.4	16.3	10.8	2.35	85.1	
1.8	98.7	1.9	11.9	0.3	9.1	15.1	6.2	25.1	9.9	20.6	27.1	1.31	59.9	
3.5	96.2	2.3	13.6	0.3	13.2	14.5	8.3	14.8	7.2	25.9	35.1	1.03	45.7	
5.1	93.9	2.4	14.0	0.3	14.3	14.8	7.9	13.3	5.9	27.1	36.2	0.98	43.9	
10.8	80.2	2.5	13.2	0.2	15.9	11.8	8.2	13.4	6.9	27.9	37.3	0.83	40.5	
14.1	76.5	2.5	12.9	0.2	15.9	11.1	7.9	13.0	6.6	29.9	36.7	0.81	39.8	
21.7	66.7	2.6	13.5	0.2	16.7	12.3	8.1	14.5	6.9	25.2	38.3	0.81	41.3	
33.2	53.0	2.6	12.3	0.2	16.7	9.0	6.8	11.8	5.5	35.0	35.9	0.74	37.0	
36.2	47.6	2.6	12.5	0.2	17.3	8.8	6.9	12.0	5.5	34.2	36.7	0.72	36.4	
47.7	35.9	2.5	11.7	0.2	16.6	7.6	6.2	10.9	5.0	39.2	34.6	0.71	35.1	
49.4	32.0	3.0	13.6	0.2	19.2	8.7	7.1	12.5	5.6	30.2	39.8	0.71	35.0	
Selectivities (>50%)		2.2	12.3	0.2	13.1	12.7	6.8	19.3	7.4	26.0	32.2	1.07	49.2	

Run No.	M6				WHSV (g/g/hr)	0.5			Calcination Temp.	500				
Catalyst	ZM760				Temp. (deg.C)	400			Sat.Temp. (C)	30				
Mass (g)	0.5				Part.press. (kPa)	21			MFC Setting	11				
Date	17-12-1991				Calcination	Shallow bed			GC Trace Nos.	1751-1762				
Time (hours)	Ox.Conv. (%)	Methane	Ethene	Ethane	Propene	Propane	Butene	Butane	C5	C6+	C2-C4 (olefin selectivities)	C2/C3	% Paraf. C2-C4	
		(Hydrocarbon selectivities : wt%)												
0.3	97.4	1.7	7.7	0.4	3.5	20.1	1.3	29.8	6.1	29.5	12.5	2.24	80.1	
2.0	99.0	6.8	17.1	0.7	15.6	16.2	8.9	11.5	5.9	17.4	41.6	1.09	40.5	
3.8	86.3	9.1	19.4	0.5	23.3	11.5	8.9	7.4	4.1	15.8	51.6	0.83	27.4	
6.1	73.8	8.5	20.0	0.5	25.6	12.3	9.0	8.8	4.1	11.2	54.6	0.78	28.3	
9.0	65.5	7.9	18.9	0.4	25.0	11.5	8.6	9.0	3.9	14.8	52.4	0.76	28.6	
12.3	50.5	8.0	18.2	0.5	25.4	10.2	8.3	9.1	3.6	16.7	52.0	0.72	27.6	
21.5	22.5	9.8	17.7	0.7	25.7	8.3	8.1	9.2	3.5	17.0	51.5	0.69	26.1	
29.5	15.3	9.4	15.5	0.7	22.8	7.0	7.3	8.6	3.6	25.1	45.6	0.68	26.3	
33.1	13.7	9.1	14.2	0.6	21.0	6.3	6.6	8.2	3.4	30.5	41.9	0.68	26.5	
Selectivities (>50%)		7.0	16.9	0.5	19.7	13.6	7.5	12.6	4.6	17.6	44.1	1.07	38.7	

Run No.	M7			WHSV (g/g/hr)	1			Calcination Temp.	500				
Catalyst	ZM760			Temp. (deg.C)	400			Sat.Temp. (C)	16				
Mass (g)	0.5			Part.press. (kPa)	10.5			MFC Setting	50.9				
Date	19-12-1991			Calcination	Shallow bed			GC Trace Nos.	1763-1770				
Time (hours)	Ox.Conv. (%)	Methane	Ethene	Ethane	Propene	Propane	Butene	Butane	C5	C6+	C2-C4 (olefin selectivities)	C2/C3	% Paraf. C2-C4
		(Hydrocarbon selectivities : wt%)											
0.3	50.0	1.2	6.0	0.1	8.2	5.4	3.3	10.1	3.2	62.5	17.5	0.72	47.2
2.2	95.9	2.9	7.0	0.2	10.9	2.8	5.4	2.3	2.5	66.0	23.4	0.64	18.3
4.3	78.9	1.5	3.8	0.1	5.4	1.6	2.0	1.5	1.0	83.2	11.1	0.70	22.4
6.5	74.0	1.0	2.1	0.1	3.0	0.8	1.0	0.8	0.4	90.8	6.1	0.72	21.6
10.0	48.4	1.3	1.9	0.1	2.3	0.5	0.5	0.6	0.3	92.5	4.8	0.82	19.5
18.4	27.7	1.7	0.8	0.1	0.8	0.1	0.1	0.1	2.6	93.7	1.7	1.04	13.0
24.2	27.3	1.1	0.3	0.0	0.3	0.0	0.0	0.0	6.0	92.3	0.6	1.28	0.0
Selectivities (>50%)		1.6	4.7	0.1	6.9	2.7	2.9	3.7	1.8	75.6	14.5	0.70	27.4

Run No.	M8			WHSV (g/g/hr)	1			Calcination Temp.	500				
Catalyst	ZM760			Temp. (deg.C)	400			Sat.Temp. (C)	45.5				
Mass (g)	0.5			Part.press. (kPa)	42			MFC Setting	8.8				
Date	23-12-1991			Calcination	Shallow bed			GC Trace Nos.	1771-1782				
Time (hours)	Ox.Conv. (%)	Methane	Ethene	Ethane	Propene	Propane	Butene	Butane	C5	C6+	C2-C4 (olefin selectivities)	C2/C3	% Paraf. C2-C4
		(Hydrocarbon selectivities : wt%)											
0.2	95.6	2.1	6.8	0.5	3.9	25.5	1.6	35.2	6.7	15.9	14.2	2.24	81.1
2.4	90.5	3.6	9.2	0.3	10.4	6.9	4.6	4.3	2.5	58.3	24.2	0.89	32.2
5.3	79.4	6.4	16.9	0.5	21.4	12.1	7.5	8.4	3.2	23.6	45.8	0.79	31.3
7.4	70.7	5.4	14.0	0.4	18.7	9.4	6.3	7.4	2.6	35.8	39.0	0.75	30.6
12.7	50.9	5.8	14.1	0.5	19.8	8.2	6.4	7.8	2.8	34.7	40.2	0.71	29.2
22.4	31.4	5.3	11.3	0.4	16.4	6.1	5.4	7.0	2.7	45.3	33.1	0.69	29.1
27.9	28.7	5.1	9.2	0.4	13.5	4.7	4.4	5.6	2.2	54.9	27.1	0.68	28.4
31.8	25.2	6.4	7.8	0.5	11.3	3.4	3.5	4.1	1.6	61.2	22.7	0.69	26.2
Selectivities (>50%)		4.7	12.6	0.4	14.8	12.4	5.3	12.6	3.6	33.7	32.7	1.08	40.9

Run No.	M9	WHSV (g/g/hr)	2	Calcination Temp.	500
Catalyst	ZM760	Temp. (deg.C)	400	Sat.Temp. (C)	30
Mass (g)	0.5	Part.press. (kPa)	21	MFC Setting	44.1
Date	06-01-1992	Calcination	Shallow bed	GC Trace Nos.	1783-1790

Time (hours)	Ox.Conv. (%)	Methane	Ethene	Ethane	Propene	Propane	Butene	Butane	C5	C6+	C2-C4 (olefin selectivities)	C2/C3	% Paraf. C2-C4
		(Hydrocarbon selectivities : wt%)											
0.3	96.2	3.0	11.7	0.4	15.1	12.2	7.3	20.6	7.5	22.3	34.1	0.78	49.3
2.0	87.4	4.4	13.2	0.3	19.2	7.9	9.7	7.2	5.5	32.6	42.1	0.69	26.8
3.7	73.7	3.2	10.8	0.2	16.5	6.3	7.7	6.6	4.5	44.2	35.0	0.65	27.2
5.5	66.5	2.9	10.4	0.2	15.9	5.9	6.9	6.5	4.2	46.9	33.2	0.65	27.6
8.2	51.0	3.2	11.2	0.2	17.4	6.1	7.2	7.2	4.5	43.0	35.8	0.65	27.5
11.5	37.7	3.2	11.0	0.2	17.1	5.7	6.7	7.1	4.3	44.6	34.9	0.64	27.3
25.1	12.4	5.4	15.6	0.3	22.7	6.8	7.1	8.2	3.3	30.6	45.4	0.69	25.2
Selectivities (>50%)		3.4	11.5	0.3	16.8	7.7	7.8	9.6	5.2	37.8	36.0	0.68	31.7

Run No.	M10	WHSV (g/g/hr)	1	Calcination Temp.	500
Catalyst	ZM760	Temp. (deg.C)	400	Sat.Temp. (C)	30
Mass (g)	0.5	Part.press. (kPa)	21	MFC Setting	22
Date	07-01-1992	Calcination	Shallow bed	GC Trace Nos.	1791-1801

Time (hours)	Ox.Conv. (%)	Methane	Ethene	Ethane	Propene	Propane	Butene	Butane	C5	C6+	C2-C4 (olefin selectivities)	C2/C3	% Paraf. C2-C4
		(Hydrocarbon selectivities : wt%)											
0.2	94.6	1.3	7.3	0.3	4.0	15.6	1.5	29.1	6.2	34.7	12.9	1.80	77.7
2.0	98.0	5.2	13.9	0.4	15.5	9.2	8.0	5.9	4.1	37.9	37.4	0.89	29.3
3.8	86.9	4.9	12.3	0.3	15.4	7.5	5.8	5.1	2.8	45.9	33.6	0.80	27.7
5.6	77.6	4.0	10.9	0.2	14.4	6.5	5.0	5.0	2.4	51.6	30.3	0.76	28.0
7.4	71.2	3.5	9.9	0.2	13.4	5.8	4.5	4.8	2.2	55.8	27.8	0.74	27.9
11.6	49.3	4.2	11.5	0.2	16.2	6.2	5.3	5.9	2.5	48.0	33.0	0.71	27.1
13.5	44.0	3.8	10.0	0.2	14.2	5.1	4.6	5.1	2.1	55.0	28.7	0.70	26.7
17.7	32.4	3.7	8.9	0.2	12.5	4.2	4.0	4.6	1.8	60.0	25.4	0.71	26.3
22.4	23.8	3.2	6.9	0.2	9.7	3.1	3.0	3.7	1.4	68.8	19.5	0.71	26.4
25.4	22.1	3.0	6.8	0.2	9.6	2.9	3.0	3.5	1.4	69.7	19.4	0.71	25.1
Selectivities (>50%)		3.8	10.8	0.3	12.6	8.9	5.0	10.0	3.5	45.2	28.4	1.00	38.1

Run No.	M11			WHSV (g/g/hr)	1			Calcination Temp.	500					
Catalyst	ZM760			Temp. (deg.C)	400			Sat.Temp. (C)	45.5					
Mass (g)	0.5			Part.press. (kPa)	42			MFC Setting	8.8					
Date	08-01-1992			Calcination	Shallow bed			GC Trace Nos.	1802-1813					
Time (hours)	Ox.Conv. (%)	Methane	Ethene	Ethane	Propene	Propane	Butene	Butane	C5	C6+	C2-C4	C2/C3	% Paraf. C2-C4	
		(Hydrocarbon selectivities : wt%)									(olefin selectivities)			
0.3	90.4	2.2	8.5	0.5	3.9	23.4	1.7	38.2	8.8	12.9	14.1	2.19	81.5	
2.3	94.7	6.5	18.5	0.5	20.4	14.8	8.7	9.2	4.5	16.9	47.6	0.91	33.9	
4.6	85.6	5.9	18.1	0.4	21.8	14.4	8.3	9.7	4.2	17.2	48.1	0.83	33.8	
7.4	77.4	5.6	18.1	0.4	22.7	13.7	8.1	10.3	4.2	17.0	48.9	0.80	33.3	
10.8	67.2	5.2	17.6	0.4	23.3	12.6	8.3	10.8	4.5	17.4	49.2	0.76	32.6	
16.1	51.1	4.8	16.6	0.3	23.1	10.7	8.1	10.5	4.4	21.4	47.9	0.72	31.0	
19.2	45.9	4.5	15.5	0.3	22.1	9.5	7.6	9.9	4.1	26.6	45.2	0.70	30.3	
22.6	36.2	4.6	15.3	0.3	22.2	8.9	7.5	9.8	4.0	27.4	45.0	0.69	29.6	
25.8	28.5	4.4	15.4	0.3	23.3	9.0	8.3	10.5	4.5	24.3	47.0	0.66	29.6	
35.2	19.1	4.2	13.2	0.3	19.8	6.9	6.9	9.0	4.0	35.7	39.9	0.67	28.8	
43.6	16.0	3.6	10.8	0.2	16.4	5.3	5.8	7.6	3.5	46.7	33.1	0.66	28.5	
Selectivities (>50%)		5.0	16.2	0.4	19.2	14.9	7.2	14.8	5.1	17.1	42.6	0.89	41.0	

Run No.	M12			WHSV (g/g/hr)	1			Calcination Temp.	500					
Catalyst	ZM760			Temp. (deg.C)	400			Sat.Temp. (C)	30					
Mass (g)	0.5			Part.press. (kPa)	21			MFC Setting	22					
Date	13-01-1992			Calcination	Shallow bed			GC Trace Nos.	1814-1821					
Time (hours)	Ox.Conv. (%)	Methane	Ethene	Ethane	Propene	Propane	Butene	Butane	C5	C6+	C2-C4	C2/C3	% Paraf. C2-C4	
		(Hydrocarbon selectivities : wt%)									(olefin selectivities)			
0.3	98.2	2.6	9.3	0.3	10.5	9.7	5.4	13.8	5.3	43.2	25.2	0.89	48.5	
2.0	91.6	3.2	7.8	0.2	10.5	4.6	5.0	4.2	3.0	61.5	23.3	0.75	27.8	
3.7	87.6	2.7	7.0	0.2	9.4	4.3	4.3	3.7	2.5	66.0	20.7	0.74	28.4	
5.9	80.7	2.9	8.0	0.2	11.0	4.9	4.8	4.5	2.8	60.9	23.8	0.73	28.8	
9.2	70.0	3.2	9.2	0.2	13.0	5.5	5.6	5.9	3.5	53.9	27.7	0.70	29.6	
14.6	56.6	2.8	8.1	0.2	12.0	4.5	4.8	5.0	3.0	59.7	24.9	0.67	27.9	
24.1	24.4	3.4	8.5	0.2	12.5	3.9	4.1	4.7	2.1	60.7	25.1	0.68	25.9	
Selectivities (>50%)		2.9	8.2	0.2	11.1	5.6	5.0	6.2	3.3	57.5	24.3	0.75	31.8	

Run No.	M13	WHSV (g/g/hr)	1	Calcination Temp.	520
Catalyst	M1-4AR	Temp. (deg.C)	400	Sat.Temp. (C)	30
Mass (g)	0.5	Part.press. (kPa)	21	MFC Setting	22
Date	27-01-1992	Calcination	Shallow bed	GC Trace Nos.	1822-1828

Time (hours)	Ox.Conv. (%)	Methane	Ethene	Ethane	Propene	Propane	Butene	Butane	C5	C6+	C2-C4	C2/C3	% Paraf. C2-C4
		(Hydrocarbon selectivities : wt%)									(olefin selectivities)		
0.2	99.8	2.2	12.0	0.4	10.1	11.9	5.5	10.6	3.9	43.4	27.6	1.19	45.4
1.9	50.4	3.8	1.6	0.1	1.6	0.2	0.8	0.3	0.7	90.8	4.0	1.05	14.5
4.0	36.1	3.0	0.6	0.1	0.4	0.0	0.1	0.1	0.3	95.6	1.0	1.59	11.8
5.7	45.0	1.4	0.2	0.0	0.1	0.0	0.0	0.0	0.0	98.2	0.4	1.70	7.8
8.0	34.1	1.9	0.2	0.0	0.1	0.0	0.1	0.0	0.2	97.5	0.4	1.80	6.6
12.8	25.5	2.4	0.2	0.0	0.0	0.0	0.1	0.0	0.2	97.1	0.3	-	10.1
Selectivities (>50%)		3.0	6.8	0.2	5.8	6.1	3.1	5.5	2.3	67.1	15.8	1.12	30.0

Run No.	M14	WHSV (g/g/hr)	1	Calcination Temp.	520
Catalyst	M1-2AR	Temp. (deg.C)	400	Sat.Temp. (C)	30
Mass (g)	0.5	Part.press. (kPa)	21	MFC Setting	22
Date	30-01-1992	Calcination	Shallow bed	GC Trace Nos.	1829-1838

Time (hours)	Ox.Conv. (%)	Methane	Ethene	Ethane	Propene	Propane	Butene	Butane	C5	C6+	C2-C4	C2/C3	% Paraf. C2-C4
		(Hydrocarbon selectivities : wt%)									(olefin selectivities)		
0.2	98.2	0.8	6.3	0.2	3.7	7.8	1.6	11.8	2.4	65.4	11.6	1.73	63.1
1.8	85.2	1.9	3.7	0.1	8.7	0.8	5.3	3.0	3.0	73.5	17.7	0.42	18.0
3.5	69.8	0.9	0.9	0.0	3.5	0.0	2.8	0.9	1.5	89.4	7.2	0.27	11.9
5.4	57.5	0.9	0.6	0.0	1.6	0.0	1.5	0.4	1.0	94.1	3.7	0.38	9.6
8.1	43.8	0.9	0.3	0.0	0.3	0.0	0.1	0.0	0.2	98.2	0.7	1.24	2.7
14.0	38.9	0.8	0.2	0.0	0.1	0.0	0.1	0.0	0.1	98.7	0.5	1.56	0.0
22.8	30.6	0.7	0.1	0.0	0.1	0.0	0.2	0.0	0.1	98.7	0.4	1.88	0.0
Selectivities (>50%)		1.1	2.9	0.1	4.4	2.1	2.8	4.0	2.0	80.6	10.0	1.07	25.7

Run No.	M15			WHSV (g/g/hr)	1			Calcination Temp.	520					
Catalyst	M1-2AR			Temp. (deg.C)	400			Sat.Temp. (C)	30					
Mass (g)	0.5			Part.press. (kPa)	21			MFC Setting	22					
Date	01-02-1992			Calcination	Shallow bed			GC Trace Nos.	1839-1846					
Time (hours)	Ox.Conv. (%)	Methane	Ethene	Ethane	Propene	Propane	Butene	Butane	C5	C6+	C2-C4 (olefin selectivities)		C2/C3	% Paraf. C2-C4
		(Hydrocarbon selectivities : wt%)												
0.3	99.1	1.8	11.6	0.4	7.2	12.4	3.8	17.3	5.0	40.7	22.5		1.61	57.2
2.0	85.9	2.2	4.7	0.1	9.7	1.7	5.9	4.4	3.7	67.8	20.2		0.48	23.4
5.5	58.0	1.0	1.0	0.1	2.9	0.3	2.9	1.1	2.0	88.7	6.8		0.35	17.0
7.8	39.6	1.1	0.5	0.0	0.6	0.0	0.5	0.3	0.7	96.2	1.7		0.91	13.6
11.0	25.0	1.4	0.4	0.0	0.2	0.0	0.0	0.0	0.1	97.9	0.7		1.76	0.0
24.4	18.2	1.0	0.3	0.0	0.1	0.0	0.0	0.0	0.3	98.3	0.4		2.04	0.0
Selectivities (>50%)		1.6	5.8	0.2	6.6	4.8	4.2	7.6	3.6	65.7	16.5		0.81	32.5

Run No.	M16			WHSV (g/g/hr)	1			Calcination Temp.	520					
Catalyst	M1-H			Temp. (deg.C)	400			Sat.Temp. (C)	30					
Mass (g)	0.5			Part.press. (kPa)	21			MFC Setting	22					
Date	03-02-1992			Calcination	Shallow bed			GC Trace Nos.	1849-1853					
Time (hours)	Ox.Conv. (%)	Methane	Ethene	Ethane	Propene	Propane	Butene	Butane	C5	C6+	C2-C4 (olefin selectivities)		C2/C3	% Paraf. C2-C4
		(Hydrocarbon selectivities : wt%)												
0.4	98.0	4.6	25.9	0.9	19.4	24.0	5.6	6.6	2.5	10.4	50.9		1.33	38.3
2.2	25.8	5.9	13.8	0.6	12.3	5.1	3.2	3.2	1.9	53.9	29.3		1.12	23.4
4.2	22.2	5.0	10.0	0.4	9.6	4.4	2.7	3.3	2.0	62.8	22.3		1.04	26.5
5.9	21.3	3.8	7.3	0.3	7.3	3.4	2.4	2.7	1.9	71.0	16.9		1.00	27.4
Selectivities (>50%)		5.0	21.9	0.8	17.1	17.7	4.8	5.5	2.3	24.9	43.7		1.26	33.3

Run No.	M17	WHSV (g/g/hr)	1	Calcination Temp.	520
Catalyst	M1-2AW	Temp. (deg.C)	400	Sat.Temp. (C)	30
Mass (g)	0.5	Part.press. (kPa)	21	MFC Setting	22
Date	04-02-1992	Calcination	Shallow bed	GC Trace Nos.	1854-1857

Time (hours)	Ox.Conv. (%)	Methane	Ethene	Ethane	Propene	Propane	Butene	Butane	C5	C6+	C2-C4 (olefin selectivities)	C2/C3	% Paraf. C2-C4
		(Hydrocarbon selectivities : wt%)											
0.3	96.7	11.2	7.9	5.9	2.4	44.4	1.0	5.5	0.9	20.7	11.3	3.33	83.2
2.0	14.1	5.5	2.2	0.9	1.3	7.1	1.4	0.9	1.0	79.7	5.0	1.70	63.9
3.8	15.9	2.0	0.6	0.2	0.4	1.1	1.0	0.1	1.2	93.6	1.9	1.50	42.2
Selectivities (>50%)		9.3	6.0	4.3	2.0	32.0	1.2	3.9	0.9	40.3	9.2	2.79	76.7

Run No.	M18	WHSV (g/g/hr)	1	Calcination Temp.	520
Catalyst	M2-H	Temp. (deg.C)	400	Sat.Temp. (C)	30
Mass (g)	0.5	Part.press. (kPa)	21	MFC Setting	22
Date	06-02-1992	Calcination	Shallow bed	GC Trace Nos.	1861-1865

Time (hours)	Ox.Conv. (%)	Methane	Ethene	Ethane	Propene	Propane	Butene	Butane	C5	C6+	C2-C4 (olefin selectivities)	C2/C3	% Paraf. C2-C4
		(Hydrocarbon selectivities : wt%)											
0.2	97.5	17.2	10.9	16.3	5.4	34.8	2.1	3.9	1.4	8.1	18.3	2.01	75.0
1.9	32.7	5.7	6.5	4.5	5.7	14.9	3.0	4.2	3.1	52.3	15.3	1.14	60.8
3.5	16.5	1.9	1.9	0.5	2.0	2.3	1.1	1.5	1.8	87.1	5.0	0.96	45.7
5.4	11.5	1.6	1.1	0.2	1.0	0.8	1.4	0.5	1.2	92.2	3.4	1.10	30.7
Selectivities (>50%)		13.3	9.4	12.4	5.5	28.2	2.4	4.0	2.0	22.9	17.3	1.72	70.2

Run No.	M19	WHSV (g/g/hr)	1	Calcination Temp.	520
Catalyst	M2-4AR	Temp. (deg.C)	400	Sat.Temp. (C)	30
Mass (g)	07-02-1992	Part press. (kPa)	21	MFC Setting	22
Date	08-01-1992	Calcination	Shallow bed	GC Trace Nos.	1899-1878

Time (hours)	Ox.Conv. (%)	Methane	Ethene	Ethane	Propene	Propane	Butene	Butane	C5	C6+	C2-C4 (olefin selectivities)	C2/C3	% Paraf. C2-C4
		(Hydrocarbon selectivities : wt%)											
0.1	97.7	1.6	5.1	1.1	0.9	40.7	0.5	28.9	8.0	13.3	6.4	5.82	91.7
1.9	45.5	5.7	12.6	0.6	21.2	2.0	11.4	5.7	7.4	33.5	45.2	0.59	15.5
3.6	15.3	4.7	5.1	0.3	4.7	0.0	1.8	0.5	1.0	81.9	11.6	1.08	6.7
5.7	12.8	3.2	1.5	0.1	1.0	0.0	0.1	0.0	4.1	90.0	2.5	1.54	4.9
Selectivities (>50%)		3.0	7.6	0.9	7.6	27.8	4.1	21.1	7.8	20.0	19.3	4.07	66.3

Run No.	M20	WHSV (g/g/hr)	1	Calcination Temp.	520
Catalyst	M2-2AR	Temp. (deg.C)	400	Sat.Temp. (C)	30
Mass (g)	0.5	Part.press. (kPa)	21	MFC Setting	22
Date	08-02-1992	Calcination	Shallow bed	GC Trace Nos.	1871-1875

Time (hours)	Ox.Conv. (%)	Methane	Ethene	Ethane	Propene	Propane	Butene	Butane	C5	C6+	C2-C4 (olefin selectivities)	C2/C3	% Paraf. C2-C4
		(Hydrocarbon selectivities : wt%)											
0.2	99.4	4.2	8.1	2.7	2.1	35.3	1.0	22.3	3.8	20.4	11.3	3.80	84.2
1.9	12.3	3.0	7.0	0.5	7.0	0.0	1.2	0.9	0.6	79.7	15.2	1.00	8.7
3.6	13.1	1.4	1.3	0.1	1.0	0.0	0.2	0.0	0.1	95.8	2.6	1.25	5.2
5.6	13.0	0.9	0.4	0.0	0.3	0.0	0.2	0.0	0.2	98.0	0.9	1.17	0.0
Selectivities (>50%)		3.8	7.8	2.0	3.7	23.6	1.1	15.2	2.7	40.2	12.6	2.87	59.0

Run No.	M21	WHSV (g/g/hr)	1	Calcination Temp.	520
Catalyst	m2-2aw	Temp. (deg.C)	400	Sat.Temp. (C)	30
Mass (g)	0.5	Part.press. (kPa)	21	MFC Setting	22
Date	09-02-1992	Calcination	Shallow bed	GC Trace Nos.	1876-1880

Time (hours)	Ox.Conv. (%)	Methane	Ethene	Ethane	Propene	Propane	Butene	Butane	C5	C6+	C2-C4	C2/C3	% Paraf. C2-C4
		(Hydrocarbon selectivities : wt%)									(olefin selectivities)		
0.2	96.2	15.3	14.0	15.7	6.8	19.9	2.6	2.2	1.6	21.9	23.4	2.05	61.8
1.9	16.0	2.3	5.5	1.9	4.8	2.5	1.4	0.7	0.7	80.1	11.7	1.14	30.4
3.6	11.5	0.6	1.2	0.0	0.9	0.0	0.0	0.0	2.8	94.5	2.1	1.27	0.0
5.5	12.7	0.3	0.5	0.0	0.4	0.0	0.0	0.0	0.1	98.7	0.8	1.36	0.0
Selectivities (>50%)		11.0	11.1	11.1	6.2	14.1	2.2	1.7	1.3	41.3	19.5	1.74	51.3

Run No.	M22	WHSV (g/g/hr)	1	Calcination Temp.	520
Catalyst	M1-4AR	Temp. (deg.C)	400	Sat.Temp. (C)	30
Mass (g)	0.5	Part.press. (kPa)	21	MFC Setting	22
Date	10-02-1992	Calcination	Shallow bed	GC Trace Nos.	1881-1887

Time (hours)	Ox.Conv. (%)	Methane	Ethene	Ethane	Propene	Propane	Butene	Butane	C5	C6+	C2-C4	C2/C3	% Paraf. C2-C4
		(Hydrocarbon selectivities : wt%)									(olefin selectivities)		
0.2	99.1	1.3	12.2	0.4	8.3	16.9	3.9	29.4	8.4	19.3	24.4	1.47	65.7
1.9	79.9	3.9	15.0	0.3	25.3	2.0	13.6	5.0	6.4	28.5	53.9	0.59	11.8
4.1	30.9	4.9	7.0	0.3	17.8	0.0	12.9	3.2	1.4	52.5	37.7	0.39	8.4
8.2	13.8	4.5	2.4	0.2	2.4	0.0	0.5	0.0	0.3	89.7	5.3	1.01	2.8
9.9	12.3	4.2	1.9	0.0	1.6	0.0	0.3	0.0	0.6	91.5	3.7	1.21	0.0
Selectivities (>50%)		2.6	13.6	0.4	16.8	9.4	8.8	17.2	7.4	23.9	39.1	1.03	38.8

Run No.	M23	WHSV (g/g/hr)	1	Calcination Temp.	520
Catalyst	MN-4AR	Temp. (deg.C)	400	Sat.Temp. (C)	30
Mass (g)	0.5	Part.press. (kPa)	21	MFC Setting	22
Date	11-02-1992	Calcination	Shallow bed	GC Trace Nos.	1888-1892

Time (hours)	Ox.Conv. (%)	Methane	Ethene	Ethane	Propene	Propane	Butene	Butane	C5	C6+	C2-C4 (olefin selectivities)	C2/C3	% Paraf. C2-C4
		(Hydrocarbon selectivities : wt%)											
0.2	99.1	1.8	6.8	1.1	1.7	35.4	0.8	21.7	3.3	27.4	9.3	4.01	86.2
1.8	14.1	5.5	3.8	0.8	3.2	1.1	1.6	0.9	0.9	82.1	8.6	1.21	24.9
3.5	17.5	1.4	0.6	0.1	0.4	0.0	0.0	0.0	0.1	97.4	1.0	1.50	10.0
5.4	14.9	1.0	0.3	0.0	0.2	0.0	0.1	0.0	0.1	98.2	0.7	1.49	0.0
Selectivities (>50%)		3.1	5.8	1.0	2.2	24.0	1.1	14.8	2.5	45.6	9.1	3.08	65.8

Run No.	M24	WHSV (g/g/hr)	1	Calcination Temp.	520
Catalyst	MN-2AR	Temp. (deg.C)	400	Sat.Temp. (C)	30
Mass (g)	0.5	Part.press. (kPa)	21	MFC Setting	22
Date	12-02-1992	Calcination	Shallow bed	GC Trace Nos.	1893-1896

Time (hours)	Ox.Conv. (%)	Methane	Ethene	Ethane	Propene	Propane	Butene	Butane	C5	C6+	C2-C4 (olefin selectivities)	C2/C3	% Paraf. C2-C4
		(Hydrocarbon selectivities : wt%)											
0.2	99.2	3.3	5.2	2.4	0.6	43.7	0.3	17.2	2.2	25.1	6.1	8.10	91.1
1.9	12.6	4.1	1.6	0.9	1.1	0.5	0.4	0.2	0.1	91.2	3.0	1.47	34.2
3.7	13.1	1.4	0.4	0.2	0.3	0.0	0.0	0.0	0.4	97.3	0.7	1.53	20.7
Selectivities (>50%)		3.6	4.0	1.9	0.8	29.3	0.3	11.5	1.5	47.1	5.1	5.89	72.2

Run No.	M25	WHSV (g/g/hr)	1	Calcination Temp.	520
Catalyst	MN-H	Temp. (deg.C)	400	Sat.Temp. (C)	30
Mass (g)	0.5	Part.press. (kPa)	21	MFC Setting	22
Date	13-02-1992	Calcination	Shallow bed	GC Trace Nos.	1897-1901

Time (hours)	Ox.Conv. (%)	Methane	Ethene	Ethane	Propene	Propane	Butene	Butane	C5	C6+	C2-C4 (olefin selectivities)	C2/C3	% Paraf. C2-C4
		(Hydrocarbon selectivities : wt%)											
0.2	98.5	8.0	6.2	7.5	1.0	41.0	0.5	7.7	1.1	26.9	7.8	6.04	87.8
1.9	17.7	5.9	4.6	1.0	5.0	4.1	3.4	3.6	3.0	69.3	13.0	0.91	40.2
3.7	16.3	1.0	0.4	0.1	0.3	0.0	0.0	0.1	0.4	97.6	0.8	1.31	20.2
5.5	14.0	0.7	0.2	0.0	0.1	0.0	0.0	0.0	0.2	98.8	0.3	1.41	0.0
Selectivities (>50%)		7.3	5.7	5.3	2.4	28.7	1.5	6.3	1.8	41.1	9.5	4.33	72.0

Run No.	M26	WHSV (g/g/hr)	1	Calcination Temp.	520
Catalyst	MN-2AW	Temp. (deg.C)	400	Sat.Temp. (C)	30
Mass (g)	0.5	Part.press. (kPa)	21	MFC Setting	22
Date	17-02-1992	Calcination	Shallow bed	GC Trace Nos.	1907-1910

Time (hours)	Ox.Conv. (%)	Methane	Ethene	Ethane	Propene	Propane	Butene	Butane	C5	C6+	C2-C4 (olefin selectivities)	C2/C3	% Paraf. C2-C4
		(Hydrocarbon selectivities : wt%)											
0.2	99.8	4.6	6.1	3.3	1.1	37.5	0.5	14.4	2.0	30.5	7.8	5.38	87.7
1.9	17.5	2.0	0.8	0.5	0.6	0.3	0.3	0.2	0.2	95.1	1.7	1.44	37.3
3.5	26.3	0.6	0.2	0.1	0.2	0.1	0.1	0.1	0.1	98.5	0.5	1.33	35.6
Selectivities (>50%)		3.7	4.4	2.4	0.9	25.1	0.5	9.7	1.4	52.0	5.7	4.07	70.9

Catalyst : MN-H (M10) Calc. Temp. (C) : 400
Date : 17-11-1989 Calc. Time (hr) : 10

Conditions	Period	Gas Product g/g cat/hr	Liquid Product g/g cat/hr	WHSV g/g cat/hr	Total Conversion %	Propene Conversion %	Cumulative Liquid product g/g cat/hr
200 deg.C	1	11.15	0.41	11.57	3.56	4.06	0.41
Ramp	1	11.11	0.55	11.66	4.68	5.34	0.96
250 deg.C	1	11.32	1.33	12.64	10.49	11.96	2.28
Ramp	1	9.85	1.16	11.01	10.56	12.04	3.45
300 deg.C	1	9.96	2.10	12.06	17.38	19.82	5.54
Ramp	1	10.62	1.50	12.12	12.39	14.13	7.04
350 deg.C	1	11.37	1.10	12.47	8.81	10.04	8.14
350 deg.C	1	10.56	0.34	10.90	3.08	3.52	8.48

Catalyst : MN-2AW (M40) Calc. Temp. (C) : 400
Date : 20-02-1991 Calc. Time (hr) : 10

Conditions	Period	Gas Product g/g cat/hr	Liquid Product g/g cat/hr	WHSV g/g cat/hr	Total Conversion %	Propene Conversion %	Cumulative Liquid product g/g cat/hr
200 deg.C	1	12.19	0.00	12.19	0.00	0.00	0.00
Ramp	1	13.37	0.00	13.37	0.00	0.00	0.00
250 deg.C	1	12.33	0.00	12.33	0.00	0.00	0.00
Ramp	1	11.93	0.00	11.93	0.00	0.00	0.00
300 deg.C	1	12.34	0.00	12.34	0.00	0.00	0.00
Ramp	1	12.43	0.00	12.43	0.00	0.00	0.00
350 deg.C	1	11.96	0.00	11.96	0.00	0.00	0.00
350 deg.C	1	11.96	0.10	12.06	0.83	0.95	0.10

Catalyst : MN-2AR (M41) Calc. Temp. (C) : 400
Date : 21-02-1991 Calc. Time (hr) : 10

Conditions	Period	Gas Product g/g cat/hr	Liquid Product g/g cat/hr	WHSV g/g cat/hr	Total Conversion %	Propene Conversion %	Cumulative Liquid product g/g cat/hr
200 deg.C	1	11.66	0.00	11.66	0.00	0.00	0.00
Ramp	1	12.13	0.00	12.13	0.00	0.00	0.00
250 deg.C	1	11.80	0.00	11.80	0.00	0.00	0.00
Ramp	1	11.75	0.00	11.75	0.00	0.00	0.00
300 deg.C	1	12.34	0.00	12.34	0.00	0.00	0.00
Ramp	1	12.07	0.00	12.07	0.00	0.00	0.00
350 deg.C	1	11.23	0.09	11.32	0.80	0.91	0.09
350 deg.C	1	12.70	0.08	12.78	0.63	0.71	0.17

Catalyst : MN-4AR (M42) Calc. Temp. (C) : 400
Date : 22-02-1991 Calc. Time (hr) : 9

Conditions	Period	Gas Product g/g cat/hr	Liquid Product g/g cat/hr	WHSV g/g cat/hr	Total Conversion %	Propene Conversion %	Cumulative Liquid product g/g cat/hr
200 deg.C	1	11.66	0.00	11.66	0.00	0.00	0.00
Ramp	1	11.43	0.22	11.65	1.89	2.15	0.22
250 deg.C	1	12.69	0.31	13.00	2.38	2.72	0.53
Ramp	1	10.86	0.19	11.05	1.72	1.96	0.72
300 deg.C	1	11.98	0.18	12.16	1.48	1.69	0.90
Ramp	1	12.07	0.17	12.24	1.39	1.58	1.07
350 deg.C	1	10.67	0.49	11.16	4.39	5.01	1.56
350 deg.C	1	12.15	0.33	12.48	2.64	3.02	1.89

Catalyst : ZM510 (M46) Calc. Temp. (C) : 400
Date : 29-03-1991 Calc. Time (hr) : 8

Conditions	Period	Gas Product g/g cat/hr	Liguid Product g/g cat/hr	WHSV g/g cat/hr	Total Conversion %	Propene Conversion %	Cumulative Liquid product g/g cat/hr
200 deg.C	1	10.00	0.56	10.56	5.30	6.05	0.56
Ramp	1	11.51	0.63	12.14	5.19	5.92	1.19
250 deg.C	1	10.74	0.84	11.58	7.25	8.27	2.03
Ramp	1	10.69	0.94	11.63	8.08	9.22	2.97
300 deg.C	1	9.30	1.73	11.03	15.68	17.88	4.70
Ramp	1	9.53	2.10	11.63	18.06	20.59	6.80
350 deg.C	1	8.33	3.79	12.12	31.27	35.66	10.59
350 deg.C	1	9.47	2.81	12.28	22.88	26.09	13.40

Catalyst : ZM760 (M45) Calc. Temp. (C) : 400
Date : 25-03-1991 Calc. Time (hr) : 8

Conditions	Period	Gas Product g/g cat/hr	Liguid Product g/g cat/hr	WHSV g/g cat/hr	Total Conversion %	Propene Conversion %	Cumulative Liquid product g/g cat/hr
200 deg.C	1	12.05	0.64	12.69	5.04	5.75	0.64
Ramp	1	11.11	0.62	11.73	5.29	6.03	1.26
250 deg.C	1	10.73	1.51	12.24	12.34	14.07	2.77
Ramp	1	10.74	1.83	12.57	14.56	16.60	4.60
300 deg.C	1	9.09	2.58	11.67	22.11	25.21	7.18
Ramp	1	9.16	2.71	11.87	22.83	26.03	9.89
350 deg.C	1	9.07	3.30	12.37	26.68	30.42	13.19
350 deg.C	1	10.00	2.57	12.57	20.45	23.31	15.76

Catalyst : ZM980 (M47) Calc. Temp. (C) : 400
Date : 01-04-1991 Calc. Time (hr) : 8.5

Conditions	Period	Gas Product g/g cat/hr	Liquid Product g/g cat/hr	WHSV g/g cat/hr	Total Conversion %	Propene Conversion %	Cumulative Liquid product g/g cat/hr
200 deg.C	1	12.19	1.00	13.19	7.58	8.64	1.00
Ramp	1	11.20	1.33	12.53	10.61	12.10	2.33
250 deg.C	1	9.95	1.58	11.53	13.70	15.63	3.91
Ramp	1	10.38	1.37	11.75	11.66	13.29	5.28
300 deg.C	1	10.42	2.07	12.49	16.57	18.90	7.35
Ramp	1	8.88	2.30	11.18	20.57	23.46	9.65
350 deg.C	1	8.00	4.02	12.02	33.44	38.13	13.67
350 deg.C	1	8.33	4.11	12.44	33.04	37.67	17.78

Catalyst : M1-H (M11) Calc. Temp. (C) : 400
Date : 22-11-1991 Calc. Time (hr) : 10

Conditions	Period	Gas Product g/g cat/hr	Liquid Product g/g cat/hr	WHSV g/g cat/hr	Total Conversion %	Propene Conversion %	Cumulative Liquid product g/g cat/hr
200 deg.C	1	9.36	0.38	9.74	3.86	4.40	0.38
Ramp	1	11.62	0.84	12.46	6.74	7.69	1.22
250 deg.C	1	10.29	1.50	11.79	12.72	14.51	2.72
Ramp	1	9.57	1.47	11.04	13.32	15.18	4.19
300 deg.C	1	9.36	2.52	11.88	21.21	24.19	6.71
Ramp	1	9.15	2.24	11.39	19.67	22.42	8.95
350 deg.C	1	10.95	2.25	13.20	17.05	19.44	11.20
350 deg.C	1	11.39	0.91	12.30	7.39	8.43	12.11

Catalyst : M1-2AW (M16) Calc. Temp. (C) : 400
Date : 30-03-1991 Calc. Time (hr) : 8

Conditions	Period	Gas Product g/g cat/hr	Liquid Product g/g cat/hr	WHSV g/g cat/hr	Total Conversion %	Propene Conversion %	Cumulative Liquid product g/g cat/hr
200 deg.C	1	11.67	0.48	12.15	3.95	4.51	0.48
Ramp	1	12.32	0.34	12.67	2.72	3.10	0.82
250 deg.C	1	10.95	0.88	11.83	7.40	8.44	1.70
Ramp	1	10.95	0.77	11.72	6.55	7.47	2.47
300 deg.C	1	10.43	1.72	12.14	14.12	16.11	4.18
Ramp	1	9.88	1.95	11.83	16.48	18.79	6.13
350 deg.C	1	8.89	3.19	12.07	26.38	30.08	9.32
350 deg.C	1	9.86	2.31	12.17	19.00	21.67	11.63

Catalyst : M1-2AR (M17) Calc. Temp. (C) : 400
Date : 30-04-1990 Calc. Time (hr) : 11.3

Conditions	Period	Gas Product g/g cat/hr	Liquid Product g/g cat/hr	WHSV g/g cat/hr	Total Conversion %	Propene Conversion %	Cumulative Liquid product g/g cat/hr
200 deg.C	1	10.69	1.57	12.25	12.77	14.56	1.57
Ramp	1	10.94	1.49	12.43	11.98	13.66	3.05
250 deg.C	1	10.83	3.10	13.93	22.24	25.36	6.15
Ramp	1	8.72	3.34	12.05	27.68	31.57	9.49
300 deg.C	1	8.96	6.22	15.17	40.97	46.72	15.71
Ramp	1	5.01	7.97	12.98	61.39	70.00	23.67
350 deg.C	1	4.30	9.42	13.73	68.65	78.27	33.10
350 deg.C	1	5.22	7.25	12.47	58.15	66.31	40.35

Catalyst : M1-2AR(NH3)(M18) Calc. Temp. (C) : 400
Date : 05-04-1991 Calc. Time (hr) : 12

Conditions	Period	Gas Product g/g cat/hr	Liquid Product g/g cat/hr	WHSV g/g cat/hr	Total Conversion %	Propene Conversion %	Cumulative Liquid product g/g cat/hr
200 deg.C	1	10.36	1.48	11.84	12.50	14.25	1.48
Ramp	1	11.24	1.62	12.86	12.60	14.36	3.10
250 deg.C	1	9.54	2.99	12.53	23.86	27.21	6.09
Ramp	1	9.05	3.33	12.38	26.90	30.67	9.42
300 deg.C	1	6.47	5.73	12.20	46.97	53.55	15.15
Ramp	1	5.22	8.00	13.22	60.51	69.00	23.15
350 deg.C	1	4.13	9.22	13.35	69.06	78.75	32.37
350 deg.C	1	5.33	7.18	12.51	57.39	65.44	39.55

Catalyst : M1-4AR (M48) Calc. Temp. (C) : 400
Date : 06-04-1991 Calc. Time (hr) : 8

Conditions	Period	Gas Product g/g cat/hr	Liquid Product g/g cat/hr	WHSV g/g cat/hr	Total Conversion %	Propene Conversion %	Cumulative Liquid product g/g cat/hr
200 deg.C	1	10.02	1.45	11.47	12.63	14.40	1.45
Ramp	1	11.02	1.74	12.76	13.65	15.56	3.19
250 deg.C	1	6.74	2.48	11.22	22.12	25.22	5.67
Ramp	1	7.97	2.71	10.67	25.36	28.92	8.38
300 deg.C	1	6.22	4.98	11.21	44.46	50.70	13.36
Ramp	1	5.33	6.14	11.47	53.53	61.04	19.50
350 deg.C	1	5.40	6.45	11.84	54.44	62.07	25.95
350 deg.C	1	6.02	5.09	11.10	45.81	52.23	31.03

Catalyst : M1-4AR(NH3)(M43) Calc. Temp. (C) : 400
Date : 27-02-1991 Calc. Time (hr) : 16

Conditions	Period	Gas Product g/g cat/hr	Liquid Product g/g cat/hr	WHSV g/g cat/hr	Total Conversion %	Propene Conversion %	Cumulative Liquid product g/g cat/hr
200 deg.C	1	11.58	1.50	13.08	11.46	13.07	1.50
Ramp	1	10.86	1.44	12.31	11.74	13.38	2.94
250 deg.C	1	9.43	2.53	11.96	21.14	24.10	5.47
Ramp	1	10.17	2.76	12.93	21.37	24.37	8.24
300 deg.C	1	6.36	4.49	10.85	41.36	47.16	12.72
Ramp	1	7.08	6.86	13.94	49.20	56.10	19.58
350 deg.C	1	4.96	6.60	11.56	57.09	65.10	26.18
350 deg.C	1	5.94	6.03	11.97	50.35	57.41	32.21

Catalyst : M2-H (M50) Calc. Temp. (C) : 400
Date : 26-07-1991 Calc. Time (hr) : 18

Conditions	Period	Gas Product g/g cat/hr	Liquid Product g/g cat/hr	WHSV g/g cat/hr	Total Conversion %	Propene Conversion %	Cumulative Liquid product g/g cat/hr
200 deg.C	1	9.16	0.75	9.91	7.52	8.58	0.75
Ramp	1	14.73	0.87	15.60	5.59	6.38	1.62
250 deg.C	1	11.65	0.84	12.49	6.70	7.63	2.45
Ramp	1	11.98	0.40	12.38	3.23	3.68	2.85
300 deg.C	1	11.15	0.69	11.84	5.84	6.66	3.55
Ramp	1	11.24	0.82	12.05	6.79	7.74	4.36
350 deg.C	1	11.65	2.27	13.93	16.32	18.61	6.64
350 deg.C	1	9.60	2.04	11.64	17.50	19.95	8.67

Catalyst : M2-2AW (M52) Calc. Temp. (C) : 400
Date : 01-08-1991 Calc. Time (hr) : 13

Conditions	Period	Gas Product g/g cat/hr	Liquid Product g/g cat/hr	WHSV g/g cat/hr	Total Conversion %	Propene Conversion %	Cumulative Liquid product g/g cat/hr
200 deg.C	1	20.13	0.00	20.13	0.00	0.00	0.00
Ramp	1	8.10	0.00	8.10	0.00	0.00	0.00
250 deg.C	1	8.85	0.32	9.17	3.45	3.94	0.32
Ramp	1	10.63	0.68	11.32	6.04	6.89	1.00
300 deg.C	1	8.37	1.58	9.95	15.91	18.14	2.58
Ramp	1	10.92	2.08	13.00	16.03	18.27	4.67
350 deg.C	1	9.43	3.80	13.23	28.72	32.74	8.47
350 deg.C	1	8.80	3.77	12.57	29.97	34.18	12.23

Catalyst : M2-2AR (M44) Calc. Temp. (C) : 400
Date : 23-03-1991 Calc. Time (hr) : 14

Conditions	Period	Gas Product g/g cat/hr	Liquid Product g/g cat/hr	WHSV g/g cat/hr	Total Conversion %	Propene Conversion %	Cumulative Liquid product g/g cat/hr
200 deg.C	1	12.40	0.00	12.40	0.00	0.00	0.00
Ramp	1	12.53	0.00	12.53	0.00	0.00	0.00
250 deg.C	1	11.10	0.00	11.10	0.00	0.00	0.00
Ramp	1	13.02	0.00	13.02	0.00	0.00	0.00
300 deg.C	1	11.45	0.00	11.45	0.00	0.00	0.00
Ramp	1	12.08	0.00	12.08	0.00	0.00	0.00
350 deg.C	1	11.80	0.33	12.13	2.72	3.10	0.33
350 deg.C	1	12.03	0.20	12.23	1.64	1.86	0.53

Catalyst : M2-4AR (M54) Calc. Temp. (C) : 400
Date : 08-08-1991 Calc. Time (hr) : 12

Conditions	Period	Gas Product g/g cat/hr	Liquid Product g/g cat/hr	WHSV g/g cat/hr	Total Conversion %	Propene Conversion %	Cumulative Liquid product g/g cat/hr
200 deg.C	1	11.72	0.56	12.28	4.60	5.24	0.56
Ramp	1	11.22	1.01	12.24	8.27	9.43	1.58
250 deg.C	1	9.69	1.67	11.36	14.70	16.76	3.25
Ramp	1	10.91	1.40	12.31	11.38	12.97	4.65
300 deg.C	1	8.76	2.35	11.12	21.16	24.13	7.00
Ramp	1	8.31	3.67	11.98	30.65	34.95	10.67
350 deg.C	1	9.75	3.20	12.95	24.70	28.17	13.87
350 deg.C	1	10.42	2.44	12.86	18.94	21.59	16.31

Catalyst : ZM760 (M20) Calc. Temp. (C) : 400
Date : 21-05-1990 Calc. Time (hr) : 11

Conditions	Period	Gas Product g/g cat/hr	Liquid Product g/g cat/hr	WHSV g/g cat/hr	Total Conversion %	Propene Conversion %	Cumulative Liquid product g/g cat/hr
250 deg.C	1	11.54	1.32	12.86	10.23	11.66	1.32
250 deg.C	1	11.29	1.06	12.35	8.59	9.80	2.38
250 deg.C	1	11.47	0.97	12.44	7.81	8.91	3.35
250 deg.C	1	11.82	0.90	12.72	7.10	8.09	4.25
250 deg.C	2	11.11	0.75	11.86	6.32	7.21	5.75
250 deg.C	1	11.99	0.73	12.72	5.74	6.54	6.48
250 deg.C	1	12.35	0.64	12.99	4.93	5.62	7.12

Catalyst : M1-2AR(NH3)(M19) Calc. Temp. (C) : 400
Date : 19-05-1990 Calc. Time (hr) : 12

Conditions	Period	Gas Product g/g cat/hr	Liquid Product g/g cat/hr	WHSV g/g cat/hr	Total Conversion %	Propene Conversion %	Cumulative Liquid product g/g cat/hr
250 deg.C	1	8.07	3.61	11.68	30.91	35.25	3.61
250 deg.C	1	10.07	3.24	13.31	24.33	27.74	6.85
250 deg.C	1	10.33	2.37	12.70	18.69	21.31	9.22
250 deg.C	1	10.14	1.90	12.04	15.78	18.00	11.12
250 deg.C	1	10.30	1.62	11.92	13.62	15.53	12.75
250 deg.C	1	10.65	1.42	12.07	11.77	13.42	14.17
250 deg.C	1	10.81	1.32	12.12	10.85	12.37	15.48
250 deg.C	1	11.18	1.15	12.33	9.33	10.64	16.63

APPENDIX VII : Calculation of number of Al^{VI} per mordenite channel

The number of aluminium atoms per channel ($Al^{VI}_{channel}$) may be calculated using the number of extra-framework aluminium atoms per unit cell (Al^{VI}_{uc}), the average length of a unit cell (L_{uc}) and the average length of a channel running through the crystallite ($L_{crystallite}$) :

$$Al^{VI}/_{channel} = Al^{VI}/_{uc} \times L_{crystallite} / L_{uc}$$

$L_{crystallite}$ = 2E-6 m
L_{uc} = 7.48E-10 m
$Al^{VI}/_{uc} = Al^{tot}/_{uc}$ x %Al in octahedral coordination

For the M2-H sample, the %Al in octahedral coordination calculated from the peak areas of the ^{27}Al MAS NMR spectrum below is 12.1%.

$$Al^{VI}/_{channel} = 0.121 \times Al^{VI}/_{uc} \times 2E\text{-}6 / 7.48E\text{-}10$$
$$Al^{VI}/_{channel} = 323.53\ Al^{VI}/_{uc}$$

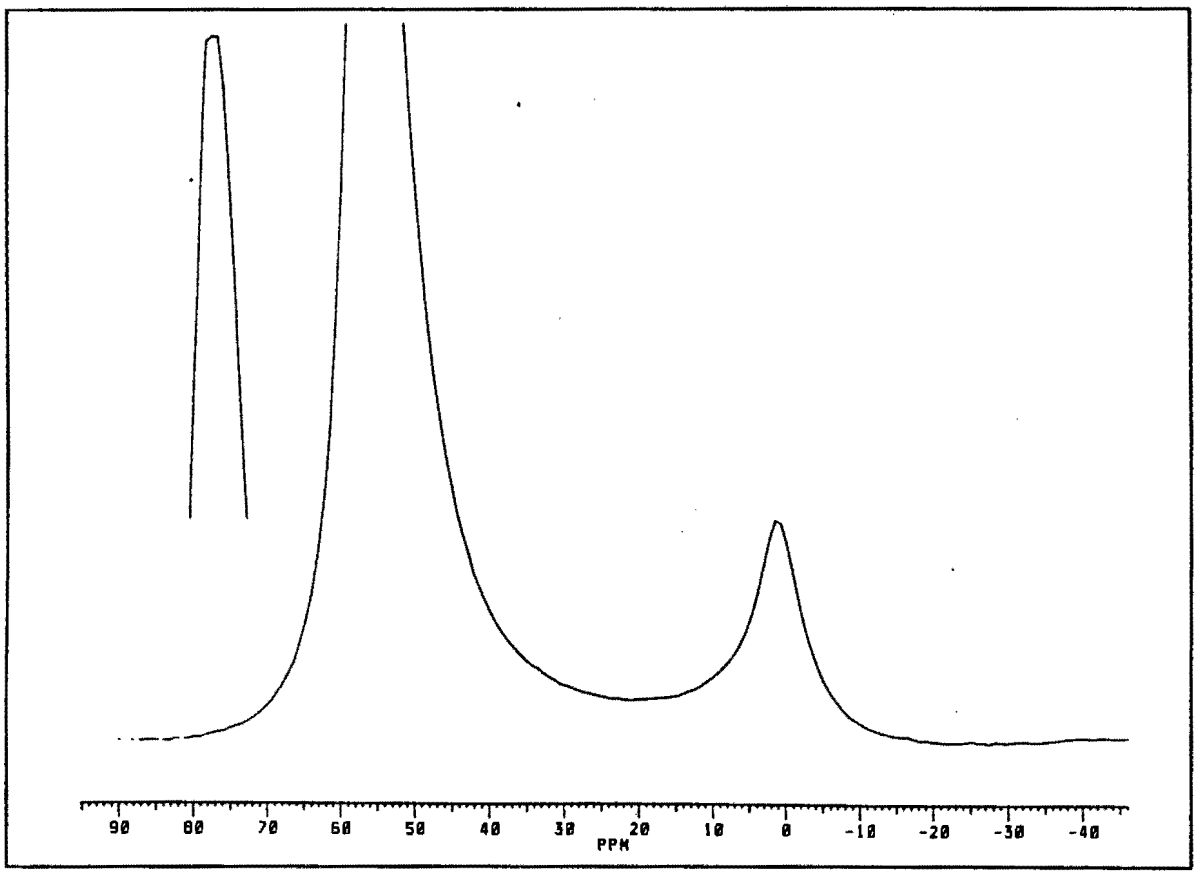

From the last equation, it can be seen that in order to calculate an average $Al^{VI}/_{channel}$, it is necessary to calculate the overall extraframework aluminium content per unit cell ($Al^{VI}/_{uc}$). For this calculation it is assumed that silicon is not removed from the framework during dealumination thereby fixing the number of silicon atoms per unit cell. For the M2-H catalyst the overall catalyst aluminium content (mass basis) is 6.70% (see Table 3.2), all of which is assumed to be in the framework after synthesis, enabling calculation of the Si content (MW_z denotes the molecular mass of the element "z") :

$$6.70/100 = \text{Mass of Al per unit cell / Total mass of unit cell}$$
$$= Al^{tot}/_{uc}\, MW_{Al} / (Al^{tot}/_{uc}\, MW_{Al} + Si^{tot}/_{uc}\, MW_{Si} + O^{tot}/_{uc}\, MW_O + H^{tot}/_{uc}\, MW_H)$$

For an ideal mordenite structure :

$H^{tot}/_{uc} = Al^{tot}/_{uc}$ (H charge balances Al)

$O^{tot}/_{uc} = 2\,(Al^{tot}/_{uc} + Si^{tot}/_{uc})$ (2 oxygen atoms per T atom)

Simplifying and using the above relationships and the appropriate molecular masses :

$$0.067 = 27\, Al^{tot}/_{uc} / (28\, Al^{tot}/_{uc} + 28\, Si^{tot}/_{uc} + 16\, O^{tot}/_{uc})$$

For the unmodified catalyst :

$Si^{tot}/_{uc} = 48 - Al^{tot}/_{uc}$ (48 T atoms per unit cell)

$O^{tot}/_{uc} = 48 \times 2 = 96$

$$0.067 = 27\, Al^{tot}/_{uc} / (28\, Al^{tot}/_{uc} + 1344 - 28\, Al^{tot}/_{uc} + 1536)$$
$$= 27\, Al^{tot}/_{uc} / 2880$$

Simplifying : $Al^{tot}/_{uc} = 7.15$

Now, the number of extra-framework aluminium atoms per channel may be calculated :

$$Al^{VI}/_{channel} = 323.53\, Al^{VI}/_{uc} = 2313$$

REFERENCES

REFERENCES

Alberty, R.A., *Chem.Eng.Sci.*, **42** No 10, 2325 (1987).

Andersen, B., PhD Thesis, University of Cape Town, 1991.

Anderson, J.R, Chang, Y.-F. and Western, R.J., *J.Catal.*, **124**, 259 (1990).

Appleby, W.G., Gibson, J.W. and Good, G.M., *I&EC Proc.Des.Dev.*, **1**, 102 (1962).

Avidan, A.A., *in* "Methane Conversion" (D.M. Bibby, C.D. Chang, R.F. Howe and S. Yurchak, Eds.), p.307. Elsevier, Amsterdam, 1988.

Bajpai, P.K., Rao, M.S. and Gokhale, K.V.G.K., *in* "Thermal analysis, International conference proceedings", **1**, 558 (1982).

Bandiera, J., Hamon, C. and Naccache, C., *in* "Proceedings of the 6th International Zeolite Conference" (D. Olson and A. Bisio, Eds.), p. 337. Butterworths, London, 1984.

Barrer, R.M., *in* "Hydrothermal chemistry of zeolites", p.2. Academic Press, Londen, 1982.

Barrer, R.M., *Brit.Chem.Eng.*, **4**, 267 (1959).

Barrer, R.M. and Ibbitson, D.A., *Trans.Faraday Soc.*, **32**, 947 (1944).

Barrer, R.M., *in* "Zeolites and Clay Minerals as sorbents and molecular sieves", p.358. Academic Press, London, 1978.

Barrer, R.M. and Peterson, D.L., *Proc.Roy.Soc.London,* **280A**, 468 (1964).

Barrer, R.M. and Sutherland, J.W., *Proc.Roy.Soc.Londen*, **137A**, 439 (1956).

Bennet, J.M. and Marcus, B.K., *in* "Innovation in zeolite materials science" (P.J. Grobet, W.J. Mortier, E.F. Vansant and G. Schulz-Ekloff, Eds.), p.269. Elsevier, Amsterdam, 1988.

Beyer, H.K. and Belenykaja, I., *in* "Catalysis by zeolites" (B.Imelik, C.Naccache, Y.Ben Taarit, J.C.Vedrine, G.Coudurier and H.Praliaud, Eds.), p.303. Elsevier, Amsterdam, 1980.

Beyer, H.K., Belenykaja, I.M., Mishin, I.V. and Borbely, G., *in* "Proceedings of the Conference on the Structure and Reactivity of Modified Zeolites" (P.A. Jacobs, N. Jaeger, P. Jiru, G. Schulzekloff and V.B. Kazansky, Eds.), p.133. Elsevier Scientific Publishing Company, Amsterdam, 1984.

Beyerlein, R.A., McVicker, G.B., Yacallo, L.N. and Ziemiak, J.J., *J.Phys.Chem.*, **92**, 1967 (1988).

Bhavikatti, S.S. and Patwardhan, S.R., *Ind.Eng.Chem.Prod.Res.Dev.*, **20**, 102 (1981).

Bibby, D.M., Milestone, N.B., Patterson, J.E., Aldridge, L.P., *J.Catal.*, **97**, 493 (1986).

Breck, D.W., *in* "Zeolite Molecular Sieves", p.418. Wiley, New York, 1974.

Breck, D.W., *in* "Zeolite Molecular Sieves", p.2. Wiley, New York, 1984.

Bremer, H., Reschetilowski, W., Ahmed, A.S., Wendlant, K.P., Nau, P.E. and Mishin, I.V., *Z.Chem.*, **23**, 381 (1983).

Brunner, E., Ernst, H., Freude, D., Hunger, M., Krause, C.B.,Prager, D., Reschetilowski, W., Schweiger, W. and Bergk, K.-H., *Zeolites*, **9**, 282 (1989).

Chang, C.D., Lang, W.H. and Smith, R.L., *J.Catal.*, **56** (1979).

Chang, C.D., Chu, C.T.W. and Socha, R.F., *J.Catal.*, **86**, 289 (1984).

Chang, C.D. and Silvestri, A.J., *J.Catal.*, **47**, 249 (1977).

Chang, C.D. and Silvestri, A.J., *Chemtech* (1987).

Chang, C.D., Hellring, S.D. and Pearson, J.A., *J.Catal.*, **115**, 282 (1989).

Chen, N.Y., *J.Phys.Chem.*, **80**, 60 (1976).

Chen, N.Y. and Garwood, W.E., *Catal.Rev., Sci.Eng.*, **28**, 185 (1986).

Chen, N.Y. and Reagan, W.J., *J.Catal.*, **59** , (1979).

Chen, N.Y., Garwood, W.E., and Dwyer, F.G., *in* "Shape selective catalysis in industrial applications", p.56. Marcel Dekker Inc., New York, 1988.

Chen, N.Y., Lucki, S.J. and Mower, E.B., *J.Catal.*, **13**, 329 (1969).

Chon, H. and Park, D.H., *J.Catal.*, **114** (1988).

Chu, C.T.W. and Chang, C.D., *J.Catal.*, **86**, 297 (1984).

Clarke, J.K.A., Darcy, R., Hegarty, B.F., O'Donoghue, E., Ebrahimi, V.A. and Rooney, J.J., *J.Chem.Soc., Chem.Comm.*, 425 (1986).

Coudurier, G., Naccache, C. and Vedrine, J.C., *J.Chem.Soc., Chem.Comm.*, **24**, 1413 (1982).

Coudurier, G. and Vedrine, J.C., *Pure & Appl.Chem.*, **58**, 1389 (1986).

Dass D.V., Martin W.R. and Odell A.L., *J.Catal.*, **106**, 153 (1987).

Davis, R., *Min.Mag.*, **31**, 887 (1958).

Davis, M.E., Saldattiage, C., Montes, C., Graces, J. and Crowder, C., *Nature*, **331**, 698 (1988).

De Armando, M., Gnep, N. and Guisnet, M., *J.Chem.Res.*, **1**, 8 (1981).

Deffeyes, K.S., *in* "Molecular sieves", p.7. Soc.Chem.Ind., Londen, 1968.

Dejaifve, P., Vedrine, J.C., Bolis, V. and Derouane, E.G., *J.Catal.*, **63**, 331 (1980).

Dejaifve, P., Auroux, A., Gravelle, P.C., Vedrine, J.C., *J.Catal.*, **70**, 123 (1981).

Dessau, R.M., *J.Catal.*, **99**, 111 (1986).

Dessau, R.M. *J.Catal.*, **103**, 526 (1987).

Dry, M.E., *Catalysis Today*, **6**, 183 (1990).

Ducarme, V. and Vedrine, J.C., *Appl.Catal.*, 175 (1985).

Durgakumari, V., Narayanan, S. and Guczi, L., *Catal.Lett.*, **5**, 377 (1990).

Dunken, H. and Stephanowitz, R., *Z.Chem.*, **23**, 353 (1983).

Eberly, P.E, *J.Phys.Chem.*, **67**, 2404 (1963).

Eberly, P.E. and Kimberlin, C.N., *Ind.Eng.Chem.Prod.Res.Dev.*, **9**, 335 (1970).

Eisenbach, D., Gallei, E., *J.Catal.*, **56**, 377 (1979).

Fejes, P., Hannus, I. and Kiricsi, I., *Zeolites*, **4**, 73 (1984).

Fejes, P., Hannus, I., Kiricsi, I., Pfeifer, H., Freude, D. and Oehme, W., *Zeolites*, **5**, 45 (1985).

Fejes, P., Kiricsi, I., Hannus, I., Schobel, Gy, *in* "Catalysis on zeolites" (D. Kallo and Kh.M. Minachev, Eds.), p.205. Akademiai Kiado, Budapest, 1988.

Fejes, P., Kiricsi, I., Tasi, Gy., Hannus, I., Bertoti, I. and Szekely, T., *Zeolites*, **9**, 392 (1988).

Fernandez, C., Lefebvre, F., Nagy, J.B. and Derouane, E.G, *in* "Innovation in zeolite materials science" (P.J. Grobet et al., Eds.), p.223. Elsevier, Amsterdam, 1988.

Flanigen, E.M., *in* "Zeolite Chemistry and Catalysis" (J.A.Rabo, Ed.), ACS Monograph Ser., **171**, Ch. 2. Am.Chem.Soc., Washington DC, 1976.

Flanigen, E.M., *in* "Introduction to zeolite science and practice" (H. van Bekkum, E.M. Flanigen and J.C.Jansen, Eds.), p.13. Elsevier, Amsterdam, 1991.

Flanigen, E.M., Patton, R.L. and Wilson, S.T., *in* "Innovation in zeolite materials science" (P.J. Grobet, W.J. Mortier, E.F. Vansant and G. Schulz-Ekloff, Eds.), p.13. Elsevier, Amsterdam, 1988.

Flanigen, E.M., Lok, B.M., Patton, R.L. and Wilson, S.T., *in* "New developments in zeolite science and technology" (Y. Murakami, A. Iijima and J.W. Ward, Eds.),p.103. Elsevier, New York, 1986.

Froment G.F., *in* "Progress in catalyst deactivation", (Ed. J.L. Figriredo), NATO Advanced Study Institutes Series - E54, Vyhoff The Hague (1982).

Gaffney, T., Pierantozzi, R. and Seger, M., *in* "Zeolite synthesis", (M.L.Ocelli and H.E.Robson, Eds.), ACS Symp.Ser., **398**, p.374. Am.Chem.Soc., Washington DC, 1989.

Gallezot, P., Lequercq, C., Guisnet, M., Magnoux, P., *J.Catal.*, **114**, 100 (1988).

Ghosh, A.K. and Curthoys, G., *J.Chem.Soc., Faraday Trans. 1*, **79**, 805 (1983).

Ghosh, A.K. and Curthoys, G., *J.Catal.*, **86**, 454 (1984).

Gianneti, J.P. and Perrotta, A.J., *Ind.Eng.Chem., Process Des.Develop.*, **14**, 86 (1975).

Giordano, W., Vitarelli, P., Cavallaro, S., Otanna, R. and Lembo, R., *in* "Proceedings of the 6th International Zeolite Conference" (D.Olson and A.Bisio, Eds.), p. 331, Butterworths, London, 1984.

Goovaerts, F., Vansant, E.F., Pilippaerts, J., De Hulsters, P. and Gelan, J., *J.Chem.Soc., Faraday Trans.I*, **85**, 3675 (1989).

Goepper, M., Guth, F., Delmotte, L., Guth, J.L. and Kessler, H., *in* "Zeolite: Facts, Figures and Future", Proceedings of the 8th International Conference on Zeolites (P.A. Jacobs and R.van Santen, Eds.), p.857. Elsevier, Amsterdam, 1989.

Guisnet, M. and Magnoux, P., *Appl.Catal.*, **54**, 1 (1989).

Ha, B., Guidot, J. and Barthomeuf, D., *J.Chem.Soc., Faraday Trans.I*, **75**, 1245 (1979).

Haas, J., Fetting, F. and Gubicza, L., *Acta Phys.Chem.*, **31**, 659 (1985)

Hamon, C. Personal communication, Siege Social 154, Rue de L'Universite, Paris, 1991.

Herrmann, C., Haas, J. and Fetting, F., *Appl.Catal.*, **35**, 299 (1987).

Hibino, T., Niwa, M. and Murakami, Y., *J.Catal.*, **128**, 551 (1991).

Hidalgo, C.V., Itoh, H., Hattori, T., Niwa, M. and Murakami, Y., *J.Catal.*, **85**, 362 (1984).

Hocevar, S., Rajic, N., Zagar, T. and Levec, J., *in* "Synthesis and properties of new catalysts: Utilization of novel materials, components and synthetic techniques" (E.W. Corcoran and M.J. Ledoux, Eds.), p.29. Materials Reaearch Society, Boston, 1990.

Holderich, W.F. and van Bekkum, H., *in* "Introduction to zeolite science and practice" (H. van Bekkum, E.M. Flanigen and J.C.Jansen, Eds.), p.631. Elsevier, Amsterdam, 1991.

Hunter, R., Hutchings, G.J. and Pickl, W., *J.Chem.Soc., Chem.Comm.*, 1369 (1987).

Hutchings, G.J., Hall, M.V.M. and Hunter, R., *J.Catal.*, **101**, 224 (1986).

Hutchings, G.J. and Hunter, R., *Catal.Today*, **6**, 279 (1990).

Inaoka, W., Kasahara, S., Fukushima, T. and Igawa, K., *in* "Chemistry of microporous crystals", p.37. Kodansha Ltd, Tokyo, 1991.

Inui, T., Matsuda, H., Okaniwa, H. and Miyamoto, A., *Appl.Catal.*, **58**, 155 (1990a).

Inui, T., Phatnasari, S. and Matsuda, H., *J.Chem.Soc., Chem.Commun.*, 206 (1990b).

Inui, T., European Patent 0 418 142 A1 (1990).

Inui, T., *in* "Structure-activity and selectivity relationships in heterogeneous catalysis" (R.K. Grasselli and A.W. Sleight, Editors), p.233. Elsevier, Amsterdam, (1991).

Itabashi, K., Fukushima, T. and Igawa, K., *Zeolites*, **6**, 30 (1986).

Itoh, H., Hattori, T. and Murakami, Y., *Appl.Catal.*, **2**, 19 (1982).

Jacobs, P.A., *in* "Carboniogenic activity of zeolites", p.52. Elsevier, Amsterdam, 1977.

Kaeding, W.E. and Butter, S.A., *J.Catal.*, **61**, 153 (1980).

Kaiser, S.W., *Arab.J.Sci.Eng.*, 361 (1985).

Kanazirev, V., Tsoncheva, T. and Minchev, Chr., *Z.Phys.Chem.Neue Folge*, **149**, 237 (1986).

Karge, H.G., *in* "Introduction to zeolite science and practice" (H. van Bekkum, E.M. Flanigen and J.C.Jansen, Eds.), p.531. Elsevier, Amsterdam, 1991.

Karge, H.G. and Dondur, V., *J.Phys.Chem.*, **94**, 765 (1990).

Karge, H.G., Boldingh, E.P., *Catalysis Today*, **3**, 379 (1988).

Karge, H.G. and Weitkamp, J, Chem.Ing.Tech., **58**, 946 (1986).

Karge, H.G., Boldingh, E.P., Lange, J.-P., and Gutsze, A., *Acya Phys.Chem.*, **31**, 369 (1985).

Karge, H.G., Wada, Y., Weitkamp, J., Ernst, S., Girrbach, U. and Beyer, H.K., in "Catalysis on the Energy Scene" (S.Kaliaguine and A.Mahay, Eds.), p. 101, Elsevier, Amsterdam, 1984.

Karge, H.G., Laniecki, M., Ziolek, M., Onyestyak, G., Kiss, A., Kleinschmit, P. and Siray, M., *in* "Zeolite: Facts, Figures and Future", Proceedings of the 8th International Conference on Zeolites (P.A. Jacobs and R.van Santen, Eds.), p.1327. Elsevier, Amsterdam, 1989.

Keogh, A.H. and Sand, L.B, *J.Am.Chem.Soc.*, **83**, 3536 (1961).

Kerr, G.T., *J.Phys.Chem.*, 73 (1969) 2780

Kiovsky, J.R., Goyette, W.J. and Notermann, T.M., *J.Catal.*, **52**, 25 (1978).

Kokatailo, G.T., Personal communication, University of Cape Town, 1989.

Koradia, P.B., Kiovsky, J.R. and Asim, M.Y., J.Catal., **66**, 290 (1980).

Kranich, W.L., Ma, H.Y., Sand, L.B., Weiss, A.H. and Zwiebel, I., *Adv,Chem.Ser.* **101**, 502 (1971).

Lago, R.M., Haag, W.O., Mokovsky, R.J., Olson, D.H., Hellring, S.D., Schmitt, K.D. and Kerr, G.T., *in* "Proceedings of the 7th International Zeolite Conference" (Y. Murakami, A. Lijima and J.P. Ward, Eds.), p.677. Elsevier, Amsterdam, (1986).

Langner, B., *App.Catal.*, **2**, 289 (1982).

Liang, J., Li, H., Zhao, S., Guo, W., Wang, R. and Ling, M., *Appl.Catal*, **64**, 31 (1990).

Lin, D.H., Ducarme, V., Coudurier, G. and Vedrine, J.C., *in* "Zeolites as catalysts, sorbents and detergent builders" (H.G. Karge and J. Weitkamp, Eds.), p.615. Elsevier, Amsterdam, 1989.

Lok, B.M., Messina, C.A., Patton, R.L., Gajek, R.T., Cannan, T.R. and Flanigen, E.M., US Patent 4 440 871; *J.Amer.Chem.Soc.*, **104**, 1146 (1984).

Magnoux, P., Cartraud, P., Mignard, S., Guisnet, M., *J.Catal.*, **106**, 235 (1987).

Magnoux, P., Cartraud, P., Mignard, S., Guisnet, M., *J.Catal.*, **106**, 242 (1987).

Marchi, A.J. and Froment, G.F., *Appl.Catal.*, **72**, 1403 (1991).

Maxwell, W.E. and Stork, *in* "Introduction to zeolite science and practice" (H. van Bekkum, E.M. Flanigen and J.C.Jansen, Eds.), p.571. Elsevier, Amsterdam, 1991.

McLaughlin, K.W. and Anthony, R.G., *AIChE J.*, **31** No 6, 927 (1985).

Meier, W.M., *in* "New developments in zeolite science and technology" (Y. Murakami, A. Iijima and J.W. Ward, Eds.),p.13. Elsevier, New York, 1986.

Meier, W.M., *Z.Chem.*, **115**, 439 (1961).

Meier, W.M., *in* "Molecular sieves", p.12. Soc.Chem.Ind., Londen, 1968.

Meisel, S.C., McCullough, J.P., Lechtaler, C.H. and Weitz, P.B., *Chemtech*, **86**, 6 (1976).

Mertens, M.M., Martens, J.A., Grobet, P.J. and Jacobs, P.A., *in* "Guidlines for mastering the properties of molecular sieves" (D.Barthomeuf, Ed), p.1. Plenum Press, New York, 1990.

Messina, C.A., Lok, B.M. and Flanigen, E.M., US Patent 4 544 143 (1985).

Meyers, B.L., Ely, S.R., Kutz, N.A., Kadic, J.A. and van den Bosch, E., *J.Catal.*, **91**, 352 (1985).

Meyers, B.L., Fleisch, T.H., Ray, G.J., Miller, J.T. and Hall, J.B., *J.Catal.*, **110**, 84 (1988).

Miradatos, C., Ha, B.H., Otsuka, K. and Barthomeuf, D., *in* "Proceedings of the 5th International Zeolite Conference" (L.Rees, Ed.), p. 382, Heyden, London, 1980.

Mishin, I.V., Piloyan, G.A., Klyachko-Gurvich, L.A., Rubenshtein, A.M., Izv.Akad.Nauk. USSR, Se.Khim., (1973) 1343

Mishin, I.V., Klyachko-Gurvich, L.A., Rubenshtein, A.M., *Izv.Akad.Nauk. USSR, Se.Khim.*, (1973) 445

Mole, T., *J.Catal.*, **84**, 423 (1983).

Mole, T., Bett, G. and Seddon, D., *J.Catal.*, **84**, 435 (1983).

Mole, T. and Whiteside, J.A., *J.Catal.*, **75**, 284 (1982).

Moscou, L. and Mone, R., *J.Catal.*, **30**, 417 (1973).

Moscou, L.,*in* "Introduction to zeolite science and practice" (H. van Bekkum, E.M. Flanigen and J.C.Jansen, Eds.), p.1. Elsevier, Amsterdam, 1991.

Murakami, Y., Kobayashi, T., Hattori, T. and Masuda, M., *Ind.Eng.Chem.(Fund.)*, **7**, 599 (1968).

Musa, M., Tarina, V., Stoica, A.D., Ivanov, E., Postinaru, D., Pop, E., Pop, Gr., Ganea, R., Birjega, R., Musca, G. and Paukshtis, E.A., *Zeolites*, **7**, 431 (1987).

Naccache, C., Chen F.R., Coudurier, G., *Chemistry Express*, **1**, 691 (1986).

Namba, S., Unaka, A. and Yashima, T., *Zeolites*, **16**, (1986).

Niwa, M., Kato, M., Hattori, T. and Murakami, Y., *J.Chem.Soc.Faraday Trans. 1*, **80**, 3135 (1984).

Niwa, M., Kato, M., Hattori, T. and Murakami, Y., J.Phys.Chem., 90 (1986), 6233

Niwa, M., Sawa, M. and Murakami, Y., *in* "Proceedings of the 9th International Catalysis Congress" (M.J.Phillips and M.Ternan, Eds.), p. 380, Chemical Institute of Canada, Ottawa (1988).

Ono, Y. and Mori, T., *Z.Chem.*, **115**, 99 (1979).

Ono, Y. and Mori, T., *J.Chem.Soc.Faraday Trans. 1*, **77**, 2209 (1981).

Pardillos, J., Coq, B. and Figueras, F., *Appl.Catal.*, **51**, 285 (1989).

Passaglia, E, *Conrtib.Mineral petrol*, **50** (1975) 65

Peeters, G., Thijs, A., Fansant, E.F. and De Bievre, P., *in* "Proceedings of the 6th International Zeolite Conference" (D. Olson and A. Bisio, Eds.), p. 651. Butterworths, London, 1984.

Pellet, R.J., Long, G.N. and Rabo, J.A., *in* "New developments in zeolite science and technology" (Y. Murakami, A. Iijima and J.W. Ward, Eds.),p.843. Elsevier, New York, 1986.

Pellet, R.J., Coughlin, P.K., Shamshoum, E.S. and Rabo, J.A., *in* "Perspectives in molecular seive science" (W.H.Flank and T.E.Whyte, Eds.), p.512. American Chemical Society, Washington DC, 1988.

Pichat, P., Beaumont, R. and Barthomeuf, D., J.Chem.Soc., Faraday Trans.I, **70**, 1402 (1974).

Post, M.F., *in* "Introduction to zeolite science and practice" (H. van Bekkum, E.M. Flanigen and J.C.Jansen, Eds.), p.391. Elsevier, Amsterdam, 1991.

Prinz, D. and Riekert, L., *Appl.Catal.*, **37**, 139 (1988).

Pujado, P.R., Rabo, J.A., Antos, G.J., Gembicki, S.A., *Catalysis Today,* **13**, 113 (1992).

Purcell, K.F. and Kotz, J.C., *in* "Inorganic Chemistry". Everbest Printing Co, Hong Kong, 1977.

Quann, R.J., Green, L.A., Tabak, S.A. and Krambeck, F.J., *Ind.Eng.Chem.Res.*, **27**, 565 (1988).

Raatz, F., Freund, E. and Marcilly, C., *J.Chem.Soc., Faraday Trans.I*, **79**, 2299 (1983).

Rabo, J.A., *Chem.Eng.*, **32** No2, 211 (1988).

Rastelli, H., Lok, B.M., Duisman, J.A., Earls, D.E. and Mullhaupt, J.T., *J.Chem.Eng.*, **60**, 44 (1982).

Rollman, L.D. and Walsh, D.E., *J.Catal.*, **56**, 139 (1979).

Sand, L.B., *in* "Molecular sieves", p.71. Soc.Chem.Ind., Londen, 1968.

Sanders, J.V., *Zeolites*, **5**, 81 (1985).

Santilli, D.S. and Zones, S.I., *Catal.Lett.*, **7**, 383 (1990).

Satterfield, C.N. and Frabetti, A.J., *AIChE J.*, **13** No4, 731 (1967).

Sawa, M., Niwa, M. and Murakami, Y., *Appl.Catal.*, **53**, 169 (1989).

Sawa, M., Niwa, M. and Murakami, Y., *Zeolites*, **10**, 532 (1990).

Sawa, M., Niwa, M. and Murakami, Y., *Zeolites*, **12**, 175 (1992).

Sayed, M.B., *Spectrochim.Acta*, **43A**, No8, 991 (1987).

Sayed, M.B., Auroux, A. and Vedrine, J.C., *J.Catal.*, **116**, 1 (1989).

Scherzer, J., (Whyte, T.E. et al. Eds.), A.C.S. Symp. Ser. Vol. 248, 157, Am.Chem.Soc., Washington DC, 1984.

Schulz, H., Bohringer, W., Baumgartner, W. and Siwei, Z., *in* "Catalyst deactivation 1987" (B. Delmon and G.F. Froment, Eds.), p.479. Elsevier, Amsterdam, 1987.

Schulz, H., Baarth, D and Siwei, Z., *in* "Catalyst deactivation 1991" (C.H. Bartholomew and J.B. Butt, Eds.), p783. Elsevier, Amsterdam, 1991.

Schwarz, S., Kojima, M. and O'Connor, C.T., *Appl.Catal.*, **68**, 81 (1991).

Schwarz, S., PhD Thesis, University of Cape Town, 1991.

Sherman, J.D. and Bennet, J.M., *Adv,Chem.Ser.*, **152**, 54 (1973).

Shiring, F.J., Venkatadri, R., Goodwin, J.G., *Canad.J.Chem.Eng.*, **61**, 218 (1983).

Skupinska, J., *Chem.Rev.*, **91** (1991).

Smith, J.V., *in* "Zeolite chemistry and catalysis", (J.A. Rabo, Ed), ACS Monograph Ser., **171**, p.1. Am.Chem.Soc., Washington DC, 1979.

Sugimoto, M., Katsuno, H., Takatsu, K. and Katawa, N., *Zeolites*, **7**, 503 (1987).

Sunavala, K.P and Sunavala, P.D., *Ind.J.Tech.*, **26**, 515 (1988).

Suzuki, K., Kiyozumi, Y., Matsuzaki, K. and Shin, S., *Appl.Catal.*, **35**, 401 (1987).

Suzuki, K., Kiyozumi, Y., Matsuzaki, K. and Shin, S., *Appl.Catal.*, **42**, 35 (1989).

Suzuki, K., Kiyozumi, Y., Matsuzaki, K. and Shin, S., *J.Catal.*, **42**, 35 (1988).

Szostak, R.,*in* "Introduction to zeolite science and practice" (H. van Bekkum, E.M. Flanigen and J.C.Jansen, Eds.), p.153. Elsevier, Amsterdam, 1991.

Tabak, S.A. and Yurchak, S., *Catal.Today*, **6**, 307 (1990).

Tabak, S.A., Krambeck, F.J. and Garwood, W.G., *AIChE J.*, **32** No9, 1526 (1986).

Tarramasso, M., Perego, G. and Notari, B., *in* "Proceedings of the 5th International Zeolite Conference", p.40. Heyden & Sons, Londen, 1980.

Taylor, W.H., *Z.Kristallogr.*, **74**, 1 (1930).

Thomson, R., Montes, C., Davis, M.E. and Wolf, E.E., *J.Catal.*, **124**, 401 (1990).

Thijs, A., Peeters, G., Vansant, E.F., Verhaert, I. and De Bievre, P., *J.Chem.Soc., Faraday Trans.1*, **79**, 2821 (1986).

Ueda, S., Murata, H., Koizumi, M., *Am.Mineral.*, **65**, 1012 (1980).

van Geem, P.C., Scholle, K.F.M., van der Velden, G.P.M. and Veeman, W.S., *J.Phys.Chem.*, **92**, 1585 (1988).

van Koningsveld, H., *in* "Introduction to zeolite science and practice" (H. van Bekkum, E.M. Flanigen and J.C.Jansen, Eds.), p.35. Elsevier, Amsterdam, 1991.

Vaughan, J.S., Unpublished data, University of Cape Town, 1991.

Walsh, D.E. and Rollman, L.D., *J.Catal.*, **49**, 369 (1977).

Weisz, P.V., *Chemtech*, **3**, 498 (1973).

Weller, S.W. and Brauer, J.M., AIChE Annual Meeting, Washington DC, 1969.

Wendlandt, K.-P., Reschitilowski, W.P., Unger, B., Romanovskij, B.V., Suchkova, E.V. and Freude, D., *in* "Innovation in zeolite materials science" (P.J. Grobet, W.J. Mortier, E.F. Vansant and G. Schulz-Ekloff, Eds.), p.207. Elsevier, Amsterdam, 1988.

Weyda, H. and Lechert, H., *Zeolites*, **10**, 251 (1990).

Whittemore, O.J., *Amer.Mineral.*, **57**, 1146 (1972).

Wilson, S.T., Lok, B.M. and Flanigen, E.M., U.S. Patent 4 310 440 (1982).

Wilson, S.T. and Flanigen, E.M., U.S. Patent 4 567 029 (1986).

Wu, M.M. and Kaeding, W.W., *J.Catal.*, **88**, 478 (1984).

Wu, P. and Ma, Y.H., *AEChE Symp.Ser. No219,* **78**, 90 (1988).

Xu, Y., Grey, C.P., Thomas, J.M. and Cheetham, K., *Catal.Lett.*, **4**, 251 (1990).

Yurchak, S., *in* "Methane Conversion" (D.M. Bibby, C.D. Chang, R.F. Howe and S. Yurchak, Eds.), p.251. Elsevier, Amsterdam, 1988.